University of Catania

Department of Chemical Sciences

International Ph.D. program in Chemical Sciences

Academic year 2019/2023

Mass spectrometric and proteomic investigations of mammalian body fluid proteins

Agatino Zammataro

Academic Tutor:
Professor Rosaria Saletti

Industrial Tutor:
Doctor Ilenia Abbate

Rostock University Tutor:
Professor Michael. O. Glocker

Ph.D. Coordinator:
Professor Salvatore Sortino

XXXV Cycle Ph.D. Programme

PON Ricerca e Innovazione 2014-2020-D.D.n. 2008 del 22/10/2019.

In partnership with: SIFI S.p.A.

Rostock University, Department for Proteome Research

Fatti non foste a viver come bruti,

ma per seguir virtute e canoscenza

Divine Comedy, Canto XXVI, Hell

Dante Alighieri

Abstract

The present work is divided into two sections based on the mammalian body fluid type under consideration (tears and serum). Different mass spectrometry methods and proteome analysis studies were applied with both biological fluids which had been collected from rabbits (Figure 1).

The first section, dedicated to tear samples, is entitled "*Proteomic profiles study on rabbit tears treated with a postbiotic-based medical device*" (Section 1). This study was performed at SIFI S.p.A, a pharmaceutical company operating in the ophthalmic field, and at the University of Catania. Tear samples were collected from 5 untreated rabbit (NT), and from 10 rabbits in which left eyes were treated with placebo ocular drops (PL) and right eyes were treated with ocular drops of a medical device based on postbiotic product (PB). Then, the proteomic profile of each sample was defined, to obtain information about the possible effect of this medical device for treating ocular allergies and dry eye syndrome (Section 1A). In addition, a protocol designed to perform a rapid quantitative analysis of principal components using an integrated analytical method, was developed and used to characterise the postbiotic product, derived from the fermentation of *Lactobacillus paracasei* (Section 1B).

The second section is dedicated to rabbit serum analysis, it is entitled "*Development of an MS-based method for determining serum conversion and epitope characterisation*" (Section 2). This study was performed at the Proteome Center Rostock, University of Rostock. The first research goal was to develop a rapid method for the extraction of immunoglobulins (IgG) from rabbit serum avoiding expensive affinity chromatography. This method can be used for the extraction of IgG from serum which di-

rectly are suitable for mass spectrometric investigations (Section 2A). IgG solutions from seroconverted serum was used for epitope mapping using an innovative MS-based method (Section 2B), termed Intact Transition Epitope Mapping (ITEM)". The purpose of this study is to open up the possibility to use this MS-based ITEM method for detecting specific antibody reactivities within serum from patients after infections with pathogens, upon suffering from autoimmune diseases, or with allergy problems.

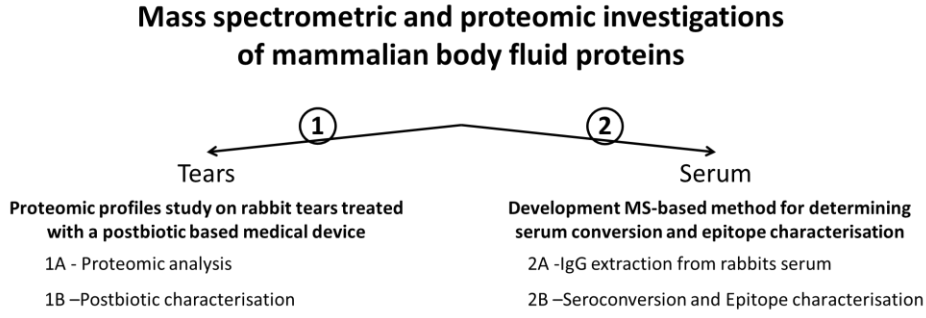

***Figure 1**. Work structure*

Index

1. List of abbreviations

aa= amino acid

Abs= Absorbance

ADDE= Aqueous Deficient Dry Eye

AFM= Atomic Force Microscope

AKC= Atopic Kerato Conjunctivities

APPI= atmospheric pressure photoionization

AUC= Area Under the Curve

CAP= F- actin-capping protein

CE= Capillary electrophoresis

CH= Constant heavy chain

CI= Chemical Ionization

CID= Collision Induced Dissociation

CL= Constant light chain

CRT= Calreticulin

CTRL= Control solution

DED= Dry Eye Diseases

Dev.Std= Standard deviation

DMSO= Dimethyl sulfoxide

DNA= Deoxyribonucleic acid

DTT= Dithiothreitol

EDTA= Ethylenediaminetetraacetic acid

EI= Electron Impact

ELISA= enzyme-linked immunosorbent assay

EM= Expectation-Maximization

EPIT= Epi Cutaneous Immune Therapy

ER= Endoplasmic Reticulum

ESCi= electrospray and atmospheric pressure chemical ionization

ESI= Electro Spray Ionization

ETD= Electron-Transfer Dissociation

FDR= False Discovery Rate

FOS= Fructo OligoSaccharides

FT-IR= Fourier Transform Infrared Spectroscopy

GOS= Galacto OligoSaccharides

GBI-30= Bacillus coagulans

GPC= Giant Papillary Conjunctivitis

GPMAW= General Protein/Mass Analysis for Windows

HCD= High-energy Collision Dissociation

hnRNP K= Heterogeneous nuclear ribonucleoprotein K

HT-Buffer= High TRIS concentrated buffer

IAA= Iodoacetamide

IgE= Immunoglobulins E

IgG= Immunoglobulins G

IR= Infrared spectroscopy

IT= Ion Trap

ITEM= Intact Transition Epitope Mapping

LC= Liquid Chromatography

LT= Low TRIS concentrated buffer

MALDI= Matrix Assisted Laser Desorption/Ionization

MCP= MicroChannel Plate

MOPS= 3-(N-morpholino) propanesulfonic acid

MS= Mass Spectrometer

MS-MS= Mass-Mass technique

MTBE= Methyl tert-butyl ether

MudPIT= Multidimensional Protein Identification Technology

nESI= nano Electro Spray ionization

NHE-RF1= Na(+)/H(+) exchange regulatory cofactor

NMR= Nuclear Magnetic Resonance

NST= Non-Stimulated Tears

NT= Untreated rabbits

PAC= Perennial Allergic Conjunctivitis

PB= Postbiotic treated rabbits

PBS= Phosphate-buffered saline

PCO= Posterior Capsular Opacification

PCTF= PreCorneal Tear Film

PDX= PolyDextrose

PES= Polyethersulfone

PL= Placebo treated rabbits

PLA= Phospholipase A2

PLGS= ProteinLynx Global Server

PSM = Peptide Spectral Matches

PVDF= polyvinylidene difluoride

Q= Quadrupole

RF lens= Radio frequency lenses

RP-HPLC= Reverse Phase-High Pressure Liquid Chromatography

SAC= Seasonal Allergic Conjunctivitis

SCIT= SubCutaneous Immune Therapy

SDS= Sodium dodecyl sulfate

SDS-PAGE= sodium dodecyl sulfate–polyacrylamide gel electrophoresis

SEM= Scanning Electron Microscope

SIFI S.p.A.= Società Industria Farmaceutica Italiana

IgA= Immunoglobulins A

SLIT= SubLingual Immune Therapy

SPF rabbits, NZW= Specific Pathogen-Free rabbits, New Zealand White

SPR= Surface Plasmon Resonance

ST= Stimulated Tears

STD= Standard solution

STS= Schirmer Test Strip

TFOS= Tear Film and Ocular surface Society

TIC= Total Ion Current

TNFs= Tumor Necrosis Factors

ToF= Time of Flight

Tpm= Tropomyosin beta chain

TRIS= tris (hydroxymethyl) amin methane

UHPLC= Ultra High-Performance Liquid Chromatography

USA= United States of America

VH= Variable heavy chain

VKC= Vernal KeratoConjunctivities

VL= Variable light chain

WO= Wash Out

2. Proteomic profiles study on rabbit tears treated with a postbiotic-based medical device (Section 1)

2.1. Introduction

2.1.1. The tear film

The precorneal tear film (PCTF), that covers the ocular surface, has different functions. For example, it works like a barrier which is able to protect the eye from microorganisms, has lubrification and nutritive functions for tissues without blood vessels, and an appropriate refraction index that permits a clear vision.[1]

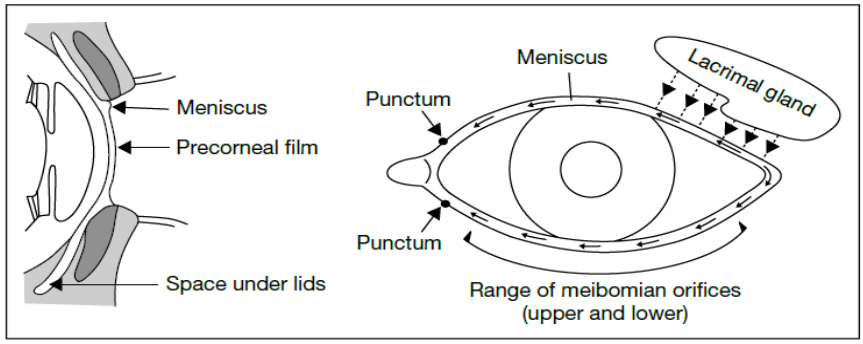

Figure 2. Position of tear film. *Left,* sagittal section indicating different regions of the tear film. *Right,* front view showing position of main lacrimal gland and other structures influencing the teat film

The lacrimal film has a thickness of about 3-11 μm and is constituted by two layers: lipidic and aqueous/mucous.[2]

The lipid layer originates from Meibomian glands and is the superior layer of the lacrimal film. Its main role is to slow down the evaporation of the underlying aqueous layer.

The aqueous layer originates from lacrimal glands and contains electrolytes, proteins, peptides and mucins (Figure 2).

Mucins are glycoproteins produced by the epithelium tissues and mucous; they protect these tissues thanks to its antioxidant, antimicrobial and lubrification properties. In normal conditions the lacrimal film production is of about 0.5-2.2 µl/min, and the total volume present in the eye is between 7 and 10 µl (Table 1).

The cycle of production, evaporation, drainage, and absorption of tears highlight the establishment of a dynamic equilibrium of tears presence upon ocular surface. The composition of the tears makes them viscous (the viscosity is between 1.3 and 5.9 cP) enough to protect and lubricate the ocular surface without damaging the eye.[3,4]

Table 1. Properties of PCTF[6]

Volume	7-10 µl
Flow (secretory velocity)	0.5-2.2 µl/min
Osmolarity	≤290 mOsmol/l
Turnover rate	16%/min
Layers	1- Aqueous; 2-Lipid/oily
Thickness	3-11 µm
Total protein concentration	7 g/l

External factors and stimuli can irritate the eye and the irritation changes the physiology of the lacrimal film, which also changes according to the different times of the day. These reasons make harder the extrapolation of significant data that can describe, in an exhaustive way, the normal composition of this biological fluid.

The lacrimal film is a complex fluid, which despite its little volume, contains a lot of solubilized species (Table 2). In particular, in the

tears the normal concentration of proteins is about 7 g/l, and the sampling method can affect their relative concentrations.[5]

Table 2. Layers of tears: origins, components, and main roles

PCTF layers	Produced by/origin	Components	Main roles
Aqueous layer	Globelet cells, corneal and conjunctival epithelia, main lascrimal gland, accessory lacrimal gland of Krause and Wolfring	Sectreted and transmembrane mucin, immunoglobulins, salts, urea, enzymes, glucose, leukocytes, water, antimicrobial agents, cytokines, hormones, growth factors, neurotrophic factors, cell adhesion molecules, matrix metalloproteinase, insulin, vitamis, electrolytes, 60-500 different proteins	Protection against pathogens, increase stability of the overlying tear film, regulation of epithelial growth, cellular signaling, movement of lipids, transport of proteins, lubrification and cleaning of the ocular surface, antimicrobial activity
Lipid layer	Meibomian glands, glands of Moil and Zeiss, lacrimal glands, epithelial cells	Polar lipids, non-polar lipids	polar surface layer formation, evaporation reduction, smooth optical surface

Most of these proteins have important roles in the inflammatory processes and eyes protection. The most common proteins that have been found are: lactoferrin, lysozyme, immunoglobulin, lipocalin etc.[6,7]

These alone represent 90% of the total proteins that are contained in the tear fluid.

2.1.2. Tear sampling

The quantitative and qualitative protein tear determination is an interesting ophthalmic topic in the worldwide, but the work is difficult and is affected by sampling technological problems. The sampling problems are due to the little volume and the complexity of the fluid.[8]

Direct method is conducted with glass microcapillaries or micropipettes (Figure 3), and requests to stimulate the eye before sampling. This stimulus can be done by instillation of a saline solution (100-200 µl) in the conjunctival sac.

After mixing the saline solution with tears, through the opening and closing eyelids, it is possible to collect the sample.

This method, called ST (Stimulated Tears), is affected by dilution of the species which are solubilised in the lacrimal film.[9]

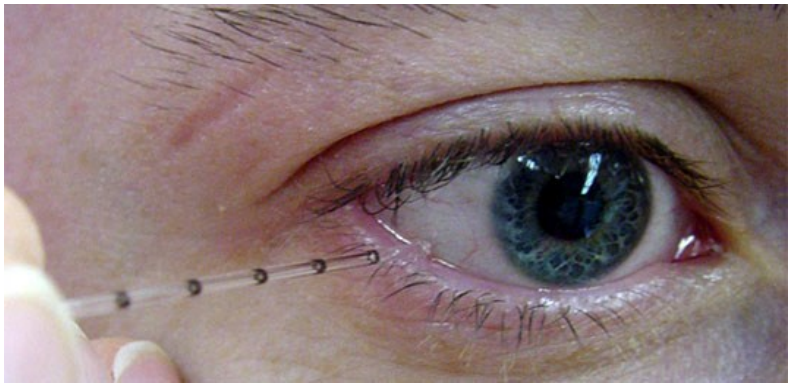

Figure 3. Direct sampling method by sterilised glass microcapillary

Non-stimulated sampling (NST) has been introduced for the first time by Kalsow et al. [12] in lacrimal cytokine studies. The tears from inferior conjunctiva of both eyes were collected through a sterilized 10 µl glass microcapillary.m5 µl of lacrimal fluid were rapidly transferred into a sterilized 0.2 ml Eppendorf, previously filled with 49.5 µl of storage solution, so a 10 times more diluted solution was obtained. Finally, the Eppendorf was stored at -80°C.[10]

These two sampling methods produce two different protein profiles. ST method has more proteins which came from lacrimal glands,[11] instead NST method produces a representative protein profile about in-

flammatory state of the ocular surface, but its volume is limited, especially if the patient is affected by dry eye syndrome.
Therefore, even if the NST method causes less local irritation thanks to limited eyes contact, and the relative concentration of the solubilised species is well represented, the volume of sample (2-3 µl) that can be collected is small.[3]

A method to increase the volume of the samples is the wash out method (WO). This technique is leaded through instillation of 10 µl of saline solution in the inferior conjunctiva, before the sampling. Monitoring immunoglobin IgA concentration, which decreases with the tear stimulus increasing, Markoulli et al. have found a immunoglobulin relative concentration comparable in both NST and WO methods.[12] They have demonstrated that WO method is a valid choice, it is better than NST because it produces a major volume of sample and does not stimulate the lacrimation.
Unfortunately, ST makes samples not representative of the effective state of the eye, because it is affected by dilution and by overproduced molecules which are involved in the response of an external stimulus.

Indirect methods are performed using absorbent materials such as Schirmer test strips (STS), paper disks (Figure 4)[13] or cellulose sponges.[14]

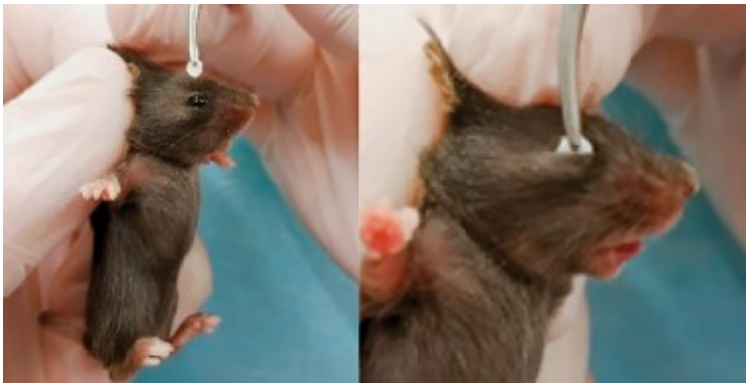

Figure 4. *Left*, Mice were restrained gently by hand via the loose skin of the scruff of their neck. *Right*, the smooth edge of the circular filter paper pieces was placed inside the lower lid margin (inferior fornix) of the eye, allowing tear secretion by the Meibomian ducts

STS (Figure 5) is the most common method. The samples collected in this way have high quantity of mucous, lipids and cells.
Unfortunately, the elution of proteins is incomplete and irregular on the filter, indeed the STS and direct methods produce different proteins profiles. In conclusion, the correct sampling with microcapillary remains the most representative.[15]

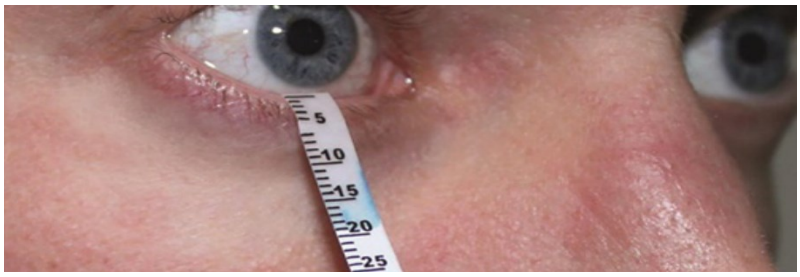

Figure 5. Schirmer test strip for lacrimal sample collection and volume measurement

STS method is advantaged by the large volume collected but is disadvantaged by lacrimal reflex and irritation that change normal proteins profile.

These results, which are obtained comparing different kinds of samples highlight that the STS method has an impact on the protein pro-

file. We must pay attention to choose the best sampling method to obtain the best correlation between reality, data and hypothesis.

2.1.3. Eye diseases

The ***dry eye disease*** (DED) is defined as multifactorial pathology that involves the lacrimal film and the ocular surface. The symptoms are pain, disturbed vision, inflammation, redness, lacrimal film instability and potential damage of the ocular surface.[16] The ocular surface tissues involved in DED are the cornea, conjunctiva, Meibomian glands, and lacrimal glands.[17] Recent studies show that DED has numerous aspects in common with autoimmune pathologies, and the trigger factor is the ocular stress, that can be originated by environmental or genetic factors, infections etc. In DED onset, the involved mechanism promotes secretion of cytokines, chemokines and metalloproteins, which encourage a strong immune response. This response promotes a successive overproduction of these species and so on, and the situation become a vicious circle.[18] The DED has been subdivided into two different categories: the first is the aqueous-deficient (ADDE), due to the decreased tear secretion, the second is the hypervaporative, due to the more rapid evaporation of the tears film (Figure 6). 10% of the patients with DED are affected by the aqueous-deficient type, other 10 % of them are affected by the hypervaporization which is due to the Meibomian glands disfunctions, and the remaining 80 % of the patients are affected by both pathologies.[19]

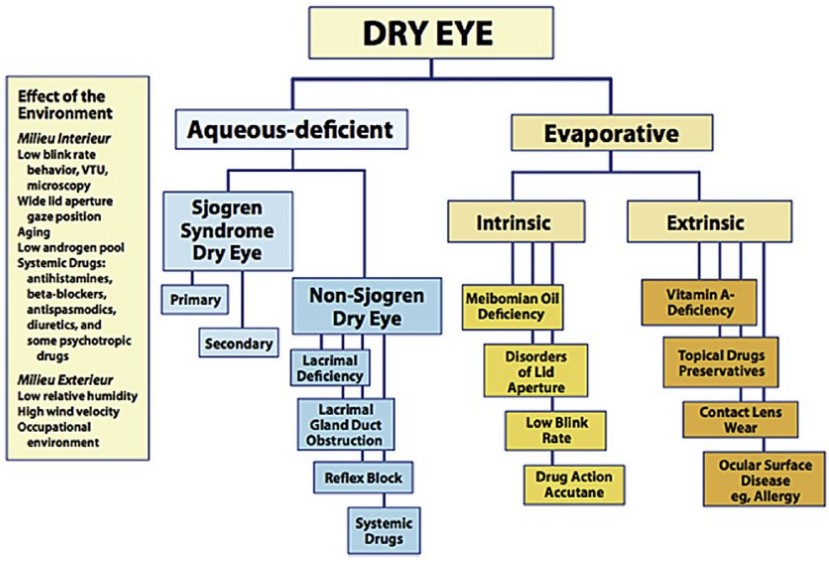

Figure 6. Dry eye classification from the 2007 TFOS Report[16]

The world population which is affected by DED is of about 15-34% with an age-related increase.[20] DED can damage vision, make it difficult to read paper and screens, drive, etc.[21] In general, DED reduces the quality of life and affect daily actions in 60% of cases, while 38% of patients show a decline in work performance.[22] DED is associated with depression in 37.7% of the cases.[23] In addition, DED is an expensive problem for sanitary system, only in the USA it costs about 3.84 million of dollar each year.[24] DED symptoms are redness, burning sensation, itching, photophobia, pain, and potential damage, severe or low, of the conjunctiva with epithelial erosion,[25] Meibomian gland's orifice (Figure 7) could be obstructed by a solid secretion.[26]

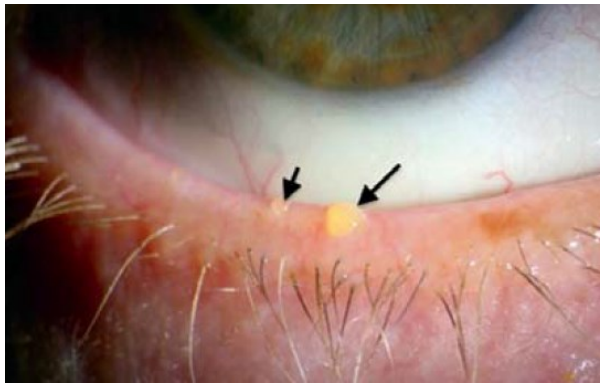

Figure 7. Meibomian gland orifices on the eyelid margin blocked by thickened meibomian secretion

In the most aggressive DED, the patients can be affected by scaring of the conjunctiva. These scars are due to the cornea's ulcerations and perforations. Severe situations are not common, but they can be observed in some kinds of DED like Sjogren's syndrome, Stevens-Johnson syndrome and in the xeropthalmia, all of these can lead at the blindness.[27]

The therapies against DED are long and without immediate effects, is common a gradual approach based on the seriousness of the case. The approaches must pay attention at the possible disfunction of the Meibomian glands, inflammatory state of the ocular surface etc.[28] It is also recommended to avoid the risk factors, which can worsen the situation, such as smoke of cigarette, hot or dry air etc.[24]

The most common therapy uses artificial tears, randomized studies have demonstrated that their use is able to increase the lacrimal film stability, reduce stress upon ocular surface and improve the optical quality of the eyes and life quality.[29]

A wide number of artificial tears are based on the polyvinyl alcohol, povidone, Guar gum, cellulose, and hyaluronic acid derivates. Based

on the case, the patients can choose among various products which have high or low viscosity. Against the Meibomian glands dysfunctions, it is possible to use artificial tears with lipids as triglycerides, phospholipids and castor oil; often anti-inflammatories are contained too.[30] Some kinds of artificial tears are produced by patient's serum, with a variable concentration from 20% to 100%. These products present a high content of grow factors for the epithelial cells, and anti-inflammatories species. This strategy can be used only in the severe cases, and the production of these artificial tears is regulated by the regulatory bodies.[31] Topical corticosteroids application, for 2 or 4 weeks, improve patients' conditions. The improvement starts from the second week with a regression of symptoms on the 42% of the cases or with complete regression on the 57% of cases. After the treatment, the symptoms are still reduced for few weeks. But this kind of therapy promote different complications. In particular, it grows intraocular pressure which can favour the onset of glaucoma or can promote the onset of cataract.[32] Another topical treatment involves an immune suppressor, the Ciclosporin A, which inhibits the calcineurin phosphatase through the complexation of cyclophilin, and thanks to this reaction the synthesis of cytokines, which activate the T-cells, is reduced. The topical application of this drug improves the lacrimal film production. A study leaded with a topical preparation, which include 0.05% of Ciclosporin A, applied twice a day, showed an improvement of the keratopathies, an enhancement of the Schirmer test strip results, and also a reduction of the symptoms.[33] The same results are obtained with tacrolimus and pimecrolimus.[34] Tetracyclines are bacteriostatic drugs with anti-inflammatory effects. These kinds of molecules can reduce the synthesis of the metalloproteins,

interleukins, TNFs (tumour necrosis factors), and are B-cells activator. The effect of the tetracyclines in Meibomian glands disfunctions has been studied. When a dose from 40 to 400 mg at day of doxycycline and a dose from 50 to 100 mg at day of minocycline was used, an improvement in tear film stability was seen already at the lowest dose, with optimization of lacrimal secretion and reduction of the symptoms. These molecules have also some collateral effects, like gastrointestinal and skin disturbs, but they appear at high dosage. The recommended therapy suggests an application for 6 or 12 weeks at the minimum dosage.[35] Azithromycin is a macrolide with antibiotics and anti-inflammatory effects, which if used at a concentration of 1% has positive effects on the Meibomian glands (normalization of lipidic secretions an reduction of symptoms).[36] Omega 3 and 6 are essential fatty acids for the ocular surface homeostasis, omega 3 can block proinflammatory eicosanoids and reduces the inflammatory activity of cytokines.[37]

Ocular allergy is a pathology which has origin from a group of immune disorders. It is related with the IgE mast cells overproduction, in presence of allergens. The allergy can appear in different ways and affect different tissues. The sites can be nose, respiratory apparatus, eyes, gastrointestinal tissues, and skin. The development of allergies is in constant increasing in the world, especially during the scholastic age, about 50% of the children have one kind of allergy.[38]

Ocular allergies are characterized by conjunctiva inflammation, and they are originated from exposition to allergens. Most common forms of these kind of allergies are seasonal allergic conjunctivitis (SAC), and perennial allergic conjunctivitis (PAC). The last one is due to the

indoor allergens; the SAC is due to the outdoor allergens like pollen (Figure 8)

The most common diseases promoted by this pathology are atopic keratoconjunctivitis (AKC), vernal keratoconjunctivitis (VKC) and giant papillary conjunctivitis (GPC). The AKC is the most severe form and can lead at an opaque cornea and at vascularization. The VKC is most common in children affected by giant papillae in the tarsal conjunctiva, and the GPC is not directly related to the allergy, but it often appears as one of the symptoms with redness, itching and swelling.[39]

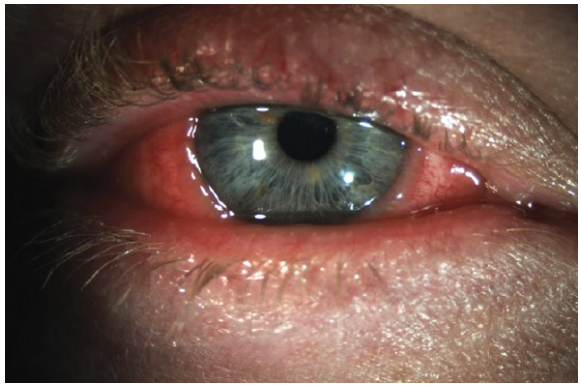

Figure 8. Example of eye with ocular allergy manifestation

Numerous topical pharmacological therapies against ocular allergy consist of mast cells stabilizers and may also contain antihistaminic. Other drugs can contain steroids or immunomodulators. The simultaneous action of both pharmacological therapies and non-pharmacological therapies (like cold compresses) improvement the treatment efficacy.[40] Cetirizine is an effective antihistaminic which can reduce itching sensation and conjunctiva redness,[41] therefore, it is able to give a rapid sense of relief to the patients. Its effectiveness improves if it is used with a catechins, which are extracted from some

plants, which are histidine decarboxylase inhibitors.[42] Cyclodextrins are a valid means for Olopatadine delivery, in this way the action of the drug is more constant and long-lasting.[43] Contact lenses are a barrier against the allergens which can arrive on the ocular surface, and they could be use as drug delivery systems. In a work the surface of the contact lenses have been covered with Epinastine and Olopatadine, and consequently, prolonged release time of the drugs improved their efficacy.[44] Sub lingual immune therapy (SLIT) uses tabs or drops with the allergen,[45] that was extracted from grass. More than 50% of patients, who were treated with these drugs, during the next season had not allergic symptoms like rhinitis, itching etc.[46] Sub cutaneous immune therapy (SCIT) is another innovative therapy, which uses a protein extracted from Gramineae. After three weeks of therapy, the patients have obtained positive results.[47] Epicutaneous immune therapy (EPIT) is a method in which the contact between allergens and the patients skin is direct, and it is able to decrease the conjunctivitis.[48] Probiotics are an unconventional approach for the ocular allergy treatment. Recent studies have demonstrated that the introduction of mandarin yogurt in the patients' diet can reduces redness, itching and chemosis. This result is possible thank to the Nobiletin and β-lactoglobulin which are contain in this kind of yogurts, and this highlights that the use of pro-biotics improves the life quality of the allergic patients.[49] In the lacrimal film of subjects with ocular allergy there are an overproduction of prostaglandins,[50] these species and their receptors could offer new pharmacological targets.[51]

2.1.4. Probiotics, prebiotics and postbiotics

Biotics is a word that takes origin from the Greek expression biōtikós which means "belonging to life." Biotic products are a mix of bioactive compounds generated during a microbial fermentation. In recent years, these products have sparked increasing interest for their proven beneficial effects,[52] for example, in patients with lactose intolerance[53] or insulin resistance.[54] They have also been shown to be effective in lowering blood pressure[55] and cholesterol[56] and appear to exhibit anti-inflammatory, immunomodulatory, anti-proliferative and antioxidant activities[57]. Biotic products are classified as probiotics, prebiotic and postbiotic.

Probiotics are made up of living microorganism originated for example from fermented yoghurts, grains, or pickles; commercial development of probiotics focuses on only a few genera, the most common being *Lactobacillus spp.*, *Bifidobacterium spp.*, *Bacillus spp.* and *Weissella spp.*[58] The administration of probiotic appear to affect the intestinal microbiota through suppression[59] and/or inhibition of pathogens[60]. In particular, immunomodulatory[61] and antiinflammation[62] effects were shown for the *Lactobacillus* genera.

Prebiotics are substrate used selectively by host microorganisms, which confer health benefits.[63] These type of products may be involved in modifying the composition of the microbiota, as they can stimulate the growth of particular species.[64] Commonly used prebiotics are fermentable carbohydrates such as galacto-oligosaccharides (GOS), fructo-oligosaccharides (FOS), and polydextrose (PDX).[65]

Postbiotics, the new entry in the biotic family, are a mixture of biological molecules originating from the fermentation of microorgan-

ism, in which microbial cells are not viable.[66] To obtain a postbiotic preparation, bacterial cell lysis can be performed using various technological strategies, such as heat treatment, sonication and dehydration.[67,68] The administration of postbiotics may be safer than the administration of probiotics, since the absence of microorganisms avoids the possibility of microbial translocation and the consequent infection and inflammation[69]. These products appear to have a beneficial effect on patience health perhaps because due to the additional bioactivity provided by the presence of the obtained bioproducts[70, 71].

Although the molecular mechanisms behind their beneficial effects are not fully understood, it is known that there is an interaction between the host and key compounds generated during microbial fermentation; for example, the lipopolysaccharides produced have been related to immunomodulatory activities by stimulating the innate immune system[72].

Their effects, therefore, are not led by the living bacterial availability; this was demonstrated by different studies in which probiotics, postbiotics and different microbial products fractions were compared.[73] In a major part of the studies about postbiotics, this bioproducts were obtained from *Lactobacillus* and *Bifidobacterium*, to cite some instance De Oliveira et al. reported an exhibition of antioxidant activity using both intracellular and extracellular contents of *Lactobacillus*[74], the same effect was reported by other authors as Amaretti et al. in which intracellular postbiotic of *Bifidobacterium* was used, they found that the antioxidant features are based on the used strain[75], Aguilar et al. found that between intracellular content and cell wall fraction the first one has higher antioxidant activity[76]. Effects on

apoptotic process and antiproliferative activity are reported by Maghsood et al. in their studies they saw that postbiotics from *Lactobacillus ruteri* have inhibitor effects on colon cancer stem-like cells thanks to an increased apoptosis and downregulation of metalloproteinase-9[77], in addition, Nozari et al. reported an inhibition of cell growth of human colon carcinoma cell line by cell wall protein fractions from *Lactobacillus paracasei*[78], Chuah et al. found out a cytotoxic activity performed by a postbiotic product based on *L. planatrum* strain[79], similar induced apoptosis in colon carcinoma cell line was demonstrated by Karimi et al.[80] Antimicrobial activity were reported by Kareem et al. they found that postbiotics from *L. plantarum* strains produce bacteriocin-like products against different pathogens bacteria[81], same result are showed by Moradi et al. using different strains of *Lactobacillus*[82], Posados et al. reported that products based on S. cerevisiae seems to have greater binding adhesion against phatogenic Gram-positive and Gram-negative.[83] Immunostimulant activity thanks to an increasing gene expression of some cytokines and chemokines were reported by Balzaretti et al.[84]; Qi et al. took under consideration different postbiotics compound from *L. rhamnosus GG* in order to evaluate their immunomodulatory properties, they reported that the major part of used postbiotics involve the inhibition of extracellular regulated protein kinases, activation of toll-like receptor and mitogen-activated protein kinases which can bring to an anti-inflammatory activity[85]. Immunomodulatory and anti-inflammatory effects were found by using cell wall components from *Bacillus coagulans GBI-30* by Jensen et al.[86] Principal components of postbiotics are proteins and derivatives, carbohydrates and derivatives, inorganic salts, lipids and derivatives.[87, 88, 89, 90] Indeed, the mixture of

these components contains complex molecules, this means that are necessary sophisticated analysis with appropriate instruments and standards; the choose is based on which kind of information the operator is focused on, if it is necessary to perform qualitative or quantitative analysis, or if the task is, for example, knowing the exact carbohydrates compositions or lipids compositions. For instance, gas chromatography is the common used technique to identify short-chain fatty acids or aminoacids[91]. For protein determination liquid chromatography coupled with mass spectrometry is used; in this way was possible to find a novel secreted protein called HM0539 in *Lactobacillus rhamnosus*[92], lipoteichoic acids produced by *Lactobacillus plantarum*[93] or characterise the glycolipids from the wall cell of *Bifidobacterium longum* spp[94]. NMR spectroscopy was used to obtain information about the amount of cell-free supernatants metabolites as monosaccharides, ketones or amino acids[95]. To characterise antifungal metabolites from *Lactobacillus brevis* were used IR spectroscopy techniques.[96]

Other instruments like SEM, AFM, FTIR and Raman spectroscopy were used.[97, 98, 99]

2.1.5. Proteomics methods

Proteomics is the study of set of proteins which are synthetised by genome within a cell or tissue in a specific moment. The old idea that declares: "at each gene corresponds one protein" is not true. This idea does not consider post-translational changes. Post-translational modifications produce a wide variety of proteins which are produced by the same gene. These dynamic modifications are based on a specific life moment of the organism, external environmental conditions,

pharmacological treatments etc. Therefore, the proteome is more complex than the genome, and in addition it is dynamic. Proteomic studies can be conducted by two approaches: top-down and bottom-up.

Top down approach consists in the study of intact protein ions and their direct fragmentation within the instrument without previous digestion.[100] The accurate molecular mass and the sequence information can then be used for the bioinformatic research in order to identify the protein (Figure 9).

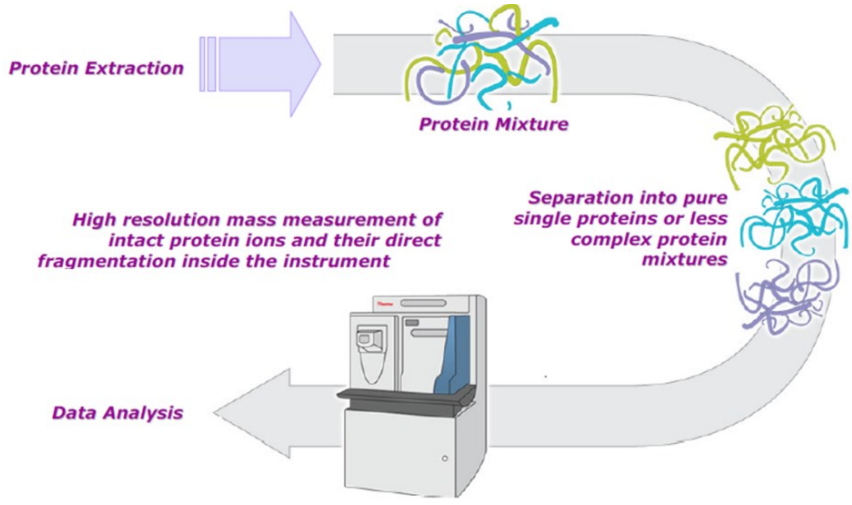

Figure 9. Schematic representation of Top-down approach

This approach requires very expensive instrumentation and does not allow for the characterization of high molecular weight proteins.

The bottom-up method is subdivided in gel-based and gel-free approaches. The most common ***gel-free*** method is "Multidimensional Protein Identification Technology" (MudPIT)[101]. This approach consists in whole protein pool digestion and in separation of resulting peptides through two chromatography steps: ion exchange and RP-HPLC (Figure 10 and 11).

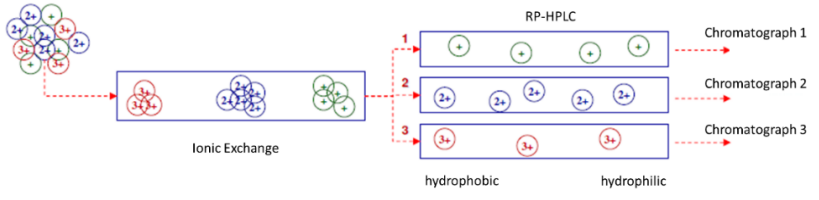

Figure 10. Schematic representation of chromatographic steps

Finally, the isolated peptides are analysed by ESI/MS-MS mass spectrometry.

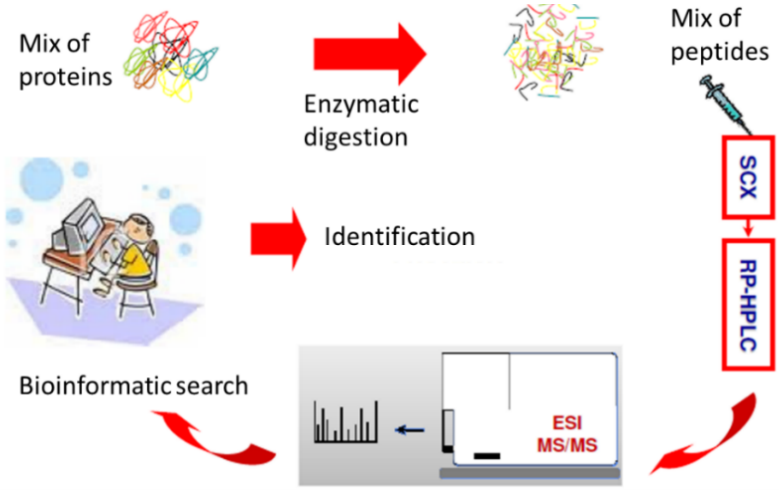

Figure 11. Schematic representation of the workflow for Multidimensional protein identification (MudPIT)

The advantage of this method is the simultaneous characterization of multiple proteins, but the system is very complex, and it is difficult to identify proteins present in lower amount.

By using ***gel-based approach***, a complex mixture of proteins is separated by 1-D or 2-D electrophoresis. Subsequently, the protein of interest is excised from the gel and subjected to reduction of disulfide bonds, block of the cysteine residues to avoid disulphide bridges restoring, and enzymatic digestion. This procedure is followed by mass spectrometry analysis (MALDI-ToF or RP-HPLC/nESI/MS-MS) and bioinformatics research.

2.1.6. Proteomic analysis

Proteomics is useful to study ocular diseases. Thanks to the technology improvement and the more sensitive instruments, nowadays it is possible to analyse a small sample quantity and detect proteins present in trace amount. Moreover, by means of advanced analytic techniques and bioinformatic research, we can characterise the protein profile of a health eye and compare it with that of a sick eye, to identify biomarkers of specific pathologies. These biomarkers are essential for understanding the disease and developing early diagnosis methods, new pharmacological targets, and personalised therapies.

2.1.7. HPLC

HPLC (High-Performance Liquid Chromatography) is a chromatographic technique that permits complex mixtures separation. It is based on the formation of a pseudo-equilibrium between each component of the sample, the stationary phase, and the mobile phase. At the head of the column there is a pump to apply a pressure, thanks to this pressure the system can elute the liquid mobile phase through the stationary phase which is constituted by particles with size comprised between 3 and 10 μm. In this way the separation is efficient, the resolution is high, and, thanks to the pump, it is faster than other chromatographic techniques. Reverse-phase chromatography (RP-HPLC) uses apolar stationary phase which is constituted by alkyl chains (C4, C12, C18) linked to small silica spheres. Polar mobile phase is in general a mixture of two or more different solvents, whose flow rate is regulated by the respective pump. In this way is possible to work in two different flow conditions:

- isocratic conditions: same mobile phase composition during whole analysis.

- gradient elution: in this case the solvent composition and polarity are variable during the analysis. The gradient can separate the different analytes contained in function of their affinity for the specific mobile phase compared to the stationary phase.

  At the beginning of the separation based on elution gradient the mobile phase is rich in more polar solvent and, thereafter, the solvent with non-polar characteristics is increased over the time. Usually, the solvents were used in RP-HPLC are water and methanol (or acetonitrile). In this way, initially the more polar components of the mixture are eluted, whereas the more apolar ones, which have a greater affinity for the organic eluent are eluted later. The main components of a modern HPLC are (Figure 12):
- containers for solvents with degassing system.
- pumps.
- system for the sample introduction (sampling loop).
- column with different dimensions and characteristics depending on the type of analyses to be performed, the system used, the type of detector and the amount of sample.
- detector, the kind of detector that is used depends by the nature of the sample.

Usually, the detectors used for liquid chromatography are based on the measure of the absorption of ultraviolet or visible light by the sample. For instance, detection of proteins is conducted at 220-224 nm. On the other hand, a particularly sensitive and versatile detector is represented by a mass spectrometer with electrospray ionization (ESI), which today is widely used in proteomic studies.

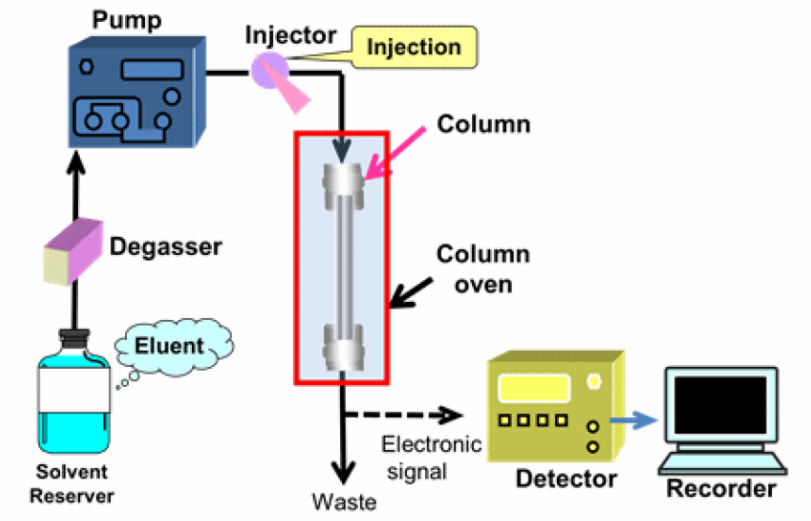

Figure 12. Schematic representation of an HPLC system

2.1.8. Mass spectrometry

Mass spectrometry is an analytical technique based on the ionized molecules production, the subsequent separation based on their different mass/charge ratio (m/z) and detection of the ions produced. The results are shown in a graph of relative abundance versus m/z ratio.

The principal mass spectrometer components are (Figure 13):

- system for the introduction of the sample.
- source, where the ionization of the sample occurs.
- analyser, which performs a separation of the ions produced in the source according to their m/z ratio.
- detector, where the separated ions are detected.
- vacuum system, whose task is to keep the various parts of the instrument under vacuum, the presence of which (the pressure is around 10^{-6}-10^{-8}Torr) is needed primarily to avoid the collision of the ions produced with the atmospheric gases.

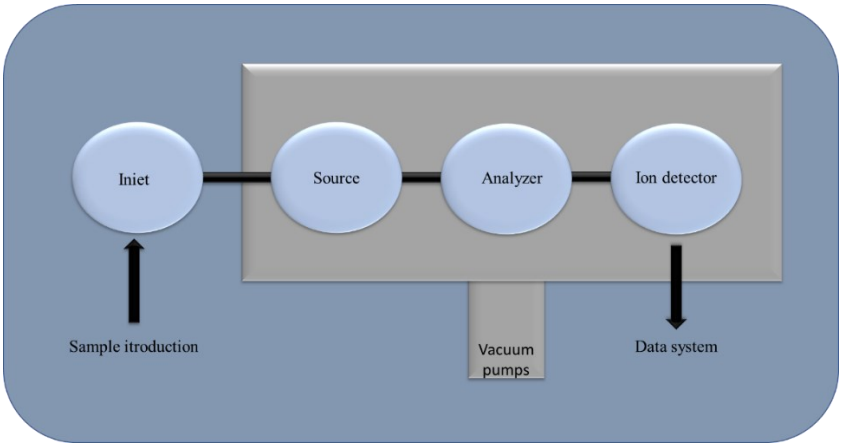

Figure 13. Block diagram of a mass spectrometer

Electron impact (EI) and chemical ionization (CI) were the first sources for samples ionization which are constituted by low molecular weight species that are easy to transfer in the gas phase.

Only thanks to develop of MALDI (Matrix-Assisted Laser Desorption/Ionization) and ESI (Electrospray Ionization), mass spectrometry was permitted the study and characterisation of biomolecules.

Electrospray ionization (ESI) is a soft ionization technique that does not produce sample fragmentation. This ionization technique is the ideal interface for the online coupling of a chromatographic system (RP-HPLC/ESI MS) and a mass spectrometer. It assumed an important role in the field of mass spectrometry for the ability to bring into gas phase and ionize macromolecules of biological origin. Electrospray mass spectrometry (ESI-MS) allows to obtain, from a solution of analyte introduced into the source by direct infusion or coming from a chromatographic column, single-charged ions and multiple charged ions which are thus sent to the analyser and to the detection system.

By using a capillary tube of silica, the protein solution is introduced into the source. Inside the ionization chamber, a spray is produced between the metallic tip of the needle and a counter electrode, where it is present a strong electric field (3-5 kV) that disperses the solution emerging from the needle into an aerosol of droplets with a high charge concentration. The desolvation of the droplets of the spray is obtained by using a stream of nitrogen suitably heated or just the high temperature of the capillary tube. The generally used solvent is water mixed with an organic solvent (acetonitrile, methanol, or propanol) and small amounts of weak acid (trifluoroacetic acid, acetic or formic acid) or a weak base (ammonia solution) to facilitate the ionization of the sample and the formation, respectively, of positive or negative ions. The mechanism through which the ions are formed starting from the charged drops of sample has not yet been completely clarified; several models have been proposed, including a qualitative model compatible with the mechanisms proposed by Smith, Fenn and Röllgen.[102,103] According to this model, in a first moment the formation of micro-droplets whose dimensions are related to their surface tension is observed; the hot gas stream causes the desolvation of these micro-droplets, tending to bring together the charged molecules. When the Coulomb repulsion force equals the droplet surface tension (Rayleigh limit), they explode producing other smaller droplets (nano-droplets)[104] which are subjected to further desolvations (Figure 14).

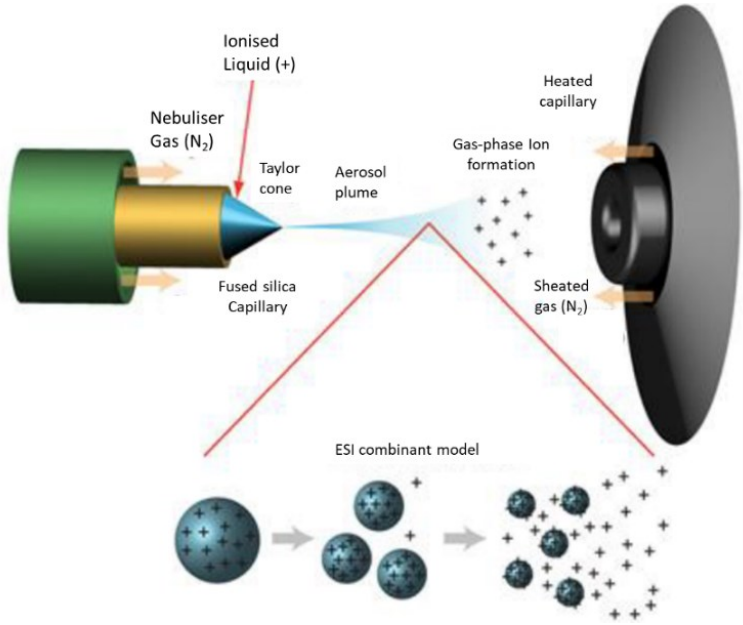

Figure 14. ESI source and model of ions formation

The pre-chamber is located at a pressure of 10^{-1}-10^{-2} Torr, only a part of the ions arrives to this part of the instrument. Subsequently, the ion beam is focused, through a series of electrostatic lenses (skimmers), and reaches the analyser (10^{-6} - 10^{-7} Torr), where separation takes place based on the m/z ratio value. The formation of multiple charged ions allows to display ions with high masses even working with analysers that have limited mass range and, therefore, makes this ionization method an excellent tool for the analysis of peptides and proteins. A typical ESI spectrum of positive ions of a protein consists of a set of peaks, each of which is generated from the analyte that has linked a specific number of protons. The proteins are usually analysed as positive ions because a series of multi-charged protein ions generated in the source is mainly related to the protonation of basic sites of molecules. In general, in a protein, the number of basic amino acid residues determines the maximum number of protons that the

molecule can take. The ESI spectrum of small molecules shows a precise correlation between the number of basic sites which are present in the structure and multi-charged ions. When the molecule size increases, this correlation is not so rigorous because some of the basic sites will be located inside the protein itself according to a particular conformation and will be protonable with difficulty. The capacity to protonate a protein of high molecular weight is closely related to the conformation that the protein assumes in solution under the experimental conditions (pH, temperature, presence of denaturing agents). ESI mass spectrometry constitutes a particularly powerful and versatile detector for high performance liquid chromatography (HPLC). Tandem mass spectrometry is employed in order to select an ion with a given m/z ratio ("precursor" ion) and subsequently to fragment it; fragmentation leads to the formation of lower mass ions ("fragment" ions), which are analysed in a second stage of analysis of mass.[105] The characteristic fragmentation peaks in the MS/MS spectra allow to obtain important information on the molecular structure of the precursor ion. In the case of peptides, the fragment ions are generated by cleavage of the peptide bond with retention of the positive charge at the N-terminal (b series) or in the C-terminal part (y series) along the main chain (Figure 15) and allow to go back to the amino acid sequence of the precursor peptide.

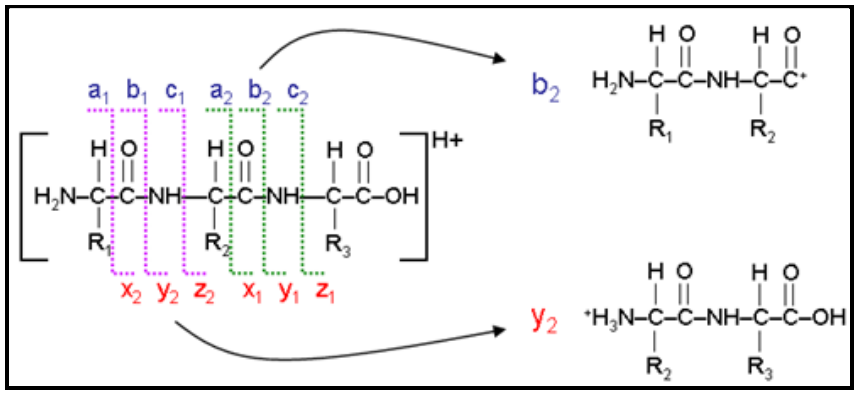

Figure 15. Typical peptide fragmentation in mass spectrometry analysis

The ion source can be interfaced with different mass analysers. The most used are quadrupole (Q), ion trap (IT), time-of-flight (ToF) and Orbitrap. The characteristics of these mass analysers are different both in principles of operation and performance. Orbitrap (Figure 16) is a new mass analyser constituted by an inner electrode (central) and external electrode, axially symmetrical, which create a combined square logarithmic electrostatic potential.

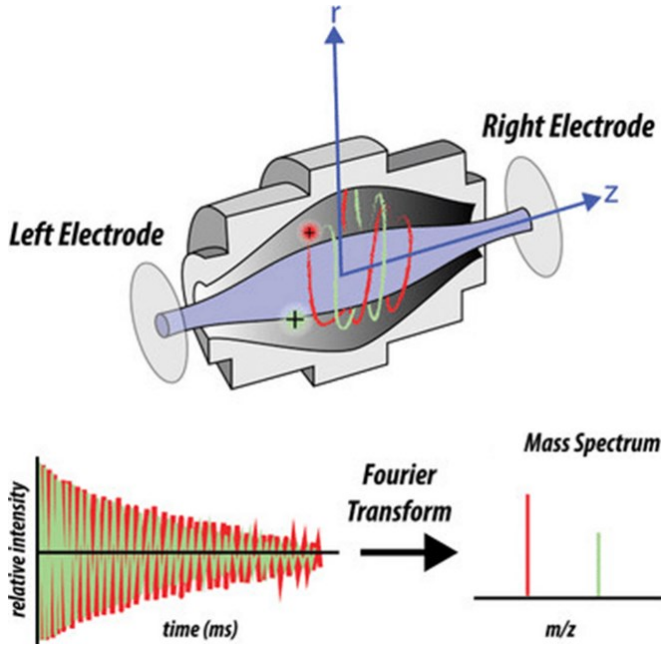

Figure 16. Schematic representation of Orbitrap analyser

The ions rotate around at central electrode and oscillate with harmonic motion along its axis (z direction) with a frequency characteristic of their m/z values. As mentioned, within this analyser, the axial symmetric electrodes create a square logarithmic **U** (electrostatic potential), which can be calculated through the equation:

$$U(r,z) = \frac{k}{2}\left(z^2 - \frac{r^2}{2}\right) + \frac{k}{2}(Rm)^2 \ln\left(\frac{r}{Rm}\right) + C$$

where **r** and **z** are the cyclic coordinates, **C** is a constant, **k** is the field curvature and **Rm** is the characteristic radius. In this U field, a rotational motion around the electrode and an oscillatory motion along the axes create stable trajectories of the ions, which result in a complex spiral. The equations that describe this motion for this mass analyser are very complex. From these equations it follows that the mass and the charge are correlated with the frequency of axial oscillations, expressed in radiant/second:

$$\omega = \sqrt{\left(\frac{q}{m}\right)k}$$

ω is completely independent of the energy and position of the ions, and thus can be used for analysis of mass (in fact in the expression appears the ratio q/m). All ions have then a harmonic oscillatory motion of the same amplitude but of different ω frequency. These frequencies are measured in a non-destructive way by a differential amplifier, which acquires the signals of the current image in the time domain. For each ion is produced a wave function; therefore, a mixture of ions gives rise to overlapped signals that can be converted to a mass spectrum thanks to Fourier transform.

Orbitrap Fusion Tribrid Mass Spectrometer (Figure 17) combines the best of quadrupole, linear ion trap and Orbitrap mass analysis in a new instrument. The resolution of this instrument is up to 450.000 FWHM. Moreover, the precursor selection using a quadrupole mass filter allows the ion trap and Orbitrap mass analyser to operate in parallel for excellent sensitivity and selectivity. Also, multiple dissociation techniques (CID, HCD and ETD) are possible.

Collision Induced Dissociation (CID) in the most commonly method of fragmentation in proteomics.[106] By using anelastic collision, selected precursor ions are collided with an inert gas. CID fragmentation occurs at the peptide bond between the carboxyl group and amino group. The produced fragments are y-ions and b-ions.[107] High-energy Collision Dissociation (HCD) is a fragmentation method which produces the same y/b-ions as CID. It can be performed only in instrument with HCD fragmentation cell and uses higher energy than CID. The theory of precursor ion fragmentation in Electron-transfer dissociation (ETD) is still debated, but it is known that ETD produces fragments of c/z-type, given complementary information about peptide sequence.

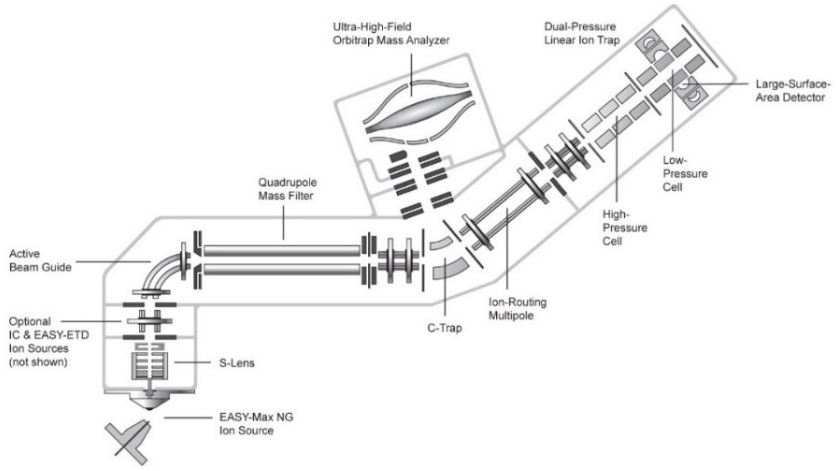

Figure 17. Representation of the Orbitrap® Fusion Mass Spectrometer instrument

2.1.9. Bioinformatic research

Adequate support of software to analyse the collected data is fundamental in proteomic analysis. Today, there are a variety of algorithms for the interpretation of peptide fragmentation data. LC-MS/MS data in this work were processed using PEAKS X (Bioinformatics Solutions Inc.) software. PEAKS X uses an algorithm to compute the best peptide sequences (de novo Peptide sequencing approach) whose fragment ions can best interpret the peaks in the MS/MS spectrum. Then, PEAKS combines de novo sequencing results with those of a database search to identify peptides and proteins. Particularly, de novo peptide sequences are aligned with protein database entries to provide additional information about PMTs, mutations, homologous peptides, and novel peptides. [108]

2.1.10. Label free

Label-free quantification is included in the PEAKS X module. It is used in the study of large-scale proteomics to obtain a fast protein profiling. This quantification method is based on the detection of peptide features (mass, retention time and signal intensity) in multi-

ple samples. For each sample is obtained a feature detection and then by using the EM (expectation-maximization) algorithm, these features can be overlapped. The features of the same peptide from different samples are aligned together using a high performance retention time alignment algorithm.[109]Mass spectrometry plays an important role in proteomic analysis. The new techniques, developed in recent years, gel-free based "shotgun" proteomic, such as Multidimensional Protein Identification (MudPIT) allow to study the protein production in complex biological system.[110] Proteomic studies can be performed to obtain both absolute (using internal standards) or relative quantification by different techniques including label-based and label-free approaches. In label-based approach a stable isotope is used to label the sample by biosynthetic or chemical reactions.[111] Labelling strategies are often preferred because they are considered more accurate in quantitating protein abundances. However, this technique requires expensive isotope labels, specific software and expertise to analyse data.[112] Moreover, most of the label-based methods require more steps in sample preparation and higher sample concentration, are more expensive and can only be performed for a limited number of samples.[113] MS-based label-free quantitative proteomics avoids the use of isotopes to label the samples under investigation and this approach can be used in "shotgun" analysis (analysis of the whole proteome) or in targeted analysis (analysis of specific proteins) and it can be applied when labelling is not possible.[114] There is a correlation between protein abundance and peaks areas[115] or number of MS/MS spectra.[116] Today, label-free methods are divided in two groups: (i) measurement of the intensity of the ion precursor signal or area under the curve (AUC) and (ii) spectral counting, which is

based on counting of the number of peptides assigned to a protein in an MS/MS experiment. Regardless of which label-free quantitative proteomics method is used, the analysis includes the following fundamental steps:

- sample preparation including extraction, reduction, alkylation, and digestion.
- sample separation using liquid chromatography and ESI-MS/MS.
- data analysis, including protein identification, quantification, and statistical analysis.

After the acquisition of MS/MS spectra, the raw data need to be processed by a software. Label-free proteomics software workflows typically consist of multiple steps: peptide peak picking, peptide identification, feature finding, matching of the features with identified peptide, alignment of the features in different samples. Protein quantifications is finally obtained from quantified peptides.[117]

2.2. Aims of the work (Section 1)

In this first section, proteomics techniques are used in ophthalmic field to obtain and compare protein profiles from lacrimal fluid of untreated eyes, placebo and postbiotic-based medical device treated eyes. Lacrimal samples have been collected from rabbits' eyes without ocular diseases. Determination and comparison of the protein profiles are directed to evaluate the effects of the postbiotic-based medical device upon lacrimal fluid proteome. In addition to monitor the composition and reproducibility of the batch-to-batch preparation of the postbiotic product, rapid methods for quantitative characterization of major components are desirable. In this work, a protocol designed to perform a rapid quantitative analysis of principal components using an integrated analytical method, was developed and used to characterise the postbiotic derived from *Lactobacillus paracasei* fermentation.

The aims of this first section are: 1A) Proteomic analysis; 1B) Postbiotic characterisation

Keywords: Postbiotic, Carbohydrates assay, Lipids assay, Proteins quantification, Inorganic salts quantification, Colorimetric assay, Incineration, *Lactobacillus paracasei,* Proteomic profile, Tear proteins, Rabbit tears.

2.3. Materials and Methods: Proteomic analysis (1A)

All chemicals were of the highest purity commercially available and were used without further purification. Methanol, Acetonitrile and Hydrochloric Acid (HCl) were purchased from Carlo Erba (Milan, Italy). Formic Acid, Ammonium Acetate, Ammonium Bicarbonate, Dithiothreitol (DTT) and Iodoacetamide (IAA) were obtained from Aldrich (St. Louis, Missouri, USA). Modified Porcine Trypsin was purchased from Promega (Madison, WI, USA). Water and Acetonitrile (OPTIMA® LC/MS grade) for LC/MS analyses were purchased from Fisher Scientific (Milan, Italy).

Tolerability study was conducted by SIFI S.p.A. (Società Industria Farmaceutica Italiana, ophthalmic pharmaceutical company). It consists in a 28 days' treatment of 10 Specific Pathogen-Free (SPF) rabbits, New Zealand White (NZW). Each right eye of the rabbits was treated with 50 µl/2.5 h of topical medical device containing postbiotic as ingredient and each left eye of the rabbits were treated with a placebo (Tris-isosmotic, pH 7.4). After 28 days the 20 samples (10 from placebo treated eyes and 10 from postbiotic-based medical device treated eyes) were collected by NST method using a sterilized glass microcapillary. Each sample (2-5 µl) was transferred in a 0.5 ml Eppendorf using a nitrogen flux and diluted adding 50 µl of a solution of ammonium bicarbonate 50 mM, pH 8. Samples were stored at -80 °C until use.

Untreated rabbit lacrimal fluid samples were collected with NST method from 5 SPF rabbits NZW, using sterilised glass microcapillary. The 10 collected samples were approximately 1 µl and each of them was transferred in a 0.5 ml Eppendorf using N_2 flux, diluted with 50 µl

of ammonium bicarbonate 50 mM, pH 8, and stored at -80 °C until use.

All animals were treated according to the Directive 2010/63/UE European Convention for the Protection of Vertebrate Animals used for Experimental and Other Scientific Purposes.

2.3.1. In-solution digestion of proteins in rabbit tear samples

Placebo and postbiotic-based medical device treated rabbit samples were reduced adding 8.5 µl of solution constituted by 771 µg of DTT in 400 µl of ammonium bicarbonate 0.1 M, pH 8. The solutions were gently mixed for 3 h at 25 °C, then alkylated with 5.4 µl of a solution constituted by 5810 µg of IAA in 800 µl of ammonium bicarbonate 0.1 M (pH 8), and gently mixed in the dark for 1 h at 25 °C.

Enzymatic digestion was performed adding, to each sample, 64.5 µl of solution constituted by 10 µl of porcine trypsin (1 µg/10 µl of HCl 0.1 % solution in distilled water) diluted with 140 µl of ammonium bicarbonate 0.1 M (pH 8), the solutions were gently mixed overnight at 37 °C.

Untreated rabbit samples were reduced as mentioned before, but the volume of DTT solution used was 3 µl, 3.6 µl of IAA and 21 µl of trypsin solution.

All samples were then transferred in 1.5 ml Eppendorf tubes, dried under Speedvac RVC 2-25 (Martin Christ Drying Systems, Osterode am Harz, Germany), and the residues were solubilized in 30 µl of 5 % formic acid in LC-MS water (pH 2.6). Subsequently, due to the high Total Ion Current (TIC) registered during a preliminary injection at mass spectrometer, the samples coming from placebo (PL) and

postbiotic-based medical device (PB) treated eyes were diluted of 1:30 with 0.1% formic acid solution in LC-MS water (pH 2.6); samples coming from untreated eyes (NT) were diluted of 1:5 with 0.1% formic acid solution in LC-MS water (pH 2.6), and analysed by LC-MS/MS (Figure 18).

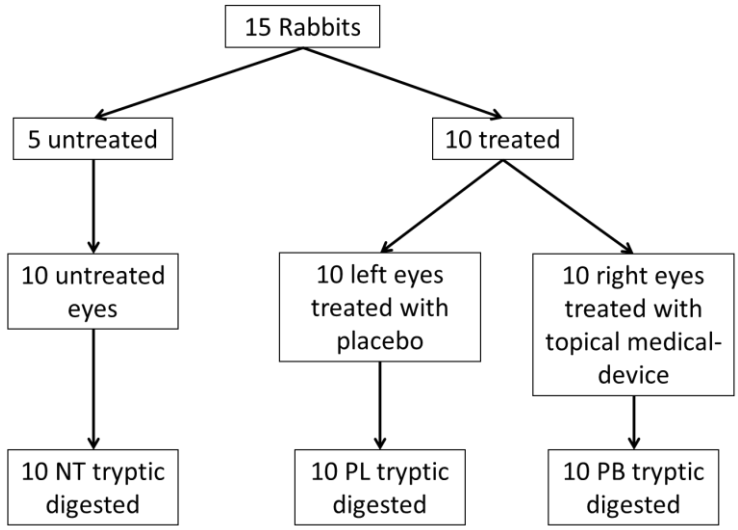

Figure 18. *Rabbits' tear samples treatment workflow*

2.3.2. LC–MS/MS analysis

Mass spectrometry data were acquired in triplicate by an Orbitrap Fusion Tribrid (Q-OT-qIT) mass spectrometer (Thermo Fisher Scientific, Bremen, Germany) equipped with a Thermo Fisher Scientific Dionex UltiMate 3000 RSLCnano system (Sunnyvale, California). 1 µl of each reconstituted sample was loaded onto an Acclaim ®Nano Trap C18 Column (100 µm i.d. x 2 cm, 5 µm particle size, 100 Å). After washing the trapping column with solvent A (LC-MS water + 0.1% formic acid in LC-MS water, pH 2.6) for 3 minutes at a flow rate of 7 µl/minute, the peptides were eluted from the trapping column onto a PepMap® RSLC C18 EASY-Spray column (75 µm i.d. x

50 cm, 3 m particle size, 100 Å). Peptides were separated by elution at a flow rate of 0.25 µl/minute at 40°C with a linear gradient of solvent B (Acetonitrile + 0.1% formic acid in LC-MS water, pH 2.6) in A, 5% for 3 minutes, followed by 5% to 20% in 32 minutes, 20% to 40% in 30 minutes, 40% to 60% in 20 minutes and 60% to 98% in 15 minutes. At the end it was finished by holding 98% B for 5 minutes, 98% to 5% in 1 minute, and re-equilibrating the column at 5% B for 20 minutes. The eluting peptide cations were converted to gas-phase ions by electrospray ionization using a source voltage of 1.75 kV and introduced into the mass spectrometer through a heated ion transfer tube (275°C). Survey scans of peptide precursors from m/z 200 to m/z 1600 were performed at 120 K resolution (m/z 200). Tandem MS was performed by isolation at 1.6 Th with the quadrupole, HCD fragmentation with normalized collision energy of 35 V, and rapid scan MS analysis in the ion trap. Only those precursors with charge states 2÷4 and an intensity above the thresh-old of $5 \cdot 10^3$ were sampled for MS. The dynamic exclusion duration was set to 60 seconds with a 10 ppm tolerance around the selected precursor and its isotopes. Monoisotopic precursor selection was turned on. The instrument was run in top speed mode with 3 seconds/cycle, meaning that the instrument would continuously perform MS^2 events until the list of non-excluded precursors diminishes to zero or 3 seconds, whichever is 25 shorter. MS/MS spectral quality was enhanced enabling the parallelizable time option (i.e., by using all parallelizable time during full scan detection for MS/MS precursor injection and detection). Mass spectrometer calibration was performed by using the Pierce® LTQ Velos ESI Positive Ion Calibration Solution (ThermoFisher Scientific, Bremen, Germany). MS data acquisition was carried out by

utilizing the Xcalibur v. 3.0.63 software (ThermoFisher Scientific, Bremen, Germany).

2.3.3. Protein identification

LC–MS/MS raw data were processed using PEAKS X de novo sequencing software (Bioinformatics Solutions Inc., Waterloo, Canada). Data were searched against a dedicated protein database of *Oryctolagus cuniculus* from UniProt and downloaded in SwissProt (13680 entries, released in May 2020). Database search was carried out using the following parameters: i) full tryptic peptides with a maximum of 3 missed cleavage sites; ii) cysteine carbamidomethylation as fixed modification; iii) oxidation of methionine, transformation of N-terminal glutamine and N-terminal glutamic acid residue in the pyroglutamic acid form as variable modifications. The precursor mass tolerance threshold was 10 ppm, and the maximum fragment mass error was set to 0.6 Da. Peptide spectral matches (PSM) were validated using a Target Decoy PSM Validator node based on q-values at a 0.1% FDR. A protein was considered identified if a minimum of two peptides were matched. Proteins containing the same set or sub-set of peptides and that could not be differentiated based on MS/MS analysis alone were grouped to satisfy the principles of parsimony (groups of parsimony).

The same procedure and parameters were also used to search data from postbiotic-based medical device treated eyes against a dedicated protein database of *Lactobacillus paracasei* from UNIPROT and downloaded in SwissProt (301 entries, released in February 2021). No proteins were identified by this database search.

Once the list of all identified proteins was obtained, a Wilcoxon rank sum test was used to assess the basis for further analysis, we first looked at the overall differences in protein identification frequencies between the three group. The Wilcoxon rank sum test is a non-parametric test used to make comparisons between two independent groups of non-normally distributed data. It was used to compare the NT group against PL then against PB group, and to compare PL against PB group. Therefore, the null hypothesis for all these three comparisons was that there is not statistical difference of identification frequency, the alternative hypothesis was that there is. Considering a confidence interval of 95%, if the p-value is greater than 0.05 there is no statistical difference of protein identification frequency; if the p-value is less than 0.05 there is a statistical difference of protein identification frequency. Relative increases were not used because different proteins had zero identifications into PL and NT group.

2.4. Results and Discussions: Proteomic analysis (1A)

To assess the reproducibility of the MS data, the tryptic mixture of the 30 samples were subjected to triplicate RP-nUHPLC/nESI-MS/MS analysis and database search. Triplicate analysis demonstrated that the data obtained are highly reproducible.

To compile the final list of proteins identified in each sample, only those proteins that were identified at least in two LC-MS/MS runs out of the three replicates, proteins with a sequence coverage >5 %; and identified with at least two peptides were considered.

The complete lists of the proteins identified in each sample is reported in the Supporting info (Chapter 5.1 from Table S 1 to S 30).

From PL samples were found in average 68.7±23.5 proteins, for PB were 89.4±17.2 and for NT 60.8±21.8, for a total of 152 different proteins identified (Figure 19).

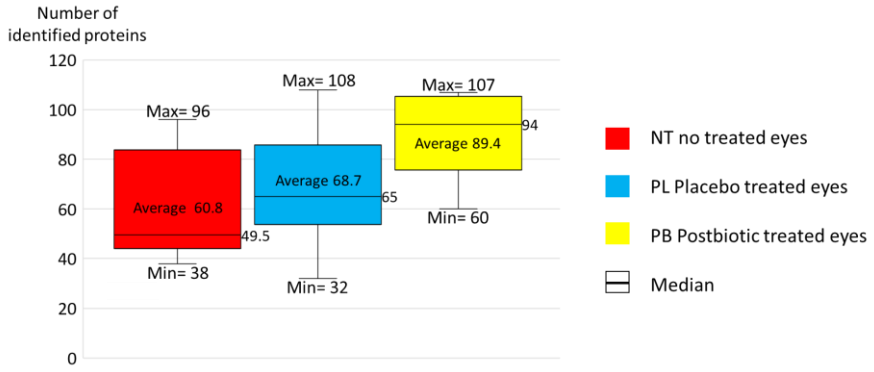

Figure 19. Box and whiskers plot of identified proteins. For each group is reported the maximum and the minimum number of identified proteins among the 10 samples, the average number of identified protein and the median value for each group is reported.

Wilcoxon rank sum test was used to find out which of the three group of samples have a significant statistical difference of protein identification frequency. The difference between PB and NT is significant, p-value= 0.0045; between PB and PL is significant, p-value= 0.035; between PL and NT is not significant, p-value= 0.5. This means that the use of the postbiotic-based medical device has some effects on changing the proteomic profile of rabbit's tears. Proteins with a score higher or equal to 5 (Table 3), obtained performing a comparison between the mean of PL and NT group against PB group are considered (Supporting info chapter 5.1 Table S 31). These proteins are the most correlated with the modification of the proteomic profile due to the administration of postbiotic-based medical device.

Table 3. *Oryctolagus cuniculus* proteins (score higher or equal to 5 in Wilcoxon rank sum test) involved in proteomic profile changing due to the administration of the postbiotic-based medical device. Information from UNIPROT.org

Accession number	Description	Molecular weight	Score
P58776	Tropomyosin beta chain (Tpm)	32.837 kDa	6.5
P15253	Calreticulin (CRT)	48.275 kDa	6
O19049	Heterogeneous nuclear ribonucleoprotein K (hnRNP K)	50.960 kDa	5
P14422	Phospholipase A2 membrane associated (PLA)	7.592 kDa	5
Q09YN4	F-actin-capping protein subunit alpha-2 (CAP)	32.951 kDa	5
Q28619	Na(+)/H(+) exchange regulatory cofactor NHE-RF1 (NHE-RF1)	38.562 kDa	5

The protein Heterogeneous Nuclear Ribonucleoprotein K (hnRNP K) plays an important role in the DNA (Deoxyribonucleic acid) damage response and in the induction of apoptosis, but not in cell cycle arrest.
A study conducted on optic axons of *Xenopus laevis* was focused on hnRNP K protein to understand the regeneration ability of this organism. The study demonstrated that hnRNP K is an essential component of a novel pathway that regulates the intrinsic response to injury leading to successful axon regeneration[118]. The role of hnRNP K as response to DNA damage was reported in various studies (e.g. Moumen A. et al.[119]; Eder S. et al.[120]). Its property to repair DNA damage and to influence the apoptosis cycle also implicates hnRNP K also in tumour growing and its higher concentration could be used as biomarker.[121, 122]

The protein Calreticulin (CRT) is a calcium-binding chaperone that promotes folding, oligomeric assembly and quality control in the endoplasmic reticulum (ER) and is involved in calcium homeostasis, binding of calcium, carbohydrates and unfolded proteins binding, protein folding and stabilisation.[123] CRT is associated with a wide variety of signalling processes, such as cardio genesis, adipocyte differentiation and the adaptability of cellular stress responses adaptability to hyperosmotic stress exposure.[124] Its correlation has also been demonstrat-

ed in wound healing, immune response against tumor[125] and apoptotic cells clearance.[126]

The protein Tropomyosin beta chain (Tpm) plays a central role, in association with the troponin complex, in the calcium regulation, identical protein binding, protein heterodimerization and homodimerization activity. Some studies showed that Tpm, a family of cytoskeleton proteins, are involved in the regulation and stabilization of actin microfilaments in lens epithelial cells[127, 128] and in wound healing[129] but on the other hand the high concentration of Tpm proteins seems to be involved in the onset of posterior capsular opacification (PCO)[130, 131]. Conversely, a low level of this family of protein appears to inhibit PCO[132] but increase the chance of cataract formation.[129]

The protein Phospholipase A2 (PLA) plays an important role in host antimicrobial defence, inflammatory response and tissue regeneration, contributes to the lipid remodelling of cellular membranes and the elimination of pathogen. The bactericidal activity against Gram-positive bacteria is due to the ability to hydrolyse the phospholipids of the bacterial membrane.[133]

The protein F-actin-capping protein subunit alpha (CAP) plays an important role in the growth of the actin filament. Delalle et al. demonstrated that mutations in the Drosophila orthologues of the alpha and beta subunits of the F-actin capping protein may be related to tissue degeneration. The first abnormality observed in mutant clones is an accumulation of actin, consistent with the known function of the α/β-heterodimer in capping actin filaments and arresting their growth[134]. Hopmann et al. have previously described disorganized actin filaments in bristles of cpb mutants.[135]

The protein Na(+)/H(+) exchange regulatory cofactor (NHE-RF1) is involved in the regulation of cytoskeletal actin and surface expression. Georgescu et al. report in their review the role of NHE-RF1 as a linker between membrane proteins and the cytoskeletal network.[136] Other studies describe NHE-RF1 as an important player in cancer progression depending on its cellular distribution. It can also be a tumour suppressor when is localised on the plasma membrane. [137, 138]

2.5. Conclusions: Proteomic analysis (1A)

The MS-based shotgun approach, employed here, allowed the qualitative characterisation of the proteomic profiles of untreated, placebo and postbiotic-based medical device treated rabbits' tears. As previously described, an average of 68.7±23.5 proteins were identified in PL samples, 89.4±17.2 in PB and 60.8±21.8 in NT, for a total of 152 different proteins identified.

Among these 152 proteins 6 were identified with significant frequency in PB samples.

All appear to have a key role in wound healing, especially hnRNP K which is involved in axon regeneration, CRT and PLA which are also involved in the immune response against tumour and apoptotic cells clearance and Tpm in avoiding the formation of cataract but, on the other hand it also seems play a role in PCO triggering.

In summary, the postbiotic-based medical device administration appears to have no short negative effects on ocular health. The rabbits subjected to the tolerability study did not show any discomfort, redness or itching of their eyes. Moreover, during tear sampling the eyes ap-

peared healthy on visual inspection and no differences were found in frequency rate protein identification between eyes treated with PL and those untreated. In addition, during the proteomic study pro-inflammatory cytokines and chemokines were not found among the three groups of samples.

The results seems to indicate that the administration of postbiotic-based medical device on ocular surface could be beneficial for wound healing and maintenance of calcium homeostasis. Other effects such as inhibition of cataract formation, immune response against tumour and clearance of apoptotic cells may occur. However, further in-depth studies and more data will be required to fully clarify the effect of the postbiotic-based medical device administration on ocular surface.

2.6. Materials and Methods: Postbiotic characterization (1B)

All chemicals were of the highest purity commercially available and were used without further purification. Methanol was purchased from Carlo Erba (Milan, Italy). Formic acid, Methyl tert-butyl ether (MTBE), Sunflower oil and Vanillin were obtained from Aldrich (Milan, Italy). Acetone, Chloroform, D-Glucose, Sulfuric acid 98% and Dimethyl sulfoxide (DMSO) were purchased from Merck (Milan, Italy). Phenol was purchased from Euroclone (Milan, Italy). Qubit Protein Assay kit with the Qubit 1.0 Fluorometer from ThermoFisher Scientific (Milan, Italy). The postbiotic product is a lactate ferment from a single strain culture of Lactobacillus Paracasei strain CNCM I-5220 from Postbiotica (Milan, Italy).

2.6.1. Quantitative determination of proteins

The determination of proteins was carried out with the QuBit fluorometer. This instrument can detect all kind of proteins without interferences from amino acids, DTT and DNA.

The sample solution was prepared by solubilizing 20.7 mg of postbiotic in 50 µl of 5% formic acid in distilled water (pH 2.6) and stored at 5°C until use. The amount of proteins was determined using the Qubit protein assay kit. The calibration standards were prepared freshly each time, according to the manufacturer's recommendations.

2.6.2. Quantitative determination of carbohydrates

The determination of sugars was carried out with the Molisch assay[139]. This method can detect almost all carbohydrates and derivatives, like pentoses, hexoses and their derivatives (di- and poly- sac-

charides). Instead, alditols, like mannitol, are not detected. With this test glycosidic bonds are hydrolysed by sulfuric acid, thus only monosaccharides are obtained. Monosaccharides change into furfural (for pentoses) and into hydroxymethylfurfural (for hexoses). These compounds react with phenol and the solution turns to yellow.

Stock solution was prepared by solubilising 10.6 mg of D-Glucose in distilled water to a final volume of 100 ml, obtaining a concentration of 106 µg/ml.

Sample solution was prepared solubilising 201.4 mg of postbiotic in distilled water to a final volume of 50 ml.

Five standard solutions (STD) were prepared by adding distilled water to 0.4, 0.5, 0.6, 0.7 and 0.8 ml of stock solution to a final volume of 2 ml , into glass test tubes. The concentrations of the five standard solutions were 21.2, 26.5, 31.8, 37.1 and 42.4 µg/ml respectively.

Quality control sample (CTRL) whit a concentration of 24.4 µg/ml was prepared by adding distilled water to 0.46 ml of stock solution to a final volume of 2 ml into a glass test tube.

The blank consist in 2 ml of distilled water in a glass test tube.

The sample was prepared by adding 1 ml of distilled water to 1 ml of sample solution. All solutions were stored at 5°C until use.

53 µl of phenol 75% in water were added to all the test tubes. The mixtures were vortexed for 1 minute. Then 5 ml of sulfuric acid 98% were added. The solutions were vortexed for 1 minute, kept for 20 minutes at room temperature and vortexed again. The absorbance

(Abs) at 490 nm was read in triplicate against the blank by an UV-Vis spectrophotometer (Perkin Elmer Instruments, Milan, Italy)[139]

Calibration: for each STD, which were prepared as reported before, was read the Abs in triplicate against the blank, in the UV-Vis Spectrophotometer at 490 nm (Table 4), using the obtained average Abs the calibration curve was built (Figure 20).

Table 4. Standard Abs for quantitative carbohydrates determination

Standard	µg/ml	Abs1	Abs2	Abs3	Avg.Abs	Dev. Std
1	21.2	0.341	0.342	0.342	0.342	0.001
2	26.5	0.473	0.473	0.473	0.473	0
3	31.8	0.606	0.607	0.607	0.607	0.001
4	37.1	0.656	0.657	0.657	0.657	0.001
5	42.4	0.734	0.735	0.735	0.735	0.001

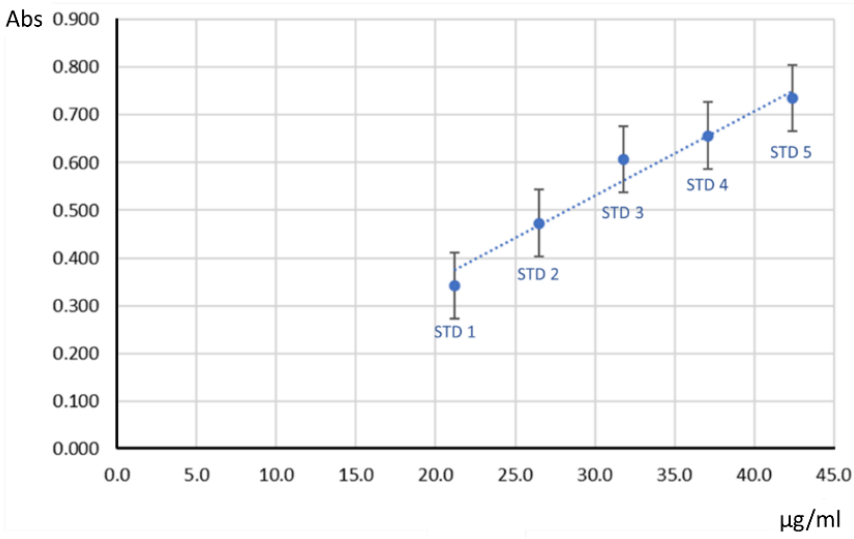

Figure 20. Relation between absorbance (Abs) and concentration of carbohydrates (µg/ml) at 490 nm. The obtained calibration curve for quantitative carbohydrates determination, using STD concentration, have a linear trend. The equation is $y = 0.0177x$ and the R^2 value is 0.998.

2.6.3. Quantitative determination of lipids

The determination of lipids was carried out by the Vanillin-Phosphoric Acid assay[140]. This method can detect all kind of lipids (neutral and polar).

Vanillin-Phosphoric acid solution was prepared solubilising 123.6 mg of Vanillin in 20 ml of distilled water and adding Phosphoric acid 85% to a final volume of 100 ml (pH 2.3).

Polar and neutral lipids extraction was obtained by adding 1.5 ml of methanol to 257 mg of postbiotic. The suspension mixture was vortexed for 1 minute, then 5 ml of MTBE were added and the suspension mixture was vortexed again for 1 minute and shaken for 45 minutes. Subsequently, 2 ml of distilled water were added, the solution was vortexed for 1 minute and allowed to rest for 10 minutes. Finally, the organic phase was collected by pipetting in a 15 ml Falcon tube and dried under nitrogen flux.[141] Sample solution was obtained reconstituting the dried organic phase with 2 ml of Chloroform/Methanol solution (1:1).

Stock solution was prepared mixing 51.4 mg of Sunflower seed oil with chloroform to a final volume of 100 ml, obtaining a concentration of 514 µg/ml.
All these solutions can be stored at 5°C until use.

Five standard samples were prepared by drying into a water bath at 60°C, 60, 120, 180, 240 and 300 µl of Sunflower seed oil stock solution in glass test tubes. The amount of sample in each test tube was 30.84, 61.68, 92.52, 123.36 and 154.20 µg, respectively.

CTRL whit 107.94 µg of Sunflower seed oil was prepared by drying 210 µl of stock solution.

The blank consist of an empty glass test tube.

The sample was prepared collecting 0.5 ml of sample solution and it was dried.

All glass test tubes were dried at 60°C into a water bath, then 100 µl of water were added. 2 ml of Sulfuric acid 98% were added to each tube, then they were vortexed for 1 minute and heated in water bath (at 90°C) for 10 minutes. Afterwards they were cooled in ice bath for 5 minutes. Subsequently 5 ml of Vanillin-Phosphoric acid solution were added, and the solutions were incubated at 37°C for 15 minutes. Exactly after 15 minutes, for each tube the Abs was read at 530 nm in the UV-Vis Spectrophotometer.[140]

Calibration: for each STD, which were prepared as reported before, was read the Abs in triplicate against the blank, in the UV-Vis Spectrophotometer at 530 nm, (Table 5). Using the obtained average Abs the calibration curve was built (Figure 21).

Table 5. Standard Abs for quantitative lipids determination

Standard	µg	Abs1	Abs2	Abs3	Avg.Abs	Dev. Std
1	30.84	0.119	0.119	0.119	0.119	0
2	61.68	0.205	0.205	0.205	0.205	0
3	92.52	0.33	0.331	0.331	0.331	0.001
4	123.36	0.394	0.395	0.395	0.395	0.001
5	154.2	0.498	0.499	0.5	0.499	0.001

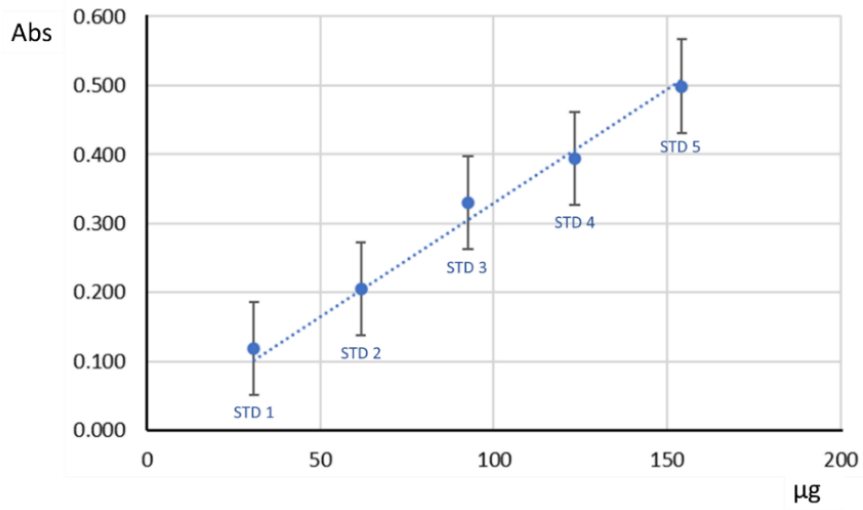

Figure 21. Relation between absorbance (Abs) and amount of lipids (µg) at 530 nm. The obtained calibration curve for lipids quantitative determination, using STD concentration, have a linear trend. The equation is y = 0.0033x and the R^2 value is 0.998.

2.6.4. Quantitative determination of inorganic salts

The determination of inorganic salts is conducted with incineration in the microwave muffle PYRO from Milestone (Bergamo, Italy), in this way is possible to remove water, crystallization water, and organic compounds from the sample.

A porcelain crucible was placed in the muffle microwave oven for 1 hour at 600°C, then was cooled to room temperature in a desiccator and weighted to determine the tare.

1 g of postbiotic was placed into the crucible and was incinerated in the muffle for 1 hour at 600°C, then was cooled to room temperature in a desiccator for 30 minutes. Incineration and cooling steps were repeated 3 times. At this point the crucible was weighted, from this value the tare was subtracted to obtain the amount of inorganic salts in 1 g of postbiotic. The experiment was repeated in triplicate.

2.7. Results and Discussions: Postbiotic characterisation (1B)

2.7.1. Quantitative determination of proteins

To determine the amount of proteins by the Qubit fluorometer assay, triplicate measurements were performed using 1 µl of sample. The results (Table 6) indicate an average amount of 28.07 µg of proteins. Considering that the amount of postbiotic contained in the sample solution was 20.7 mg, the percentage of proteins is 0.14%.

Table 6. Proteins quantitative determination by Qubit

Sample	Concentration (µg/µl)	Volume (µl)	µg
1	0.560	50	28
2	0.563	50	28.15
3	0.561	50	28.05
Average amount			28.07
Dev.Std			0.08

2.7.2. Quantitative determination of carbohydrates

Once the calibration curve was ready (chapter 2.6.2.) the Abs of the CTRL (prepared as reported in chapter 2.6.2) was read in triplicate (method in chapter 2.6.2), to monitor the validity of the method (Table 7 and Figure 22). The CTRL concentration was 24.4 µg/ml (chapter 2.6.2.), the concentration found was 23.8 µg/ml with an approximation error (E%) of -2.5%

Table 7. Abs of CTRL for quantitative carbohydrates determination

	µg/ml	Abs1	Abs2	Abs3	Avg.Abs	Dev. Std
CTRL	24.4	0.420	0.425	0.418	0.421	0.004

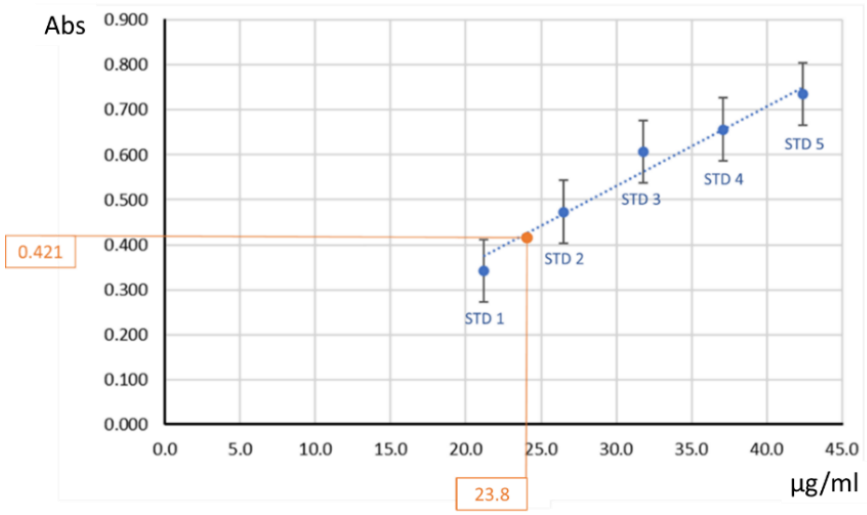

Figure 22. Relation between absorbance (Abs) and concentration of carbohydrates (µg/ml) at 490 nm. Average Abs of CTRL into carbohydrates quantitative determination calibration curve, and concentration are indicated in orange lines and boxes.

To determine the amount of sugars, 1 ml of the 50 ml of the sample solution (prepared as reported in chapter 2.6.2) was diluted 1:2 adding distilled water, it was prepared for the assay as reported before (Chapter 2.6.2) and the Abs at 490 nm was read in triplicate (Table 8) and its position into the calibration curve was found (Figure 23). The results indicated a concentration of 24.5 µg/µl, corresponding to the presence of a total of 2.45 mg of sugars, in the sample solution containing 201.4 mg of postbiotic. Thus, a percentage of 1.22% of sugars was determined.

Table 8. Abs of sample for quantitative carbohydrates determination

	Abs1	Abs2	Abs3	Avg.Abs	Dev. Std
Sample	0.433	0.432	0.433	0.433	0.001

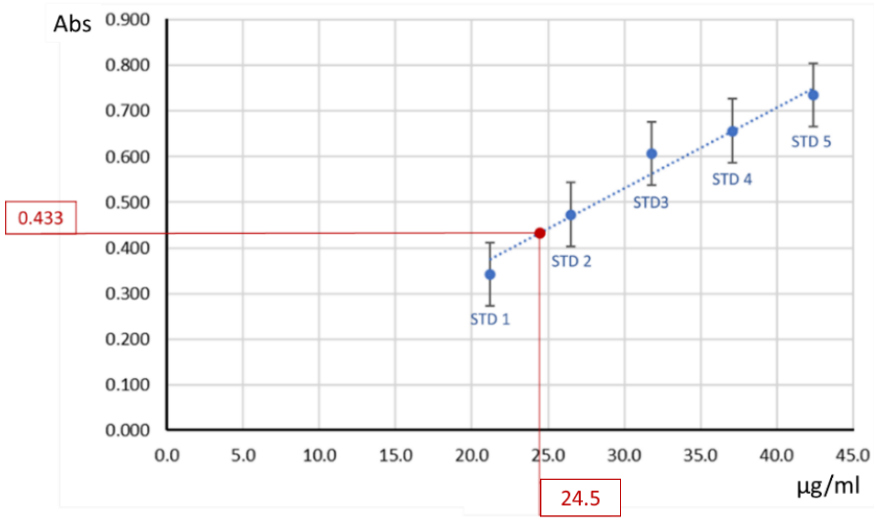

Figure 23. Relation between absorbance (Abs) and concentration of carbohydrates (µg/ml) at 490 nm. Average Abs of sample into carbohydrates calibration curve and concentration are indicated in red lines and boxes.

According to the producer, the total percentage of carbohydrates in the postbiotic preparation is 90%, because it is necessary to add a large amount of mannitol to obtain a solid residue by freeze-drying. Therefore, the percentage of mannitol, which, being an alditol is insensitive to the Molish assay, can be calculated by difference as 88.78%

2.7.3. Quantitative determination of lipids

Once the calibration curve was ready (chapter 2.6.3) the Abs of the CTRL (prepared as reported in chapter 2.6.3) was read in triplicate, to monitor the validity of the method (Table 9 and Figure 24). The CTRL concentration was 107.94 µg/ml (chapter 2.6.3), the concentration found was 114.55 µg/ml with an E% of 5.77%.

Table 9. Abs of CTRL for quantitative lipids determination

	µg	Abs1	Abs2	Abs3	Avg.Abs	Dev.Std
CTRL	107.94	0.377	0.378	0.378	0.378	0.001

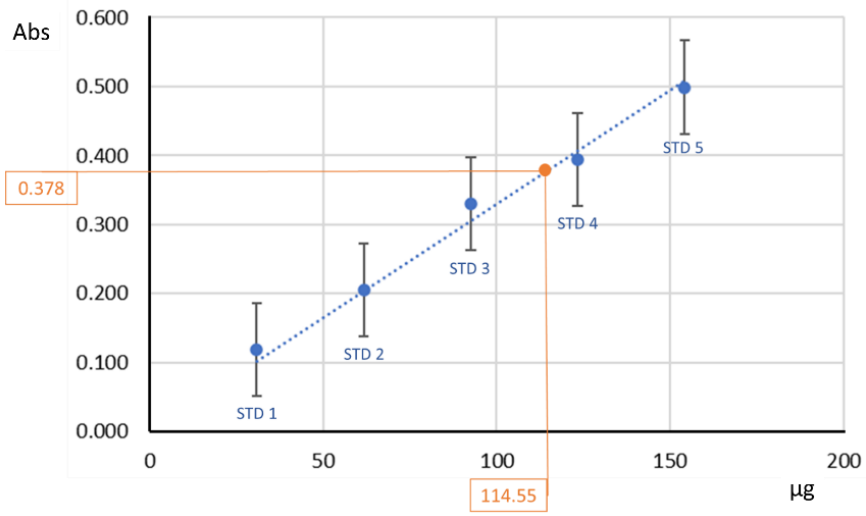

Figure 24. Relation between absorbance (Abs) and amount of lipids (µg) at 530 nm. Average Abs of CTRL into lipids calibration curve, and concentration are indicated in orange lines and boxes. The E% for lipids quantification is larger than the E% for carbohydrates test, because the Abs readings for lipids determination is time sensitive. The amount of time between the Vanillin-Phosphoric acid addition and the Abs measurement must be the same for each test tube, indeed we waited exactly 15 minutes.

To determine the amount of lipids, 0.5 ml of the 2 ml of the sample solution (prepared as reported in chapter 2.6.3), were dried and processed as described before (Chapter 2.6.3). The Abs at 530 nm was read in triplicate (Table 10, Figure 25). The original volume of the sample was 2 ml, and 0.5 ml of it were collected by pipetting in another glass test tube and dried, therefore the total amount of lipids in the sample was 221 µg. Considering that the amount of postbiotic contained in the sample solution was 257 mg, the percentage of lipids is 0.09%.

Table 10. Abs of sample for quantitative lipids determination

	Abs1	Abs2	Abs3	Avg.Abs	Dev.Std
Sample	0.182	0.182	0.183	0.182	0.001

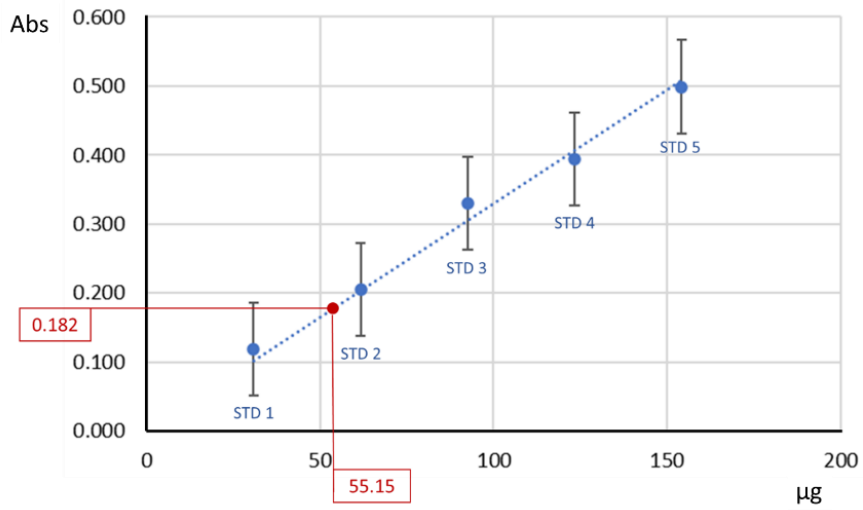

Figure 25. Relation between absorbance (Abs) and amount of lipids (µg) at 530 nm. Average Abs of sample into lipids calibration curve, and concentration are indicated in red lines and boxes.

2.7.4. Quantitative determination of inorganic salts

Inorganic salts quantification was conducted as reported before (chapter 2.6.4), the incineration process was repeated three times in triplicate, the results of the last incineration for each replicate are reported (Table 11). The determined average percentage of inorganic salts into postbiotic was 13.13%.

Table 11. Inorganic salts determination replicates

	Tare (g)	Postbiotic wheight	Gross weight (g)	Inorganic salts (g)	%
1° crucible	21.1515	1.0087	21.2815	0.1300	12.89%
2° crucible	20.8633	1.0202	20.9972	0.1339	13.12%
3° crucible	21.4151	1.0522	21.5558	0.1407	13.37%
Average Inorganic salts percentage					13.13%
Dev.Std					0.24

2.8. Conclusions: Postbiotic characterisation (1B)

In this section (1B) using an integrated analytical method, was developed a protocol designed to perform a rapid and simple quantitative analysis of the main classes of compounds included into a complex matrix, which is a postbiotic obtained by *Lactobacillus paracasei* fermentation. The used assays offer significant advantages in terms of sensitivity and selectivity, simple sample preparation and fast analysis, proved to be linear, accurate and precise. The procedure can be useful to monitor the composition and reproducibility of batch-to-batch preparations. Summarizing the results, the composition sugars, mannitol, proteins, carbohydrates, lipids and inorganic salts of *Lactobacillus paracasei* postbiotic was determined as shown (Figure 26).

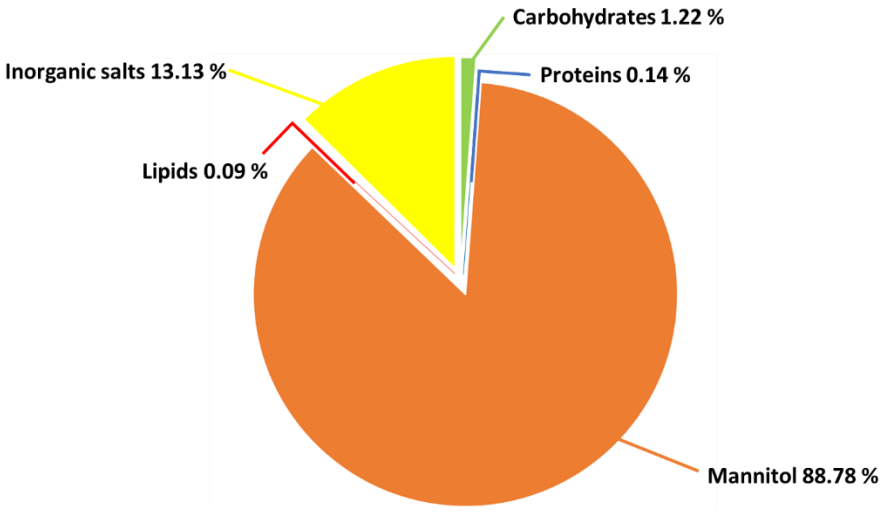

Figure 26. Pie-chart of *Lactobacillus paracasei* postbiotic main components

2.9. Future prospects (Section1)

Concerning the proteomic analysis on rabbit tears samples, extensive studies are needed to improve the statistical significance and more samples are necessary to conduct qualitative analysis. Furthermore, it could be useful to conduct in vitro studies to monitor which cells and which ocular compartments are affected by the postbiotic based tear drops.

Regarding the quantitative estimation of postbiotic components, reported results are a good starting point to perform in deep characterisation. For instance, chromatographic techniques can be used to compare postbiotic with different standards to find out what type of carbohydrates are present, lipidomic and proteomic analysis can be performed for lipidic and protein composition.

3. Development of an MS-based method for determining serum conversion and epitope mapping (Section 2)

3.1. Introduction

3.1.1. Antibody-Antigen complexes

The interaction between an antibody and an antigen at one antigenic site (epitope) generates immune complexes with strongly bound (high affinity) components, i.e. the antibody and the antigen. Each antigenic site (epitope) interacts with the antigen-binding region (paratope), formed by the variable domains of the antibody, trough non-covalent binding. The specificity of this non-covalent interaction is controlled by three factors: antibody-epitope affinity, their valence, and the shape of the interaction sites.

The definition of antigen includes each molecule that can be bound by a specific antibody. These molecules can be proteins, peptides, polysaccharides, lipids, nucleic acids, pollen grain and so on. The immune response is triggered by the presence of antigens since they are recognised by the antigen receptor, antibodies, and/or T-cell receptors. Usually, an antibody can bind just one specific antigen, some of them can cross react and bind more than one. The epitope is the portion of the antigen which is actually recognised and bound by an antibody. Non-self proteins are also called exogenous antigens, into this classification are considered such antigens which have entered the body from outside or are found in the circulation because of viral or bacterial infections. Often the immune response to exogenous antigen is subclinical. Self-proteins may also become antigens, then called endogenous antigens. They are generated during the normal

cell metabolism and are part of the host itself. Immune reactions to self proteins cause autoimmune disorders.[142]

Immune complex formation is based on hydrogen bonds, hydrophobic interactions, Van der Waals forces, and electrostatic forces. While all of them are classified as being weak because of their non-covalent nature, the combination of these forces can result in rather strong bindings (cooperative effect). Since antibody – antigen binding is of non-covalent nature, it is reversible, and the equilibrium state depends on the rate of diffusion and on the affinity. The affinity constant can vary a lot and is affected by temperature, solvent, and pH value. It can be determined by immuno sensor based Surface Plasmon Resonance (SPR). SPR involves excitation of surface metal electrons which when interfering with photons cause a change of angle of photon reflection depending on the composition and density of metal surface-attached molecules. This method is used as biosensor for immuno assays as follows. A specific antibody is immobilized on the gold surface of the chip which is exposed to the running buffer which flows through a microfluidic flow cell of the instrument. When a sample with an antigen is injected into the running buffer flow, binding between the antigen and the surface-coated antibody leads to the increase of mass near the surface and as a consequence a change in photon reflection angles.[143]

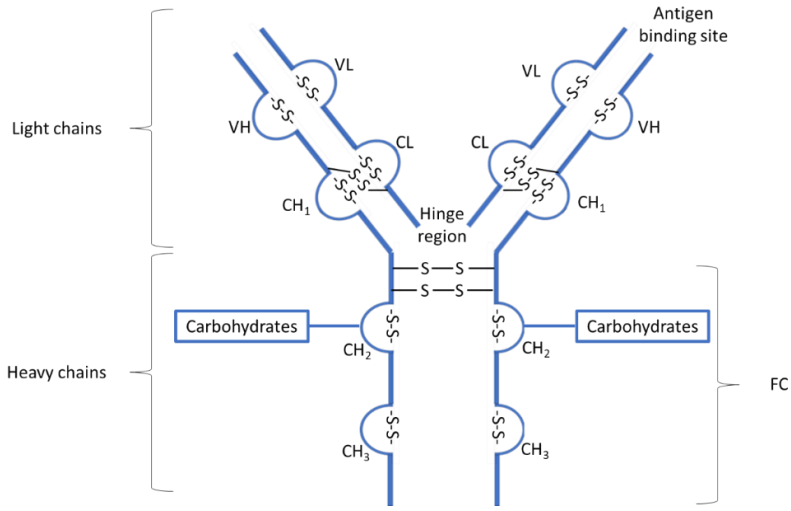

Figure 27. Schematic representation of immunoglobulin

Antibodies are constituted by four chains (Figure 27). Two identical heavy chains (H) and two identical light chains (L); the variable regions are indicated with V, they are located at the amino terminals and their amino acid sequences are varying from antibody to antibody. The constant regions are indicated with the letter C. Each H chain is composed of one variable domain and three constant domains; each L chain possesses one constant and one variable domain. The heavy chain´s average molecular mass is ca. 50 kDa and that of the light chain is ca. 25 kDa.[144, 145, 146]

Light and heavy chains are linked together by covalent interchain disulphide bonds and by non-covalent interactions, giving a symmetric structure with Y shape. Both V regions are involved in antigen binding making antibodies bivalent. The region between CH_1 and CH_2, were disulphide bonds are placed, is called the hinge region. It is flexible and therefore the distance between the two antigen binding sites can vary. The IgG antibodies´ heavy chains are called gamma

chains (IgM have mu-chains; IgA have alpha chains; IgE have epsilon chains and IgD have delta chains). [147, 148, 149]

The antigen binding site (paratope) of the antibody is formed by the three hypervariable regions of the light chains and the three hypervariable regions of the heavy chains. Usually, multiple non-covalent bonds are formed to hold an immune complex together, but on both, the epitope and the paratope, only rather small molecular portions comprising a few amino acids, each, are engaged. The strong attraction between them is due to ionic and hydrophobic forces which help the molecules to overcome their hydration energies and permits water expulsion which makes the binding spontaneous because the total entropy of the system increases.[150, 151, 152]

For immunoassay such as Western blot or ELISA, a high specificity is needed, in which an immunoglobulin recognises one antigen among other antigens and antibodies.[153, 154, 155] Their application can be extended as therapeutic agents, against cancer or autoimmune diseases, and in disease diagnostic.[156, 157, 158] Considering that the most valuable feature of Immunoglobulins is the specificity of antigen binding, the chance to obtain an experimental epitope determination is essential.

Immunoglobulins, or antibodies, are glycosylated proteins synthetised by white blood cells and are secreted into the blood plasma. Plasma is obtained from blood by centrifugation, it is the liquid component of the blood that contains proteins, hormones, and electrolytes but not cells. Immunoglobulins can also be found in blood serum which other than plasma does not contain fibrinogen. Serum is obtained by centrifugation of coagulated blood.

Immune complexes have numerous regulatory functions, such as enhancing of B cell and T cell activation.[159, 160, 161] Antibodies can be administered for preventing disease and for therapeutic purposes when treating inflammatory diseases and infections. [162, 163]

3.1.2. ESI-MS analysis of intact macromolecules

Intact macromolecules, such as peptides and proteins, are multiply protonated by ESI in positive ion mode, and the macromolecule´s ions assume a characteristic charge state distribution. Because of the multiply charging effect the mass range of macromolecules is expanded, because, since the m/z value is measured, it is possible to detect a ten-fold charged ion with a mass of 10,000 at an m/z value of 1000.[164]

Furthermore, ESI MS can be carried out without any problems with aqueous solvents under almost physiological conditions. A series of ion signals is obtained with intact protein measurements, and a Gaussian distribution is generated. Each of the ion signals of one series is distinguished by one charge (Figure 28). The maximum of this distribution is based on the parameters used during the ESI mass spectrometer measurements, on the pH value, solvent, temperature, and gas pressure in the ESI source as well as on the macromolecules properties.

To determine the charge of proteins from ESI MS spectra the following equation is applied at with consecutive signals from the same ion species but with different charge (Figure 28). This equation works with the assumption that the difference between z1 and z2 is 1.

$$z1 = \frac{(m2 - x)}{m2 - m1}$$

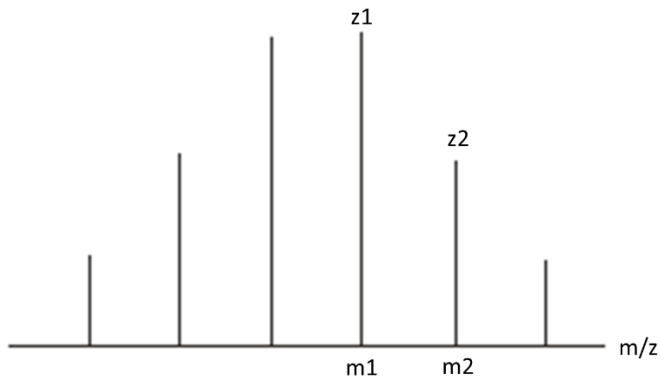

Figure 28. ESI MS spectrum example for proteins of multiply charged ion signals which follow a Gaussian distribution

Once the charge is known it is possible to calculate the mass of the macromolecule using the following equation:

$$M = z1(m1 - x)$$

M = molecular mass (Da)

z = charge of the molecule ion signal

x = mass of the charger carrier

m = m/z value of the signal

Before performing an ESI MS measurement of antibodies it is very important to exchange buffers, because antibodies are usually in buffers which contain several non-volatile components, such as glycerol, detergents, and organic polymers. These components may be necessary to keep the antibody in solution, but they commonly suppress ionization. Usually, the buffer of choice is ammonium acetate at different concentrations and with a pH range of 6-8 are, to avoid denaturation.[165, 166]

The tandem or hybrid mass spectrometer nanoESI Q-ToF is constituted by a spray source for electrospray ionization, ion optics, two

mass analyser (the first one is a quadrupole, the second is a ToF analyser used for the determination of ions m/z ratio), a reflector and a multi-channel plate (MCP) detector for the registration of the m/z ratio. This instrument type is able to work in MS mode, in which acquire mass spectra of macromolecules and non-covalent interactions between them can be investigated. In MS/MS mode is possible to select and fragment ions. This fragmentation mode is important for obtaining structural information, such as post-translation modifications or amino acid sequences of peptides. The ion selection can be done by the quadrupole analyser, the selected ions reach the collision cell, which typically is supplied with argon. Due to the collision with argon atoms the ions are fragmented. Once formed, fragment ions pass the transfer lens and are accelerated by the pusher into the ToF analyser. Then ions are reflected in the reflectron and finally reach the detector.

Electrospray ionization takes place under atmospheric pressure, but the analysis of obtained ions is done in high vacuum. To obtain an efficient nebulization, the capillary, from which the analyte is delivered, is typically cloaked by nitrogen sheath gas to improve nebulization and assist the desolvation processes. In addition, to support the spray, the source and the desolvation gas can be heated. Obtained analyte and solvent ions pass through the sample cone into the mass spectrometer and reach the first analyser while the remaining solvent evaporates because of the vacuum which is produced by a rotary pump and which is provided in the analyser region. The analyte ions are focused to an ion beam by an electro-optical lens system.

Nano ESI Q-ToF

The nanoESI Q-ToF II instrument from WATERS (Figure 29) is constituted by a nano ESI source which operates as a so-called Z-spray because the path which the formed ions follow has a Z shape. The electric lenses collimate the ion beam. The Quadrupole analyser is used to scan the different m/z ions, but it is also possible to block the transmission or to select specific m/z ions to pass through the quadrupole. The Collision Cell can be switched on which means that then a gas pressure is set as well as its voltage difference (ΔCV). When ΔCV is elevated, ions collide with higher energy with the Argon gas atoms and thereby fragment. The hexapole focuses the ion bean and leads the ions which leave the collision cell into the ToF system. The specific version of the nanoESI Q-ToF II instrument at the Proteome Center Rostock is equipped with a Speedivalve which gives the possibility to manually set the vacuum value behind the cone and using this Speedivalve allows to increase the vacuum value. This operation is essential when big ions, like immunoglobulins, are under investigation. In this way they are more likely to be desolvated.

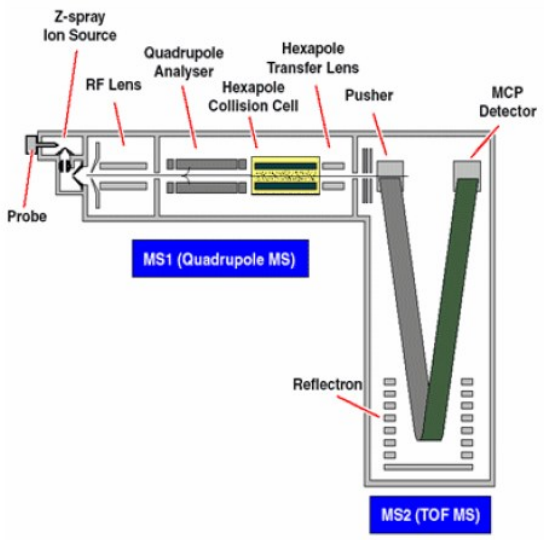

Figure 29. Schematic representation of the instrument Q-ToF for offline nanoESI-MS measurements

Synapt G2

Synapt G2 Mass Spectrometry system from WATERS is a hybrid, quadrupole orthogonal acceleration, time of flight mass spectrometer (Figure 30). Here the sample is introduced using a probe, and a lock-spray flow, containing a compound of known mass, flows through a separate ESI probe called LockSpray sprayer. The sprays can be analysed thanks to an oscillating baffle with two separate data functions. In this way the lock-mass correction is calculated and directly applied to the sample data set. The ion optics works as follows: samples from the LC or instrument's solvent delivery system are introduced at atmospheric pressure into the ionization source, the produced ions goes through the sample cone, into the vacuum system. Then the ions goes through the T-Wave ion guide reaching the quadrupole, here they are filtered based on their m/z value. The separated ions pass into the Triwave region, where they can be fragmented to the collision-induced dissociation (CID). At this point the ions goes into ToF ana-

lyser. A high-voltage pulse orthogonally accelerates the ions down the flight tube, where the dual-stage reflectron reflects them towards the ion mirror, which, in turn, reflects the ions back to the dual-stage reflectron. Here the ions are reflected to the detector. Ions of different m/z value arrive at the detector at different times, eventually a mass spectrum can be created once the signal from the detector is amplified, digitized, and sent to the MassLynx software. The system uses both quadrupole and time-of-flight (ToF) mass analysers.

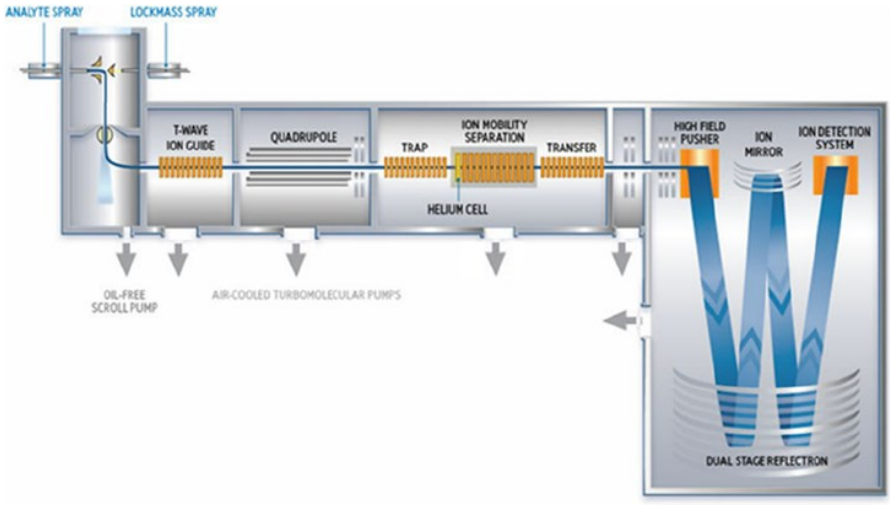

Figure 30. Schematic representation of the instrument Synapt for online nanoLC-ESI-MS^{E} measurements

3.1.3. ITEM

Intact transit epitope mapping (ITEM) is performed exploiting the possibility to use ion mobility mass filtering or quadrupole mass filtering in tandem mass spectrometers. Ion mobility and/or quadrupole filtering are mass separation steps which occur in the gas phase.[167, 168] ITEM follows the same in-solution epitope mapping steps as other mass spectrometric epitope mapping procedures do, but avoids immobilization of the immune complex. Instead, here the immune com-

plex solution is sprayed by nanoESI to yield in complex ions in the gas phase together with the other ionic species which are present in the solution, such as unbound antibody and unbound antigens.
The ITEM method is able to identify an epitope of an antigen in a single, fast and easy experiment which requires only low amounts of sample (typically pmols) in 3-5 µl volumes. The experiment encompasses (i) obtaining an immune complex and (ii) transferring the immune complex into the gas phase by nanoESI, then (iii) separation of ions is done using ion mobility or quadrupole filtering. The dissociation of the epitope (iv) from the complex occurs into a collision cell and the dissociated constituents of the immune complex are (v) separated by the ToF analyser and the ions (vi) are recorded at the mass spectrometer´s detector.[169]

The immune complex is prepared in a volatile buffer such as ammonium acetate and the antibody-epitope molar ratio should be at least 1:2.2. For complex formation it is necessary to reduce organic co-solvents and/or acidic condition. During desolvation of ions via nanoESI the conditions must be selected carefully to break weaker bonds between molecules and non-specific interactions, and simultaneously safe the stronger interactions of the antibody-antigen complex.[170] Once the quadrupole or the ion mobility mass filter is reached, the gas phase sample will be freed from smaller ions, such as unbound ligands or other peptide ions which did not bind. In this way only the complexed and uncomplexed antibodies can reach the collision cell. Here, the epitope peptide can be released from the complex by increasing the collision cell voltage difference (ΔCV), and with the help of a Synapt mass spectrometer the so freed peptides

can be fragmented afterwards. In this way just a few peptide ions will reach the mass spectrometer´s detector, which makes the spectra easy to interprete.[171] Since during ITEM experiment the complex in gas phase must reach the collision cell intact and here the energy must be high enough for releasing the epitope from the complex, success of these two steps is highly dependent on the used conditions, which must be fine-tuned. Each complex needs different conditions, depending on the stability of the complex which has been taken into consideration. [171, 170]

Three ITEM methods have been developed by the research group of the Proteome Center Rostock.

ITEM-ONE (Intact Transition Epitope Mapping - One step Non-covalent force Exploitation), where epitopes are identified by the accurate masses of the complex released peptides.[169]

ITEM-TWO (Intact Transition Epitope Mapping – Thermodynamic Weak-force Order), where epitopes and their apparent dissociation energies are identified.[172]

ITEM-THREE (Intact Transition Epitope Mapping- Targated High-Energy Rupture of Extracted Epitopes), where the epitopes are identified by partial amino acid sequencing of released peptides.[173]

3.2. Aims of the work (Section 2)

In this second section, an MS-based method, called ITEM, shall be applied to perform epitope mapping in a seroconverted rabbit serum. First of all, a valid protocol by which immunoglobulins shall be extracted from rabbit serum which avoids the use of affinity chromatography methods and produces immunoglobulin solutions ready for ESI-MS is to be developed. The to be developed extraction procedure is supposed to be easy to use and feasible to apply in all laboratories around the world. In addition, the purity of the final product must be compatible with epitope mapping methods, such as ITEM. Application of the immunoglobulin isolation procedure shall be tested with immunoglobulins which will be extracted from rabbit serum and into which shall be spiked in an ovalbumin-specific antibody. So prepared extracts will be used for traditional immuno assays, such as Western blotting as well as for ITEM, to prove the success of the seroconversion and of epitope mapping by mass spectrometry.

The aims of this second section are: 2A) IgG extraction from rabbit serum without affinity chromatography; 2B) Seroconversion and epitope characterisation of ovalbumin.

Keywords: Immune complex, Seroconversion, Rabbit serum, Immune assay, Immunoglobulins extraction, Epitope mapping.

3.3. Materials and Methods: IgG extraction from rabbit serum (2A)

All chemicals were of the highest purity commercially available and were used without further purification. Deionised Water was purchased from TKA (Milan, Italy). LC-MS Water was obtained from Biosolve Chimie (Dieuze, France). Sodium Acetate from Merck (Darmstadt, Germany). Ammonium Acetate from Fluka Chemika (Buchs, Switzerland). Octanoic Acid from Sigma-Aldrich (St. Louis, Missouri, USA). Acetone from Roth (Karlsruhe, Germany). Glacial acetic acid from J.T. Baker (Deventer, Netherlands). NaOH from Merk (Darmstadt, Germany). Rabbit Serum from Kaninchenbetrieb Pelleit (Gottin, Germany). Qubit kit for protein determination from Invitrogen/Thermo Fischer Scientific (Waltham, Massachusetts, USA). MOPS from Serva Electrophoresis (Heidelberg, Germany). TRIS from Roth (Karlsruhe, Germany). SDS from Serva Electrophoresis (Heidelberg, Germany). EDTA from Merck (Darmstadt, Germany). Ethanol from Zentralapotheke Universitätsmedizin Rostock (Rostock, Germany). Acetic acid from Baker (Deventer, Netherlands). Aluminum sulphate from Sigma-Aldrich (St.Luis, Missouri, USA). Coomassie brilliant blue G250 from Serva Electrophoresis (Heidelberg, Germany). Phosphoric acid 85% from Merck (Darmstadt, Germany). Bromophenol blue from Merck (Taufkirchen, Germany). Glycerin from Merck (Darmstadt, Germany). Prestained protein marker from Thermo Fisher Scientific (Waltham, Massachusetts, USA). $Na_2S_2O_3$ (Sodium thiosulfate) from Merk (Darmstadt, Germany). $AgNO_3$ (Silver nitrate) from Merk (Darmstadt, Germany). Na_2CO_3 (Sodium carbonate) from Merk (Darmstadt, Germany). Formaldehyde from Merk (Darmstadt, Germany). Acetonitrile from Biosolve (Valkenswaard, Netherlands). Formic

acid from Biosolve (Valkenswaard, Netherlands). Ammonium bicarbonate from Honeywell Fluka (Waltham, Massachusetts, USA). Modified Porcine Trypsin was purchased from Promega (Madison, WI, USA). DTT from Serva Electrophoresis (Heidelberg, Germany). Hydrochloric acid from Merk (Darmstadt, Germany).

3.3.1. IgG extraction procedure

Thorough literature study on protein extraction methods using techniques such as precipitations and filtrations was the starting point to obtain the following protocol. For instance, Ko et al. developed a method to extract immunoglobulins from egg yolk in high purity by consecutive steps of precipitation, filtration and centrifugation.[174] Of note, the buffer ionic strength, with which serum is diluted, affects precipitations yields.[175] Thus, the final protocol for isolation of immunoglobulins from serum, which has been developed in this work, is composed of a combination of three steps including octanoic acid precipitation, [176] acetone precipitation,[177, 178] and ultrafiltration.[179] The endpoints of each step mark break points where the procedure may be interrupted for an extended period of time. The final product is a nearly pure immunoglobulin solution in a volatile buffer (ammonium acetate) which contains just traces of other proteins such as serum albumin and transthyretin, but is ready for ESI-MS analysis.

***Step1*:** A volume of 170 µl of serum is pipetted into a 1.5 ml Eppendorf tube. Then 30 µl of deionized water and 600 µl of a 60 mM sodium acetate solution are added. The mixture is vortexed for 30 seconds. Then 20 µl of neat octanoic acid is slowly added. A white precipitate forms and the suspension is vortexed at room temperature for 30 minutes. Subsequently, the suspension is centrifuged at 10,000 g

and at 4 °C for 30 minutes to separate the white precipitate, P1, from its supernatant solution, S1. P1 is discarded. S1 (ca 0.82 ml volume) is aspirated and filled into a 2 ml syringe which is equipped with a PES syringe filter (0.45 µm pore size, 4 mm diameter). S1 is filtered into a 5 ml Eppendorf tube. The filter is washed with 180 µl of deionized water and this washing solution is added to S1. Then, S1 is split into two equal portions of ca. 500 µl, each, and filled into separate 5 ml Eppendorf tubes to obtain solutions S1a and S1b which may be kept at 4 °C overnight.

***Step2*:** To each S1a and S1b solution is added 4 ml of chilled acetone at -20°C. The mixtures are vortexed for 1 minute, each (no precipitation is visible). Then the tubes are placed into the freezer, at -20°C, overnight (flocculates appear the next day). The suspensions are centrifuged at 10,000 g and -5 °C for 30 minutes, to separate the white precipitates, P2a and P2b, from their supernatant solutions, S2a and S2b. S2a and S2b supernatants are discarded. Precipitates P2a and P2b are suspended in 100 µl of deionized water, each. Then the suspensions are centrifuged at 10,000 g and 4 °C for 30 minutes. Supernatant solutions are again discarded. This washing operation is repeated 2 times. Then the precipitate P2a (ca. 3 mg), is suspended in 100 µl of 200 mM ammonium acetate, pH 6.7, and is vortexed at room temperature overnight (10 hours). The suspension is centrifuged at room temperature and at 9,000 rpm for 3 minutes to generate supernatant S3a. Then residual precipitate is removed by aspirating S3a (ca. 0.1 ml). The S3a solution is added to the washed precipitate P2b (ca. 3 mg). The resulting suspension is vortexed at room temperature overnight (10 hours). The suspension is then centrifuged at

room temperature and at 9000 rpm for 3 minutes to generate supernatant S3. The residual precipitate is separated by aspiration of S3 (ca. 0.1 ml). S3 may be kept at 4 °C overnight.

***Step3*:** A centrifuge ultrafilter unit (Amicon) with 50 kDa cut-off, is filled with S3 (ca. 0.1 ml). Then 300 µl of 200 mM ammonium acetate, pH 6.7, are added. The solution is centrifuged at room temperature at 9,000 rpm for 5 minutes. The filtrate solution is discarded and the retentate solution, R1, is filled up with 200 mM ammonium acetate solution (ca. 300 µl). Centrifugation, discarding of filtrate solution, and refilling are repeated for eight times. Then, the centrifuge ultrafilter device is mounted onto another microcentrifuge tube which is placed in the centrifuge in an upside-down position. Centrifugation at room temperature and at 3,800 rpm is performed for 2 minutes. The retentate, R1, (ca. 80 µl) is the final solution. R1 may be kept at 4 °C for an extended period of time.

3.3.2. SDS-PAGE analysis of extracted IgG

MOPS solution was prepared by solubilising 104.6 g of MOPS, 60.6 g of TRIS (tris(hydroxymethyl)amin methane), 10 g of SDS, and 3.8 g of EDTA in 500 ml of deionised water. Then, this solution was diluted 20 times with deionised water.

Fixation solution is composed of 50% Ethanol and 10% Acetic acid in deionised water (v/v).

Coomassie brilliant blue staining solution was prepared with 100 g of $Al_2(SO_4)_3$ which is solubilised in 1.5 l of deionised water. Then 200 ml of Ethanol and 0.4 g of Coomassie Brilliant Blue G250 is added and mixed. Then 46 ml of 85% H_3PO_4 in water is added. The solution

is filled up with deionised water until 2 l. The solution is kept in a dark bottle.

Destaining solution is composed of 10% of 96% Ethanol, and 2% of 100% H_3PO_4 (or 2.3% of 85%H_3PO_4) in deionized water.

Non-reducing sample buffer was obtained by mixing 6.25 ml of 1 M TrisHCl, pH 6.8, with 2 g SDS, 0.08 g Bromophenol blue, 10 ml of Glycerol, and 3.75 ml of deionised water.

Reducing sample buffer was obtained by mixing 6.25 ml of 1 M TrisHCl, pH 6.8, with 2 g SDS, 0.08 g Bromophenol blue, 1 g DTT, 10 ml Glycerol, and 3.75 ml of deionised water.

Sensitizing solution was obtained by mixing 500 ml of deionised water with 100 mg of $Na_2S_2O_3*5H_2O$.

Silver solution was obtained by mixing 500 ml of deionised water with 1 g of $AgNO_3$ (prepared fresh each time, avoid light exposure).

Developing solution was obtained by mixing 25 ml of Sensitizing solution with 60 g of Na_2CO_3 and 975 ml of deionised water.

Stop solution was obtained by mixing 100 ml of deionised water with 1.46 g of EDTA.

R1 solutions were subjected to SDS-PAGE analysis. A volume of R1 that contained between 0.5 µg and 1 µg of protein was mixed with deionised water to reach a total volume of 16 µl. Then, 4 µl of Non-reducing sample buffer was added. The mixture was vortexed for 30 seconds and then was centrifuged for 2 minutes at room temperature and 6,000 rpm. Alternatively, 4 µl of Reducing sample buffer was added to diluted R1 (see above) and the solution was mixed and heat-

ed at 95 °C for 5 minutes. Then, the solution was vortexed for 30 seconds and centrifuged for 2 minutes at room temperature and 6,000 rpm.

The pre-cast SDS gels (NuPAGE Novex 12% Bis-Tris Gel; (Invitrogen, Carlsbad, CA, USA) were placed in the electrophoresis chamber Hoefer DALT Vertical Electrophoresis System (GE healthcare/ Amersham Biosciences, Freiburg, Germany) and the inner chamber was filled with MOPS buffer solution until the gels´ pockets were completely covered. The outer chamber was filled to cover the bottom ends of the gels. Into several gel pockets were filled 20 µl of protein-containing solutions, each, and in other pockets 3 µl of Prestained protein marker mix. Then, electrophoresis was performed using 200 V and 150 mA for 45 minutes. After separation gels were taken out and the gel pockets and the bottom bulge were removed. Then the gels were placed in fixation solution (ca. 10 ml, each) and shaken at room temperature for 1 hour. Then, gels were stained in Coomassie brilliant blue solution (ca. 10 ml, each) overnight by shaking at room temperature. Next, gels were placed up to 4 times in destaining solution (ca. 10 ml, each) and were shaken at room temperature for 20 minutes, each.[180] At this point the gels were scanned using the ScanMaker 1000XL Microtek from Microtek (Hsinchu City, Taiwan).

To perform Silver staining of protein bands (after Coomassie staining), gels were placed in fixation solution (ca. 10 ml) and shaken overnight at room temperature. Then, the gels were placed in 50% Ethanol solution (ca. 10 ml, each) and shaken for 20 minutes at room temperature. This operation is repeated 2 times. Then, the gels were placed in Sensitizing solution (ca. 10 ml, each) and shaken for 2

minutes at room temperature. Then, the gels were placed in deionised water (ca. 10 ml, each) and shaken for 1 minute at room temperature. This operation is repeated. Then, 100 ml of Silver solution were mixed with 75 µl of Formaldehyde, the gels were placed in this solution (ca. 10 ml, each) and shaken for 20 minutes at room temperature, avoiding light exposure. Then, the gels were placed in deionised water (ca. 10 ml, each) and shaken for 1 minute at room temperature. Then, the gels were placed in Developing solution (ca 10 ml, each) to which were added with 50 µl of Formaldehyde and were shaken for ca. 15 seconds at room temperature (the time is variable and needs to be monitored because too long light exposure must be avoided). Then, the gels were placed in Stop solution (ca. 10 ml, each) and shaken for 10 minutes at room temperature.[181] At this point the gels were scanned using the ScanMaker 1000XL Microtek scanner and stored between two heat-sealed plastic sheets in the fridge at 4°C.
The scans provided tif-files which were stored on computer drives and subjected to image analysis and documentation using the CorelDraw 17.0 software package.

3.3.3. In-gel digestion of extracted IgG bands

Washing solution 1 was prepared by adding 30% of acetonitrile in 25 mM ammonium bicarbonate solution (pH 8), dissolved in LC-MS water.

Washing solution 2 was prepared by adding 50% of acetonitrile in 10 mM ammonium bicarbonate solution (pH 8), dissolved in LC-MS water.

Extraction solution was prepared by adding 0.3% of formic acid in a solution of 50% acetonitrile and 50% LC-MS water.

Digestion solution with Trypsin as protease was prepared by adding to one vial of trypsin (Promega) (stored at -20°C) 2 ml of 3 mM Tris/HCL solution (pH 8.5) in LC-MS water. Directly before use mix 95 µl of this protease-containing mixture with 4 µl of 50 mM Tris/HCl and 2 µl of 250 mM DTT, dissolved in LC-MS water.

The band, which needed to be digested, was cut out from a Coomassie stained gel and was transferred into a 0.5 ml Eppendorf tube. Then, 200 µl of water were added. Water was removed by pipetting after one minute and 150 µl of washing solution 1 were added. The tube was gently shaken for 20 minutes at room temperature. Then the solution was removed by pipetting and 150 µl of washing solution 2 were added. The tube with the gel plug which contained the protein was gently shaken for 20 minutes at room temperature. Then, the solution was discarded by pipetting and 100 µl of acetonitrile were added. The tube was gently shaken for 10 minutes at room temperature. Then, the acetonitrile was discarded by pipetting. The gel plug was left to dry for 10 minutes at room temperature under the hood. Then, 5 µl of digestion solution were added. If after 1 hour the gel seemed to be dry, 5 µl of 3 mM Tris/HCl buffer solution were added. The moist gel plug was incubated overnight at room temperature. Then, 7 µl of the extraction solution were added and the tube was shaken for 60 minutes at room temperature. The supernatant (ca. 10 µl) which contained the proteolytically produced peptides was transferred by pipetting into a separate 0.5 ml Eppendorf tube and was lyophilised to dryness. The peptide mixture was dissolved in 10 µl of 3% acetonitrile and 0.1% formic acid in LC-MS water and was shaken for

20 minutes at room temperature. The solvent was collected at the bottom of the tube by centrifugation for 2 minutes at 13,000 rpm. [182]

3.3.4. Online nanoLC-ESI-MS^E analysis of in-gel digested extracted IgG bands

Online nanoLC-ESI-MS^E analysis was performed using a Synapt G2S instrument coupled with a nanoLC system (from Waters, Manchester, UK). In-gel digested final peptide solution in 3% acetonitrile and 0.1% formic acid in LC-MS water (2-3 µl) was loaded from each digested protein band. The spectra were recorded using the MassLynx 4.1 data system from Waters (Manchester, UK) and CDR-files were saved on computer drives. The MassLynx 4.1 software package was used for data analysis. The standard parameter settings were applied. Obtained online nanoLC-ESI-MS^E analysis raw data were used for protein identification by the PLGS software using standard conditions.[183]

3.3.5. Offline nanoESI-MS of extracted IgGs

R1 solutions were analysed by offline nanoESI-MS analysis using the Q-TOF II mass spectrometer from Waters (Manchester, UK). A gold coated needle for nano spray was filled with 2.5 µl of the solution and it was assembled to the nanoESI-Z spray. The capillary voltage was 1.4 kV; Cone voltage 130 V, Extractor voltage 3V, RF Lens 1.2 V, Source temperature 40 °C, MCP 1950 V, Pusher 124 µs, Inlet vacuum was $1.49 \cdot 10^{-1}$ mbar, Analyser vacuum was $3.92 \cdot 10^{-5}$ mbar, the TOF vacuum was $3.18 \cdot 10^{-7}$ mbar and the nitrogen sheath gas flow was set to 4 psi.[184] The spectra were collected from m/z 200 to m/z 8000 for 5 minutes, each. Obtained spectra were smoothed 10 times (Window size scans ± 30, used method “mean”). Spectra were

recorded using the MassLynx 4.0 data system from Waters (Manchester, UK). The MassLynx software package was used for data analysis and spectral image preparation in conjunction with the CorelDraw 17.0 software package.[172]

3.4. Results and Discussions: IgG extraction from rabbit serum (2A)

3.4.1. SDS PAGE image analysis of extracted IgG solution from rabbit serum

Proteins concentration of each R1 replicate (Chapter 3.3.1) was obtained using the Qubit fluorometer (Supporting info Table S 34). Considering that Immunoglobulins concentration in rabbit serum is between 5 and 10 µg/µl. Assuming an Immunoglobulins concentration of ca. 7.5 µg/µl, 170 µl of serum (starting material) contains around 1275 µg of Immunoglobulins. As result the average recovery of Immunoglobulin from the serum is 5.7%.

Presence of IgG was confirmed by SDS-PAGE analysis of reduced proteins bands (Figure 31).

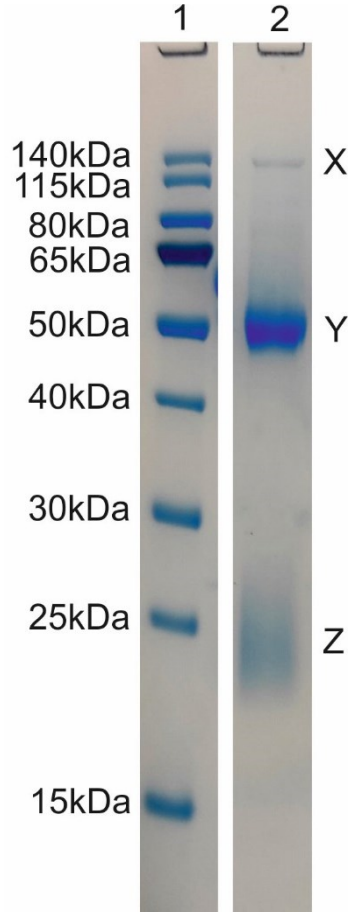

Figure 31. SDS-PAGE reduced R1 replicates
Into pocket 1 were loaded 3 µl of Prestained proteins marker; into pocket 2 were loaded 0.7 µl of R1 replicate 4, 1.46 µg/µl, in 0.2 M ammonium acetate, pH 6.7 (1 µg of total protein was loaded into pocket 2).

Band Y at the apparent mass of 50 kDa, which fit to the average mass of IgG heavy chains (50 kDa), band Z, broad and less coloured, is visible at about 25 kDa, this fit with the average mass of IgG light chains (25 kDa). The band X indicates that either the reduction was not complete or that there are other proteins present in the preparation.

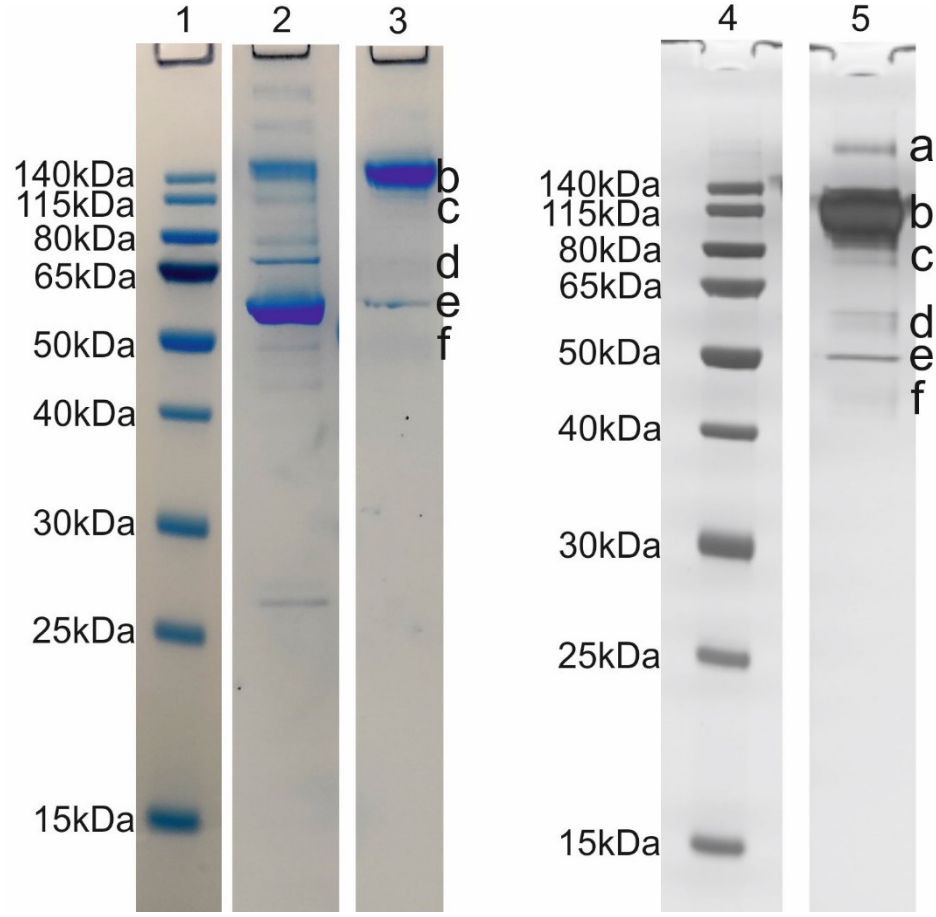

Figure 32. SDS-PAGE unreduced R1 replicates Coomassie and Silver staining.
Into pocket 1 were loaded 3 µl of Prestained proteins marker; into pocket 2 was loaded 1 µl of raw serum diluted 1:50 with Ammonium acetate solution 200 mM, pH 6.7, 1.19 µg/µl of protein concentration; into pockets 3 was loaded 0.7 µl of R1 replicate 4, 1.46 µg/µl, in ammonium acetate 0.2 M, pH 6.7 (1 µg of total proteins loaded).
For SDS-PAGE of unreduced R1 replicates Silver stained, another electrophoresis was performed as the first one. Into pocket 4 were loaded 3 µl of Prestained proteins marker; into pocket 5 was loaded 1 µl of raw serum diluted 1:50 with Ammonium acetate solution 200 mM, 1.19 µg/µl of protein concentration; into pockets B was loaded 0.7 µl of R1 replicate 4, 1.46 µg/µl, in ammonium acetate 0.2M, pH 6.7 (1 µg of total proteins loaded).

In lane 3 is possible to see band b at the apparent mass of ca. 140 kDa, which fit to the average mass of IgGs (150 kDa), please note that at high mass the separation is less efficient than low mass. The other bands can be barely seen, the only exception is the band e be-

tween 65 kDa and 50 kDa of apparent mass, this value can be related with the presence of the serum Albumin.

To visualize better other minor proteins as contaminants of IgG extracted solution, the more sensitive Silver stain method (Chapter 3.3.2) was used on another gel, obtained following the same protocol used for the first one.

The low recovery rate is compensated by high purity of the extracted material, as we can see from the gel (Figure 32, other replicates gels are reported in Supporting info Figure S 1, S 2 and S 3).

3.4.2. SDS PAGE protein bands analysis

Bands b, c, d, e and f were cut from the Coomassie stained gel (Figure 32) and obtained gel plugs were subjected to in-gel digestion (Chapter 3.3.3), band a is not visible in Coomassie stained gel so it was not possible to cut it and perform in-gel digestion and online nanoLC-ESI-MS^E measurement (set-up and instrument in Supporting info Table S 32) and PLGS analysis (set-up in Supporting info Table S 33).

From in-gel digestion 5 solutions, one for each cut gel plug, were obtained in a solvent constituted by 3% of acetonitrile and 0.1% of formic acid in LC-MS water.

Proteins identification of the reported bands were performed by online nanoLC-ESI-MS^E measurements followed by PLGS raw data analysis (Table 12).

Table 12. Protein identification of bands b, c, d, e and f by PLGS analysis using raw data from online nanoLC-ESI-MS^E

Band	Accession number	Description	Avg. Mass	Low energy ions		High energy ions		Seq. Cover(%)
				Ions found	Ions matched	Ions found	Ions matched	
b	P01870	Ig gamma chain C region	35404.33	2006	65	30134	369	30.65
c	P19007	Haptoglobin	38869.31	415	30	17968	170	13.54
d	P19134	Serotransferrin	76670.75	772	72	18575	366	20.43
d	P01870	Ig gamma chain C region	35404.33	772	72	18575	366	12.07
d	P49065	Albumin	68910.13	772	72	18575	366	6.58
e	P49065	Albumin	68910.13	211	19	10999	81	3.62
f	P07489	Transthyretin	13657.36	318	17	13746	84	20.47

3.4.3. Offline nanoESI-MS analysis of extracted IgG solution from rabbit serum

The extracted proteins in the R1 retentates were analysed by offline nanoESI-MS as reported (Chapter 3.3.5). R1 replicate 4 sprayed solution was 0.73 µg/µl, obtained by dilution 1:2 the solution R1 replicate 4 with ammonium acetate 0.2 M, pH 6.7 (Figure 33).

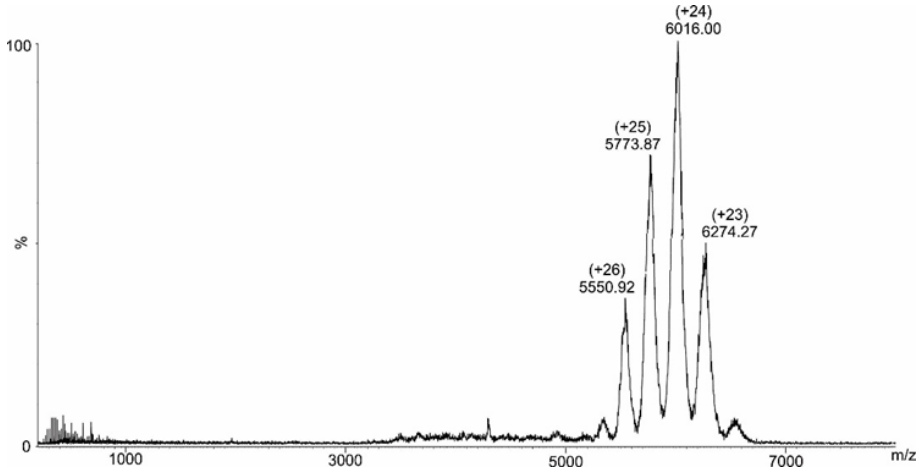

Figure 33. Offline nanoESI-MS spectra of R1 replicate 4 0.73 µg/µl. Ion signals are labelled with m/z values and charge states are given in parentheses. Solvent: 200 mM ammonium acetate, pH 6.7.

The mass spectrum shows a clean antibody solution obtained after the desalting and buffer exchange process with the typical pattern of multiply charged ion signals between m/z 5000 and m/z 6500. Ion signal intensities follow a Gaussian distribution and the most intense

ion signal is recorded for the 24-fold protonated ion. The from the multiply charged ion signals determined molecular mass is 144316.22 ± 32.88 Da. In the m/z range between m/z 3000 and m/z 4000 there are some low intensity ion signals that can be attributed to the presence of contaminants (not labelled in Figure 33). Performing the same offline measure, but this time with a lower Analyser vacuum value, which was $3.15 \cdot 10^{-5}$ mbar, the signals at low range, related to contaminants, increase in intensity (Figure 34)

Table 13. Average calculated IgGs masses from offline nanoESI-MS spectra of R1 replicates

R1 replicate	Average MS	Standard Deviation
1	145319.99	67.81
2	144979.63	32.70
3	144947.78	33.01
4	144316.22	32.88
Average mass		144890.90

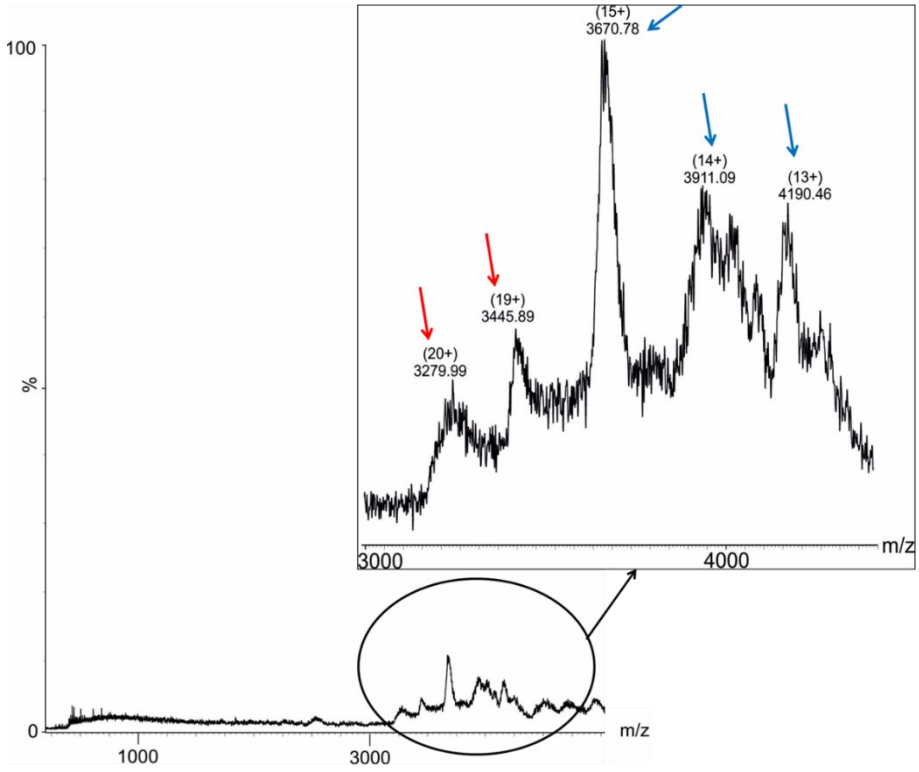

Figure 34. Offline nanoESI-MS spectra of R1 replicate 4 0.73 µg/µl. Ion signals are labelled with m/z values and charge states are given in parentheses. Solvent: 200 mM ammonium acetate, pH 6.7. The insert shows a zoom of the contaminant serum albumin and transthyretin signals between m/z 3000 and m/z 4500.

In the m/z range between m/z 3000 and m/z 4000 there are some ion signals that can be attributed to the presence of albumin (red arrows) and transthyretin (blue arrows). Respectively the from the multiply charged ion signals determination molecular mass is 65516.36 ± 89.72 Da, and 54754.51 ± 291.86 Da (Supporting info Figure S 4, 5 and 6 offline nanoESI-MS spectra of R1 replicate 1, 2 and 3).

3.5. Conclusion: IgG extraction from rabbit serum (2A)

The here developed extraction method provides IgG from rabbit serum with high purity. Only small amounts of albumin, transthyretin and other serum proteins are present. Average estimated recovery was 5.7%. The method is cheap and the steps are simple to perform with no special laboratory equipment. Most important, the final R1 retentates can be directly sprayed in ESI-MS experiments or used for protein concentration determination, SDS-PAGE, and Western Blot analysis without further manipulation.

3.6. Materials and Methods: Seroconversion and Epitope characterisation (2B)

All chemicals were of the highest purity, commercially available, and were used without further purification. Anti-Ovalbumin antibody from abcam (Cambridge, UK). Aminocaproic acid from Merck (Taufkirchen, Germany). Methanol from Roth (Karlsruhe, Germany). Odyssay Blocking buffer from LI-COR Biosciences (Lincoln, Nebraska, USA). Tween-20 from Merck (Taufkirchen, Germany). PBS from Merck (Taufkirchen, Germany). IRDye® 800 CW goat anti-mouse from Li-COR Biosciences (Lincoln, Nebraska, USA). Ammonium bicarbonate from Honeywell Fluka (Waltham, Massachusetts, USA). Ovalbumin from Merck (Taufkirchen, Germany). Urea from Bio-Rad Laboratories (Hercules, California, USA). DTT from Serva Electrophoresis (Heidelberg, Germany). IAA from Bio-Rad Laboratories (Hercules, California, USA). Trypsin from Promega Corporation (Madison, Winsconsin, USA). Acetonitrile from Biosolve (Valkenswaard, Netherlands). Formic acid from Biosolve (Valkenswaard, Netherlands).

3.6.1. Preparation of anti-Ovalbumin antibody containing solutions

Desalting of the original anti-Ovalbumin antibody solution (Solution 1)

A volume of 50 µl of the supplier´s original anti-Ovalbumin antibody solution (0.98 µg/µl) was transferred into an ultrafilter tube with 50 kDa cut-off (Amicon) and the buffer was exchanged with 0.2 M ammonium acetate, pH 6.7 (as reported in chapter 3.3.1 step 3). The so prepared anti-Ovalbumin antibody solution (Solution 1) in 0.2 M ammonium acetate, pH 6.7, has a concentration of 0.28 µg/µl.

anti-Ovalbumin antibody-containing IgG solution (Solution 2)

8 µl of IgG solution extracted from rabbit serum (R1 replicate 3; reported in chapters 3.3.1 and 5.2) 0.34 µg/µl (in ammonium acetate 0.2 M, pH 6.7) were mixed with 6 µl of anti-Ovalbumin antibody solution (Solution 1), protein concentration 0.28 µg/µl. In this way the anti-Ovalbumin antibody-containing IgG solution (Solution 2) is obtained with final concentration of IgG from rabbit serum of 0.19 µg/µl and anti-Ovalbumin antibody final concentration of 0.12 µg/µl (0.31 µg/µl of total proteins concentration).

With anti-Ovalbumin converted rabbit serum (Solution 3)

170 µl of rabbit serum 40.2 µg/µl of protein concentration measured by Qubit, were mixed with 10 µl of anti-Ovalbumin antibody (0.98 µg/µl) solution (original solution from supplier). 5 µl of this solution were mixed with 75 µl of 0.2 M ammonium acetate solution, pH 6.7, thereby obtaining converted serum solution (Solution 3) 2.38 µg/µl.

IgG extraction from with anti-Ovalbumin converted rabbit serum (Solution 4)

175 µl of converted serum solution (Solution 3) were used to perform an IgG extraction according to the preparation protocol as was reported before (Chapter 3.3.1) to yield in the respective retentate R1 (Solution 4) 1.41 µg/µl in ammonium acetate 0.2 M, pH 6.7. IgG extracted from converted rabbit serum solution (Solution 4), an aliquot of 0.75 µl, was characterised by SDS-PAGE following the protocol reported before (Chapter 3.3.2).

3.6.2. Preparation of antigen-containing solutions

Ovalbumin amino acid sequence from data base

The Ovalbumin sequence was downloaded from UNIPROT (P01012) in FASTA-file format (Figure 35).

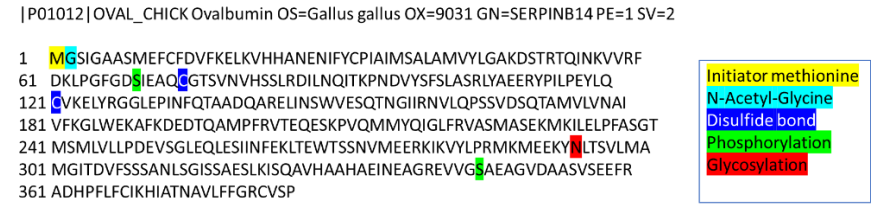

Figure 35. Ovalbumin sequence. According to the UNIPROT data base entry the first amino acid (methionine in yellow), is deleted from the sequence because it is the initiator amino acid which is not present in the final Ovalbumin protein. The Cysteine residues (blue) are alkylated by iodoacetamide, phosphorylated Serin residues (green), and the N-terminal acetylation on the Glycine residue (light blue) as well as the glycosylation on the Asparagine residue (red) are marked

Antigen-containing solution with commercial Ovalbumin (Solution 5)

Ovalbumin solution (solution 5) was prepared by solubilizing 96.6 mg of Ovalbumin in 50 mM ammonium bicarbonate, pH 8, to yield a final volume of 10 ml (protein concentration: 9.66 µg/µl).

Ovalbumin digestion with trypsin (Solution 6)

10 µl of Ovalbumin solution (Solution 5, protein concentration 9.66 µg/µl) were pipetted into a 0.5 ml Eppendorf tube and mixed with 6.8 µl of 15 M Urea dissolved in 50 mM ammonium bicarbonate solution, pH 8. Add 2 µl of 100 mM DTT dissolved in 50 mM ammonium bicarbonate solution pH 8, warm it up for 30 minutes at 57 °C. Add 1.5 µl of fresh prepared 300 mM IAA dissolved in 50 mM ammonium bicarbonate solution, pH 8, let it rest at room temperature for 30 minutes in the dark. Add 114 µl of 50 mM ammonium bicarbonate

buffer, pH 8, and 20 µl of Trypsin (0.1 µg/µl) dissolved in 3 mM TRIS/HCl, pH 9.3. Incubate overnight at 37 °C in the dark. Final Urea concentration is 0.66 M; protein/peptide concentration is 0.63 µg/µl; final volume is 154.3 µl.[185, 186, 187, 188, 189]

To check the digestion yield an SDS-PAGE run was performed, using a 1.2 µl aliquot from the digestion mixture (as reported in chapter 3.3.2).

Desalt and remove undigested Ovalbumin protein from the peptide-containing solution using a C18 OASIS cartridge. Mix 100 µl of digested ovalbumin protein/peptide solution, pH 8, with 900 µl of 0.1% formic acid solution, pH 2.6 Condition the OASIS cartridge with 1 ml of neat acetonitrile, equilibrate the cartridge with 0.1% formic acid solution (pH 2.6), and load the peptide mixture. Wash cartridge using 1 ml of 0.1% formic acid solution (pH 2.6), then with 1 ml of deionized water (LC-MS quality). Elute the peptides, first using 600 µl of 80% acetonitrile 0.1% formic acid solution in LC-MS Water, and again using 200 µl of the same elution solution. Collect the eluted volumes in a 1.5 ml Eppendorf tube. Evaporate solvent of the eluate using a SpeedVac RVC 2-25 (Martin Christ Drying Systems, Osterode am Harz, Germany) and redissolve the dried peptides in 30 µl of 0.2 M ammonium acetate, pH 6.7, to yield Ovalbumin digested solution (Solution 6). Peptide concentration of digested Ovalbumin solution (Solution 6) is 1.11 µg/µl.

Antigen-containing solution from egg white (Solution 7)

Egg white solution (Solution 7) was prepared by mixing 100 µl of egg white with deionized water to a final volume of 2 ml (0.75 µg/µl of proteins). The pH of egg white diluted solution (Solution 7) is 7.2.

Egg white protein digestion with trypsin (Solution 8)

To digest the proteins from the egg white solution (Solution 7; protein concentration 0.75 µg/µl) the same procedure was applied as reported above for Ovalbumin digestion. The only difference was that doubled volumes of each solution were used.

Then, the obtained protein/peptide mixture was directly subjected to desalting with an OASIS cartridge. The dried peptides were dissolved in 30 µl of 0.2 M ammonium acetate pH 6.7, thereby obtaining egg white digested solution (Solution 8). Peptide concentration of egg white digested solution (Solution 8) is 0.38 µg/µl.

The success of the digestion was confirmed with an SDS-PAGE electrophoresis using a 1.5 µl aliquot from the digestion mixture.

3.6.3. Preparation of control solution

No anti-Ovalbumin antibody containing antibody solution (Solution 9)

As IgG solution without anti-Ovalbumin antibody (Solution 9) was used the IgG extraction of rabbit serum, R1 replicate 3 (as reported in chapter 3.3.1 and 5.2). The solvent is ammonium acetate 0.2 M, pH 6.7, and protein concentration is 0.34 µg/µl.

3.6.4. Western blot analysis

Before starting the Western Blots ε-Buffer, HT-Buffer, LT-Buffer, Blocking Buffer solution, primary antibody solutions, secondary antibody solution and washing solution were prepared.

ε-Buffer solution was prepared solubilising in 400 ml of deionised water 2.62 g of Aminocaproic acid and 1.51 g of TRIS; Methanol was added to a final volume of 500 ml, final pH 9.4.

HT-Buffer (High TRIS Buffer) was prepared by solubilising in 400 ml of deionised water 18.16 g of TRIS and Methanol was added to a final volume of 500 ml, pH 10.4.

LT-Buffer (Low TRIS Buffer) was prepared by solubilising in 400 ml of deionised water 1.51 g of TRIS and Methanol was added to a final volume of 500 ml, pH 10.1.

Blocking solution was prepared by mixing Odyssay Blocking Buffer with PBS 1% in a ratio 1:2.

Primary antibody + converted rabbit serum (Solution 3) was prepared by adding to the Blocking Buffer solution the 0.1% of Tween-20 and mix 3 ml of this solution with 40 µl of Serum mixed with anti-Ovalbumin antibody (Solution 3).

Primary antibody + IgG extracted from converted rabbit serum solution (Solution 4) was prepared by adding to the Blocking Buffer solution the 0.1% of Tween-20 and mix 3 ml of this solution with 35 µl of IgGs extracted from rabbit serum spiked in with anti-Ovalbumin antibody (Solution 4).

Primary antibody + IgG from rabbit serum R1 replicate 3 (Solution 9) was prepared by adding to the Blocking Buffer solution the 0.1% of Tween-20 and mix 3 ml of this solution with 40 µl of R1 replicate 3, IgGs extracted from rabbit serum (Solution 9).

Secondary antibody solution was prepared by adding to the Blocking Buffer solution the 0.1% of Tween-20 and add for each 10 ml of this solution 1 µl of antiMouse-IgG antibody from goat IRDye® 800 CW.

Washing solution was prepared by adding to the PBS 1% the 0.1% of Tween-20.

Two electrophoresis gels were performed and prepared as previously reported (Chapter 3.3.2), in one gel were load 3 µl of Prestained proteins marker, 1.1 µg of Ovalbumin (Solution 5) and one pocket was left empty, this sequence was repeated three times in total in this gel. On the second gel were load 3 µl of Prestained proteins marker, 1.5 µg of egg white (Solution 7) and one pocket was left empty, this sequence was repeated three times in total in this gel. Once the electrophoresis were done, to perform the Western blot trim, for each gel, 1 PVDF membrane and 18 filter paper, previously cut to the size of the gel. Store gel after electrophoresis for a maximum of 30 minutes in ε-Buffer (ca. 10 ml), prepare membrane by shaking it in Isopropanol (ca. 10 ml), shake afterwards with water until hydrophilic (ca. 10 ml), then with LT-Buffer (ca. 10 ml). Wet bottom plate of Western Blot with ε-Buffer, put 9 layers of ε-Buffer soaked filter paper down, put the gel on it, then put membrane down, add 3 layers of LT-Buffer soaked filter paper, 6 layers of HT-Buffer soaked filter paper, wet top plate with HT-Buffer, and put top plate on the system. Sett voltage at 3500 V, set amperage to 1.2 mA/cm^2. Electrophoresis duration depend on the mobility of the proteins (molecular weight and shape) for example Immunoglobulins need ca. 2 hours and ca. 45 minutes are needed for smaller proteins like Ovalbumin and egg white proteins. After blotting, block the membrane using Blocking solution (ca. 10 ml), shake for 1 hour at room temperature. Then wash 4 times, 5 minutes each, shaking into washing solution at room temperature (ca. 10 ml). Then trim the membrane in Primary antibody shaking over-

night at 4 °C (ca. 3 ml). Afterwards wash again as before and trim the membrane in Secondary antibody solution (ca. 3 ml), shaking for 1 hour at room temperature protected from light. At this point wash the membranes protected from light 4 times, 5 minutes each, shaking it into washing solution (ca. 10 ml each time) at room temperature. The last step consists in putting the membranes into a solution of PBS 1% (ca. 10 ml) and scanning at LICOR-System scanner. Store between two heat-sealed plastic sheets into the fridge at 4°C. The scans provided tif-files which were stored on computer drives and subjected to image analysis and documentation using the CorelDraw 17.0 software package. [180]

3.6.5. nanoESI-MS analysis of antibody solutions

Anti-Ovalbumin antibody solution (Solution 1)

2.5 µl of anti-Ovalbumin antibody solution (Solution 1) were transferred into a gold-coated capillary needle. Offline nanoESI-MS analysis at the Q-ToF II instrument was performed with applying a capillary voltage of 1.6 kV. Cone voltage was set to 130 V. Extractor voltage was 3 V. RF Lens was set to 1.2 V. Source temperature was 40 °C. MCP detector voltage was 1950 V. The pusher was set to 124 µs. Inlet vacuum was $1.55 \cdot 10^{-1}$ mbar. Analyser Penning was $3 \cdot 10^{-5}$ mbar. The ToF analyser vacuum was $4.5 \cdot 10^{-7}$ mbar. The nitrogen sheath gas flow was set to 4 psi. Mass spectra were recorded from m/z 200 to m/z 8000 for 5 minutes. Obtained spectra were smoothed 10 times (Window size scans ± 30, using the method "mean"). Spectra were recorded using the MassLynx 4.0 data system from Waters (Manchester, UK). Raw data were exported to CorelDraw and graph-

ic files (CorelDraw 17.0 software package) were saved on computer drives.

Anti-Ovalbumin antibody-containing IgG solution (Solution2)

2.5 µl of anti-Ovalbumin antibody-containing IgG solution 0.31 µg/µl (Solution 2) were transferred into a gold-coated capillary needle. Offline nanoESI-MS analysis at the Q-ToF II instrument was performed as mentioned above, but this time the Analyser Penning was $3.2 \cdot 10^{-5}$ mbar.

Anti-Ovalbumin antibody-containing IgG solution after extraction from converted serum (Solution 4)

2.5 µl of anti-Ovalbumin antibody-containing IgG solution after extraction from converted serum (Solution 4) 0.17 µg/µl (obtained by dilution of 4 µl 1.41 µg/µl with 29 µl of ammonium acetate 0.2 M, pH 6.7.), were transferred into a golden coated capillary needle, which was used for offline nanoESI-MS analysis at the Q-ToF II instrument was performed as mentioned above.

3.6.6. nanoESI-MS analysis of antigen solutions

Online nanoLC-ESI-MS^E analysis of peptide mixture from digested commercial Ovalbumin (Solution 6)

Online nanoLC-ESI-MS^E analysis was performed using a Synapt G2S instrument coupled with a nanoLC system (from Waters, Manchester, UK).

Digested Ovalbumin solution (Solution 6) 1.11 µg/µl was diluted 1:2 with ammonium acetate 0.2 M, pH 6.7, and 2 µl of this solution were added to 260 µl of a solution constituted by acetonitrile 2% formic acid 0.1% in LC-MS Water, final estimated concentration was 50

fmol/l. The spectrum was recorded using the MassLynx 4.1 data system from Waters (Manchester, UK) and CDR-files were saved on computer drives. The MassLynx 4.1 software package was used for data analysis and spectral image preparation in conjunction with the CorelDraw 17.0 software package.

Obtained online nanoLC-ESI-MS^E analysis raw data were used for in deep characterisation by PLGS software and peptide assignment by BiopharmaLynx.

Offline nanoESI-MS analysis of tryptic peptide mixtures from digested Ovalbumin (Solution 6)

For offline nanoESI-MS analysis of tryptic Ovalbumin peptide mixtures from digested Ovalbumin a gold coated needle for nano spray was filled with 2.5 µl of diluted tryptic Ovalbumin peptide mixture. 1 µl of tryptic Ovalbumin peptide mixture (Solution 6; 1.11 µg/µl) was diluted with 3 µl of 0.2 M ammonium acetate, pH 6.7, to yield a final peptide concentration of 0.28 µg/µl. Offline nanoESI-MS analysis was performed as mentioned before (Chapter 3.6.5). This time the capillary voltage was 1 kV; and the spectrum was collected from m/z 50 to m/z 8000, for 5 minutes. This spectrum was compared to the offline nanoESI mass spectrum (Supporting info chapter 5.4 Figure S 10 and S 11) of native Ovalbumin (Solution 5), to confirm that undigested Ovalbumin is not into Ovalbumin digested solution (Solution 6) anymore, thanks to OASIS cartridge treatment.

Online nanoLC-ESI-MS^E analysis of tryptic peptide mixtures from digested egg white proteins (Solution 8)

Online nanoLC-ESI-MS^E analysis of tryptic peptide mixtures from digested egg white proteins (Solution 8; peptide concentration 0.38

µg/µl) was performed using a Synapt G2S instrument. 6 µl from egg with digested solution (Solution 8) were added to 259 µl of a solution constituted of 2% acetonitrile and 0.1% formic acid in LC-MS water. Final estimated peptide concentration is 100 fmol/l. The spectrum was recorded using the MassLynx 4.1 data system from Waters (Manchester, UK). The MassLynx software package was used for data analysis and spectral image preparation in conjunction with the CorelDraw 17.0 software package.

Obtained online nanoLC-ESI-MS^E raw data were used for in deep characterisation by PLGS software and peptide assignment by BiopharmaLynx.

Offline nanoESI-MS analysis of tryptic peptide mixtures from digested egg white proteins (Solution 8)

Offline nanoESI-MS analysis of tryptic peptide mixtures from digested egg white proteins was performed at the Q-ToF II instrument. 2 µl of digested egg white peptides solution (Solution 8) were diluted with 1 µl of ammonium acetate 0.2 M, pH 6.7. Peptide concentration was ca. 0.25 µg/µl. Offline nanoESI-MS analysis was performed as mentioned before (Chapter 3.6.5). This time the capillary voltage was 1 kV; the Analyser Penning was at $2.25 \cdot 10^{-5}$ mbar, the ToF Analyser vacuum was at $3.9 \cdot 10^{-7}$ mbar and the spectrum was collected from m/z 200 to m/z 2000, for 5 minutes.

3.6.7. ITEM Analysis

Positive Control 1 (Solution 1 + Solution 6):

The ratio between antibody and antigen should be at least 1:2, therefore 10 µl of anti-Ovalbumin antibody solution (Solution 1; 0.28

µg/µl; 1900 fmol/µl) were mixed with 3.1 µl of peptide mixture from digested Ovalbumin (Solution 6; 0.055 µg/µl obtained by dilution of 1 µl of ovalbumin digested solution 0.28 µg/µl with 4 µl of ammonium acetate 0.2 M, pH 6.7). The final antibody concentration is 0.21 µg/µl (1.4 pmol/µl) and final peptide concentration is 0.013 µg/µl (32 pmol/µl). After mixing, the solution was left to rest for at least 1.5 hours at room temperature.

Offline nanoESI-MS ITEM experiment was performed setting capillary voltage to 1.4 kV; Cone voltage 130 V. Extractor voltage 3 V. RF Lens 1.2 V. Source temperature 80 °C. MCP 1950 V. Pusher 124 µs. Inelet vacuum was $1.55 \cdot 10^{-1}$ mbar. Analyser Penning was $3.5 \cdot 10^{-5}$ mbar, the ToF analyser vacuum was $4.5 \cdot 10^{-7}$ mbar. The nitrogen sheath gas flow was set to 4 psi. Ion transmission was blocked via quadrupole setting at below m/z 2000 . Mass spectrum ranges was from m/z 200 to m/z 8000 . Collision gas pressure was 4 psi and collision cell voltage difference initially was 3 V. After 1.5 minutes of recording the collision cell voltage difference was increased to 10 V, and recording lasted again for 1.5 minutes. The obtained spectra were smoothed 10 times (Window size scans ± 10, used method “mean”). Spectra were recorded using the MassLynx 4.0 data system from Waters (Manchester, UK). The MassLynx software package was used for data analysis and spectral image preparation in conjunction with the CorelDraw 17.0 software package. CDR-files were saved on computer drives

Test 1 (Solution 2 + Solution 6):

7 µl of IgGs extracted from rabbit serum plus anti-Ovalbumin antibody (Solution 2) were mixed with 1 µl of peptides from digested

Ovalbumin (Solution 6; 0.055 µg/µl). In this way the final peptide concentration from digested Ovalbumin is 0.007 µg/µl and the final IgGs concentration is 0.27 µg/µl. After mixing, the solution was left to rest at least for 1.5 hours at room temperature.

Offline nanoESI-MS ITEM experiment was performed as reported above, but this time the Analyser Penning was at $4 \cdot 10^{-5}$ mbar,

Test 2 (Solution 4 + Solution 6):

5 µl of Ovalbumin digested solution (Solution 6) 0.32 µg/µl (obtained by dilution of 4 µl of ovalbumin digested solution 1.11 µg/µl with 10 µl of ammonium acetate 0.2 M, pH 6.7) were mixed with 4 µl of IgGs extracted from rabbit serum spiked in with Anti-Ovalbumin antibody (Solution 4) 1.41 µg/µl**.** Final volume 9 µl, antibody concentration 0.63 µg/µl and final peptides from digested Ovalbumin concentration is 0.18 µg/µl. After mixing the solution was left to rest at least 1.5 hours at room temperature.

Offline nanoESI-MS ITEM experiment was performed as mentioned at the beginning of this chapter (3.6.7) but this time the Analyser Penning was at $4.4 \cdot 10^{-5}$ mbar.

Positive Control 2 (Solution 1 + Solution 8):

8 µl of Anti-Ovalbumin antibody desalted solution (Solution 1) 0.28 µg/µl were mixed with 2.5 µl of egg white digested solution (Solution 8) 0.05 µg/µl (obtained by dilution of 2 µl of egg white digested solution 0.38 µg/µl with 13 µl of ammonium acetate 0.2 M, pH 6.7). The final volume is 10.5 µl, final Anti-Ovalbumin antibody concentration is 0.21 µg/µl (1400 fmol/µl), final peptides from digested egg

white concentration is 0.013 µg/µl (32000 fmol/µl). After mixing the solution was left to rest at least 1.5 hours at room temperature.

Offline nanoESI-MS ITEM experiment was performed as mentioned at the beginning of this chapter (3.6.7), but this time the capillary voltage was 1.6 kV and the Analyser Penning was at $4.5 \cdot 10^{-5}$ mbar.

The whole set-up was maintained constant for all measurements except for Capillary Voltage and Analyser Penning. Since the used solvent is not optimal because acid condition (that promote protonation) and organic solvent (that lower surface tension) are missing, the Capillary voltage and Analyser Penning were adapted time by time to obtain a good and stable spray, in particular the Capillary voltage had values between 1.2 to 1.8 kV, the Analyser Penning, adjusted by Speedivalve, had values between $3.5 \cdot 10^{-5}$ and $4.5 \cdot 10^{-5}$ mbar.

Negative Control 1 (Solution 9 + Solution 6):

IgGs extracted from rabbit serum (Solution 9) was diluted in Ammonium acetate 0.2 M, pH 6.7, to the concentration of 0.23 µg/µl (1600 fmol/µl). 2.5 µl of Ovalbumin digested solution (Solution 6) 0.055 µg/µl. (13700 fmol/µl), were added to 10 µl of IgG from rabbit serum solution R1 replicate 3 (Solution 9) 16000 fmol/µl. The final volume is 12.5 µl, final IgGs concentration is 0.19 µg/µl (1200 fmol/µl), final peptides concentration from digested Ovalbumin is 0.011 µg/µl (34000 fmol/µl). After mixing, the solution was left to rest at least 1.5 hours at room temperature. Offline nanoESI-MS ITEM experiment was performed as mentioned at the beginning of this chapter (3.6.7).

Negative Control 2 (Solution 9 + Solution 8):

10 µl IgGs extracted from rabbit serum (Solution 9) 0.34 µg/µl were mixed with 5 µl of egg white digested solution (Solution 8) 0.05 µg/µl. Final volume 10.5 µl, final IgGs concentration 0.23 µg/µl and final peptides from digested egg white concentration is 0.017 µg/µl. After mixing the solution was left to rest at least 1.5 hours at room temperature.

Offline nanoESI-MS ITEM experiment was performed as mentioned at the beginning of this chapter (3.6.7).

Calibration of mass spectra for ITEM measurements:

Comparing ion signals from mass spectra of digested Ovalbumin (Solution 6) which were recorded in offline nanoESI mass spectrometry using both, standard settings (Non-ITEM) and ITEM conditions shows mass shifts of ion signals (Table 14). The peptide ion signals in the mass spectrum of digested Ovalbumin solution (Solution 6) which was obtained by offline nanoESI mass spectrometry with standard settings (reported in chapter 3.6.6, and chapter 3.7.2 Figure 40) differ by ca. 7 Th from those ion signals which were measured with the offline nanoESI mass spectrometry when using the ITEM conditions (reported in Supporting info chapter 5.6, Figure S 15)

Table 14. Peptides from digested Ovalbumin (Solution 6) signals shift between standard settings Non-ITEM reported in chapter 3.6.6) and ITEM condition (Chapter 5.6 Figure S 15)

Condition	Non-ITEM	ITEM	Difference
Signal 1	1555.97 Th	1548.64 Th	7.33 Th
Signal 2	1582.02 Th	1573.48 Th	8.54 Th
Signal 3	1687.12 Th	1681.13 Th	5.99 Th
Average			7.29 Th

The ion signals′ shifts are on average +7.29 Th. Therefore, mass spectra of the ITEM experiments were re-calibrated to adjust for the mass shift.

3.7. Results and discussion: Seroconversion and Epitope characterisation (2B)

3.7.1 Antibody solutions characterisation

Anti-Ovalbumin antibody solution (Solution 1)

The anti-Ovalbumin antibody solution′s (Solution 1) protein concentration was determined as 0.28 µg/µl (prepared as reported in chapter 3.6.1) and offline nanoESI mass spectrometry (Figure 36) was conducted as reported before (Chapter 3.6.5).

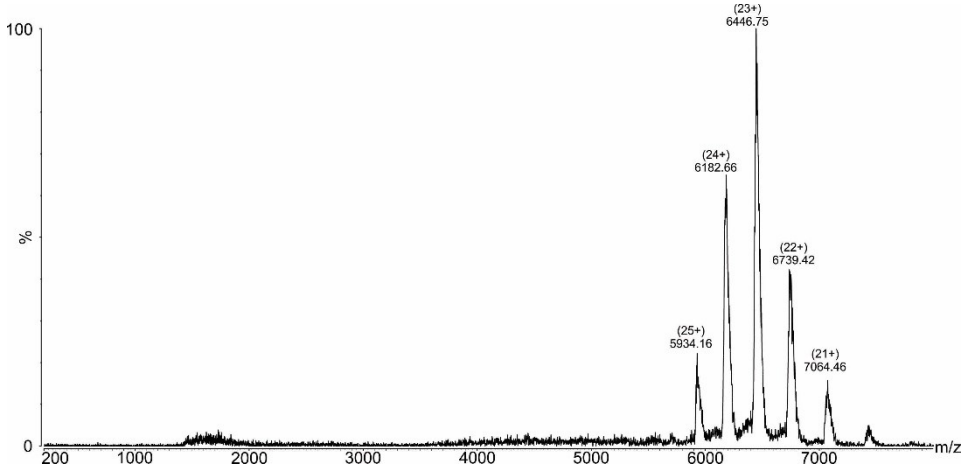

Figure 36. Offline nanoESI mass spectrum of anti-Ovalbumin antibody (Solution 1). Ion signals are labelled with m/z values and charge states are given in parentheses. Protein concentration is 0.28 µg/µl. Solvent: 200 mM ammonium acetate, pH 6.7.

The mass spectrum shows a clean anti-Ovalbumin antibody solution obtained after the desalting and buffer exchange process with the typical pattern of multiply charged ion signals between m/z 6000 and m/z 7500. Ion signal intensities follow a Gaussian distribution and the most intense ion signal is recorded for the 23-fold protonated ion.

The from the multiply charged ion signals determined molecular mass of the anti-Ovalbumin antibody is 148303.80 ± 51.71 Da.

Anti-Ovalbumin antibody-containing IgG solution (Solution 2)

The anti-Ovalbumin antibody-containing IgG solution´s (Solution 2) protein concentration was determined as 0.31 µg/µl (prepared as reported in chapter 3.6.1) and offline nanoESI mass spectrometry (Figure 37) was conducted as reported before (Chapter 3.6.5).

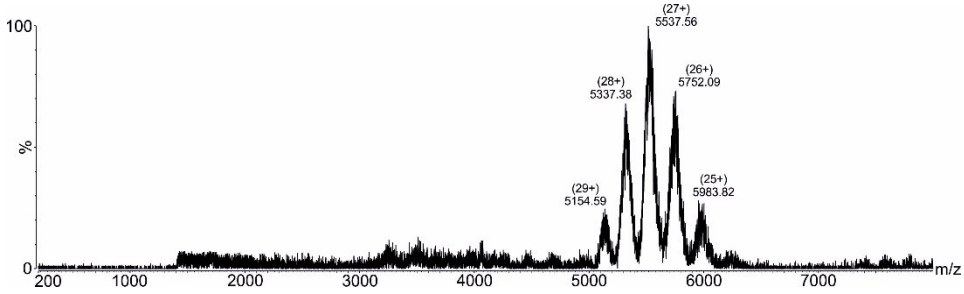

Figure 37. Offline nanoESI mass spectrum of anti-Ovalbumin antibody-containing IgG solution (Solution 2). Ion signals are labelled with m/z values and charge states are given in parentheses. Protein concentration is 0.31 µg/µl. Solvent: 200 mM ammonium acetate, pH 6.7.

The mass spectrum shows a clean antibody solution with the typical pattern of multiply charged ion signals between m/z 5000 and m/z 6500. The most intense ion signal is recorded for the 27-fold protonated ion. The width of the ion signals indicates a heterogeneous composition. The from the multiply charged ion signals determined average molecular mass of the antibodies is 149491.74 ± 59.84 Da. The contaminants, Albumin and Transthyretin, already characterised in solutions with extracted IgG from rabbit serum (Chapter 3.4), give rise to small ion signals between m/z 3000 and m/z 4500 (not labelled in Figure 37).

Anti-Ovalbumin antibody-containing IgG solution after extraction from converted serum (Solution 4)

The anti-Ovalbumin antibody-containing IgG from converted serum solution´s (Solution 4) protein concentration was determined as 1.41 µg/µl (prepared as reported in chapter 3.6.1) and offline nanoESI mass spectrometry (Figure 38) was conducted as reported before (Chapter 3.6.5).

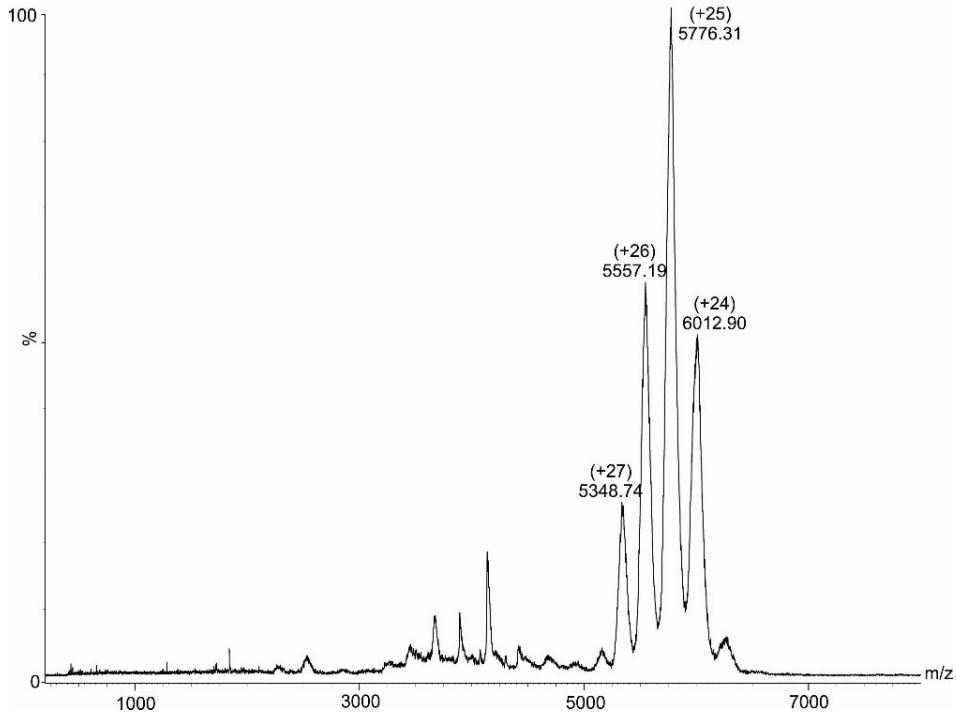

Figure 38. Offline nanoESI mass spectrum of anti-Ovalbumin antibody-containing IgG from converted serum solution (Solution 4). Ion signals are labelled with m/z values and charge states are given in parentheses. Protein concentration is 0.17 µg/µl. Solvent: 200 mM ammonium acetate, pH 6.7. Other serum protein ion signals are not labelled.

The mass spectrum shows a quite clean antibody solution which contains some contaminants. The typical pattern of multiply charged ion signals between m/z 5000 and m/z 6500 is seen. The most intense ion signal is recorded for the 25-fold protonated ion. The from the multiply charged ion signals determined average molecular mass of the an-

tibodies is 144379.64 ± 71.01 Da. Ion signals from other serum proteins are seen in the mass range between m/z 3000 and m/z 5000 (not labelled in Figure 38).

Considering that the immunoglobulin concentration in rabbit serum is between 5 and 10 µg/µl[190] and assuming an immunoglobulin concentration of ca. 7.5 µg/µl, 170 µl of serum (starting material) contains around 1275 µg of immunoglobulin and considering that 10 µl of anti-Ovalbumin antibody 0.98 µg/µl were added, the calculated recovery is 8.85%, with an estimated concentration of anti-Ovalbumin antibody of 0.011 µg/µl.

3.7.2 Antigen solutions characterisation

Peptide mixtures from digested Ovalbumin (Solution 6)

Online nanoLC-ESI-MS^E analysis

Digested Ovalbumin solution (Solution 6) was obtained as reported (Chapter 3.6.2). After the digestion and desalting processes, the peptide concentration was determined as 1.11 µg/µl. To check the digestion yield an SDS-PAGE electrophoresis (Supporting info 5.4 Figure S 9) was performed as reported (Chapter 3.3.2).

Online nanoLC-ESI-MS^E measurement (Figure 39, set-up and instrument in Supporting info Chapter 5.2 Table S 32) and PLGS analysis (set-up in Supporting info Chapter 5.4 Table S 35) were performed as reported before (Chapter 3.6.6).

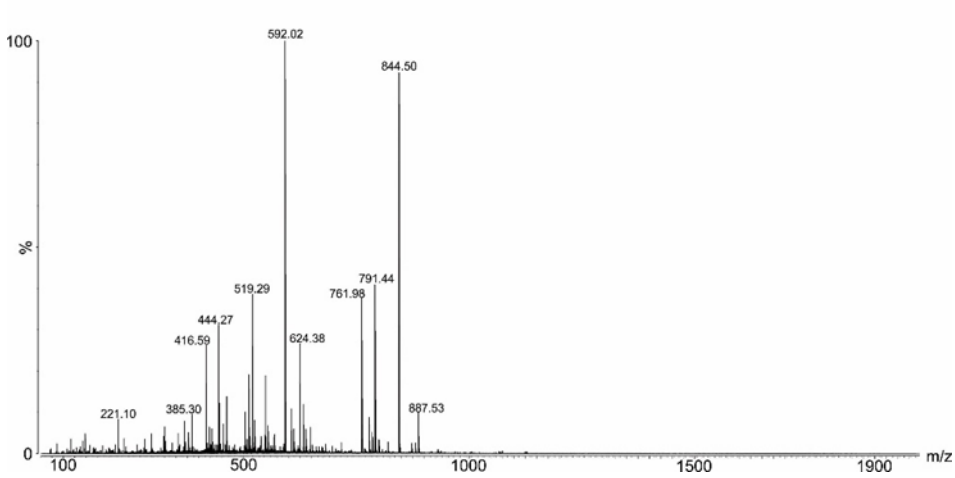

Figure 39. Online nanoLC-ESI-MS^E spectrum of Ovalbumin digested solution (Solution 6). 50 fmol/l in 0.2 M ammonium acetate, pH 6.7, with 2% of acetonitrile and 0.1% of formic acid as co-solvents.

Obtained raw data from online nanoLC-ESI-MS^E measurement provided 1711 low energy ions (mostly precursor ions) and 102862 high energy ions (mostly fragment ions). From them 132 low energy ions and 1033 high energy ions were assigned using the PLGS data analysis software package. After removing redundancy from the protein hit list leaves 10 protein entries (Supporting info chapter 5.4 Table S 38) and 4 proteins are correlated with the organism *Gallus gallus*: Ovalbumin, Ovomucoid, Serpin domain and Alpha-1-acid glycoprotein (Supporting info chapter 5.4 Table S 39).

The raw data were also subjected to peptide assignment using the BiopharmaLynx software package (set-up in Supporting info chapter 5.4 Table S 36) and provided an Ovalbumin sequence coverage of 95.8% (Figure S 12 in supporting info chapter 5.4)

Offline nanoESI-MS analysis

The digested Ovalbumin solution (Solution 6) was subjected to offline nanoESI mass spectrometry (Figure 40) as reported (Chapter 3.6.6).

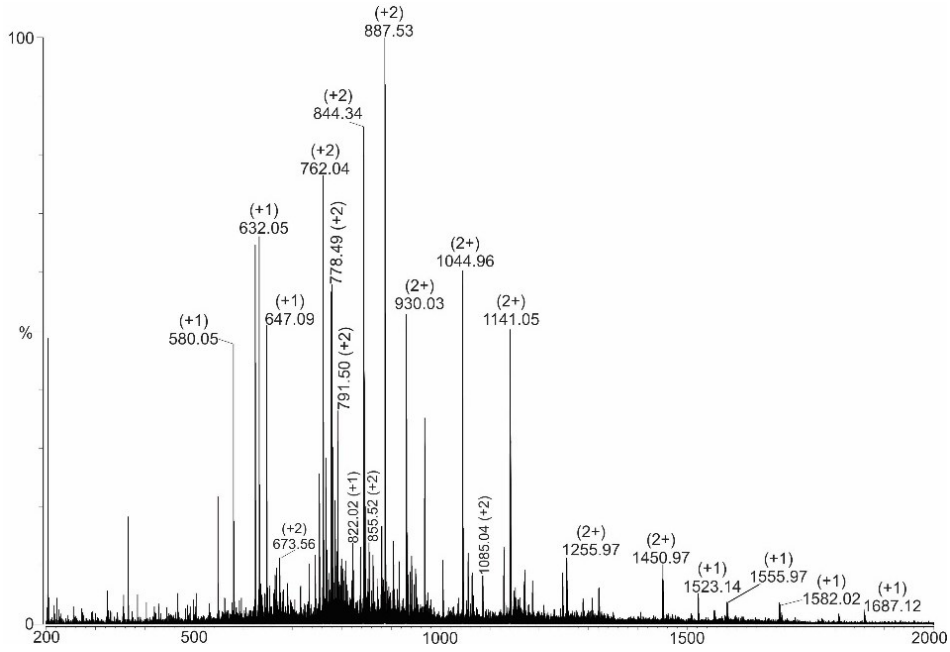

Figure 40. Offline nanoESI mass spectrum of digested Ovalbumin solution (Solution 6). Ion signals are labelled with m/z values and charge states are given in parentheses. Peptide concentration is 0.28 µg/µl. Solvent: 200 mM ammonium acetate, pH 6.7.

The mass spectrum shows 17 ion signals which were matched (Table 15) to the calculated masses from the in-silico digested Ovalbumin (list of obtained calculated peptides for Ovalbumin solution by GPMAW in supporting info chapter 5.4 Table S 37, used set-up Table S 36).

Table 15. Amino acid sequence assignments of Ovalbumin peptides (Solution 6) from the offline nanoESI mass spectrum

Amino acid sequence range	Experimental m/z value	Charge state	Calculated m/z value	Peptide amino acid sequence
59-84	1450.97	2+	1452.21	FDKLPGFGDSIEAQCGTSVNVHSSLR
59-84	967.65	3+	968.36	FDKLPGFGDSIEAQCGTSVNVHSSLR
62-84	1255.97	2+	1256.31	LPGFGDSIEAQCGTSVNVHSSLR
85-104	1141.05	2+	1141.77	DILNQITKPNDVYSFSLASR
111-122	1523.14	1+	1522.81	YPILPEYLQCVK
111-122	762.04	2+	761.91	YPILPEYLQCVK
123-126	580.05	1+	580.65	ELYR
127-142	1687.12	1+	1687.84	GGLEPINFQTAADQAR
127-142	844.34	2+	844.91	GGLEPINFQTAADQAR
143-158	930.03	2+	930.53	ELINSWVESQTNGIIR
182-186	632.05	1+	632.73	GLWEK
182-199	1085.04	2+	1085.72	GLWEKAFKDEDTQAMPFR
187-199	1555.97	1+	1556.72	AFKDEDTQAMPFR
187-199	778.49	2+	778.86	AFKDEDTQAMPFR
219-226	822.02	1+	822.95	VASMASEK
264-276	1582.02	1+	1582.71	LTEWTSSNVMEER
264-276	791.5	2+	791.86	LTEWTSSNVMEER
264-277	855.52	2+	855.95	LTEWTSSNVMEERK
280-284	647.09	1+	647.79	VYLPR
323-339	887.53	2+	887.96	ISQAVHAAHAEINEAGR
340-359	1044.96	2+	1045.54	EVVGSAEAGVDAASVSEEFR
370-381	673.56	2+	673.78	HIATNAVLFFGR

The Ovalbumin amino acid sequence coverage is 48.83%.

3.7.3. Peptide mixtures from digested egg white (Solution 8)

Online nanoLC-ESI-MS^E analysis

Digested egg white solution (Solution 8) was obtained as previously reported (Chapter 3.6.2). After the digestion and desalting processes, the concentration was determined as 0.75 µg/µl. To check the digestion yield an SDS-PAGE electrophoresis (Supporting info 5.4 Figure S 13) was performed (Chapter 3.3.2).

Online nanoLC-ESI-MS^E measurement (Figure 41, set-up and instrument in Supporting info Chapter 5.2 Table S 32) and PLGS analysis (set-up in Supporting info Chapter 5.4 Table S 35) were performed as reported (Chapter 3.6.6).

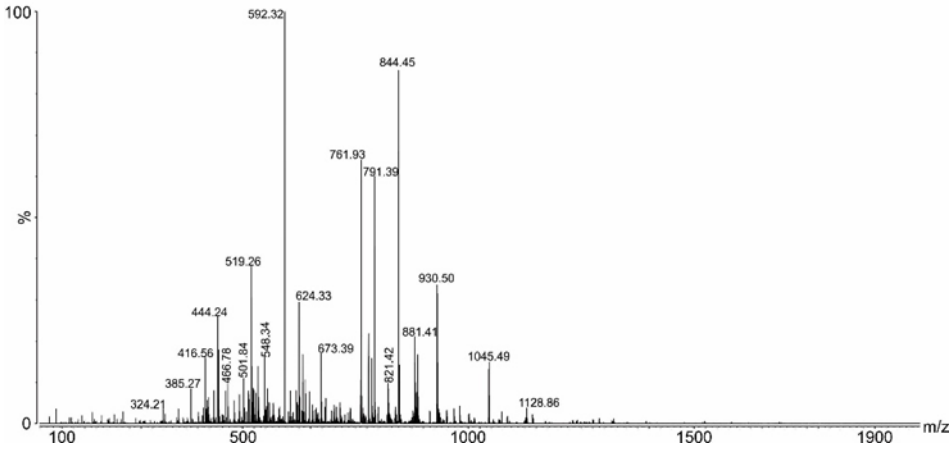

Figure 41. Online nanoLC-ESI-MS^E spectrum of digested egg white solution (Solution 6). 100 fmol/l in 0.2 M ammonium acetate, pH 6.7, with 2% of acetonitrile and 0.1% of formic acid as co-solvents.

Obtained raw data from online nanoLC-ESI-MS^E measurement provided 12877 low energy ions (mostly precursor ions) and 228395 high energy ions (mostly fragment ions). From them 8780 low energy ions and 228963 high energy ions were assigned using the PLGS data analysis software package. After removing redundancy from the protein hit list leaves 30 protein entries (Supporting info chapter 5.5 Table S 40) and 10 proteins are correlated with the organism *Gallus gallus*: Ovalbumin, Ovomucoid, Serpin domain, Alpha-1-acid glycoprotein, Folate_rec domain, Gallin protein, Lysozyme C, Ovoinhibitor, Ovotransferrin and Riboflavin-binding protein (Supporting info chapter 5.5 Table S 41).

The raw data were also subjected to peptide assignment using the BiopharmaLynx software package (set-up in Supporting info chapter

5.4 Table S 36) and provided an Ovalbumin sequence coverage of 100% (Figure S 14 in supporting info chapter 5.5)

Offline nanoESI-MS analysis

The digested egg white solution (Solution 8) was also subjected to offline nanoESI mass spectrometry (Figure 42) as reported (Chapter 3.6.6).

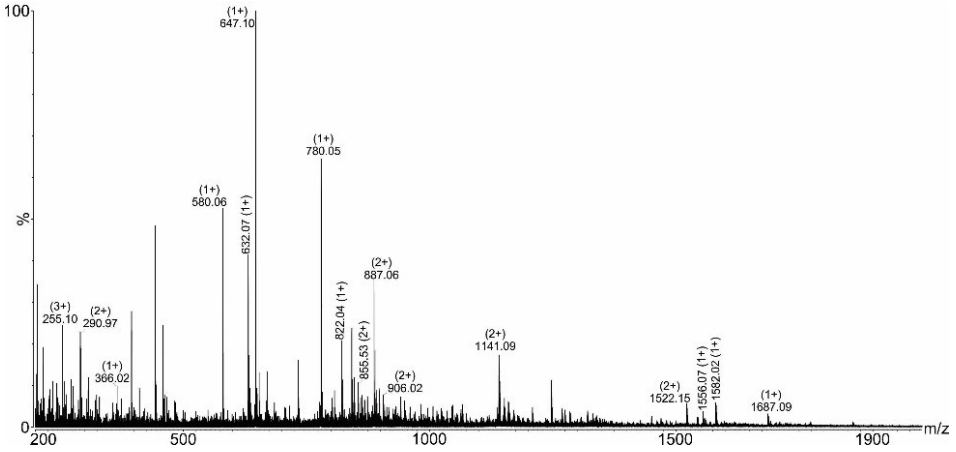

Figure 42. Offline nanoESI mass spectrum of digested egg white solution (Solution 8). Ion signals are labelled with m/z values and charge states are given in parentheses. Peptide concentration is 0.25 µg/µl. Solvent: 200 mM ammonium acetate, pH 6.7.

The mass spectrum shows 15 ion signals which were matched (Table 16) to the calculated masses from the in-silico digested Ovalbumin (list of obtained calculated peptides for Ovalbumin solution by GPMAW in supporting info chapter 5.4 Table S 37, used set-up Table S 36).

Table 16. Match between Ovalbumin calculated peptides and egg white digested (Solution 8) peptides from offline nanoESI mass spectrum

Amino acid sequence	Experimental m/z value	Charge state	Calculated m/z value	Peptide amino acid sequence
1-16	906.02	905.52	2+	GSIGAASMEFCFDVFK
56-61	255.1	255.31	3+	VVRFDK
85-104	1141.09	1141.77	2+	DILNQITKPNDVYSFSLASR
85-110	1522.15	1522.68	2+	DILNQITKPNDVYSFSLASRLYAEER
105-110	780.05	780.84	1+	LYAEER
123-126	580.06	580.65	1+	ELYR
123-126	290.97	290.83	2+	ELYR
127-142	1687.09	1687.84	1+	GGLEPINFQTAADQAR
182-186	632.07	632.73	1+	GLWEK
187-189	366.02	365.45	1+	AFK
187-199	1556.07	1556.72	1+	AFKDEDTQAMPFR
219-226	822.04	822.95	1+	VASMASEK
264-277	855.53	855.95	2+	LTEWTSSNVMEERK
264-276	1582.02	1582.71	1+	LTEWTSSNVMEER
280-284	647.1	647.79	1+	VYLPR
323-339	887.06	887.96	2+	ISQAVHAAHAEINEAGR

The Ovalbumin sequence coverage is 33.76%.

3.7.4. Immune complexes - analyses with Western blotting

Anti-Ovalbumin antibody concentration still enough to be recognised by secondary antibody in Western blot (Supporting info chapter 5.3 Figure S 7). Anti-Ovalbumin antibody-containing IgG from converted serum (Solution 4) was compared using SDS-PAGE (Supporting info chapter 5.3, Figure S 8), by loading on the gel converted rabbit serum solution (Solution 3) and R1 replicate 3 (Solution 9), the electrophoresis was performed as reported previously (Chapter 3.3.2).

Converted serum solution; anti-Ovalbumin antibody-containing IgG solution after extraction from converted serum, and IgG from rabbit serum (R1, replicate 3) solution (respectively Solutions 3, 4 and 9)

were used as primary antibody sources in another Western blot analyses (Figure 43).

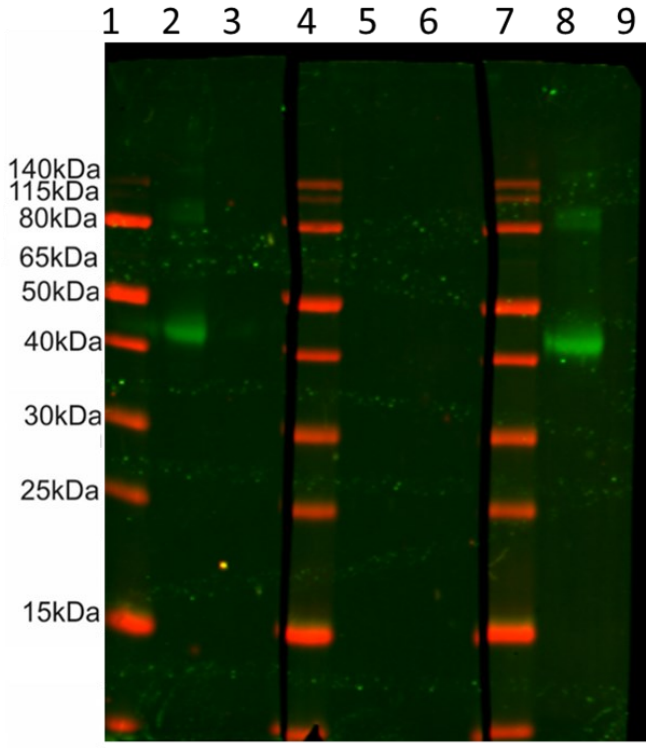

Figure 43. Western Blot with Ovalbumin solution (Solution 5). Lane 1: Apparent molecular mass marker; Lane 2: Ovalbumin band decorated with anti-Ovalbumin antibody as part of IgG solution extracted from rabbit serum with spiked in anti-Ovalbumin antibody (primary antibody; Solution 4). Lane 3: Empty; Lane 4: Apparent molecular mass marker; Lane 5: Ovalbumin band exposed to IgG solution extracted from rabbit serum (primary antibody; Solution 9); Lane 6: Empty; Lane 7: Apparent molecular mass marker; Lane 8: Ovalbumin band decorated with anti-Ovalbumin antibody as part of rabbit serum (primary antibody; Solution 3); Lane 9: Empty. Secondary antibody: Polyclonal antiMouse-IgG antibody from goat IRDye® 800 CW.

The green fluorescing band at the apparent mass between 40 and 50 kDa in lane 2 where Ovalbumin was loaded on the gel, transferred to the membrane and treated with the primary antibody solution which contains IgG extracted from rabbit serum spiked-in anti-Ovalbumin antibody (Solution 4), proves that the amount of anti-Ovalbumin antibody that "survived" the extraction process was enough to (i) decorate the Ovalbumin on the membrane and (ii) to be recognized by the

secondary antibody antiMouse-IgG antibody from goat IRDye® 800 CW. No bands are decorated in lane 5 which means that the loaded Ovalbumin was not recognized by any IgGs extracted from the rabbit serum. The green fluorescing band at the apparent mass between 40 and 50 kDa in lane 8 suggest that the Ovalbumin (ca. 45 kDa) loaded on the gel was transferred onto the membrane. During the Primary antibody treatment with serum into which was spiked-in with anti-Ovalbumin antibody (Solution 3), Ovalbumin was recognised by the anti-Ovalbumin antibody and the anti-Ovalbumin antibody was afterwards recognised by the Secondary antibody antiMouse-IgG antibody from goat IRDye® 800 CW.

Another Western Blot analysis was performed (Figure 44) by loading on the gel the diluted egg white solution (Solution 5) (chapter 3.6.4).

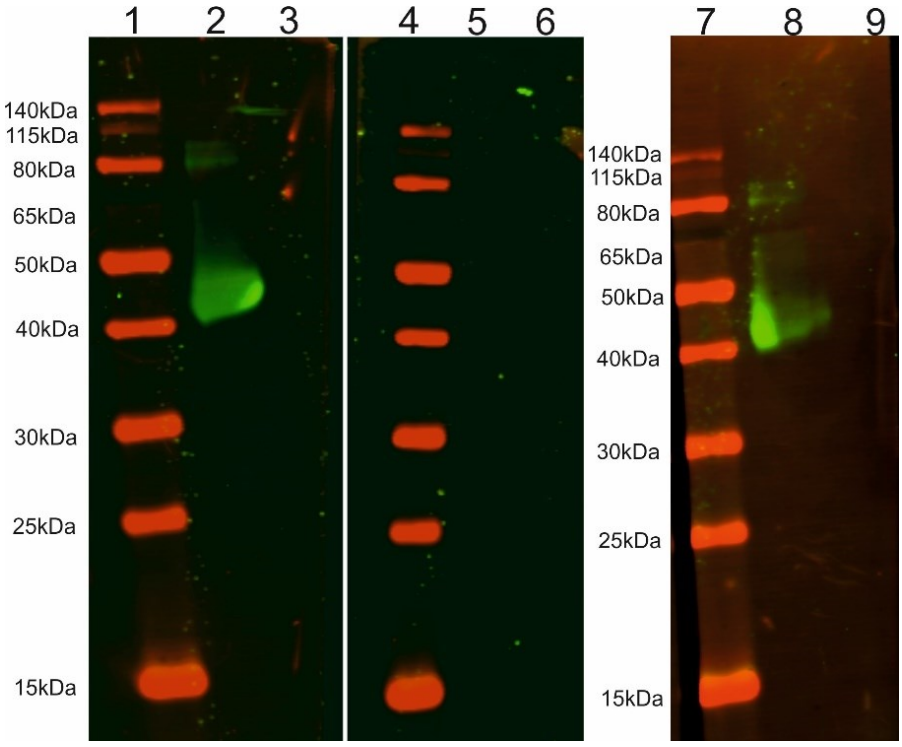

Figure 44. Western Blot with egg white solution (Solution 7). The same experiment was repeated as reported before but this time loading on the gel, instead of Ovalbumin, a solution constituted by 2 µl of egg white 0.75 µg/µl (Solution 7) mixed with, 14 µl of deionized water and 4 µl of Non reducing buffer. Lane 1: Apparent molecular mass marker; Lane 2: Ovalbumin band decorated with anti-Ovalbumin antibody as part of IgG solution extracted from rabbit serum with spiked in anti-Ovalbumin antibody (primary antibody; Solution 4). Lane 3: Empty; Lane 4: Apparent molecular mass marker; Lane 5: Ovalbumin band exposed to IgG solution extracted from rabbit serum (primary antibody; Solution 9); Lane 6: Empty; Lane 7: Apparent molecular mass marker; Lane 8: Ovalbumin band decorated with anti-Ovalbumin antibody as part of rabbit serum (primary antibody; Solution 3); Lane 9: Empty. Secondary antibody: Polyclonal antiMouse-IgG antibody from goat IRDye® 800 CW

The green fluorescing band at the apparent mass between 40 and 50 kDa in line 2 where Ovalbumin from egg white was transferred to the membrane and treated with the Primary antibody solution whit IgGs extracted from rabbit serum spiked in with anti-Ovalbumin antibody solution (Solution 4), proves that the amount of anti-Ovalbumin antibody that "survived" the extraction process was enough to (i) decorate the Ovalbumin (contained in the egg white) on the membrane and (ii) to be recognized by the secondary antibody antiMouse-IgG

antibody from goat IRDye® 800 CW. No bands are present in line 5, it means that the loaded Ovalbumin contained in egg white was not recognized by any IgGs extracted from the rabbit serum, indeed Primary Antibody with IgGs extracted from rabbit serum solution (Solution 9) was used. Therefor no substrate was available for the Secondary antibody antiMouse-IgG antibody from goat IRDye® 800 CW. The green fluorescing band at the apparent mass between 40 and 50 kDa in line 8 suggest that the Ovalbumin present into egg white, which was loaded on the gel, was transferred to the membrane, during the Primary antibody with serum mixed with anti-Ovalbumin antibody (Solution 3) treatment, Ovalbumin was recognized by anti-Ovalbumin antibody, and it was afterwards recognized by the Secondary antibody antiMouse-IgG antibody from goat IRDye® 800 CW.

3.7.5. Immune complexes - analyses with ITEM

Quadrupole transmission: to perform ITEM experiments the value of quadrupole transmission blocking was m/z 2000. In this way ions having value less than m/z 1400 cannot reach the detector. Between m/z 1400 and m/z 2000 some ions can reach the detector despite blocking settings and as a result the baseline intensity increases (Figure 47). The number of ions that reach the detector despite blocking quadrupole transmission can change based on the peptide concentration of the sprayed solution, on the vacuum gradient, and on the applied collision cell voltage difference.

Positive Control 1 : Peptide mix from digested Ovalbumin (Solution 6) plus anti-Ovalbumin antibody solution (Solution 1)

The comparison between offline nanoESI mass spectra collected with the collision cell voltage difference (ΔCV) at 3 V and 10 V, respectively, was done (Figure 45).

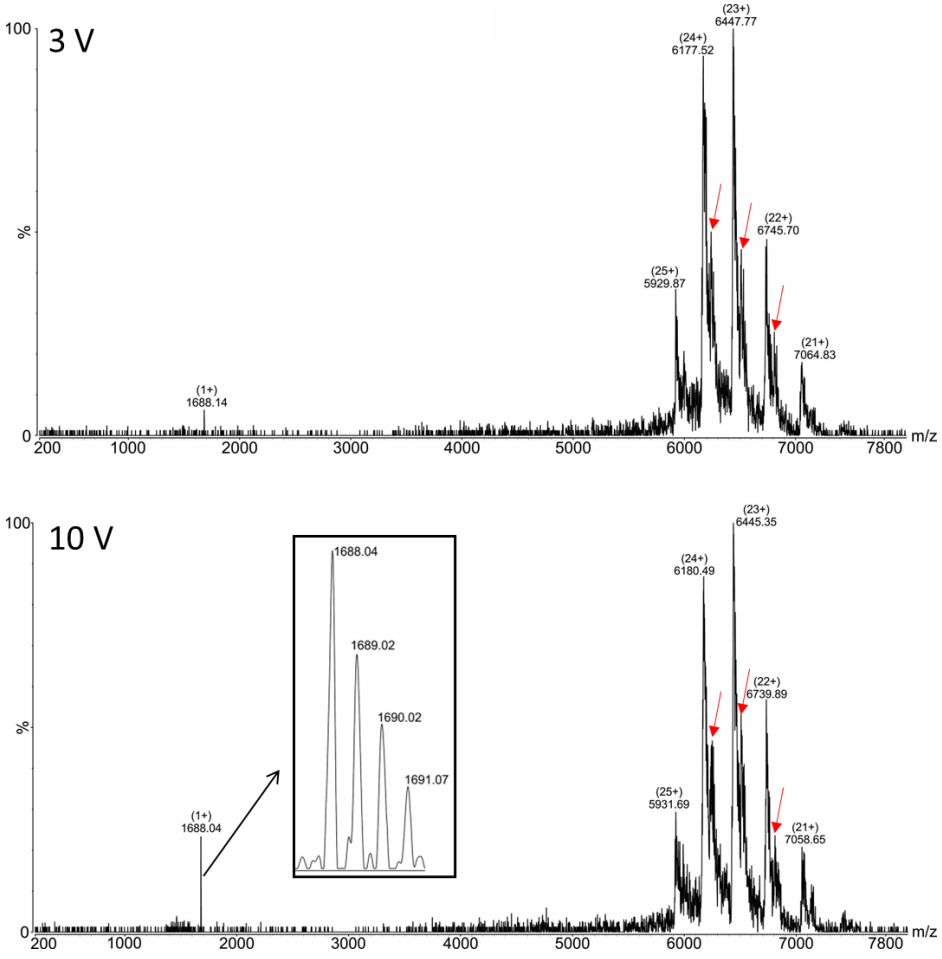

Figure 45. ITEM analysis of immune complex containing solution formed by the anti-Ovalbumin antibody plus digested Ovalbumin (Solution 1 + Solution 6). Antibody concentration: 0.21 µg/µl, antigen concentration 0.013 µg/µl. Antibody ion signals are labelled with m/z values and charge states are given in parentheses. Multiply charged satellite ion signals (marked with red arrows) indicate immune complex formation. Solvent: 200 mM ammonium acetate, pH 6.7. The insert shows a zoom of the isotope-resolved ion signal at m/z 1688.04.

By increasing the collision cell voltage difference (ΔCV), the singly charged ion signal at m/z 1688.04 increases in intensity. The isotope pattern shows that the signal is from a peptide and it is singly charged. Identification of the respective peptide aa127-142 from Ovalbumin (GGLEPINFQTAADQAR) was done by comparing this ion signal with the entries of the list of calculated masses from digested Ovalbumin (Supporting info chapter 5.4 Table S 37), and by comparison to mass spectra from offline nanoESI mass analysis of digested Ovalbumin solution (Solution 6) (Figure 40). The antibody ion signals are accompanied by satellite ion signals (marked with red arrows), which indicates immune complex formation (Supporting info chapter 5.6 Figure S 16 and Table S 42).

The immune complex-containing solution was prepared by mixing anti-Ovalbumin antibody solution (solution 1) and digested Ovalbumin peptide-containing solution (Solution 6). Then, ITEM experiments were conducted as reported (Chapter 3.6.7). The mass spectrum shows the typical pattern of multiply charged ion signals of anti-Ovalbumin antibody in the mass range between m/z 5500 and m/z 7500.

Test 1: Peptide mix from digested Ovalbumin (Solution 6) plus extracted IgG solution from serum mixed with anti-Ovalbumin antibody (Solution 2)

The comparison between offline nanoESI mass spectra collected with the collision cell voltage difference (ΔCV) at 3 V and 10 V was done (Figure 46).

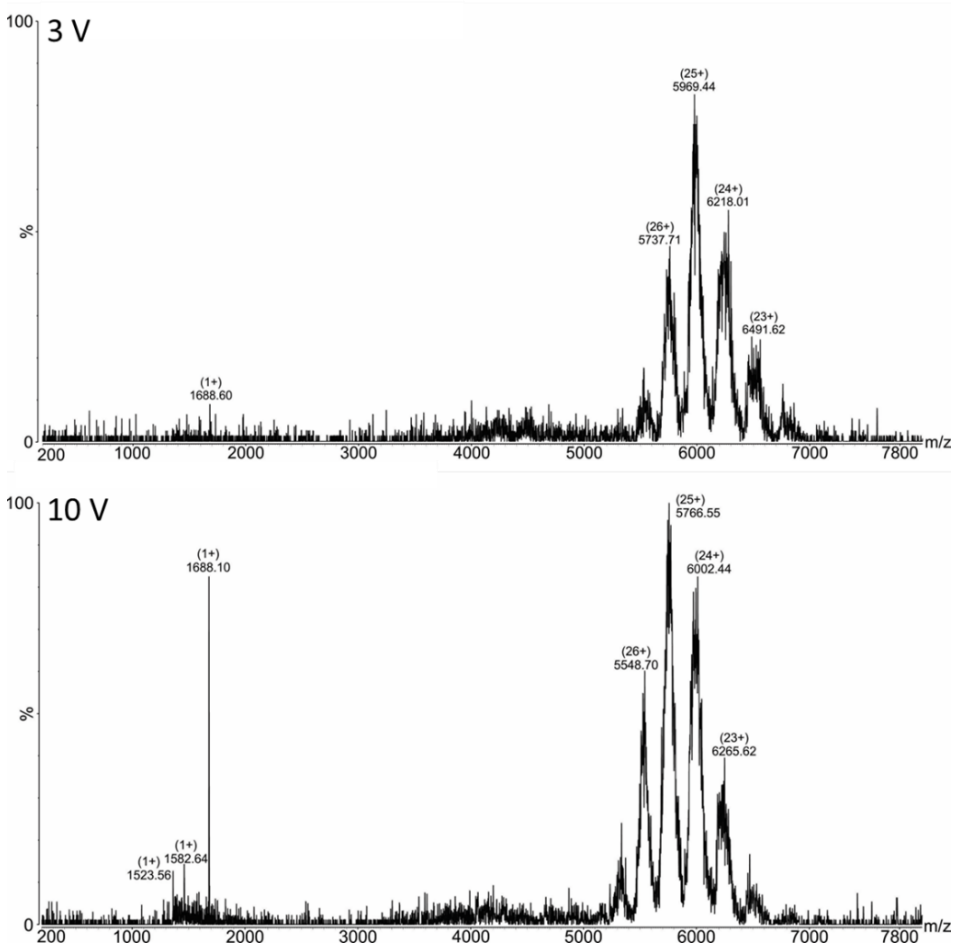

Figure 46. Test 1 ITEM experiment of IgGs extracted from rabbit serum + anti-Ovalbumin antibody + Ovalbumin digested (Solution 2 + Solution 6) respectively 0.27 µg/µl and 0.007 µg/µl. Ion signals are labelled with m/z values and charge states are given in parentheses. Solvent: 200 mM ammonium acetate, pH 6.7.

Even among other IgGs, the epitope releasing is detected by this method. This time antibody signals do not have the satellite signals because anti-Ovalbumin antibody concentration is lower than it was in the Positive Control 1. Signals identification was done by comparison against the calculated peptides from digested Ovalbumin (Supporting info chapter 5.4 Table S 37), and offline nanoESI mass spectrum of digested Ovalbumin solution (Solution 6) (Figure 40), all of them are identified as Ovalbumin peptides (Table 17).

Table 17. Signals identification in Test 1 of IgGs extracted from rabbit serum + anti-Ovalbumin antibody + Ovalbumin digested (Solution 2 + Solution 6)

From	To	MS 3V	MS 10 V	nanoESI mass spectrum of digested Ovalbumin (Solution 6)	Calculated MS	Charge	Sequence
111	122		1523.56	1523.14	1522.81	1+	YPILPEYLQCVK
127	142	1688.60	1688.10	1687.12	1687.84	1+	GGLEPINFQTAADQAR
264	276		1582.64	1582.02	1582.71	1+	LTEWTSSNVMEER

The immune complex containing solution was prepared by mixing an IgG solution which was extracted from rabbit serum and into which had been spiked-in an anti-Ovalbumin antibody solution (Solution 2) and to which was added a solution with peptides from Ovalbumin digestion (Solution 6). The ITEM experiments were conducted as reported (Chapter 3.6.7). The mass spectrum shows the antibodies typical pattern of multiply charged ion signals.

TEST 2: Peptide mix from digested Ovalbumin (Solution 6) plus extracted IgG solution from with anti-Ovalbumin antibody converted serum (Solution 4)

The comparison between spectra collected with collision cell voltage difference (ΔCV) at 3 V and 10 V was done (Figure 47).

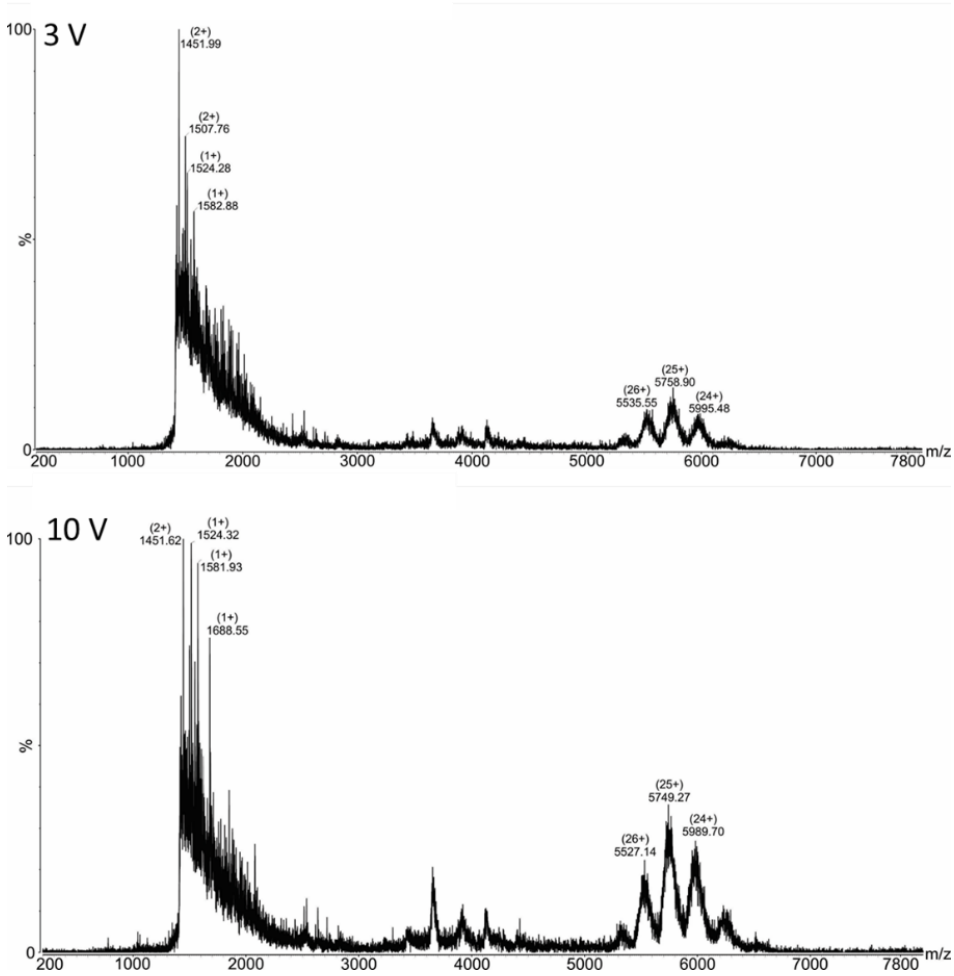

Figure 47. Test 2 ITEM experiment of IgGs extracted from rabbit serum spiked in with anti-Ovalbumin antibody + Ovalbumin digested (Solution 4 + Solution 6) respectively 0.63 µg/µl and 0.18 µg/µl. Ion signals are labelled with m/z values and charge states are given in parentheses. Solvent: 200 mM ammonium acetate, pH 6.7.

Increasing the collision cell voltage difference (ΔCV) to 10 V the epitope popped out. Epitope determination using ITEM experiment

worked even increasing the complexity of condition. Complex formation was also demonstrated by Western Blot (Figure 43 line 2). This time anti-Ovalbumin antibody was extracted together with different IgGs from rabbit serum, its concentration estimated after extraction and complex preparation was only 0.007 µg/µl out of a total IgGs concentration of 0.63 µg/µl. At low m/z value the noise is very high because of the high concentration of digested ovalbumin peptides (Solution 6). These signals can be related to Ovalbumin peptides (Table 18) using calculated peptides from digested Ovalbumin (Supporting info chapter 5.4 Table S 37) and offline nanoESI mass spectrum of digested Ovalbumin solution (Solution 6) (Figure 40).

Table 18. Signals identification in Test 2 of IgGs extracted from rabbit serum spiked in with anti-Ovalbumin antibody + Ovalbumin digested (Solution 4 + Solution 6)

From	To	MS 3V	MS 10 V	nano ESI mass spectrum of digested Ovalbumin (Solution 6)	Calculated MS	Charge	Sequence
59	84	1451.99	1451.62	1450.97	1452.03	2+	FDKLPGFGDSIEAQCGTSVNVHSSLR
111	122	1524.28	1524.32	1523.14	1523.81	1+	YPILPEYLQCVK
127	142		1688.55	1687.12	1687.84	1+	GGLEPINFQTAADQAR
264	276	1582.88	1581.93	1582.02	1582.71	1+	LTEWTSSNVMEER
360	385	1507.76	1507.79		1510.27	2+	ADHPFLFCIKHIATNAVLFFGRCVSP

Test 2 solution was prepared mixing IgGs extracted from rabbit serum spiked in with anti-Ovalbumin antibody and Ovalbumin digested (Solution 4 and 6) and the ITEM experiments were conducted as reported before (Chapter 3.6.7). The mass spectrum shows the antibodies typical pattern of multiply charged ion signals The from the multiply charged ion signals determined average molecular mass of the antibodies is 143705.06 ± 24.62 Da. This time is possible to see signals, between m/z 3500 and m/z 4500, correlated with Albumin and Transthyretin that still contaminate IgG extracted from converted serum solution (Solution 4) after IgGs extraction.

Negative Control 1: Peptide mix from digested Ovalbumin (Solution 6) plus extracted IgG solution from serum (Solution 9)

The comparison between spectra which were collected with the collision cell voltage difference (ΔCV) at 3 V and 10 V was done (Figure 48).

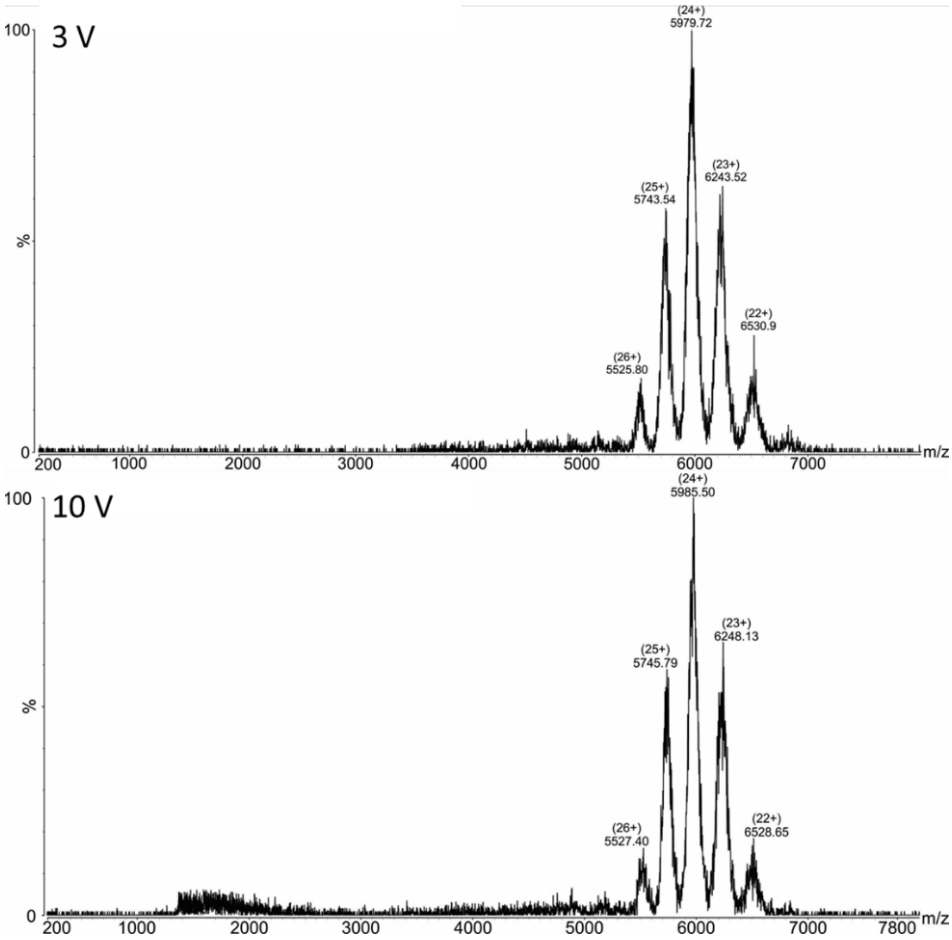

Figure 48. Negative Control 1 ITEM experiment of IgGs extracted from rabbit serum + Ovalbumin digested (Solution 9 + Solution 6) respectively 0.19 µg/µl and 0.011 µg/µl. Ion signals are labelled with m/z values and charge states are given in parentheses. Solvent: 200 mM ammonium acetate, pH 6.7.

As expected, since into IgGs extracted from rabbit serum (Solution 9) there are not antibodies able to bind Ovalbumin, as it was also

demonstrated by Western Blot (Figure 43 line 5), no epitope was found.

The negative control experiment was performed by preparing a solution with mixing IgGs extracted from rabbit serum (Solution 9) and digested Ovalbumin solution (Solution 6). Then, the ITEM experiment was conducted as reported before (Chapter 3.6.7). The mass spectrum shows antibodies typical pattern of multiply charged ion signals.

Positive Control 2: Peptide mix from digested egg white (Solution 8) plus anti-Ovalbumin antibody solution (Solution 1)

The comparison between spectra collected with collision cell voltage difference (ΔCV) at 3 V and 10 V was done (Figure 49).

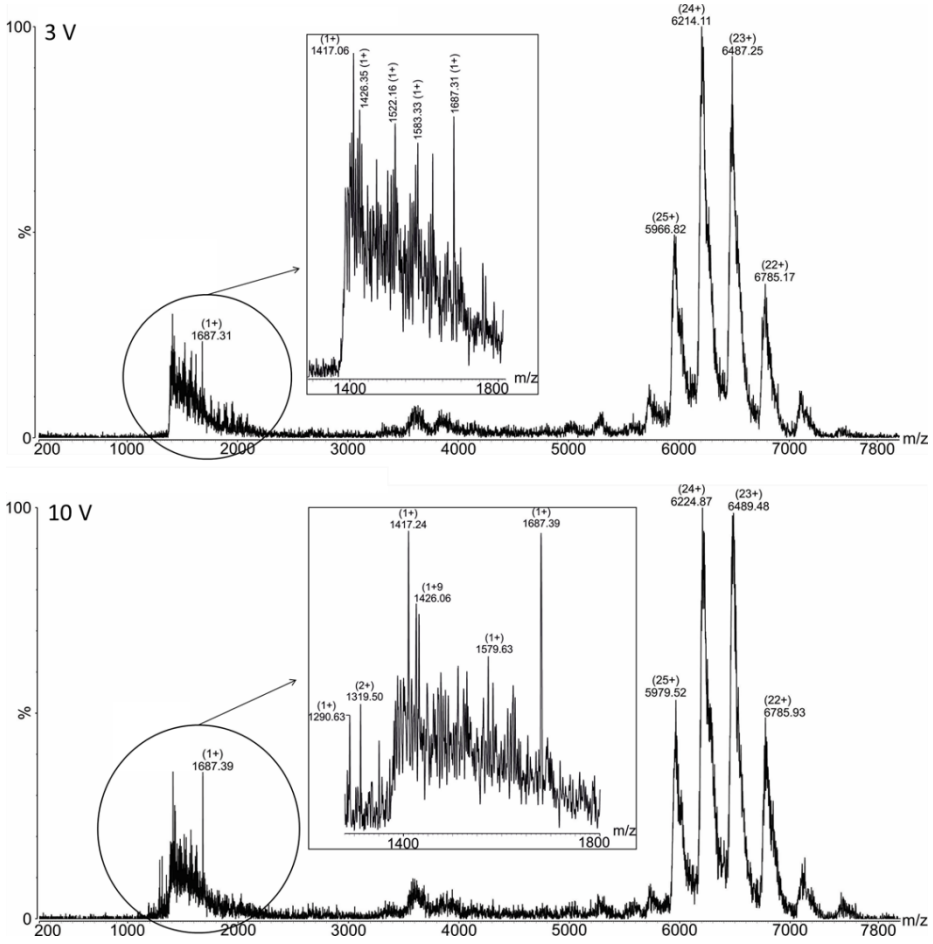

Figure 49. Positive Control 2 ITEM experiment of anti-Ovalbumin antibody + egg white digested (Solution 1 + Solution 8) respectively 0.21 µg/µl and 0.013 µg/µl. Ion signals are labelled with m/z values and charge states are given in parentheses. Solvent: 200 mM ammonium acetate, pH 6.7. The insert shows a zoom of the peptides ion signals between m/z 1300 and m/z 1800.

Increasing the collision cell voltage, only the epitope signal at m/z 1687.39 increase in intensity. These signals can be related (Table 19) with calculated peptides from digested Ovalbumin (Supporting info

chapter 5.4 Table S 37), and signal at ca. m/z 1319 with a peptide present in digested egg white (Solution 8) offline nanoESI mass spectrum (Figure 42 and zoomed spectrum in Supporting info chapter 5.6. Figure S 17). Epitope determination using ITEM experiment worked even increasing the conditions complexity. This time the epitope was among different peptides from digested egg white solution.

Table 19. Signals identification in Positive Control 2 of anti-Ovalbumin antibody + egg white digested (Solution 1 + Solution 8)

From	To	MS 3V	MS 10 V	nano ESI mass spectrum of digested Ovalbumin (Solution 6)	Calculated MS	Charge	Sequence
47	58	1417.06	1417.24		1417.59	1+	DSTRTQINKVVR
111	122	1522.16		1522.15	1522.81	1+	YPILPEYLQCVK
127	142	1687.31	1687.39	1687.09	1687.84	1+	GGLEPINFQTAADQAR
264	284		1290.63		1290.99	2+	LTEWTSSNVMEERKIKVYLPR
264	276	1583.33	1579.63	1582.02	1582.71	1+	LTEWTSSNVMEER
280	290	1426.35	1426.06		1424.75	1+	VYLPRMKMEEK
			1319.50	1320.99		1+	

Positive Control 2 solution was prepared mixing anti-Ovalbumin antibody and egg white digested (Solution 1 and 8) and the ITEM experiments were conducted as reported before (Chapter 3.6.7). As reported previously (Chapter 3.7.1) the mass spectrum shows for anti-Ovalbumin antibody the antibodies typical pattern of multiply charged ion signals. The from the multiply charged ion signals determined molecular mass of the antibody is 149292.13 ± 71.90 Da.

Negative Control 2: Peptide mix from digested egg white (solution 8) plus extracted IgG solution from serum (Solution 9)

The comparison between spectra collected with collision cell voltage difference (ΔCV) at 3 V and 10 V was done (Figure 50).

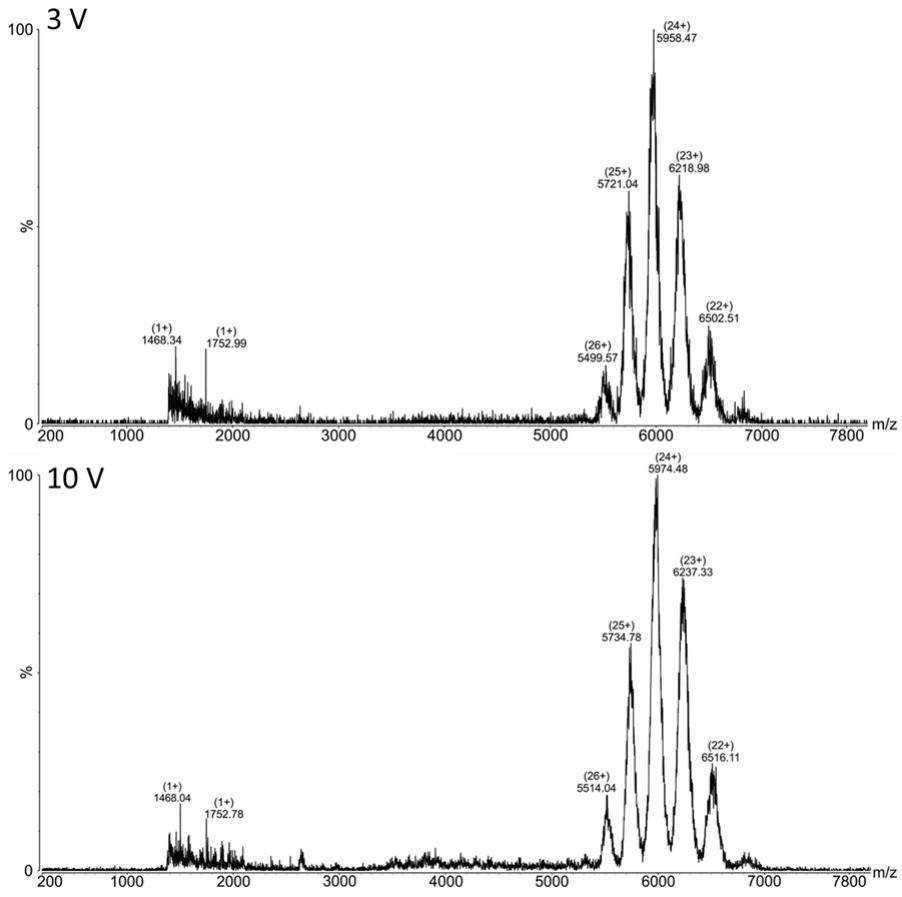

Figure 50. Negative Control 2 ITEM experiment of IgGs extracted from rabbit serum + egg white digested (Solution 9 + Solution 8) respectively 0.23 µg/µl and 0.017 µg/µl. Ion signals are labelled with m/z values and charge states are given in parentheses. Solvent: 200 mM ammonium acetate, pH 6.7.

No epitope was found. Signal at ca. m/z 1752 can be related to an Ovalbumin peptide (using calculated peptides from digested Ovalbumin reported in Supporting info chapter 5.4 Table S 37), and signal at ca. m/z 1468 is related to one of the peptides present in digested

egg white (offline nanoESI mass spectrum of Solution 8 in Figure 42 and zoomed spectra in Supporting info chapter 5.6. Figure S 17). Both of them does not increase by increasing the collision cell voltage difference (Table 20).

Table 20. Signal identification in Negative Control 2 of IgGs extracted from rabbit serum + egg white digested (Solution 9 + Solution 8)

From	To	MS 3V	MS 10 V	nano ESI mass spectrum of digested Ovalbumin (Solution 6)	Calculated MS	Charge	Sequence
1	16	1752.99	1752.78		1750.99	1+	GSIGAASMEFCFDVFK
		1468.34	1468.04	1470.01		1+	

Negative Control 2 solution was prepared mixing IgGs extracted from rabbit serum and egg white digested (Solution 9 and 8) and the ITEM experiments were conducted (Chapter 3.6.7). As reported previously (Chapter 3.7.1) the mass spectrum shows antibodies typical pattern of multiply charged ion signals. The from the multiply charged ion signals determined average molecular mass of the antibodies is 143363.01 ± 42.19 Da. As expected, since into IgGs extracted from rabbit serum (Solution 9) there are not antibodies able to bind the Ovalbumin contained into egg white, as it was also demonstrated by Western Blot (Figure 44 line 5).

3.8. Conclusions: Development of an MS-based method for determining serum conversion and epitope mapping (Section 2)

The here developed extraction method provides IgGs from rabbit serum in high purity. Most important, the obtained solution is sufficiently pure and concentrated to be directly used for SDS-PAGE, Western Blot, and ESI-MS measurements without further manipulation. The average estimated IgG recovery was 5.7%. When murine anti-Ovalbumin antibody had been spiked-in into rabbit serum prior to antibody extraction, antibody solutions with an estimated concentration of anti-Ovalbumin antibody of 11 ng/µl had been obtained. The bands in the Coomassie brilliant blue stained SDS gel and the ion signals in the offline nanoESI-MS spectrum, both confirm that this from serum extracted solution contains predominantly IgGs and only small amounts of serum albumin and transthyretin as contaminants. The Western Blots suggest that the spike-in seroconversion of the rabbit serum was successful. In all examined assays we can see that only solutions which (i) contain IgGs extracted from rabbit serum after spike-in of Anti-Ovalbumin antibody (solution 4) or (ii) serum with spiked-in Anti-Ovalbumin antibody (Solution 3) generate upon SDS PAGE protein bands which in Western blots were decorated by the antiMouse-IgG from goat IRDye® 800 CW. More importantly, converted serum (Solution 3) and IgG extracted from rabbit converted serum solution (Solution 4) can be applied to decorate (i) commercial Ovalbumin as well as (ii) egg white-derived Ovalbumin which upon SDS PAGE had been directly transferred onto a PVDF membranes and were subjected to Western blot analysis. IgG from rabbit serum solution R1 replicate 3

(Solution 9) which contains just the extracted IgGs from rabbit serum does not contain antibodies which were recognized by the antiMouse-IgG from goat IRDye® 800 CW.

The epitope on the surface of Ovalbumin which is engaged in the immune complex formation between Ovalbumin and the anti-Ovalbumin antibody was identified using ITEM experiments.

The by ITEM detected peptide ion signal at ca. m/z 1688 fits with a peptide ion signal which is also seen in mass spectra of a mixture of peptides from digested Ovalbumin (Solution 6). Comparing this experimentally determined peptide mass with the calculated peptide masses of tryptically digested Ovalbumin identifies the epitope peptide sequence as GGLEPINFQTAADQAR. When performing ITEM analyses, the ion signal at m/z 1688 is the only one that increases in intensity with increasing collision cell voltage difference (ΔCV), because more energy is given to the immune complex dissociation reaction and, hence, more epitope peptide ions are released from it.

Of note, the epitope peptide was still found at low concentration of the anti-Ovalbumin antibody (estimated at 7 ng/µl) and even when the anti-Ovalbumin antibody was applied as one among other IgGs from rabbit serum. Consistent with the above mentioned results, the epitope peptide was also found in the mass spectra recorded under ITEM conditions when using anti-Ovalbumin antibody (Solution 1) which was exposed to digested egg white protein/peptide mixtures (Solution 8). Here, the epitope peptide with m/z 1688 (GGLEPINFQTAADQAR) could be identified even as one among other peptides from other proteins.

Positive controls, where the anti-Ovalbumin antibody (Solution 1) was mixed with digested Ovalbumin (Solution 6) or with digested egg white (Solution 8) showed that the IgG ion signals were accompanied by satellite ion signals, according with complex formation, with average differences between two ion signals of the same charge state which fits to the epitope peptide mass.

3.9. Future prospects: Development of an MS-based method for determining serum conversion and epitope mapping (Section 2)

The here developed IgG extraction method can be applied also for investigations of IgG from human blood serum to generate IgG solutions ready to be used in MS investigations, electrophoresis, and immune assay such as Western blot.

Seroconversion analysis is of importance for determining antibody titres of known antigens. Then it should be possible to detect if a specific antibody is present in a blood sample of an individual by epitope release. This kind of analysis allows to monitor the presence of specific antibodies after infections or vaccinations.

In case of food allergies, specific antibodies can be extracted from serum or other body fluids (e.g. sputum, tears, mucosal swabs, etc.) and the obtained antibody solutions can be used for epitope identification by ITEM experiments as well.

Once an epitope is identified respective peptides can be synthetized to see if changing the amino acids one by one influences the binding strength. This information can be useful for investigations where it shall be interrogated which possible genetic modification / mutation on the allergen produces which antigen – antibody interaction. In this way

one can promote the synthesis of an antigen-related but now harmless protein that is not recognised by the allergen-inducing antibody, thereby avoiding an allergic episode even upon exposure to the respective modified target protein.

Epitope mapping by ITEM investigations can be further developed to allow multiplexing, i. e. the ITEM experiment might be performed by mixing one specific antibody with other antibodies which are also able to bind to the same antigen. Then ITEM experiments identified at the same time two different immune complexes by release of either the same epitope peptide or more.

4. Acknowledgment

Thanks to:

Michael O. Glocker for guiding me, professionally supporting my work, teaching me on a daily basis during my final Ph.D. year, critically reading the thesis, giving me access to his laboratory, sharing his experiences and being a mentor.

Claudia Röwer for helping me with online nanoLC-ESI-MS^E spectrometer and ITEM experiments.

Kira Billinger for sharing her knowledge on Electrophoresis and Western blot.

Cornelia Koy for helping me with offline nanoESI-MS spectrometer.

Elias Projahn for providing his expertise on bioinformatic analysis.

Stefan Mikkat for providing his expertise on online nanoLC-ESI-MS^E spectrometer measurements.

Manuela Ruβ for sharing her knowledge on many laboratories procedure.

Giovanna Cafiso for critically reading the thesis.

Ilenia Abbate and Elena Solfato for guiding me, professionally support my work, and for critically reading the thesis.

Donato Spina for professionally support my work and for sharing his knowledge on HPLC and HPLC/MS methods.

Rosaria Saletti for guiding me, professionally support my work, sharing her expertise on proteomic field and for critically reading the thesis.

Valentina Giglio for providing her expertise on Fusion Tribrid mass spectrometer.

Antonella di Francesco for sharing her knowledge in proteomic field.

Salvatore Foti and Vincenzo Cunsolo for professionally support my work and sharing their expertise on proteomic.

5. Supporting info

5.1. Proteomic analysis (1B)

Table S 1. Identified proteins in Untreated rabbit 1, right eye.

Protein Group	Accession	-10lgP	Coverage (%)	Peptides	Unique	Avg. Mass
1	P01832|PIGR_RABIT	412.15	48	41	41	83887
2	P19134|TRFE_RABIT	351.24	48	33	31	76670
3	P19007|HPT_RABIT	322.28	61	19	14	38869
4	P49065|ALBU_RABIT	333.24	49	24	24	68910
5	P60990|PIP_RABIT	233.51	61	14	14	16871
8	Q95218|DMBT1_RABIT	270.71	15	14	14	172763
9	P51662|ANXA1_RABIT	284.02	50	14	14	38735
11	P23108|IGJ_RABIT	213.46	60	7	7	15556
13	P29751|ACTB_RABIT	232.11	36	8	5	41756
14	P01879|IGHA_RABIT	265.64	39	8	8	32256
16	Q9XSC5|CLUS_RABIT	227.18	20	9	9	51851
17	Q8MI17|AL1A1_RABIT	224.65	23	8	8	54341
20	Q29426|K2C3_RABIT	197.58	17	9	5	64341
21	P01870|IGHG_RABIT	179.06	28	4	4	35404
31	P39056|OSTCN_RABIT	175.55	90	5	5	5431
32	C0HJA6|OBP2_RABIT	119.82	61	3	3	1831
33	C0HJA9|OBP3_RABIT	147	58	2	2	4721
35	Q9TTC6|PPIA_RABIT	138.66	37	5	5	17837
36	P68135|ACTS_RABIT	169.11	14	4	1	42051
36	P62740|ACTA_RABIT	169.11	14	4	1	42009
38	P68105|EF1A1_RABIT	155.62	15	5	5	50141
38	Q71V39|EF1A2_RABIT	100.87	7	3	3	50470
43	Q6Q6X0|1433T_RABIT	107.67	10	2	2	27778
44	O97862|CYTC_RABIT	127.1	25	4	4	16346
47	P46406|G3P_RABIT	162.62	14	3	3	35780
50	P11974|KPYM_RABIT	137.74	13	5	5	58048
51	P01840|KAC4_RABIT	162.74	43	3	3	11043
53	P62160|CALM_RABIT	117.23	31	3	3	16838
56	P25704|ENOB_RABIT	159.11	11	3	3	47069
58	P46409|GSTMU_RABIT	136.89	27	4	4	25417
65	P13490|LDHB_RABIT	81.29	10	2	2	24134
66	P35543|SAA3_RABIT	136.94	13	2	2	13806
67	P01692|KV11_RABIT	110.52	17	2	2	9469
68	P24480|S10AB_RABIT	113.91	26	2	2	11429
69	Q28631|WFDC2_RABIT	120.59	33	2	2	12803
71	Q8WN94|ACBP_RABIT	120.36	39	2	2	9915
74	P80191|FETUA_RABIT	115.39	9	2	2	38387
85	P26890|IL1RA_RABIT	76.93	16	2	2	20214

Table S 2. Identified proteins in Untreated rabbit 1, left eye.

Protein Group	Accession	-10lgP	Coverage (%)	Peptides	Unique	Avg. Mass
1	P01832|PIGR_RABIT	413.48	48	45	45	83887
2	P19134|TRFE_RABIT	365.31	51	36	36	76670
3	P19007|HPT_RABIT	322.99	59	22	22	38869
4	P60990|PIP_RABIT	251.74	61	15	15	16871
5	P49065|ALBU_RABIT	318.2	47	24	24	68910
9	P01870|IGHG_RABIT	278.79	51	14	14	35404
10	Q95218|DMBT1_RABIT	251.78	15	15	15	172763
11	P51662|ANXA1_RABIT	293.1	51	15	15	38735
12	P23108|IGJ_RABIT	220.33	68	9	9	15556
14	P01879|IGHA_RABIT	267.48	39	12	12	32256
15	Q9XSC5|CLUS_RABIT	240.29	25	12	12	51851
17	Q8MI17|AL1A1_RABIT	226.24	20	8	8	54341
18	P29751|ACTB_RABIT	234.48	39	9	9	41756
18	P68135|ACTS_RABIT	166.35	13	4	4	42051
18	P62740|ACTA_RABIT	166.35	13	4	4	42009
20	C0HJA6|OBP2_RABIT	119.87	61	3	3	1831
25	P01840|KAC4_RABIT	188.33	41	3	3	11043
26	P30801|S10A6_RABIT	133.52	59	5	5	10154
28	Q29426|K2C3_RABIT	170.08	10	5	3	64341
30	P46406|G3P_RABIT	225.69	29	6	6	35780
31	P39056|OSTCN_RABIT	167.05	90	5	5	5431
33	P13491|LDHA_RABIT	162.59	27	7	6	36565
34	Q9TTC6|PPIA_RABIT	145.93	43	6	6	17837
36	P13490|LDHB_RABIT	145.87	22	4	3	24134
38	P68105|EF1A1_RABIT	187.53	16	5	5	50141
38	Q71V39|EF1A2_RABIT	132.66	8	3	3	50470
41	Q6Q6X0|1433T_RABIT	122.13	22	4	4	27778
42	C0HJA9|OBP3_RABIT	163.12	58	3	3	4721
44	P46409|GSTMU_RABIT	135.5	20	3	3	25417
47	P25704|ENOB_RABIT	155.74	8	2	2	47069
49	Q08863|GSTA1_RABIT	147.86	18	4	4	25691
50	P62160|CALM_RABIT	132.01	31	3	3	16838
53	P16973|LYSC_RABIT	172.17	38	5	5	14722
57	P00939|TPIS_RABIT	136.68	33	5	5	26757
58	O97862|CYTC_RABIT	129.58	19	3	3	16346
59	P47845|LEG3_RABIT	105.88	16	3	3	25502
60	P31097|OSTP_RABIT	110.83	9	2	2	35172
63	Q28631|WFDC2_RABIT	112.8	33	2	2	12803
65	P24480|S10AB_RABIT	113.52	26	2	2	11429
67	P80508|PE2R_RABIT	112.06	10	2	2	36670
71	P80191|FETUA_RABIT	109.87	9	2	2	38387
72	P01692|KV11_RABIT	108.87	17	2	2	9469
73	P01696|KV15_RABIT	76.34	19	2	1	11596
74	P35543|SAA3_RABIT	130.84	13	2	2	13806
75	P01697|KV16_RABIT	67.92	18	2	1	12112
82	P08628|THIO_RABIT	88.57	27	2	2	11761

Table S 3. Identified proteins in Untreated rabbit 2, right eye.

Protein Group	Accession	-10lgP	Coverage (%)	Peptides	Unique	Avg. Mass
1	P49065|ALBU_RABIT	466.85	68	79	79	68910
2	P01832|PIGR_RABIT	455.13	52	59	59	83887
3	P19134|TRFE_RABIT	426.88	55	62	62	76670
4	P19007|HPT_RABIT	325.35	56	19	16	38869
5	P60990|PIP_RABIT	242.96	54	14	14	16871
6	P29751|ACTB_RABIT	300.56	46	13	1	41756
8	P51662|ANXA1_RABIT	332.22	56	21	21	38735
9	Q8MI17|AL1A1_RABIT	318.73	54	27	27	54341
13	P23108|IGJ_RABIT	236.7	74	12	12	15556
14	P68105|EF1A1_RABIT	281.74	43	15	15	50141
14	Q71V39|EF1A2_RABIT	212.15	19	6	6	50470
15	P46406|G3P_RABIT	264.72	42	13	13	35780
16	Q95218|DMBT1_RABIT	233.61	8	9	9	172763
17	P11974|KPYM_RABIT	268.88	34	15	15	58048
18	Q28640|HRG_RABIT	278.74	23	15	15	58877
19	P80191|FETUA_RABIT	277.69	49	9	9	38387
20	P01879|IGHA_RABIT	265.44	31	11	11	32256
21	P01870|IGHG_RABIT	239.73	42	9	9	35404
22	P09809|APOA1_RABIT	244.91	43	11	11	30591
25	P62740|ACTA_RABIT	203.74	19	6	1	42009
25	P68135|ACTS_RABIT	203.74	19	6	1	42051
26	Q9XSC5|CLUS_RABIT	248.31	25	12	12	51851
29	O97529|ANXA8_RABIT	226.93	34	8	8	36680
30	Q9TTC6|PPIA_RABIT	183.85	55	9	9	17837
32	P21195|PDIA1_RABIT	228.42	27	9	9	56808
33	P13491|LDHA_RABIT	180.28	29	8	7	36565
34	O77791|S10AC_RABIT	180.91	71	6	6	10668
35	Q29504|UBA1_RABIT	214.52	13	9	9	117688
36	Q8HZQ5|EZRI_RABIT	185.17	19	8	8	69220
41	Q6Q6X0|1433T_RABIT	183.56	27	5	5	27778
43	P00883|ALDOA_RABIT	213.66	39	8	8	39343
44	Q29426|K2C3_RABIT	199.04	17	9	5	64341
48	P30946|HS90A_RABIT	206.37	16	8	4	79733
49	P30947|HS90B_RABIT	203.52	19	9	5	83467
50	P00567|KCRB_RABIT	219.4	28	8	8	42663
51	P01840|KAC4_RABIT	224.02	94	5	5	11043
52	Q95MF9|CLIC1_RABIT	197.61	57	9	9	26925
53	P16973|LYSC_RABIT	195.42	45	6	6	14722
56	P30801|S10A6_RABIT	125.11	36	5	5	10154
57	P53789|VTDB_RABIT	162.91	26	7	7	52912
58	P20058|HEMO_RABIT	180.36	20	7	7	51767
59	P62160|CALM_RABIT	191.28	46	4	4	16838
63	Q28706|K1C12_RABIT	152.41	17	7	2	45727

65	P47845|LEG3_RABIT	143.78	22	4	4	25502
67	P46409|GSTMU_RABIT	175.39	22	4	4	25417
72	P25704|ENOB_RABIT	175.47	13	3	3	47069
75	O19049|HNRPK_RABIT	163.46	22	6	6	50960
76	P15122|ALDR_RABIT	132.49	21	4	4	35763
77	P13490|LDHB_RABIT	152.6	15	3	2	24134
78	O19048|PCBP1_RABIT	167.07	25	6	6	37498
81	P35543|SAA3_RABIT	167.7	13	2	2	13806
83	C0HJA6|OBP2_RABIT	106.72	61	2	2	1831
84	P14422|PA2GA_RABIT	130.67	40	3	3	7607
88	Q8WN94|ACBP_RABIT	188.52	60	4	4	9915
90	Q28631|WFDC2_RABIT	142.79	52	3	3	12803
91	C0HJA9|OBP3_RABIT	152.74	58	2	2	4721
94	Q28658|SPRR3_RABIT	137.39	27	3	3	24139
95	P10160|IF5A1_RABIT	134.41	23	3	3	16816
97	P00939|TPIS_RABIT	140.07	28	4	4	26757
98	O97862|CYTC_RABIT	141.72	25	4	4	16346
99	P50117|S10A9_RABIT	137.77	33	4	4	14787
100	P11909|GPX1_RABIT	113.89	28	3	3	21883
103	P08628|THIO_RABIT	145.9	37	3	3	11761
105	P24480|S10AB_RABIT	145.61	26	2	2	11429
106	P29562|IF4A1_RABIT	132.6	11	3	3	45291
107	P39056|OSTCN_RABIT	101.53	80	2	2	5431
110	P79226|ALDOB_RABIT	120.75	16	4	4	39605
111	P19943|RLA2_RABIT	149.61	82	3	3	4695
112	P25227|A1AG_RABIT	91.06	11	2	2	23028
113	P08855|ICAL_RABIT	112.89	6	3	3	76966
115	Q28618|YBOX1_RABIT	84.48	11	2	2	35824
116	P12337|EST1_RABIT	123.15	6	2	2	62292
117	O77622|TCPZ_RABIT	88.11	7	2	2	58024
119	P06813|CPNS1_RABIT	110.11	13	2	2	28239
120	P01692|KV11_RABIT	117.11	17	2	2	9469
123	Q08863|GSTA1_RABIT	120.14	11	2	2	25691
128	P09212|SODC_RABIT	87.85	14	2	2	15819
130	P01684|KV03_RABIT	89.18	20	2	1	11512
131	P26890|IL1RA_RABIT	106.59	16	2	2	20214
132	P01847|LAC_RABIT	107.14	33	2	2	11484
134	Q9XS70|COR1B_RABIT	104.65	9	2	2	53609
140	P01685|KV04_RABIT	86.18	32	2	1	11182
141	P53787|EF1D_RABIT	75.47	9	2	2	31075
143	P62975|UBIQ_RABIT	103.14	33	2	2	8565
154	P27170|PON1_RABIT	84.39	9	2	2	40010
156	P31097|OSTP_RABIT	94.25	9	2	2	35172

Table S 4. Identified proteins in Untreated rabbit 2, left eye.

Protein Group	Accession	-10lgP	Coverage (%)	Peptides	Unique	Avg. Mass
1	P19134|TRFE_RABIT	421.47	58	61	58	76670
2	P01832|PIGR_RABIT	416.65	48	39	39	83887
3	P19007|HPT_RABIT	339.91	58	21	18	38869
4	P60990|PIP_RABIT	259.8	61	14	14	16871
5	P49065|ALBU_RABIT	323.95	54	27	27	68910
9	Q8MI17|AL1A1_RABIT	282.76	48	16	16	54341
11	Q95218|DMBT1_RABIT	252.51	12	13	13	172763
12	P51662|ANXA1_RABIT	303.11	51	14	14	38735
13	P46406|G3P_RABIT	284.87	42	12	12	35780
15	P29751|ACTB_RABIT	259.72	40	10	1	41756
19	P23108|IGJ_RABIT	213.16	60	8	8	15556
20	P13491|LDHA_RABIT	216.23	31	8	7	36565
21	C0HJA6|OBP2_RABIT	129.3	100	3	3	1831
23	P13490|LDHB_RABIT	194.59	27	6	5	24134
24	P01870|IGHG_RABIT	208.33	33	6	6	35404
25	Q9XSC5|CLUS_RABIT	228.82	21	10	10	51851
28	P01879|IGHA_RABIT	234.28	31	7	7	32256
30	P25704|ENOB_RABIT	227.92	23	6	6	47069
35	Q9TTC6|PPIA_RABIT	148.59	37	5	5	17837
36	P26203|P15B_RABIT	182.29	36	5	5	15626
36	P26202|P15A_RABIT	182.29	36	5	5	15675
39	Q29426|K2C3_RABIT	174.7	12	6	4	64341
40	P68105|EF1A1_RABIT	207.19	22	6	6	50141
40	Q71V39|EF1A2_RABIT	151.85	8	3	3	50470
41	P11974|KPYM_RABIT	167.85	18	7	7	58048
43	Q6Q6X0|1433T_RABIT	154.93	27	5	5	27778
44	P39056|OSTCN_RABIT	146.37	90	3	3	5431
46	C0HJA9|OBP3_RABIT	138.5	58	2	2	4721
48	O97529|ANXA8_RABIT	145.85	15	4	4	36680
49	Q8HZQ5|EZRI_RABIT	142.17	6	3	3	69220
50	P01840|KAC4_RABIT	179.97	68	3	3	11043
51	P46409|GSTMU_RABIT	153.59	27	4	4	25417
54	P47845|LEG3_RABIT	100.32	10	2	2	25502
57	P25230|CAP18_RABIT	155.73	23	3	3	19805
58	O77791|S10AC_RABIT	125.45	48	3	3	10668
61	Q08863|GSTA1_RABIT	152.16	15	3	3	25691
62	P62160|CALM_RABIT	151.1	31	3	3	16838
69	P02252|H14_RABIT	108.48	11	2	2	21897
70	O97862|CYTC_RABIT	128.96	11	2	2	16346
71	P16973|LYSC_RABIT	123.45	19	2	2	14722
72	Q28631|WFDC2_RABIT	115.98	33	2	2	12803
73	O19048|PCBP1_RABIT	141.34	13	3	3	37498
77	P00883|ALDOA_RABIT	94.04	12	2	2	39343
78	Q95MF9|CLIC1_RABIT	91.29	10	2	2	26925
79	P24480|S10AB_RABIT	123.24	26	2	2	11429
80	P08628|THIO_RABIT	107.04	37	3	3	11761
81	P00939|TPIS_RABIT	70.47	11	2	2	26757
86	P29562|IF4A1_RABIT	74.94	8	2	2	45291
95	Q28640|HRG_RABIT	75.23	7	2	2	58877

Table S 5. Identified proteins in Untreated rabbit 3, right eye.

Protein Group	Accession	-10lgP	Coverage (%)	Peptides	Unique	Avg. Mass
1	P49065|ALBU_RABIT	447.9	66	63	63	68910
2	P01832|PIGR_RABIT	450.41	48	50	50	83887
3	P19134|TRFE_RABIT	403.59	52	43	39	76670
4	P19007|HPT_RABIT	386.9	64	31	25	38869
5	P60990|PIP_RABIT	256.49	51	13	13	16871
6	P29751|ACTB_RABIT	319.32	52	18	1	41756
8	P51662|ANXA1_RABIT	365.72	60	22	22	38735
9	Q8MI17|AL1A1_RABIT	311.16	49	19	19	54341
11	P68105|EF1A1_RABIT	311.12	42	14	14	50141
11	Q71V39|EF1A2_RABIT	228.24	17	5	5	50470
12	P01879|IGHA_RABIT	305.03	39	13	13	32256
13	P46406|G3P_RABIT	254.89	36	8	8	35780
14	P23108|IGJ_RABIT	236.84	60	8	8	15556
15	P11974|KPYM_RABIT	305.86	39	16	16	58048
18	P68135|ACTS_RABIT	217.69	25	8	1	42051
18	P62740|ACTA_RABIT	217.69	25	8	1	42009
21	P30801|S10A6_RABIT	172.56	50	6	6	10154
22	P01870|IGHG_RABIT	242.1	47	8	8	35404
24	P00883|ALDOA_RABIT	253.14	56	11	11	39343
25	Q9TTC6|PPIA_RABIT	197.49	49	8	8	17837
26	P13491|LDHA_RABIT	191.37	26	7	6	36565
27	Q9XSC5|CLUS_RABIT	249.81	29	12	12	51851
30	P09809|APOA1_RABIT	222.64	47	11	11	30591
31	P80191|FETUA_RABIT	239.44	34	7	7	38387
32	Q29504|UBA1_RABIT	231.83	13	8	8	117688
33	P21195|PDIA1_RABIT	243.52	25	8	8	56808
34	P62160|CALM_RABIT	202.59	46	5	5	16838
37	Q95218|DMBT1_RABIT	165.18	6	6	6	172763
39	Q8HZQ5|EZRI_RABIT	193.79	17	7	7	69220
40	Q95MF9|CLIC1_RABIT	196.72	38	6	6	26925
41	P39056|OSTCN_RABIT	204.98	90	5	5	5431
42	P30946|HS90A_RABIT	218.19	15	8	4	79733
43	Q6Q6X0|1433T_RABIT	178.93	27	5	5	27778
44	P30947|HS90B_RABIT	189.47	16	8	3	83467
45	O97529|ANXA8_RABIT	210.91	31	8	8	36680
46	Q28640|HRG_RABIT	229.18	15	7	7	58877
49	P16973|LYSC_RABIT	204.54	45	6	6	14722
51	P20058|HEMO_RABIT	192.12	16	5	5	51767
52	O77791|S10AC_RABIT	187.23	71	6	6	10668
53	C0HJA9|OBP3_RABIT	191.44	58	4	4	4721
56	P00567|KCRB_RABIT	197.08	16	5	5	42663
58	P47845|LEG3_RABIT	144.63	22	4	4	25502
59	Q29426|K2C3_RABIT	179.3	13	7	5	64341

61	O19049|HNRPK_RABIT	162.01	15	4	4	50960
62	P01840|KAC4_RABIT	195.57	91	4	4	11043
63	P25704|ENOB_RABIT	191.3	13	4	4	47069
64	P13490|LDHB_RABIT	146.94	15	3	2	24134
66	Q8WN94|ACBP_RABIT	197.85	60	4	4	9915
67	P24480|S10AB_RABIT	167.69	58	3	3	11429
70	O19048|PCBP1_RABIT	176.65	25	6	6	37498
71	P08855|ICAL_RABIT	144.08	11	4	4	76966
74	P46409|GSTMU_RABIT	176.53	22	4	4	25417
76	O97862|CYTC_RABIT	172.72	37	5	5	16346
77	P35543|SAA3_RABIT	167.33	13	3	3	13806
80	P12247|CO3_RABIT	135.84	7	4	3	81844
81	Q08863|GSTA1_RABIT	159.91	15	3	3	25691
82	C0HJA6|OBP2_RABIT	103.68	61	2	2	1831
86	P00939|TPIS_RABIT	142.97	28	4	4	26757
87	P10160|IF5A1_RABIT	167.78	23	3	3	16816
88	P08628|THIO_RABIT	153.01	27	2	2	11761
89	P26203|P15B_RABIT	164.85	36	4	4	15626
89	P26202|P15A_RABIT	164.85	36	4	4	15675
90	Q28631|WFDC2_RABIT	160.15	59	4	4	12803
94	P29562|IF4A1_RABIT	146.9	11	3	3	45291
97	P02057|HBB_RABIT	132.06	24	3	3	16133
100	P09212|SODC_RABIT	138.27	37	3	3	15819
102	P11909|GPX1_RABIT	103.72	14	2	2	21883
104	P25230|CAP18_RABIT	141.72	23	3	3	19805
106	P06813|CPNS1_RABIT	102.43	13	2	2	28239
107	Q28619|NHRF1_RABIT	102.94	11	3	3	38562
112	O77622|TCPZ_RABIT	90.12	7	2	2	58024
114	Q8MK67|PEBP1_RABIT	135.52	26	2	2	20994
116	P01692|KV11_RABIT	111.61	17	2	2	9469
117	P79226|ALDOB_RABIT	112.06	13	3	3	39605
118	Q28618|YBOX1_RABIT	87.04	11	2	2	35824
119	P53789|VTDB_RABIT	111.45	9	2	2	52912
121	P02252|H14_RABIT	103.58	11	2	2	21897
122	Q28658|SPRR3_RABIT	89.51	17	2	2	24139
123	P23612|SYWC_RABIT	99.84	7	2	2	53799
126	P34032|TYB4_RABIT	100.11	32	2	2	5037
130	O19053|ADHX_RABIT	104.28	10	2	2	39596
132	Q9XS70|COR1B_RABIT	127.29	9	2	2	53609
142	P01948|HBA_RABIT	107.26	26	2	2	15589

Table S 6. Identified proteins in Untreated rabbit 3, left eye.

Protein Group	Accession	-10lgP	Coverage (%)	Peptides	Unique	Avg. Mass
1	P01832|PIGR_RABIT	434.2	51	47	47	83887
2	P19134|TRFE_RABIT	382.73	52	38	38	76670
3	P49065|ALBU_RABIT	402.14	63	44	44	68910
4	P19007|HPT_RABIT	360.64	63	27	22	38869
5	P60990|PIP_RABIT	258	51	13	13	16871
9	P01879|IGHA_RABIT	278.75	39	12	12	32256
10	Q95218|DMBT1_RABIT	239.63	10	11	11	172763
11	P23108|IGJ_RABIT	225.66	76	10	10	15556
13	P51662|ANXA1_RABIT	297.94	51	14	14	38735
14	Q29426|K2C3_RABIT	242.79	24	13	8	64341
15	P29751|ACTB_RABIT	252.51	38	9	5	41756
18	Q28706|K1C12_RABIT	202.46	30	9	8	45727
19	P01870|IGHG_RABIT	227.82	37	7	7	35404
21	Q8MI17|AL1A1_RABIT	237.43	35	10	10	54341
24	Q9XSC5|CLUS_RABIT	246.52	20	8	8	51851
28	P46406|G3P_RABIT	218.2	34	8	8	35780
32	C0HJA9|OBP3_RABIT	176.04	58	3	3	4721
34	C0HJA6|OBP2_RABIT	113.49	61	3	3	1831
36	Q9TTC6|PPIA_RABIT	153.2	37	5	5	17837
39	P13491|LDHA_RABIT	163.27	22	6	5	36565
40	P01840|KAC4_RABIT	205.19	68	3	3	11043
41	P13490|LDHB_RABIT	166.3	27	5	4	24134
42	P39056|OSTCN_RABIT	177.52	90	4	4	5431
44	P25704|ENOB_RABIT	190.98	19	5	5	47069
45	P62740|ACTA_RABIT	171.42	16	5	1	42009
45	P68135|ACTS_RABIT	171.42	16	5	1	42051
48	Q28640|HRG_RABIT	164.81	13	5	5	58877
50	P12247|CO3_RABIT	153.14	10	4	3	81844
52	P46409|GSTMU_RABIT	149.36	27	4	4	25417
57	P09809|APOA1_RABIT	159.64	24	5	5	30591
58	O97862|CYTC_RABIT	154.46	25	4	4	16346
59	P16973|LYSC_RABIT	146.67	38	4	4	14722
62	P80191|FETUA_RABIT	178.59	19	4	4	38387
64	Q6Q6X0|1433T_RABIT	110	10	2	2	27778
66	P35543|SAA3_RABIT	160.87	19	3	3	13806
67	P31097|OSTP_RABIT	124.89	15	3	3	35172
71	Q8WN94|ACBP_RABIT	154.4	39	2	2	9915
72	P62160|CALM_RABIT	127.55	31	3	3	16838
74	P02252|H14_RABIT	100.09	11	2	2	21897
78	O97529|ANXA8_RABIT	105.42	8	2	2	36680
81	P20058|HEMO_RABIT	97.06	7	2	2	51767
82	Q28631|WFDC2_RABIT	122.28	33	2	2	12803
83	P24480|S10AB_RABIT	123.54	26	2	2	11429
84	P01687|KV06_RABIT	97.55	31	2	2	11281
88	Q08863|GSTA1_RABIT	127.83	11	2	2	25691
91	O77791|S10AC_RABIT	96.27	36	2	2	10668
92	P26890|IL1RA_RABIT	76.07	16	2	2	20214

Table S 7. Identified proteins in Untreated rabbit 4, right eye.

Protein Group	Accession	-10lgP	Coverage (%)	Peptides	Unique	Avg. Mass
1	P19134|TRFE_RABIT	420.81	66	64	64	76670
2	P01832|PIGR_RABIT	449.28	51	52	52	83887
3	P49065|ALBU_RABIT	409.96	63	49	49	68910
4	P19007|HPT_RABIT	368.54	67	37	29	38869
5	P60990|PIP_RABIT	273.4	61	22	22	16871
6	P29751|ACTB_RABIT	290.09	53	15	1	41756
7	P51662|ANXA1_RABIT	339.63	57	21	21	38735
8	Q8MI17|AL1A1_RABIT	280.29	52	19	19	54341
12	Q95218|DMBT1_RABIT	248.36	14	15	15	172763
14	P01879|IGHA_RABIT	289.1	39	13	13	32256
15	P23108|IGJ_RABIT	216.87	68	10	10	15556
16	P68105|EF1A1_RABIT	259.16	33	11	11	50141
16	Q71V39|EF1A2_RABIT	206.86	19	6	6	50470
17	P46406|G3P_RABIT	283.27	49	14	14	35780
18	P01870|IGHG_RABIT	216.82	37	7	7	35404
19	Q9XSC5|CLUS_RABIT	252.88	25	12	12	51851
22	P11974|KPYM_RABIT	215.56	28	10	10	58048
23	P39056|OSTCN_RABIT	220.71	90	7	7	5431
24	Q29426|K2C3_RABIT	212.51	19	11	8	64341
26	P68135|ACTS_RABIT	196.02	26	9	1	42051
26	P62740|ACTA_RABIT	196.02	26	9	1	42009
27	P13491|LDHA_RABIT	192.67	34	9	8	36565
29	O77791|S10AC_RABIT	191.5	71	6	6	10668
30	P00883|ALDOA_RABIT	221.41	44	9	9	39343
31	Q9TTC6|PPIA_RABIT	171.98	49	7	7	17837
32	C0HJA9|OBP3_RABIT	197.9	58	5	5	4721
36	P13490|LDHB_RABIT	177.08	31	7	6	24134
37	C0HJA6|OBP2_RABIT	122.05	61	3	3	1831
39	P30801|S10A6_RABIT	134.97	51	7	7	10154
40	P01840|KAC4_RABIT	207.89	91	5	5	11043
42	Q6Q6X0|1433T_RABIT	182.12	26	6	6	27778
44	Q29504|UBA1_RABIT	164.65	10	6	6	117688
45	Q28640|HRG_RABIT	196.16	14	7	7	58877
46	P15122|ALDR_RABIT	150.29	29	6	6	35763
48	Q28706|K1C12_RABIT	152.82	17	7	2	45727
56	P25704|ENOB_RABIT	183.28	13	3	3	47069
58	P00567|KCRB_RABIT	157.64	14	4	4	42663
59	Q8HZQ5|EZRI_RABIT	142.41	9	4	4	69220
60	P46409|GSTMU_RABIT	160.18	27	4	4	25417
61	P10160|IF5A1_RABIT	151.21	23	3	3	16816
62	P62160|CALM_RABIT	152.64	31	3	3	16838
64	O19048|PCBP1_RABIT	168.34	25	6	6	37498
67	Q8WN94|ACBP_RABIT	187.89	60	4	4	9915

71	P35543|SAA3_RABIT	163.57	19	3	3	13806
72	P47845|LEG3_RABIT	110.97	16	3	3	25502
76	P30946|HS90A_RABIT	159.53	9	5	3	79733
79	P09809|APOA1_RABIT	159.49	34	7	7	30591
80	P00939|TPIS_RABIT	124.5	28	4	4	26757
81	Q28658|SPRR3_RABIT	138.18	27	3	3	24139
82	P14422|PA2GA_RABIT	115.46	40	3	3	7607
85	Q95MF9|CLIC1_RABIT	110.6	15	3	3	26925
86	O97862|CYTC_RABIT	140	18	3	3	16346
87	P08628|THIO_RABIT	136.27	37	3	3	11761
88	P24480|S10AB_RABIT	162.56	58	3	3	11429
93	P30947|HS90B_RABIT	106.88	7	4	2	83467
94	P09212|SODC_RABIT	103.3	37	3	3	15819
95	Q28631|WFDC2_RABIT	139.01	40	3	3	12803
96	P80508|PE2R_RABIT	133.37	13	3	3	36670
97	P16973|LYSC_RABIT	130.89	38	3	3	14722
98	P50117|S10A9_RABIT	96.59	23	2	2	14787
99	P02252|H14_RABIT	108.37	18	3	3	21897
100	P21195|PDIA1_RABIT	140	12	3	3	56808
102	P12247|CO3_RABIT	97.43	6	3	3	81844
103	P01692|KV11_RABIT	112.89	17	2	2	9469
104	P29562|IF4A1_RABIT	112.01	11	3	3	45291
105	Q08863|GSTA1_RABIT	128.2	11	2	2	25691
106	P80191|FETUA_RABIT	127.02	11	2	2	38387
109	P31097|OSTP_RABIT	89.93	11	2	2	35172
111	P06813|CPNS1_RABIT	108.61	13	2	2	28239
112	O77622|TCPZ_RABIT	83.23	7	2	2	58024
113	P01685|KV04_RABIT	76.33	23	2	2	11182
115	P26890|IL1RA_RABIT	90.84	16	2	2	20214
117	P26203|P15B_RABIT	88.52	18	2	2	15626
117	P26202|P15A_RABIT	88.52	18	2	2	15675
121	P62493|RB11A_RABIT	71.03	11	2	2	24394

Table S 8. Identified proteins in Untreated rabbit 4, left eye.

Protein Group	Accession	-10lgP	Coverage (%)	Peptides	Unique	Avg. Mass
1	P01832|PIGR_RABIT	412.15	48	41	41	83887
2	P19134|TRFE_RABIT	351.24	48	33	31	76670
3	P19007|HPT_RABIT	322.28	61	19	14	38869
4	P49065|ALBU_RABIT	333.24	49	24	24	68910
5	P60990|PIP_RABIT	233.51	61	14	14	16871
8	Q95218|DMBT1_RABIT	270.71	15	14	14	172763
9	P51662|ANXA1_RABIT	284.02	50	14	14	38735
11	P23108|IGJ_RABIT	213.46	60	7	7	15556
13	P29751|ACTB_RABIT	232.11	36	8	5	41756
14	P01879|IGHA_RABIT	265.64	39	8	8	32256
16	Q9XSC5|CLUS_RABIT	227.18	20	9	9	51851
17	Q8MI17|AL1A1_RABIT	224.65	23	8	8	54341
20	Q29426|K2C3_RABIT	197.58	17	9	5	64341
21	P01870|IGHG_RABIT	179.06	28	4	4	35404
31	P39056|OSTCN_RABIT	175.55	90	5	5	5431
32	C0HJA6|OBP2_RABIT	119.82	61	3	3	1831
33	C0HJA9|OBP3_RABIT	147	58	2	2	4721
35	Q9TTC6|PPIA_RABIT	138.66	37	5	5	17837
36	P68135|ACTS_RABIT	169.11	14	4	1	42051
36	P62740|ACTA_RABIT	169.11	14	4	1	42009
38	P68105|EF1A1_RABIT	155.62	15	5	5	50141
38	Q71V39|EF1A2_RABIT	100.87	7	3	3	50470
43	Q6Q6X0|1433T_RABIT	107.67	10	2	2	27778
44	O97862|CYTC_RABIT	127.1	25	4	4	16346
47	P46406|G3P_RABIT	162.62	14	3	3	35780
50	P11974|KPYM_RABIT	137.74	13	5	5	58048
51	P01840|KAC4_RABIT	162.74	43	3	3	11043
53	P62160|CALM_RABIT	117.23	31	3	3	16838
56	P25704|ENOB_RABIT	159.11	11	3	3	47069
58	P46409|GSTMU_RABIT	136.89	27	4	4	25417
65	P13490|LDHB_RABIT	81.29	10	2	2	24134
66	P35543|SAA3_RABIT	136.94	13	2	2	13806
67	P01692|KV11_RABIT	110.52	17	2	2	9469
68	P24480|S10AB_RABIT	113.91	26	2	2	11429
69	Q28631|WFDC2_RABIT	120.59	33	2	2	12803
71	Q8WN94|ACBP_RABIT	120.36	39	2	2	9915
74	P80191|FETUA_RABIT	115.39	9	2	2	38387
85	P26890|IL1RA_RABIT	76.93	16	2	2	20214

Table S 9. Identified proteins in Untreated rabbit 5, right eye.

Protein Group	Accession	-10lgP	Coverage (%)	Peptides	Unique	Avg. Mass
1	P19134|TRFE_RABIT	457.32	65	85	80	76670
2	P01832|PIGR_RABIT	475.87	53	63	63	83887
3	P60990|PIP_RABIT	308.63	62	20	20	16871
4	P19007|HPT_RABIT	374.36	61	31	26	38869
5	P49065|ALBU_RABIT	359.82	55	29	29	68910
7	P23108|IGJ_RABIT	249.71	76	14	14	15556
8	Q95218|DMBT1_RABIT	299.23	16	17	17	172763
9	C0HJA6|OBP2_RABIT	138.09	100	4	4	1831
10	P01870|IGHG_RABIT	273.08	40	11	11	35404
12	P01879|IGHA_RABIT	295.4	35	13	13	32256
14	Q9XSC5|CLUS_RABIT	266.04	27	13	13	51851
16	P51662|ANXA1_RABIT	326.99	48	13	13	38735
19	Q8MI17|AL1A1_RABIT	240.42	36	10	10	54341
20	C0HJA9|OBP3_RABIT	257.85	58	9	9	4721
21	P39056|OSTCN_RABIT	232.93	90	8	8	5431
23	P46406|G3P_RABIT	223.66	27	5	5	35780
28	P01840|KAC4_RABIT	209.63	91	4	4	11043
29	P35543|SAA3_RABIT	220.76	26	6	6	13806
30	Q29426|K2C3_RABIT	184.61	15	8	5	64341
33	P11974|KPYM_RABIT	198.02	17	6	6	58048
35	P68105|EF1A1_RABIT	218.44	16	5	5	50141
35	Q71V39|EF1A2_RABIT	160.29	8	3	3	50470
36	Q9TTC6|PPIA_RABIT	176.65	31	4	4	17837
40	Q28706|K1C12_RABIT	176.81	11	3	3	45727
44	P62740|ACTA_RABIT	177.75	14	4	1	42009
44	P68135|ACTS_RABIT	177.75	14	4	1	42051
45	P46409|GSTMU_RABIT	165.54	27	4	4	25417
47	P31097|OSTP_RABIT	135.24	25	4	4	35172
49	O97862|CYTC_RABIT	165.22	25	4	4	16346
53	Q8WN94|ACBP_RABIT	179.87	60	4	4	9915
56	P24480|S10AB_RABIT	159.06	58	3	3	11429
59	P25704|ENOB_RABIT	173.85	16	4	4	47069
60	Q6Q6X0|1433T_RABIT	136.85	19	4	4	27778
61	Q28631|WFDC2_RABIT	144.35	33	2	2	12803
62	P13490|LDHB_RABIT	107.6	10	2	2	24134
63	P62160|CALM_RABIT	119.31	19	2	2	16838
64	P16973|LYSC_RABIT	142.4	29	2	2	14722
72	P00567|KCRB_RABIT	112.39	10	2	2	42663
73	P31347|ANGI_RABIT	92.66	25	2	2	14361
76	Q28658|SPRR3_RABIT	109.68	16	2	2	24139
82	P34032|TYB4_RABIT	100.65	32	2	2	5037
86	O97529|ANXA8_RABIT	96.75	8	2	2	36680
87	Q08863|GSTA1_RABIT	108.35	11	2	2	25691
88	P26203|P15B_RABIT	98.19	18	2	2	15626
88	P26202|P15A_RABIT	98.19	18	2	2	15675
91	Q95MF9|CLIC1_RABIT	91.49	10	2	2	26925
92	P01692|KV11_RABIT	107.69	17	2	2	9469
94	P21195|PDIA1_RABIT	102.67	9	2	2	56808
96	P26890|IL1RA_RABIT	106.33	16	2	2	20214
103	P01687|KV06_RABIT	99.88	31	2	2	11281

Table S 10. Identified proteins in Untreated rabbit 5, left eye.

Protein Group	Accession	-10lgP	Coverage (%)	Peptides	Unique	Avg. Mass
1	P19134|TRFE_RABIT	457.33	67	91	87	76670
2	P01832|PIGR_RABIT	487.6	55	69	69	83887
3	P60990|PIP_RABIT	294.11	61	20	20	16871
4	P49065|ALBU_RABIT	417.66	64	53	53	68910
5	P19007|HPT_RABIT	370.77	62	31	26	38869
6	P29751|ACTB_RABIT	341.53	59	19	1	41756
7	P51662|ANXA1_RABIT	372.52	60	23	23	38735
9	Q95218|DMBT1_RABIT	327.24	20	21	21	172763
10	P23108|IGJ_RABIT	254.6	68	15	15	15556
11	Q8MI17|AL1A1_RABIT	310.04	58	19	19	54341
12	P01879|IGHA_RABIT	287.1	35	14	14	32256
14	P01870|IGHG_RABIT	254.01	35	8	8	35404
15	P46406|G3P_RABIT	295.95	50	14	14	35780
17	P11974|KPYM_RABIT	308.03	42	16	16	58048
18	P68105|EF1A1_RABIT	295.91	37	12	7	50141
19	P62740|ACTA_RABIT	231.28	22	7	1	42009
19	P68135|ACTS_RABIT	231.28	22	7	1	42051
21	C0HJA6|OBP2_RABIT	131.18	100	4	4	1831
22	Q9XSC5|CLUS_RABIT	261.31	29	12	12	51851
23	P30801|S10A6_RABIT	196.15	59	8	8	10154
24	P00883|ALDOA_RABIT	273.39	56	11	11	39343
25	P21195|PDIA1_RABIT	275.62	36	11	11	56808
26	P00567|KCRB_RABIT	256.76	24	7	7	42663
27	Q9TTC6|PPIA_RABIT	217.36	61	10	10	17837
29	P39056|OSTCN_RABIT	197.56	90	5	5	5431
30	Q28706|K1C12_RABIT	199.04	28	9	8	45727
32	Q29426|K2C3_RABIT	207.37	20	10	8	64341
35	C0HJA9|OBP3_RABIT	217.02	58	7	7	4721
37	Q6Q6X0|1433T_RABIT	206.36	27	5	5	27778
40	P12337|EST1_RABIT	202.26	16	7	7	62292
42	P24480|S10AB_RABIT	166.92	58	3	3	11429
45	Q29504|UBA1_RABIT	218.94	12	7	7	117688
46	P13490|LDHB_RABIT	174.67	27	6	5	24134
48	P13491|LDHA_RABIT	186.1	23	6	5	36565
49	O19049|HNRPK_RABIT	175.54	17	6	6	50960
52	P11909|GPX1_RABIT	163.09	41	6	6	21883
53	P35543|SAA3_RABIT	174.25	21	3	3	13806
54	P62160|CALM_RABIT	185.57	46	4	4	16838
55	P30946|HS90A_RABIT	179.93	15	6	5	79733
57	P14422|PA2GA_RABIT	145.6	38	3	3	7607
58	P25230|CAP18_RABIT	187.86	23	4	4	19805
59	P25704|ENOB_RABIT	207.75	16	4	4	47069
60	P00939|TPIS_RABIT	186.24	48	7	7	26757

62	P16973|LYSC_RABIT	183.78	37	5	5	14722
65	P01840|KAC4_RABIT	211.57	94	5	5	11043
66	P26202|P15A_RABIT	205.12	36	5	5	15675
66	P26203|P15B_RABIT	205.12	36	5	5	15626
67	O19048|PCBP1_RABIT	170.95	21	5	5	37498
71	P30947|HS90B_RABIT	138.85	9	4	2	83467
73	P47845|LEG3_RABIT	148.68	28	5	5	25502
74	P80508|PE2R_RABIT	167.8	21	5	5	36670
75	P46409|GSTMU_RABIT	181.98	22	5	5	25417
76	O77791|S10AC_RABIT	140.78	70	4	4	10668
78	P00389|NCPR_RABIT	167.93	12	5	5	76588
79	P09809|APOA1_RABIT	157.54	30	6	6	30591
80	Q8HZQ5|EZRI_RABIT	140.95	8	3	3	69220
81	Q95MF9|CLIC1_RABIT	171.45	34	5	5	26925
82	Q8WN94|ACBP_RABIT	208.75	60	5	5	9915
83	O19053|ADHX_RABIT	183.75	29	5	5	39596
84	P09212|SODC_RABIT	176.18	49	4	4	15819
87	P02252|H14_RABIT	136.85	18	4	4	21897
88	P00949|PGM1_RABIT	150.53	17	5	5	61558
89	P06815|CAN1_RABIT	160.75	32	6	6	35275
90	Q28640|HRG_RABIT	152.65	11	5	5	58877
92	P29562|IF4A1_RABIT	156.28	11	3	3	45291
93	P41316|CRYAB_RABIT	146.68	38	5	5	20107
94	P08628|THIO_RABIT	152.92	37	4	4	11761
95	Q28631|WFDC2_RABIT	165.67	59	4	4	12803
96	P15253|CALR_RABIT	114.26	14	3	3	48275
97	O77622|TCPZ_RABIT	140.55	17	4	4	58024
99	P15128|CP4B1_RABIT	140.96	9	3	3	58604
100	Q08863|GSTA1_RABIT	146.05	23	3	3	25691
101	P10160|IF5A1_RABIT	183.18	23	3	3	16816
103	O97862|CYTC_RABIT	155.23	31	4	4	16346
104	P80191|FETUA_RABIT	164.46	22	4	4	38387
105	P50117|S10A9_RABIT	110.63	23	2	2	14787
106	P00169|CYB5_RABIT	120.23	34	3	3	15349
109	P08855|ICAL_RABIT	98.34	6	3	3	76966
110	P00489|PYGM_RABIT	142.42	9	5	5	97289
112	Q9N1E2|G6PI_RABIT	100.94	6	2	2	62747
113	P02057|HBB_RABIT	114.26	17	2	2	16133
114	P31097|OSTP_RABIT	97.55	19	3	3	35172
115	Q28739|BPI_RABIT	157.33	12	3	3	48837
116	P12247|CO3_RABIT	116.92	6	3	3	81844
119	P62493|RB11A_RABIT	86.02	11	2	2	24394
122	P23612|SYWC_RABIT	98.74	7	2	2	53799
124	P01696|KV15_RABIT	84.19	19	2	1	11596
125	O62695|H2AV_RABIT	79.9	15	2	2	13481
126	P01697|KV16_RABIT	79.78	18	2	1	12112
127	P34032|TYB4_RABIT	106.14	32	2	2	5037
130	P79226|ALDOB_RABIT	101.89	13	3	3	39605
131	O18750|ENPL_RABIT	100.79	6	3	2	82608
136	Q8MK67|PEBP1_RABIT	115.5	32	2	2	20994
137	P19943|RLA2_RABIT	123	73	2	2	4695
152	P53789|VTDB_RABIT	78.81	9	2	2	52912
154	Q9XS70|COR1B_RABIT	84.95	9	2	2	53609

Table S 11. Identified proteins in placebo treated rabbit 1, left eye.

Protein Group	Accession	-10lgP	Coverage (%)	Peptides	Unique	Avg. Mass
1	P49065|ALBU_RABIT	439.89	70	79	79	68910
2	P01832|PIGR_RABIT	460.98	53	64	64	83887
3	P19134|TRFE_RABIT	433.3	59	72	66	76670
4	P19007|HPT_RABIT	376.96	67	41	29	38869
5	P51662|ANXA1_RABIT	361.1	62	24	24	38735
7	P29751|ACTB_RABIT	331.6	64	24	1	41756
10	P60990|PIP_RABIT	264.81	58	19	19	16871
12	Q8MI17|AL1A1_RABIT	328.3	58	28	28	54341
13	P46406|G3P_RABIT	289.39	48	17	17	35780
16	Q95218|DMBT1_RABIT	270.51	13	13	13	172763
17	P23108|IGJ_RABIT	228.71	74	11	11	15556
18	P11974|KPYM_RABIT	312.48	48	20	20	58048
19	P01870|IGHG_RABIT	257.47	49	13	13	35404
20	Q9TTC6|PPIA_RABIT	286.75	65	14	14	17837
21	P68135|ACTS_RABIT	218.34	25	10	1	42051
21	P62740|ACTA_RABIT	214.12	22	9	1	42009
22	P01879|IGHA_RABIT	286.14	39	14	14	32256
23	P68105|EF1A1_RABIT	283.83	42	14	14	50141
23	Q71V39|EF1A2_RABIT	207.66	20	8	8	50470
24	Q9XSC5|CLUS_RABIT	266.14	29	15	15	51851
25	Q29504|UBA1_RABIT	238.12	20	14	14	117688
26	P30947|HS90B_RABIT	246.21	27	15	10	83467
29	P09809|APOA1_RABIT	235.06	47	12	12	30591
32	P00883|ALDOA_RABIT	259.16	56	12	12	39343
33	P15122|ALDR_RABIT	174.88	45	10	10	35763
35	P30946|HS90A_RABIT	242.75	24	13	9	79733
36	P00567|KCRB_RABIT	268.7	49	12	12	42663
37	Q28640|HRG_RABIT	245.93	23	12	12	58877
38	P80191|FETUA_RABIT	252.87	40	7	7	38387
41	C0HJA6|OBP2_RABIT	130.75	100	3	3	1831
44	P53789|VTDB_RABIT	187.39	27	10	10	52912
45	P21195|PDIA1_RABIT	227.08	31	11	11	56808
46	P62160|CALM_RABIT	203.12	50	8	8	16838
49	Q6Q6X0|1433T_RABIT	200.13	37	8	8	27778
50	P13491|LDHA_RABIT	211.2	33	10	9	36565
51	P47845|LEG3_RABIT	172.59	43	8	8	25502
53	P00939|TPIS_RABIT	201.23	58	9	9	26757
54	P12247|CO3_RABIT	198.31	16	8	5	81844
57	P20058|HEMO_RABIT	193.32	20	7	7	51767
58	Q08863|GSTA1_RABIT	176.54	28	6	6	25691
61	Q95MF9|CLIC1_RABIT	192.49	43	7	7	26925
64	P30801|S10A6_RABIT	140.55	74	8	8	10154
65	Q8WN94|ACBP_RABIT	204.74	60	5	5	9915

66	P31097|OSTP_RABIT	169.76	35	6	6	35172
67	P12337|EST1_RABIT	182.56	20	8	8	62292
69	Q8MK67|PEBP1_RABIT	228.04	71	8	8	20994
70	O77791|S10AC_RABIT	139.12	71	5	5	10668
72	P13490|LDHB_RABIT	170.4	28	7	6	24134
73	P80508|PE2R_RABIT	188.84	24	7	6	36670
74	O19048|PCBP1_RABIT	160.85	23	6	6	37498
76	P08855|ICAL_RABIT	183.64	17	7	7	76966
77	P01840|KAC4_RABIT	198.77	83	4	4	11043
79	Q29426|K2C3_RABIT	159.19	10	6	3	64341
84	P29562|IF4A1_RABIT	181	19	6	6	45291
85	Q8HZQ5|EZRI_RABIT	155.7	10	5	5	69220
89	P11909|GPX1_RABIT	153.89	42	5	5	21883
90	P25704|ENOB_RABIT	174.58	16	4	4	47069
93	O19053|ADHX_RABIT	147.57	21	5	5	39596
95	P06813|CPNS1_RABIT	151.07	37	6	6	28239
98	P16973|LYSC_RABIT	141.51	41	5	5	14722
101	P00489|PYGM_RABIT	128.18	8	5	5	97289
102	O97862|CYTC_RABIT	153.51	30	4	4	16346
103	P02057|HBB_RABIT	139.42	36	4	4	16133
104	P39056|OSTCN_RABIT	131.06	90	3	3	5431
107	P79226|ALDOB_RABIT	142.13	11	3	3	39605
109	P15253|CALR_RABIT	109.47	15	4	4	48275
110	P10160|IF5A1_RABIT	138.34	35	3	3	16816
111	Q28631|WFDC2_RABIT	140.47	59	4	4	12803
113	O97529|ANXA8_RABIT	130.99	19	5	5	36680
114	P29694|EF1G_RABIT	125.64	11	3	3	50049
116	O77506|LASP1_RABIT	101.18	10	2	2	29935
118	P62493|RB11A_RABIT	98.27	16	3	3	24394
119	P35543|SAA3_RABIT	144.51	13	2	2	13806
121	P19943|RLA2_RABIT	114.54	80	2	2	4695
122	P14422|PA2GA_RABIT	110.14	38	2	2	7607
123	P41316|CRYAB_RABIT	88.43	16	3	3	20107
124	P58776|TPM2_RABIT	84.05	11	3	2	32837
125	P00169|CYB5_RABIT	94.64	34	3	3	15349
126	P09212|SODC_RABIT	124.04	44	3	3	15819
127	P01692|KV11_RABIT	116.99	17	2	2	9469
128	P08628|THIO_RABIT	117.57	34	3	3	11761
131	P06815|CAN1_RABIT	85.84	11	3	3	35275
132	P46409|GSTMU_RABIT	110.2	18	3	3	25417
133	P24480|S10AB_RABIT	155.56	58	4	4	11429
134	Q9XS70|COR1B_RABIT	104.87	6	2	2	53609
137	P27170|PON1_RABIT	96.58	12	3	3	40010
138	P01696|KV15_RABIT	99.34	31	3	1	11596
139	Q9N1E2|G6PI_RABIT	86.13	6	2	2	62747

140	P50117|S10A9_RABIT	105.01	23	2	2	14787
141	P58772|TPM1_RABIT	61.57	8	2	1	32681
144	P41975|SODE_RABIT	73.81	9	2	2	25688
145	P23612|SYWC_RABIT	67.88	7	2	2	53799
146	P04221|MUCM_RABIT	81.59	6	2	2	52351
146	P03988|IGHM_RABIT	81.59	6	2	2	49897
147	P01697|KV16_RABIT	72.53	18	2	1	12112
148	P01847|LAC_RABIT	93.55	33	2	2	11484
149	P62943|FKB1A_RABIT	83.77	25	2	2	11951
151	P01894|HA1A_RABIT	72.81	10	2	2	40447
151	P06140|HA1B_RABIT	72.81	10	2	2	40455
153	P34032|TYB4_RABIT	104.94	32	2	2	5037
154	P07466|DEF6_RABIT	69.19	21	2	2	10122
160	P34826|EF1B_RABIT	97.41	12	2	2	24749
172	P53787|EF1D_RABIT	79.7	13	2	2	31075

Table S 12. Identified proteins in placebo treated rabbit 2, left eye.

Protein Group	Accession	-10lgP	Coverage (%)	Peptides	Unique	Avg. Mass
1	P19007|HPT_RABIT	426.77	65	47	34	38869
2	P19134|TRFE_RABIT	435.21	63	60	58	76670
3	P49065|ALBU_RABIT	411.01	63	49	49	68910
4	P01832|PIGR_RABIT	447.17	51	45	45	83887
5	P60990|PIP_RABIT	286.88	61	21	21	16871
6	C0HJA6|OBP2_RABIT	155.31	100	4	4	1831
9	P29751|ACTB_RABIT	342.1	57	18	1	41756
10	Q95218|DMBT1_RABIT	308.36	18	17	17	172763
12	P51662|ANXA1_RABIT	336.46	56	19	19	38735
13	Q8MI17|AL1A1_RABIT	307.99	50	21	21	54341
14	P15122|ALDR_RABIT	240.05	58	13	13	35763
16	P46406|G3P_RABIT	272.48	44	14	14	35780
17	Q9TTC6|PPIA_RABIT	278.46	67	12	12	17837
19	P11974|KPYM_RABIT	284.21	41	14	14	58048
20	P01870|IGHG_RABIT	238.83	45	8	8	35404
21	P68105|EF1A1_RABIT	265.41	39	13	13	50141
21	Q71V39|EF1A2_RABIT	155.2	13	5	5	50470
22	Q9XSC5|CLUS_RABIT	265.94	25	11	11	51851
23	P68135|ACTS_RABIT	214.06	22	7	1	42051
23	P62740|ACTA_RABIT	208.23	19	6	1	42009
24	P01879|IGHA_RABIT	240.16	39	7	7	32256
25	P23108|IGJ_RABIT	187.94	54	6	6	15556
26	P30946|HS90A_RABIT	229.51	20	9	6	79733
28	Q29504|UBA1_RABIT	237.36	16	10	10	117688
30	P39056|OSTCN_RABIT	172.14	90	3	3	5431
31	P00883|ALDOA_RABIT	223.97	27	6	6	39343
32	P30947|HS90B_RABIT	182.65	17	9	6	83467
33	Q08863|GSTA1_RABIT	200.77	37	5	5	25691
36	P80191|FETUA_RABIT	233.64	28	5	5	38387
37	P21195|PDIA1_RABIT	212.53	19	6	6	56808
38	P30801|S10A6_RABIT	181.13	59	6	6	10154
39	P13491|LDHA_RABIT	155.66	20	5	5	36565
40	Q6Q6X0|1433T_RABIT	169.6	15	4	4	27778
41	P13490|LDHB_RABIT	158.16	29	7	7	24134
42	P25704|ENOB_RABIT	197.19	16	4	4	47069
43	P24480|S10AB_RABIT	187.95	58	4	4	11429
47	P62160|CALM_RABIT	188.99	40	4	4	16838
48	O19048|PCBP1_RABIT	170.79	16	4	4	37498
49	O97862|CYTC_RABIT	197.17	40	5	5	16346
50	Q28640|HRG_RABIT	176.83	11	6	6	58877
51	P15253|CALR_RABIT	156.62	20	5	5	48275
52	P08628|THIO_RABIT	170.97	49	4	4	11761
53	P00939|TPIS_RABIT	180.8	33	5	5	26757

54	Q8HZQ5|EZRI_RABIT	134.43	6	3	3	69220
55	Q95MF9|CLIC1_RABIT	155.24	23	4	4	26925
56	O77791|S10AC_RABIT	151.17	58	3	3	10668
57	P29562|IF4A1_RABIT	172.31	15	5	5	45291
58	O97529|ANXA8_RABIT	178.12	20	5	5	36680
59	C0HJA9|OBP3_RABIT	157.91	58	2	2	4721
60	P00567|KCRB_RABIT	191.37	18	4	4	42663
62	P09809|APOA1_RABIT	130.92	9	2	2	30591
63	P46409|GSTMU_RABIT	158.74	22	3	3	25417
66	P06813|CPNS1_RABIT	140.74	23	3	3	28239
67	Q8WN94|ACBP_RABIT	185.07	60	5	5	9915
68	P16973|LYSC_RABIT	143.09	35	4	4	14722
73	Q8MK67|PEBP1_RABIT	156.02	48	3	3	20994
74	P11909|GPX1_RABIT	147.64	28	3	3	21883
75	Q28631|WFDC2_RABIT	159.55	52	3	3	12803
76	P08855|ICAL_RABIT	160.93	10	4	4	76966
79	P10160|IF5A1_RABIT	179.32	35	3	3	16816
80	P80508|PE2R_RABIT	119.94	14	3	3	36670
83	O19053|ADHX_RABIT	105.63	11	2	2	39596
84	P35543|SAA3_RABIT	155.48	13	2	2	13806
87	P79226|ALDOB_RABIT	131.11	8	2	2	39605
88	Q28685|DAG1_RABIT	97.44	11	3	3	97030
90	P09212|SODC_RABIT	148.7	37	3	3	15819
91	P53789|VTDB_RABIT	103.65	9	2	2	52912
93	P20058|HEMO_RABIT	110.24	7	2	2	51767
96	P31347|ANGI_RABIT	89.45	25	2	2	14361
98	P31097|OSTP_RABIT	108.03	23	3	3	35172
99	P50117|S10A9_RABIT	99.12	21	2	2	14787
100	P34032|TYB4_RABIT	108.26	32	2	2	5037
105	P98065|TSG6_RABIT	95.24	13	2	2	31081
108	P34826|EF1B_RABIT	106.93	21	2	2	24749
109	P62943|FKB1A_RABIT	80.6	25	2	2	11951
110	P07466|DEF6_RABIT	75.27	21	2	2	10122
113	Q9N1E2|G6PI_RABIT	74.28	6	2	2	62747
114	P02252|H14_RABIT	91.8	12	2	2	21897
116	O77506|LASP1_RABIT	99.84	17	3	3	29935
118	Q09YN4|CAZA2_RABIT	72.46	11	2	2	32951

Table S 13. Identified proteins in placebo treated rabbit 3, left eye.

Protein Group	Accession	-10lgP	Coverage (%)	Peptides	Unique	Avg. Mass
1	P01832|PIGR_RABIT	476.57	54	90	90	83887
2	P19134|TRFE_RABIT	381.57	59	46	44	76670
3	P19007|HPT_RABIT	366.15	65	30	21	38869
4	P49065|ALBU_RABIT	350.95	59	33	33	68910
5	Q95218|DMBT1_RABIT	305.11	20	19	19	172763
6	P60990|PIP_RABIT	257.53	61	19	19	16871
7	P23108|IGJ_RABIT	261.79	68	19	19	15556
10	P01870|IGHG_RABIT	289.19	57	18	18	35404
11	P01879|IGHA_RABIT	280.16	35	16	16	32256
13	Q9XSC5|CLUS_RABIT	275.74	34	16	16	51851
15	P29751|ACTB_RABIT	287.73	51	14	1	41756
17	Q8MI17|AL1A1_RABIT	250.05	44	13	13	54341
20	P01840|KAC4_RABIT	237.24	94	8	8	11043
21	P51662|ANXA1_RABIT	272.89	46	11	11	38735
24	C0HJA6|OBP2_RABIT	110.31	61	3	3	1831
25	P46406|G3P_RABIT	240.95	50	12	12	35780
30	P31097|OSTP_RABIT	199.95	46	8	8	35172
31	Q9TTC6|PPIA_RABIT	181.75	63	8	8	17837
33	Q29426|K2C3_RABIT	196.25	18	10	5	64341
35	C0HJA9|OBP3_RABIT	209.33	58	6	6	4721
39	P35543|SAA3_RABIT	214.21	26	6	6	13806
42	Q28706|K1C12_RABIT	213.12	27	8	4	45727
43	P13491|LDHA_RABIT	163.58	24	6	5	36565
45	P62740|ACTA_RABIT	185.37	16	5	1	42009
45	P68135|ACTS_RABIT	185.37	16	5	1	42051
46	Q08863|GSTA1_RABIT	200.5	29	6	6	25691
47	P13490|LDHB_RABIT	162.16	28	6	5	24134
48	P39056|OSTCN_RABIT	147.29	90	4	4	5431
49	P25704|ENOB_RABIT	184.5	16	4	4	47069
53	P01685|KV04_RABIT	152.66	32	2	1	11182
54	P30801|S10A6_RABIT	139.85	58	5	5	10154
61	O97862|CYTC_RABIT	164.28	40	5	5	16346
63	P62160|CALM_RABIT	151.81	46	4	4	16838
65	P80191|FETUA_RABIT	182.11	22	4	4	38387
66	Q28680|CD14_RABIT	120.09	17	5	5	39992
69	P12247|CO3_RABIT	161.86	12	5	3	81844
72	P01687|KV06_RABIT	148.7	31	2	2	11281
77	P01847|LAC_RABIT	109.75	33	2	2	11484
78	P68105|EF1A1_RABIT	138.32	8	2	2	50141
80	P11974|KPYM_RABIT	150.1	14	5	5	58048
81	P16973|LYSC_RABIT	133.31	38	3	3	14722
82	P24480|S10AB_RABIT	159.31	58	3	3	11429
85	P21195|PDIA1_RABIT	132.28	12	3	3	56808

86	P02252|H14_RABIT	105.81	18	3	3	21897
87	Q6Q6X0|1433T_RABIT	113.35	14	3	3	27778
88	P14422|PA2GA_RABIT	107.93	38	2	2	7607
89	Q95MF9|CLIC1_RABIT	96.54	20	3	3	26925
90	O77791|S10AC_RABIT	104.01	36	2	2	10668
97	P26203|P15B_RABIT	115.02	27	3	3	15626
97	P26202|P15A_RABIT	115.02	27	3	3	15675
98	Q28631|WFDC2_RABIT	97.42	33	2	2	12803
99	P25230|CAP18_RABIT	142.22	23	3	3	19805
104	Q8WN94|ACBP_RABIT	156.5	39	2	2	9915
105	P34032|TYB4_RABIT	96.2	32	2	2	5037
106	P07466|DEF6_RABIT	67.33	21	2	2	10122
107	P00883|ALDOA_RABIT	112.6	9	2	2	39343
109	P01692|KV11_RABIT	98.76	17	2	2	9469
112	P46409|GSTMU_RABIT	86.25	14	2	2	25417
113	P50117|S10A9_RABIT	84.33	21	2	2	14787
125	P53789|VTDB_RABIT	67.45	9	2	2	52912

Table S 14. Identified proteins in placebo treated rabbit 4, left eye.

Protein Group	Accession	-10lgP	Coverage (%)	Peptides	Unique	Avg. Mass
1	P19007|HPT_RABIT	363.87	65	29	22	38869
2	P01832|PIGR_RABIT	378.7	46	32	32	83887
3	P49065|ALBU_RABIT	334.56	56	32	28	68910
5	P19134|TRFE_RABIT	329.73	43	29	29	76670
6	P60990|PIP_RABIT	256.18	57	16	16	16871
9	P51662|ANXA1_RABIT	326.43	56	20	20	38735
11	P29751|ACTB_RABIT	312.51	53	16	1	41756
12	Q8MI17|AL1A1_RABIT	302.43	51	22	22	54341
13	C0HJA6|OBP2_RABIT	130.45	100	4	4	1831
15	Q9TTC6|PPIA_RABIT	208	63	11	11	17837
16	Q95218|DMBT1_RABIT	254.55	12	11	11	172763
19	P68105|EF1A1_RABIT	267.1	38	12	12	50141
19	Q71V39|EF1A2_RABIT	197.39	16	6	6	50470
21	P46406|G3P_RABIT	264.71	37	10	10	35780
22	P11974|KPYM_RABIT	250.27	39	13	13	58048
23	Q29426|K2C3_RABIT	233.17	22	12	7	64341
27	P00883|ALDOA_RABIT	213.8	29	9	9	39343
28	Q9XSC5|CLUS_RABIT	240.93	25	10	10	51851
30	P23108|IGJ_RABIT	180.08	54	5	5	15556
37	P01870|IGHG_RABIT	205.01	35	7	7	35404
38	P01879|IGHA_RABIT	226.12	31	8	8	32256
39	P00939|TPIS_RABIT	208.29	53	8	8	26757
41	P30947|HS90B_RABIT	198.1	18	10	5	83467
42	P13491|LDHA_RABIT	166.2	26	7	6	36565
46	P47845|LEG3_RABIT	152.89	36	6	6	25502
47	P13490|LDHB_RABIT	166.49	24	6	5	24134
48	Q28706|K1C12_RABIT	182.03	22	8	3	45727
49	Q08863|GSTA1_RABIT	190.73	29	6	6	25691
51	P62160|CALM_RABIT	177.16	46	5	5	16838
52	Q29504|UBA1_RABIT	202.3	12	8	8	117688
54	P30946|HS90A_RABIT	196.03	13	7	3	79733
56	Q6Q6X0|1433T_RABIT	163.17	31	7	7	27778
66	P21195|PDIA1_RABIT	173.03	17	5	5	56808
67	P15122|ALDR_RABIT	119.75	14	4	4	35763
68	P00567|KCRB_RABIT	180.15	29	6	6	42663
69	P11909|GPX1_RABIT	142.32	38	5	5	21883
72	P29562|IF4A1_RABIT	153.71	18	5	5	45291
74	P30801|S10A6_RABIT	104.36	43	3	3	10154
75	Q8WN94|ACBP_RABIT	161.14	60	4	4	9915
76	P80508|PE2R_RABIT	152.07	16	4	4	36670
77	P25704|ENOB_RABIT	172.94	16	4	4	47069
80	O19048|PCBP1_RABIT	126.74	16	4	4	37498
82	O97529|ANXA8_RABIT	127.14	16	4	4	36680

84	P41316|CRYAB_RABIT	128.91	25	4	4	20107
85	P08855|ICAL_RABIT	151.67	7	3	3	76966
88	Q95MF9|CLIC1_RABIT	141.24	20	3	3	26925
89	P80191|FETUA_RABIT	154.89	18	4	4	38387
91	Q8MK67|PEBP1_RABIT	171.53	55	5	5	20994
92	P46409|GSTMU_RABIT	98.73	14	2	2	25417
93	P10160|IF5A1_RABIT	124.58	35	3	3	16816
97	O97862|CYTC_RABIT	137.72	24	3	3	16346
99	O77791|S10AC_RABIT	106.71	49	3	3	10668
102	Q28631|WFDC2_RABIT	129.6	52	3	3	12803
105	P06815|CAN1_RABIT	114.8	12	3	3	35275
106	P26890|IL1RA_RABIT	92.62	16	2	2	20214
108	P79226|ALDOB_RABIT	106.78	8	2	2	39605
109	P09212|SODC_RABIT	118.62	37	2	2	15819
110	P24480|S10AB_RABIT	119.43	26	2	2	11429
111	P35543|SAA3_RABIT	142.05	13	2	2	13806
112	P62943|FKB1A_RABIT	93.22	25	2	2	11951
113	P08628|THIO_RABIT	93.91	23	2	2	11761
114	P34032|TYB4_RABIT	100.09	32	2	2	5037
115	P06813|CPNS1_RABIT	117.81	14	2	2	28239
117	P29694|EF1G_RABIT	93.53	8	2	2	50049
120	O19049|HNRPK_RABIT	86.4	6	2	2	50960
125	P02252|H14_RABIT	79.04	12	2	2	21897
127	P01840|KAC4_RABIT	120.46	40	2	2	11043
133	Q9XS70|COR1B_RABIT	82.98	9	2	2	53609
134	P12337|EST1_RABIT	77.3	6	2	2	62292

Table S 15. Identified proteins in placebo treated rabbit 5, left eye.

Protein Group	Accession	-10lgP	Coverage (%)	Peptides	Unique	Avg. Mass
1	P01832|PIGR_RABIT	426.67	51	49	49	83887
2	P19007|HPT_RABIT	339.13	55	23	19	38869
3	P19134|TRFE_RABIT	345.85	46	29	29	76670
4	P49065|ALBU_RABIT	323.01	56	30	22	68910
6	P60990|PIP_RABIT	248.33	61	15	15	16871
8	Q95218|DMBT1_RABIT	261.78	12	13	13	172763
11	P29751|ACTB_RABIT	284.96	45	12	1	41756
12	P23108|IGJ_RABIT	218.71	68	9	9	15556
13	C0HJA6|OBP2_RABIT	113.63	61	3	3	1831
15	Q8MI17|AL1A1_RABIT	236.05	38	13	13	54341
16	P01870|IGHG_RABIT	225.92	42	8	8	35404
22	P51662|ANXA1_RABIT	258.8	46	12	12	38735
23	P01879|IGHA_RABIT	245.59	31	9	9	32256
24	Q9XSC5|CLUS_RABIT	244.85	25	12	12	51851
30	O77791|S10AC_RABIT	180.93	71	6	6	10668
31	P46406|G3P_RABIT	208.97	33	7	7	35780
35	Q29426|K2C3_RABIT	165.08	12	6	3	64341
37	P68135|ACTS_RABIT	190.03	19	6	1	42051
37	P62740|ACTA_RABIT	190.03	19	6	1	42009
38	Q9TTC6|PPIA_RABIT	152.35	52	7	7	17837
49	P01840|KAC4_RABIT	183.25	68	3	3	11043
52	P11974|KPYM_RABIT	156.12	16	6	6	58048
54	O97862|CYTC_RABIT	146.17	30	4	4	16346
55	P13490|LDHB_RABIT	116.59	14	3	3	24134
56	P62160|CALM_RABIT	123.56	46	4	4	16838
59	P00883|ALDOA_RABIT	144.63	22	4	4	39343
61	Q08863|GSTA1_RABIT	133.85	20	4	4	25691
63	P25704|ENOB_RABIT	167.98	16	4	4	47069
65	P01696|KV15_RABIT	94.24	31	3	1	11596
66	P39056|OSTCN_RABIT	120.42	90	3	3	5431
68	O97529|ANXA8_RABIT	127.31	20	5	5	36680
69	Q6Q6X0|1433T_RABIT	121.7	22	4	4	27778
70	P01697|KV16_RABIT	85.57	18	2	1	12112
75	P16973|LYSC_RABIT	123.71	29	2	2	14722
76	P25230|CAP18_RABIT	157.98	23	3	3	19805
82	P50117|S10A9_RABIT	95.94	21	2	2	14787
83	P35543|SAA3_RABIT	138.12	13	2	2	13806
85	P00939|TPIS_RABIT	90.4	16	3	3	26757
89	P26203|P15B_RABIT	93.14	18	2	2	15626
89	P26202|P15A_RABIT	93.14	18	2	2	15675
92	Q28631|WFDC2_RABIT	74.37	33	2	2	12803
94	P31097|OSTP_RABIT	87.86	11	2	2	35172
95	P34032|TYB4_RABIT	81.65	32	2	2	5037
98	P02252|H14_RABIT	87.91	12	2	2	21897
103	P26890|IL1RA_RABIT	81.6	16	2	2	20214
111	P24480|S10AB_RABIT	101.64	47	2	2	11429

Table S 16. Identified proteins in placebo treated rabbit 6, left eye.

Protein Group	Accession	-10lgP	Coverage (%)	Peptides	Unique	Avg. Mass
1	P01832|PIGR_RABIT	421.29	51	54	54	83887
2	P19134|TRFE_RABIT	380.16	58	43	43	76670
3	P19007|HPT_RABIT	335.54	65	28	24	38869
4	P49065|ALBU_RABIT	318.66	53	30	30	68910
6	P60990|PIP_RABIT	259	61	18	18	16871
9	Q95218|DMBT1_RABIT	279.07	16	16	16	172763
10	P01870|IGHG_RABIT	270.54	46	15	15	35404
11	P51662|ANXA1_RABIT	298.5	57	16	16	38735
12	P29751|ACTB_RABIT	260.51	51	13	1	41756
13	P23108|IGJ_RABIT	226.81	66	12	12	15556
16	Q8MI17|AL1A1_RABIT	259.19	50	16	16	54341
18	P01879|IGHA_RABIT	269.72	39	12	12	32256
19	Q9XSC5|CLUS_RABIT	253.21	27	13	13	51851
21	P68105|EF1A1_RABIT	223.61	29	11	11	50141
21	Q71V39|EF1A2_RABIT	177.05	12	5	5	50470
22	P46406|G3P_RABIT	237.44	41	11	11	35780
26	P13491|LDHA_RABIT	159.96	25	7	7	36565
27	C0HJA6|OBP2_RABIT	124.77	61	2	2	1831
29	P68135|ACTS_RABIT	183.42	25	8	1	42051
29	P62740|ACTA_RABIT	183.42	25	8	1	42009
30	Q9TTC6|PPIA_RABIT	156.63	52	7	7	17837
31	Q29426|K2C3_RABIT	179.22	17	10	6	64341
34	P30801|S10A6_RABIT	128.18	74	8	8	10154
36	P39056|OSTCN_RABIT	156.05	90	3	3	5431
38	Q08863|GSTA1_RABIT	182.75	49	10	10	25691
42	P31097|OSTP_RABIT	165.85	37	6	6	35172
44	P13490|LDHB_RABIT	146.7	28	7	7	24134
46	P25704|ENOB_RABIT	180.56	16	4	4	47069
47	Q6Q6X0|1433T_RABIT	157.83	27	5	5	27778
48	P62160|CALM_RABIT	152.64	46	4	4	16838
51	P01840|KAC4_RABIT	189.06	54	3	3	11043
52	O97862|CYTC_RABIT	163.37	37	5	5	16346
55	Q28706|K1C12_RABIT	111.57	12	5	2	45727
58	P00939|TPIS_RABIT	142.94	33	5	5	26757
59	Q28631|WFDC2_RABIT	120	52	3	3	12803
60	C0HJA9|OBP3_RABIT	154.08	58	3	3	4721
62	P11974|KPYM_RABIT	149.57	17	6	6	58048
63	P46409|GSTMU_RABIT	139.17	22	3	3	25417
64	P16973|LYSC_RABIT	137.23	29	4	4	14722
65	P47845|LEG3_RABIT	100.23	14	3	3	25502
71	P14422|PA2GA_RABIT	121.94	40	3	3	7607
74	P35543|SAA3_RABIT	140.83	13	2	2	13806
75	P30946|HS90A_RABIT	133.58	6	3	3	79733

77	Q95MF9|CLIC1_RABIT	102.42	14	3	3	26925
79	P24480|S10AB_RABIT	133.13	58	3	3	11429
81	P01696|KV15_RABIT	98.06	22	2	1	11596
82	P80508|PE2R_RABIT	113.96	13	3	3	36670
83	O19048|PCBP1_RABIT	93.52	7	2	2	37498
85	P01847|LAC_RABIT	111.02	33	2	2	11484
87	Q8WN94|ACBP_RABIT	126.5	39	3	3	9915
88	P01685|KV04_RABIT	89.18	32	2	1	11182
89	P00567|KCRB_RABIT	93	7	2	2	42663
93	P34032|TYB4_RABIT	77.87	32	2	2	5037
95	P80191|FETUA_RABIT	116.12	15	3	3	38387
97	Q28658|SPRR3_RABIT	64.91	16	2	2	24139
104	Q8MK67|PEBP1_RABIT	68.85	21	2	2	20994

Table S 17. Identified proteins in placebo treated rabbit 7, left eye.

Protein Group	Accession	-10lgP	Coverage (%)	Peptides	Unique	Avg. Mass
1	P19134|TRFE_RABIT	437.74	67	84	81	76670
2	P01832|PIGR_RABIT	417.23	52	51	51	83887
3	P19007|HPT_RABIT	339.62	64	28	21	38869
4	P60990|PIP_RABIT	274.66	61	25	25	16871
5	P49065|ALBU_RABIT	343.79	57	30	30	68910
8	Q8MI17|AL1A1_RABIT	328.56	58	29	29	54341
9	Q95218|DMBT1_RABIT	270.77	12	13	13	172763
13	P29751|ACTB_RABIT	292.63	59	15	1	41756
14	P51662|ANXA1_RABIT	319.56	57	19	19	38735
15	P46406|G3P_RABIT	289.63	50	15	15	35780
18	P23108|IGJ_RABIT	227.91	82	12	12	15556
20	P13491|LDHA_RABIT	243.23	44	14	13	36565
21	P13490|LDHB_RABIT	229.86	51	12	11	24134
23	Q9XSC5|CLUS_RABIT	244.78	28	12	12	51851
25	P68105|EF1A1_RABIT	236.19	32	10	5	50141
27	P25704|ENOB_RABIT	222.02	19	5	5	47069
29	P68135|ACTS_RABIT	204.11	25	8	1	42051
29	P62740|ACTA_RABIT	198.71	22	7	1	42009
30	P01870|IGHG_RABIT	219.17	33	6	6	35404
35	Q08863|GSTA1_RABIT	194.15	41	7	7	25691
37	P01879|IGHA_RABIT	227.72	31	8	8	32256
38	C0HJA6|OBP2_RABIT	117.66	61	3	3	1831
40	Q9TTC6|PPIA_RABIT	164.49	49	7	7	17837
42	Q29426|K2C3_RABIT	186.93	16	9	3	64341
45	O97529|ANXA8_RABIT	193.84	30	7	7	36680
50	P00883|ALDOA_RABIT	191.21	28	6	6	39343
51	P39056|OSTCN_RABIT	158.16	90	3	3	5431
52	P62160|CALM_RABIT	169.42	46	5	5	16838
53	C0HJA9|OBP3_RABIT	157.13	58	3	3	4721
54	Q8HZQ5|EZRI_RABIT	145.3	11	6	6	69220
55	Q28706|K1C12_RABIT	139.63	17	7	2	45727
56	Q6Q6X0|1433T_RABIT	168.89	30	6	6	27778
57	P26203|P15B_RABIT	187.41	42	6	6	15626
57	P26202|P15A_RABIT	187.41	42	6	6	15675
60	P11974|KPYM_RABIT	181.26	23	8	8	58048
63	P01840|KAC4_RABIT	196.02	63	4	4	11043
64	P30801|S10A6_RABIT	123.52	67	4	4	10154
65	O97862|CYTC_RABIT	150.99	37	5	5	16346
66	P24480|S10AB_RABIT	165.06	58	3	3	11429
70	P16973|LYSC_RABIT	144.46	45	4	4	14722
71	P47845|LEG3_RABIT	102	14	3	3	25502
72	P80508|PE2R_RABIT	135.43	13	3	3	36670
76	O19049|HNRPK_RABIT	124.11	15	4	4	50960

77	P25230|CAP18_RABIT	166.75	23	3	3	19805
80	P30946|HS90A_RABIT	131.26	11	5	5	79733
81	P35543|SAA3_RABIT	152.89	13	2	2	13806
84	O19048|PCBP1_RABIT	119.1	10	3	3	37498
87	P14422|PA2GA_RABIT	104.71	38	2	2	7607
91	P00939|TPIS_RABIT	115.76	16	3	3	26757
92	P21195|PDIA1_RABIT	127.11	11	3	3	56808
94	O77791|S10AC_RABIT	105.04	58	3	3	10668
95	P46409|GSTMU_RABIT	107.5	14	2	2	25417
96	Q28739|BPI_RABIT	148.03	6	2	2	48837
97	Q95MF9|CLIC1_RABIT	93.47	14	3	3	26925
98	Q28640|HRG_RABIT	119.22	9	3	3	58877
100	P02252|H14_RABIT	105	17	3	3	21897
102	P08628|THIO_RABIT	90.02	23	2	2	11761
104	P29562|IF4A1_RABIT	105.03	11	3	3	45291
105	Q8MK67|PEBP1_RABIT	130.09	55	4	4	20994
106	P62493|RB11A_RABIT	79.9	18	3	3	24394
107	P10160|IF5A1_RABIT	121.72	35	3	3	16816
108	Q28631|WFDC2_RABIT	107.31	33	2	2	12803
109	P01684|KV03_RABIT	97.02	21	3	1	11512
110	Q8WN94|ACBP_RABIT	116.46	28	2	2	9915
111	P34032|TYB4_RABIT	82.91	32	2	2	5037
112	P50117|S10A9_RABIT	90.16	23	2	2	14787
113	P07466|DEF6_RABIT	68.88	21	2	2	10122
117	P80191|FETUA_RABIT	104.03	9	2	2	38387
118	P12337|EST1_RABIT	84.08	6	2	2	62292
122	P31097|OSTP_RABIT	73.61	9	2	2	35172
135	P09212|SODC_RABIT	70.25	32	2	2	15819

Table S 18. Identified proteins in placebo treated rabbit 8, left eye.

Protein Group	Accession	-10lgP	Coverage (%)	Peptides	Unique	Avg. Mass
1	P01832|PIGR_RABIT	442.8	52	56	56	83887
2	P19134|TRFE_RABIT	393.79	56	48	48	76670
3	P49065|ALBU_RABIT	394.03	65	48	41	68910
4	P19007|HPT_RABIT	364.22	67	41	29	38869
5	P60990|PIP_RABIT	274.26	59	22	22	16871
9	Q95218|DMBT1_RABIT	256.52	11	11	11	172763
11	P01879|IGHA_RABIT	273.06	48	13	13	32256
13	P29751|ACTB_RABIT	272.59	56	14	1	41756
14	Q29426|K2C3_RABIT	236.28	34	20	10	64341
15	Q8MI17|AL1A1_RABIT	270.93	45	17	17	54341
16	P23108|IGJ_RABIT	229.33	82	11	11	15556
17	P51662|ANXA1_RABIT	288.47	56	16	16	38735
20	P01870|IGHG_RABIT	243.55	47	10	10	35404
21	Q9XSC5|CLUS_RABIT	267.68	30	14	14	51851
23	Q28706|K1C12_RABIT	249.69	38	14	7	45727
25	P46406|G3P_RABIT	254.69	41	11	11	35780
34	Q9TTC6|PPIA_RABIT	163.62	66	10	10	17837
35	P13491|LDHA_RABIT	182.45	29	8	7	36565
36	C0HJA9|OBP3_RABIT	176.86	58	4	4	4721
43	P39056|OSTCN_RABIT	171.69	90	4	4	5431
44	Q28640|HRG_RABIT	195.04	17	8	8	58877
45	P68135|ACTS_RABIT	182.98	22	7	1	42051
45	P62740|ACTA_RABIT	182.98	22	7	1	42009
47	P13490|LDHB_RABIT	166.05	35	8	7	24134
50	P25704|ENOB_RABIT	177.35	16	4	4	47069
52	Q08863|GSTA1_RABIT	166.05	29	6	6	25691
54	P01840|KAC4_RABIT	181.54	57	4	4	11043
56	O97862|CYTC_RABIT	174.55	37	5	5	16346
58	P80191|FETUA_RABIT	183.76	26	5	5	38387
59	P12247|CO3_RABIT	169.29	14	6	4	81844
60	P09809|APOA1_RABIT	143.78	21	6	6	30591
64	C0HJA6|OBP2_RABIT	121.42	61	3	3	1831
65	P16973|LYSC_RABIT	146.14	36	4	4	14722
67	P11974|KPYM_RABIT	127.81	13	5	5	58048
68	P31097|OSTP_RABIT	153.66	30	5	5	35172
69	P35543|SAA3_RABIT	152.54	13	2	2	13806
73	O97529|ANXA8_RABIT	161.12	20	5	5	36680
74	P62160|CALM_RABIT	138.32	46	4	4	16838
76	P00883|ALDOA_RABIT	145.16	15	3	3	39343
77	P24480|S10AB_RABIT	134.91	58	3	3	11429
80	P20058|HEMO_RABIT	97.87	12	4	4	51767
83	Q6Q6X0|1433T_RABIT	123.88	22	4	4	27778
84	P30801|S10A6_RABIT	80.65	43	4	4	10154

87	Q95MF9|CLIC1_RABIT	96.9	10	2	2	26925
89	P46409|GSTMU_RABIT	88.44	14	2	2	25417
91	P21195|PDIA1_RABIT	105.37	14	4	4	56808
92	P00567|KCRB_RABIT	136.93	12	3	3	42663
94	O77791|S10AC_RABIT	96.32	49	3	3	10668
95	Q28631|WFDC2_RABIT	117.01	33	2	2	12803
96	Q8WN94|ACBP_RABIT	129.83	60	4	4	9915
98	P01696|KV15_RABIT	88.28	31	3	1	11596
99	P80508|PE2R_RABIT	105.33	13	3	3	36670
101	Q29504|UBA1_RABIT	87.29	6	4	4	117688
102	P26890|IL1RA_RABIT	97.82	17	2	2	20214
104	P01697|KV16_RABIT	74.3	18	2	1	12112
105	P01685|KV04_RABIT	70.56	32	2	1	11182
107	P47845|LEG3_RABIT	75.64	10	2	2	25502
111	P09212|SODC_RABIT	59.44	32	2	2	15819
112	P31347|ANGI_RABIT	72.1	25	2	2	14361
113	P01687|KV06_RABIT	76.99	31	2	2	11281
117	P00939|TPIS_RABIT	65.61	11	2	2	26757

Table S 19. Identified proteins in placebo treated rabbit 9, left eye.

Protein Group	Accession	-10lgP	Coverage (%)	Peptides	Unique	Avg. Mass
1	P01832|PIGR_RABIT	413.06	48	31	31	83887
2	P19134|TRFE_RABIT	369.97	47	29	28	76670
3	P19007|HPT_RABIT	312.05	55	16	13	38869
4	P49065|ALBU_RABIT	339.5	57	29	29	68910
5	P60990|PIP_RABIT	256.46	51	9	9	16871
7	Q95218|DMBT1_RABIT	279.35	14	13	13	172763
10	P29751|ACTB_RABIT	255.29	46	11	1	41756
13	P51662|ANXA1_RABIT	283.32	48	13	13	38735
14	Q9XSC5|CLUS_RABIT	246.5	29	10	10	51851
15	Q8MI17|AL1A1_RABIT	226.73	30	10	10	54341
17	P01879|IGHA_RABIT	263.44	39	7	7	32256
18	P23108|IGJ_RABIT	208.62	60	7	7	15556
19	Q29426|K2C3_RABIT	216.78	11	6	3	64341
20	P01870|IGHG_RABIT	189.79	28	4	4	35404
24	P68105|EF1A1_RABIT	237.07	31	8	8	50141
24	Q71V39|EF1A2_RABIT	198.76	17	5	5	50470
27	P39056|OSTCN_RABIT	178.49	90	4	4	5431
33	P46406|G3P_RABIT	217.17	32	6	6	35780
37	C0HJA9|OBP3_RABIT	150.96	58	3	3	4721
39	Q28706|K1C12_RABIT	160.96	14	4	4	45727
43	Q9TTC6|PPIA_RABIT	158.72	45	5	5	17837
44	P62160|CALM_RABIT	151.11	31	3	3	16838
48	O97862|CYTC_RABIT	160.51	31	4	4	16346
53	P25704|ENOB_RABIT	164.46	11	3	3	47069
59	P01840|KAC4_RABIT	164.44	40	2	2	11043
60	Q6Q6X0|1433T_RABIT	137.31	18	3	3	27778
61	P15122|ALDR_RABIT	103.95	8	2	2	35763
62	P35543|SAA3_RABIT	162.48	13	2	2	13806
72	P80191|FETUA_RABIT	143.71	15	3	3	38387
74	P24480|S10AB_RABIT	119.16	58	3	3	11429
88	Q28631|WFDC2_RABIT	114.61	33	2	2	12803
91	P00567|KCRB_RABIT	106.53	10	2	2	42663

Table S 20. Identified proteins in placebo treated rabbit 10, left eye.

Protein Group	Accession	-10lgP	Coverage (%)	Peptides	Unique	Avg. Mass
1	P19134|TRFE_RABIT	457.37	68	111	107	76670
2	P01832|PIGR_RABIT	470.54	55	78	78	83887
3	P49065|ALBU_RABIT	405.49	68	62	62	68910
4	P60990|PIP_RABIT	290.47	61	28	28	16871
5	P19007|HPT_RABIT	377.33	62	41	31	38869
6	Q95218|DMBT1_RABIT	317.8	22	24	24	172763
7	P51662|ANXA1_RABIT	364.32	60	27	27	38735
9	P29751|ACTB_RABIT	338.67	67	24	1	41756
10	Q8MI17|AL1A1_RABIT	318.28	62	26	26	54341
11	P01879|IGHA_RABIT	299.04	31	20	20	32256
12	P23108|IGJ_RABIT	246.68	74	19	19	15556
14	P11974|KPYM_RABIT	337.85	52	22	22	58048
15	P46406|G3P_RABIT	298.79	56	18	18	35780
16	P68105|EF1A1_RABIT	312.85	51	19	11	50141
19	P01870|IGHG_RABIT	267.34	44	12	12	35404
20	P30801|S10A6_RABIT	198.55	74	12	12	10154
21	P00883|ALDOA_RABIT	283.57	64	14	14	39343
22	Q9XSC5|CLUS_RABIT	254.11	25	11	11	51851
23	P68135|ACTS_RABIT	231.71	31	11	1	42051
23	P62740|ACTA_RABIT	227.94	28	10	1	42009
24	P30947|HS90B_RABIT	229.81	29	16	9	83467
25	P30946|HS90A_RABIT	237.75	33	15	9	79733
27	C0HJA6|OBP2_RABIT	127.45	61	3	3	1831
28	Q9TTC6|PPIA_RABIT	228.5	63	11	11	17837
29	C0HJA9|OBP3_RABIT	232.35	58	8	8	4721
30	Q29504|UBA1_RABIT	257.62	19	13	13	117688
31	P21195|PDIA1_RABIT	269.81	42	14	14	56808
32	P00567|KCRB_RABIT	268.32	38	9	9	42663
35	Q29426|K2C3_RABIT	215.31	20	14	6	64341
36	Q28706|K1C12_RABIT	216.34	46	14	9	45727
38	P13491|LDHA_RABIT	180.55	36	9	8	36565
41	P39056|OSTCN_RABIT	203.51	90	6	6	5431
42	P62160|CALM_RABIT	225.49	54	8	8	16838
44	P12337|EST1_RABIT	223.87	28	12	12	62292
46	O19053|ADHX_RABIT	216.64	48	10	10	39596
48	P13490|LDHB_RABIT	165.56	37	8	7	24134
49	P35543|SAA3_RABIT	208.95	32	6	6	13806
50	P16973|LYSC_RABIT	180.27	55	6	6	14722
51	Q6Q6X0|1433T_RABIT	200.72	31	7	7	27778
52	P24480|S10AB_RABIT	194.52	58	4	4	11429
59	P31097|OSTP_RABIT	201.46	46	7	7	35172
61	Q95MF9|CLIC1_RABIT	167.31	39	7	6	26925
63	P00939|TPIS_RABIT	207.82	56	9	9	26757

64	P14422|PA2GA_RABIT	166.46	38	5	5	7607
66	P25704|ENOB_RABIT	202.42	16	4	4	47069
67	P25230|CAP18_RABIT	194.21	38	5	5	19805
72	P11909|GPX1_RABIT	197.61	46	8	8	21883
74	O19048|PCBP1_RABIT	163.64	31	7	7	37498
75	O19049|HNRPK_RABIT	197.26	24	7	7	50960
76	P80191|FETUA_RABIT	200.27	26	5	5	38387
78	Q8HZQ5|EZRI_RABIT	153.51	10	5	5	69220
80	Q08863|GSTA1_RABIT	174.04	37	5	5	25691
81	P47845|LEG3_RABIT	147.7	35	6	6	25502
82	P26202|P15A_RABIT	207.88	42	6	6	15675
82	P26203|P15B_RABIT	207.88	42	6	6	15626
84	P08855|ICAL_RABIT	171.26	21	8	7	76966
85	P01840|KAC4_RABIT	201.61	91	4	4	11043
86	O97529|ANXA8_RABIT	175.58	28	6	6	36680
87	P10160|IF5A1_RABIT	188.65	43	5	5	16816
89	P09809|APOA1_RABIT	170.32	29	6	6	30591
90	P15128|CP4B1_RABIT	160.35	20	7	7	58604
92	P41316|CRYAB_RABIT	142.25	45	6	6	20107
93	P15253|CALR_RABIT	165.98	14	3	3	48275
94	P80508|PE2R_RABIT	165.77	21	5	5	36670
95	O77791|S10AC_RABIT	149.25	71	5	5	10668
97	Q28739|BPI_RABIT	178.13	16	5	5	48837
99	P00489|PYGM_RABIT	169.43	14	7	7	97289
100	P29562|IF4A1_RABIT	183.9	29	8	8	45291
101	P02252|H14_RABIT	130.91	19	5	5	21897
102	Q28640|HRG_RABIT	174.91	9	4	4	58877
103	O97862|CYTC_RABIT	168.65	37	5	5	16346
104	Q8WN94|ACBP_RABIT	179.24	51	4	4	9915
107	O77622|TCPZ_RABIT	152.87	21	6	6	58024
108	P00949|PGM1_RABIT	139.1	15	5	5	61558
109	P23612|SYWC_RABIT	158.49	17	5	5	53799
110	P09212|SODC_RABIT	130.49	49	4	4	15819
111	P00389|NCPR_RABIT	130.08	7	4	4	76588
112	P46409|GSTMU_RABIT	144.26	22	4	4	25417
113	P06813|CPNS1_RABIT	150.85	22	3	3	28239
115	Q8MK67|PEBP1_RABIT	166.84	59	4	4	20994
116	P15122|ALDR_RABIT	114.07	11	3	3	35763
117	P50117|S10A9_RABIT	134.99	33	3	3	14787
118	O18750|ENPL_RABIT	153.22	11	6	5	82608
119	Q9BGN0|PON3_RABIT	113.7	19	4	4	39507
120	P62493|RB11A_RABIT	115.28	23	4	4	24394
122	P12247|CO3_RABIT	120.24	9	4	2	81844
124	P06815|CAN1_RABIT	113.03	11	3	3	35275
125	Q28631|WFDC2_RABIT	139.67	40	3	3	12803

126	P01847|LAC_RABIT	113.44	33	2	2	11484
127	P08628|THIO_RABIT	146.85	37	4	4	11761
131	P00169|CYB5_RABIT	120.95	34	3	3	15349
134	P02057|HBB_RABIT	123.01	23	3	3	16133
135	P01696|KV15_RABIT	103.04	31	3	1	11596
138	P29694|EF1G_RABIT	113.11	9	3	3	50049
146	Q09YN4|CAZA2_RABIT	136.61	17	3	3	32951
148	P53789|VTDB_RABIT	82.63	9	2	2	52912
149	P34826|EF1B_RABIT	137.41	27	3	3	24749
150	P07466|DEF6_RABIT	83.53	21	2	2	10122
151	P34032|TYB4_RABIT	106.46	32	2	2	5037
153	P19943|RLA2_RABIT	129.24	82	3	3	4695
157	P62943|FKB1A_RABIT	92.75	25	2	2	11951
160	P79226|ALDOB_RABIT	107.39	8	2	2	39605
164	Q28619|NHRF1_RABIT	94.24	16	3	3	38562
165	P01687|KV06_RABIT	89.75	31	2	2	11281
167	P01948|HBA_RABIT	115.92	26	2	2	15589
184	P62139|PP1A_RABIT	57.75	9	2	2	37512
184	P62143|PP1B_RABIT	57.75	9	2	2	37187
190	P01885|B2MG_RABIT	116.02	22	2	2	11654

Table S 21. Identified proteins in postbiotic treated rabbit 1, right eye.

Protein Group	Accession	-10lgP	Coverage (%)	Peptides	Unique	Avg. Mass
1	P19134|TRFE_RABIT	435.05	68	79	79	76670
2	P01832|PIGR_RABIT	443.32	51	63	63	83887
3	P19007|HPT_RABIT	382.66	67	46	35	38869
4	P49065|ALBU_RABIT	372.96	62	43	43	68910
5	P60990|PIP_RABIT	260.73	61	22	22	16871
6	P51662|ANXA1_RABIT	344.34	60	24	24	38735
9	Q95218|DMBT1_RABIT	291.42	17	17	17	172763
10	P29751|ACTB_RABIT	313.21	59	18	1	41756
13	Q8MI17|AL1A1_RABIT	315.63	50	23	23	54341
17	P01870|IGHG_RABIT	268.75	57	15	15	35404
18	P23108|IGJ_RABIT	230.6	68	14	14	15556
19	P46406|G3P_RABIT	286.92	49	15	15	35780
20	Q9XSC5|CLUS_RABIT	265.05	29	14	14	51851
22	P01879|IGHA_RABIT	282	39	14	14	32256
25	C0HJA6|OBP2_RABIT	133.42	100	4	4	1831
26	Q9TTC6|PPIA_RABIT	237.06	67	11	11	17837
27	P11974|KPYM_RABIT	277.1	45	15	15	58048
28	P68105|EF1A1_RABIT	264.13	40	13	13	50141
28	Q71V39|EF1A2_RABIT	201.73	18	7	7	50470
30	P00883|ALDOA_RABIT	248.62	56	12	12	39343
32	P68135|ACTS_RABIT	207.65	25	8	1	42051
32	P62740|ACTA_RABIT	198.62	22	7	1	42009
34	Q29504|UBA1_RABIT	236.72	20	15	15	117688
36	P15122|ALDR_RABIT	202.21	50	12	12	35763
42	Q29426|K2C3_RABIT	204.55	19	12	5	64341
45	P00567|KCRB_RABIT	249.25	40	10	10	42663
47	P30946|HS90A_RABIT	221.23	19	10	6	79733
50	P62160|CALM_RABIT	199.99	50	6	6	16838
52	P47845|LEG3_RABIT	157	43	7	7	25502
54	P13491|LDHA_RABIT	163.51	23	6	6	36565
56	P30947|HS90B_RABIT	167.46	16	8	3	83467
58	P80191|FETUA_RABIT	208.65	31	6	6	38387
59	P31097|OSTP_RABIT	193.48	44	8	8	35172
61	P01840|KAC4_RABIT	187.73	91	5	5	11043
62	P39056|OSTCN_RABIT	168.75	90	3	3	5431
63	P25704|ENOB_RABIT	182.76	16	4	4	47069
64	P21195|PDIA1_RABIT	194.76	20	7	7	56808
65	P00939|TPIS_RABIT	174.43	49	8	8	26757
66	Q6Q6X0|1433T_RABIT	182.94	26	6	6	27778
67	P13490|LDHB_RABIT	142.35	29	6	6	24134
74	Q95MF9|CLIC1_RABIT	186.69	43	7	7	26925
75	O97529|ANXA8_RABIT	184.16	30	7	7	36680
76	O77791|S10AC_RABIT	138.46	71	4	4	10668
78	Q28706|K1C12_RABIT	140.78	19	7	2	45727

79	P14422|PA2GA_RABIT	144.68	38	4	4	7607
80	Q8WN94|ACBP_RABIT	205.03	60	5	5	9915
85	P08855|ICAL_RABIT	168.19	21	7	7	76966
88	Q8HZQ5|EZRI_RABIT	172.15	13	7	7	69220
89	Q28640|HRG_RABIT	174.51	15	7	7	58877
90	O97862|CYTC_RABIT	178.48	37	5	5	16346
91	P10160|IF5A1_RABIT	156.09	43	4	4	16816
92	P80508|PE2R_RABIT	170.27	24	6	6	36670
95	P30801|S10A6_RABIT	110.06	66	5	5	10154
96	Q08863|GSTA1_RABIT	132.58	25	5	5	25691
97	P35543|SAA3_RABIT	153.01	19	3	3	13806
98	O19048|PCBP1_RABIT	151.57	24	6	6	37498
101	P29562|IF4A1_RABIT	182.66	22	6	6	45291
102	C0HJA9|OBP3_RABIT	149.94	58	3	3	4721
105	P46409|GSTMU_RABIT	155.52	27	4	4	25417
106	P09809|APOA1_RABIT	132.69	26	5	5	30591
107	Q8MK67|PEBP1_RABIT	175.49	66	6	6	20994
108	P16973|LYSC_RABIT	136.45	35	4	4	14722
109	P08628|THIO_RABIT	134.77	49	4	4	11761
110	Q28631|WFDC2_RABIT	151.86	59	4	4	12803
111	P79226|ALDOB_RABIT	123.78	16	4	4	39605
112	P15253|CALR_RABIT	104.58	10	3	3	48275
114	P06813|CPNS1_RABIT	129.71	20	3	3	28239
115	P12337|EST1_RABIT	143.44	8	3	3	62292
117	Q28658|SPRR3_RABIT	125.6	24	3	3	24139
118	P11909|GPX1_RABIT	131.46	36	4	4	21883
120	P24480|S10AB_RABIT	139.5	58	3	3	11429
123	P02252|H14_RABIT	99.81	18	3	3	21897
125	P01692|KV11_RABIT	116.13	17	2	2	9469
126	P62493|RB11A_RABIT	104.15	16	3	3	24394
127	P20058|HEMO_RABIT	116.38	8	2	2	51767
129	P50117|S10A9_RABIT	111.05	33	4	4	14787
131	O18998|DNAS1_RABIT	102.48	14	3	3	31346
132	P53789|VTDB_RABIT	106.11	13	3	3	52912
133	P01696|KV15_RABIT	95.79	31	3	1	11596
134	P06815|CAN1_RABIT	90.63	8	2	2	35275
135	P35324|SPRR1_RABIT	66.54	23	2	2	14044
136	P09212|SODC_RABIT	123.02	37	3	3	15819
137	P01697|KV16_RABIT	80.36	30	3	1	12112
139	P34032|TYB4_RABIT	98.58	32	2	2	5037
143	Q28619|NHRF1_RABIT	91.06	11	2	2	38562
146	P29694|EF1G_RABIT	90.94	8	2	2	50049
147	Q28680|CD14_RABIT	66.1	8	2	2	39992
148	P01685|KV04_RABIT	71.77	32	2	1	11182
149	P58776|TPM2_RABIT	84.98	11	3	2	32837

150	P62943|FKB1A_RABIT	89.06	25	2	2	11951
153	O62695|H2AV_RABIT	63.5	15	2	2	13481
154	P03988|IGHM_RABIT	74.74	6	2	2	49897
154	P04221|MUCM_RABIT	74.74	6	2	2	52351
155	O19049|HNRPK_RABIT	81.1	8	2	2	50960
158	P13019|BLMH_RABIT	71.99	13	2	2	32579
162	Q9N0V7|CBS_RABIT	81.4	9	2	2	60212
167	P01687|KV06_RABIT	79.48	31	2	2	11281
185	P58772|TPM1_RABIT	70.24	8	2	1	32681

Table S 22. Identified proteins in postbiotic treated rabbit 2, right eye.

Protein Group	Accession	-10lgP	Coverage (%)	Peptides	Unique	Avg. Mass
1	P19007|HPT_RABIT	390.54	65	43	33	38869
2	P01832|PIGR_RABIT	451.6	53	56	56	83887
3	P49065|ALBU_RABIT	393.06	65	49	42	68910
4	P19134|TRFE_RABIT	411.3	63	58	58	76670
6	P29751|ACTB_RABIT	368.59	70	28	1	41756
7	P60990|PIP_RABIT	264.98	61	21	21	16871
8	P51662|ANXA1_RABIT	369.03	58	27	27	38735
9	P46406|G3P_RABIT	325.43	50	22	22	35780
10	P30801|S10A6_RABIT	282.12	74	17	17	10154
11	Q8MI17|AL1A1_RABIT	358.7	70	31	31	54341
12	C0HJA6|OBP2_RABIT	138.22	100	4	4	1831
14	P68105|EF1A1_RABIT	322.58	56	20	20	50141
14	Q71V39|EF1A2_RABIT	216.72	18	7	7	50470
15	Q29504|UBA1_RABIT	314.42	40	25	25	117688
16	P30946|HS90A_RABIT	294.77	43	21	15	79733
19	P11974|KPYM_RABIT	338.04	46	16	16	58048
20	Q9TTC6|PPIA_RABIT	289.84	65	14	14	17837
21	P30947|HS90B_RABIT	274.66	39	19	13	83467
22	P68135|ACTS_RABIT	246.21	31	12	1	42051
22	P62740|ACTA_RABIT	237.85	28	10	1	42009
23	P13491|LDHA_RABIT	270.84	59	19	17	36565
24	P15122|ALDR_RABIT	263.69	60	14	14	35763
25	Q95218|DMBT1_RABIT	271.03	15	13	13	172763
27	Q08863|GSTA1_RABIT	272.42	56	13	13	25691
27	Q08862|GSTA_RABIT	59.1	7	2	2	25450
28	P24480|S10AB_RABIT	236.25	58	8	8	11429
29	P00883|ALDOA_RABIT	271.24	56	12	12	39343
30	P01870|IGHG_RABIT	239.58	51	8	8	35404
31	P13490|LDHB_RABIT	242.31	38	12	10	24134
32	P00567|KCRB_RABIT	292.56	45	11	11	42663
33	P23108|IGJ_RABIT	197.48	54	8	8	15556
34	P01879|IGHA_RABIT	268.89	39	9	9	32256
35	P62160|CALM_RABIT	220.17	46	7	7	16838
37	O97529|ANXA8_RABIT	255.29	42	11	11	36680
38	Q6Q6X0|1433T_RABIT	236.98	34	9	9	27778
40	Q8HZQ5|EZRI_RABIT	232.42	23	11	11	69220
41	P06813|CPNS1_RABIT	239.7	65	10	10	28239
43	P08855|ICAL_RABIT	239.97	30	11	11	76966
44	Q9XSC5|CLUS_RABIT	266.36	27	12	12	51851
45	Q95MF9|CLIC1_RABIT	198.96	54	7	7	26925
47	P00939|TPIS_RABIT	238.52	65	10	10	26757
48	P29562|IF4A1_RABIT	235.26	40	11	11	45291
49	O19049|HNRPK_RABIT	206.99	29	9	9	50960

50	P80191|FETUA_RABIT	232.4	31	6	6	38387
53	O19048|PCBP1_RABIT	201.12	31	7	7	37498
54	P25704|ENOB_RABIT	219.2	16	4	4	47069
57	P80508|PE2R_RABIT	191.45	24	7	7	36670
58	P46409|GSTMU_RABIT	202.9	40	7	7	25417
59	O77791|S10AC_RABIT	174.12	71	6	6	10668
62	P06815|CAN1_RABIT	161.2	28	6	6	35275
63	P47845|LEG3_RABIT	129.49	29	5	5	25502
65	O19053|ADHX_RABIT	177.12	42	8	8	39596
66	P09212|SODC_RABIT	159.79	49	4	4	15819
68	P11909|GPX1_RABIT	175.93	32	5	5	21883
69	Q8WN94|ACBP_RABIT	198.6	60	5	5	9915
71	P39056|OSTCN_RABIT	176.06	90	4	4	5431
72	O97862|CYTC_RABIT	175.15	40	5	5	16346
73	P08628|THIO_RABIT	203.13	49	6	6	11761
74	Q9XS70|COR1B_RABIT	188.03	19	6	6	53609
75	O77506|LASP1_RABIT	153.97	22	4	4	29935
76	P14422|PA2GA_RABIT	128.89	38	3	3	7607
77	P16973|LYSC_RABIT	114.58	26	3	3	14722
79	P21195|PDIA1_RABIT	186.59	14	4	4	56808
80	P10160|IF5A1_RABIT	203.33	44	4	4	16816
81	C0HJA9|OBP3_RABIT	156.68	58	2	2	4721
82	P00489|PYGM_RABIT	155.88	9	5	5	97289
85	O77622|TCPZ_RABIT	172.71	24	6	6	58024
86	Q28619|NHRF1_RABIT	149.48	25	6	6	38562
89	P23612|SYWC_RABIT	172.83	14	4	4	53799
90	Q9N1E2|G6PI_RABIT	136	9	3	3	62747
94	P00949|PGM1_RABIT	152.06	15	5	5	61558
95	Q8MK67|PEBP1_RABIT	186.45	55	4	4	20994
96	Q28640|HRG_RABIT	163.32	11	5	5	58877
97	P09809|APOA1_RABIT	106.57	14	3	3	30591
98	P63150|2ABA_RABIT	146.49	22	6	6	51692
98	Q00006|2ABB_RABIT	96.99	8	2	2	48243
102	Q28631|WFDC2_RABIT	164.08	59	4	4	12803
103	P15253|CALR_RABIT	101.36	12	3	3	48275
104	P34032|TYB4_RABIT	118.16	61	3	3	5037
105	P50117|S10A9_RABIT	105.23	21	2	2	14787
106	P29694|EF1G_RABIT	122.46	9	3	3	50049
108	P41316|CRYAB_RABIT	101.71	16	3	3	20107
109	P62943|FKB1A_RABIT	129.57	42	4	4	11951
110	P48738|PIPNA_RABIT	112.59	13	2	2	31906
111	Q29426|K2C3_RABIT	119.63	9	5	3	64341
113	P79226|ALDOB_RABIT	140.68	18	4	4	39605
115	Q09YN4|CAZA2_RABIT	134.81	11	2	2	32951
116	P35543|SAA3_RABIT	168.84	13	3	3	13806

117	P31097|OSTP_RABIT	131.18	19	3	3	35172
118	P58776|TPM2_RABIT	72.98	7	2	2	32837
123	P29678|MP2K1_RABIT	105.37	10	2	2	43453
124	P01847|LAC_RABIT	95.64	33	2	2	11484
125	P34826|EF1B_RABIT	130.4	27	3	3	24749
127	P01840|KAC4_RABIT	145.87	63	3	3	11043
130	P53789|VTDB_RABIT	98.72	9	2	2	52912
131	P06814|CAN2_RABIT	130.04	14	3	3	49494
134	P62143|PP1B_RABIT	91.62	10	2	2	37187
134	P62139|PP1A_RABIT	91.62	10	2	2	37512
136	Q28719|PTGR1_RABIT	82.01	9	2	2	38219
138	P19943|RLA2_RABIT	100.19	82	2	2	4695
140	P43348|TCTP_RABIT	92	35	2	2	19537
144	P12247|CO3_RABIT	110.92	7	3	3	81844
148	P47844|CBR1_RABIT	75.65	10	2	2	30452
151	Q29513|GNMT_RABIT	108.82	13	2	2	32626
158	P07466|DEF6_RABIT	57.23	21	2	2	10122

Table S 23. Identified proteins in postbiotic treated rabbit 3, right eye.

Protein Group	Accession	-10lgP	Coverage (%)	Peptides	Unique	Avg. Mass
1	P01832|PIGR_RABIT	443.6	54	74	74	83887
2	P19007|HPT_RABIT	397.01	71	64	47	38869
3	P19134|TRFE_RABIT	409.58	66	76	71	76670
4	P60990|PIP_RABIT	286.15	61	29	29	16871
5	P49065|ALBU_RABIT	370.42	62	47	47	68910
8	P29751|ACTB_RABIT	340.08	74	28	1	41756
9	Q8MI17|AL1A1_RABIT	344.97	70	35	35	54341
11	P46406|G3P_RABIT	318.43	53	22	22	35780
14	Q95218|DMBT1_RABIT	288.43	19	19	19	172763
15	P23108|IGJ_RABIT	247.41	76	15	15	15556
16	P13491|LDHA_RABIT	266.61	61	21	19	36565
17	P51662|ANXA1_RABIT	309.81	52	17	17	38735
18	C0HJA6|OBP2_RABIT	126.8	100	4	4	1831
21	Q9TTC6|PPIA_RABIT	271.3	69	13	13	17837
22	C0HJA9|OBP3_RABIT	245.57	58	9	9	4721
23	P13490|LDHB_RABIT	235.93	55	18	16	24134
24	P01870|IGHG_RABIT	258.77	45	12	12	35404
25	P11974|KPYM_RABIT	306.28	47	19	19	58048
26	P68105|EF1A1_RABIT	282.18	48	18	18	50141
26	Q71V39|EF1A2_RABIT	209.81	20	8	8	50470
27	P01879|IGHA_RABIT	267.28	31	15	15	32256
28	Q9XSC5|CLUS_RABIT	264.95	35	16	16	51851
32	Q08863|GSTA1_RABIT	232.71	56	11	11	25691
32	Q08862|GSTA_RABIT	60.14	7	2	2	25450
36	P30946|HS90A_RABIT	240.9	35	17	11	79733
40	Q29504|UBA1_RABIT	257.22	22	16	16	117688
42	P25704|ENOB_RABIT	228.41	19	6	6	47069
43	P30947|HS90B_RABIT	218.22	26	15	9	83467
45	P00883|ALDOA_RABIT	249.86	55	11	11	39343
48	Q29426|K2C3_RABIT	195.43	20	12	6	64341
52	O19048|PCBP1_RABIT	208.79	42	9	9	37498
56	P29562|IF4A1_RABIT	209.44	27	8	8	45291
57	P30801|S10A6_RABIT	141.48	71	9	9	10154
58	Q6Q6X0|1433T_RABIT	188.47	34	8	8	27778
59	P80508|PE2R_RABIT	192.35	32	9	9	36670
60	P31097|OSTP_RABIT	172.28	39	6	6	35172
61	Q8HZQ5|EZRI_RABIT	175.59	15	8	8	69220
62	O77791|S10AC_RABIT	183.68	71	6	6	10668
63	P08855|ICAL_RABIT	212.32	27	11	10	76966
64	O19049|HNRPK_RABIT	186.63	32	11	11	50960
65	Q95MF9|CLIC1_RABIT	195.04	56	9	9	26925
66	P62160|CALM_RABIT	199.19	46	7	7	16838
67	P35543|SAA3_RABIT	203.32	32	6	6	13806

71	P06813|CPNS1_RABIT	190.56	64	8	8	28239
72	P00939|TPIS_RABIT	174.42	45	7	7	26757
73	Q28706|K1C12_RABIT	179.16	36	11	5	45727
76	P01840|KAC4_RABIT	186.14	91	5	5	11043
77	P39056|OSTCN_RABIT	180.75	90	4	4	5431
80	O97529|ANXA8_RABIT	181.11	30	7	7	36680
83	P24480|S10AB_RABIT	180.12	58	4	4	11429
85	P16973|LYSC_RABIT	176.4	52	7	7	14722
86	P80191|FETUA_RABIT	177.48	21	4	4	38387
87	P15122|ALDR_RABIT	137.66	30	7	7	35763
88	P47845|LEG3_RABIT	141.18	30	6	6	25502
89	Q8WN94|ACBP_RABIT	191.77	60	5	5	9915
90	P14422|PA2GA_RABIT	139.24	38	3	3	7607
91	P00567|KCRB_RABIT	174.43	20	6	6	42663
92	O97862|CYTC_RABIT	180.49	37	5	5	16346
94	P46409|GSTMU_RABIT	172.9	22	5	5	25417
95	P08628|THIO_RABIT	162.59	49	6	6	11761
101	P12247|CO3_RABIT	169.72	12	5	3	81844
103	Q8MK67|PEBP1_RABIT	197.16	66	6	6	20994
104	P10160|IF5A1_RABIT	184.19	43	5	5	16816
105	P11909|GPX1_RABIT	139.95	38	5	5	21883
107	P21195|PDIA1_RABIT	150.18	15	5	5	56808
109	Q28631|WFDC2_RABIT	138.77	40	3	3	12803
112	P41316|CRYAB_RABIT	112.34	25	4	4	20107
113	P09212|SODC_RABIT	113.54	49	4	4	15819
116	P01685|KV04_RABIT	129.96	32	2	1	11182
117	P02252|H14_RABIT	107.71	18	3	3	21897
118	P06815|CAN1_RABIT	113.41	21	4	4	35275
119	P31347|ANGI_RABIT	92.82	25	2	2	14361
120	P50117|S10A9_RABIT	108.2	21	2	2	14787
121	P00489|PYGM_RABIT	98.19	6	3	3	97289
122	Q28640|HRG_RABIT	118.5	9	3	3	58877
123	P01696|KV15_RABIT	99.31	31	3	1	11596
125	P26203|P15B_RABIT	149.84	36	4	4	15626
125	P26202|P15A_RABIT	149.84	36	4	4	15675
126	P53789|VTDB_RABIT	95.1	9	2	2	52912
127	O77506|LASP1_RABIT	79.49	12	2	2	29935
128	P62493|RB11A_RABIT	93.78	16	3	3	24394
129	P01847|LAC_RABIT	106.05	33	2	2	11484
130	P01697|KV16_RABIT	89.05	30	3	1	12112
131	P01687|KV06_RABIT	124.19	31	2	1	11281
132	Q28619|NHRF1_RABIT	89.15	16	3	3	38562
139	P00949|PGM1_RABIT	96.22	7	3	3	61558
140	Q09YN4|CAZA2_RABIT	107.65	17	3	3	32951
141	Q28680|CD14_RABIT	68.49	8	2	2	39992

142	P23612|SYWC_RABIT	97.42	13	4	4	53799
143	O62695|H2AV_RABIT	68.62	15	2	2	13481
144	P15253|CALR_RABIT	84.71	12	3	3	48275
145	P34032|TYB4_RABIT	104.3	61	3	3	5037
148	P01692|KV11_RABIT	107.64	17	3	3	9469
149	P12337|EST1_RABIT	95.45	6	2	2	62292
151	Q9N1E2|G6PI_RABIT	81.11	9	3	3	62747
152	P53787|EF1D_RABIT	78.98	13	2	2	31075
153	P07466|DEF6_RABIT	75.06	21	2	2	10122
156	P09809|APOA1_RABIT	70.48	10	2	2	30591
157	O77622|TCPZ_RABIT	76.08	7	2	2	58024
160	P58776|TPM2_RABIT	63.3	7	2	2	32837
162	P25230|CAP18_RABIT	116.76	15	2	2	19805
166	Q9XS70|COR1B_RABIT	91.14	6	2	2	53609

Table S 24. Identified proteins in postbiotic treated rabbit 4, right eye.

Protein Group	Accession	-10lgP	Coverage (%)	Peptides	Unique	Avg. Mass
1	P19007|HPT_RABIT	395.41	65	45	34	38869
2	P49065|ALBU_RABIT	386.91	62	51	51	68910
3	P01832|PIGR_RABIT	412.86	51	47	47	83887
4	P19134|TRFE_RABIT	375.47	49	39	39	76670
5	P60990|PIP_RABIT	277.82	58	21	21	16871
7	P29751|ACTB_RABIT	330.49	60	19	1	41756
8	P51662|ANXA1_RABIT	339.93	55	20	20	38735
11	Q95218|DMBT1_RABIT	286.14	18	16	16	172763
12	C0HJA6|OBP2_RABIT	146.08	100	4	4	1831
13	Q8MI17|AL1A1_RABIT	310.41	50	22	22	54341
16	P46406|G3P_RABIT	284.58	50	13	13	35780
17	Q9XSC5|CLUS_RABIT	268.52	27	13	13	51851
18	Q9TTC6|PPIA_RABIT	249.03	67	12	12	17837
19	P68105|EF1A1_RABIT	266.96	37	12	12	50141
19	Q71V39|EF1A2_RABIT	189.22	16	5	5	50470
20	P11974|KPYM_RABIT	283.85	46	16	16	58048
21	P01879|IGHA_RABIT	254.35	31	12	12	32256
22	P23108|IGJ_RABIT	212.38	60	10	10	15556
24	P01870|IGHG_RABIT	223.18	35	7	7	35404
25	P68135|ACTS_RABIT	210.37	25	8	1	42051
25	P62740|ACTA_RABIT	204.86	22	7	1	42009
26	P21195|PDIA1_RABIT	240.47	29	10	10	56808
27	P15122|ALDR_RABIT	177.83	53	11	11	35763
29	P00883|ALDOA_RABIT	239.31	47	10	10	39343
33	P30946|HS90A_RABIT	206.01	16	7	5	79733
34	Q29504|UBA1_RABIT	227.5	16	11	11	117688
35	Q6Q6X0|1433T_RABIT	199.95	26	6	6	27778
36	P62160|CALM_RABIT	196.36	46	5	5	16838
43	P39056|OSTCN_RABIT	166.04	90	3	3	5431
47	P30947|HS90B_RABIT	170.58	14	7	4	83467
48	P80191|FETUA_RABIT	221.8	31	6	6	38387
49	Q8HZQ5|EZRI_RABIT	150.41	9	5	5	69220
50	P30801|S10A6_RABIT	140.6	50	4	4	10154
51	Q08863|GSTA1_RABIT	164.4	25	5	5	25691
52	Q29426|K2C3_RABIT	179.5	12	7	5	64341
53	P25704|ENOB_RABIT	175.26	16	4	4	47069
55	C0HJA9|OBP3_RABIT	166.53	58	2	2	4721
56	P13490|LDHB_RABIT	136.71	18	4	4	24134
57	P79226|ALDOB_RABIT	186.91	25	6	6	39605
58	P12247|CO3_RABIT	185.57	12	5	3	81844
59	P13491|LDHA_RABIT	133.68	15	4	4	36565
60	Q95MF9|CLIC1_RABIT	166.84	36	6	6	26925
61	Q8WN94|ACBP_RABIT	200.91	60	5	5	9915

65	P29562|IF4A1_RABIT	171.29	18	5	5	45291
66	Q28640|HRG_RABIT	190.5	11	5	5	58877
70	P00939|TPIS_RABIT	164.65	47	7	7	26757
71	O97529|ANXA8_RABIT	176.94	20	5	5	36680
74	O19048|PCBP1_RABIT	138.84	22	5	5	37498
75	O97862|CYTC_RABIT	153.63	34	4	4	16346
76	P10160|IF5A1_RABIT	164.55	35	4	4	16816
77	P80508|PE2R_RABIT	135.99	16	4	4	36670
78	Q28631|WFDC2_RABIT	158.75	59	4	4	12803
79	P24480|S10AB_RABIT	160.89	58	3	3	11429
80	P08628|THIO_RABIT	135.13	37	3	3	11761
82	P08855|ICAL_RABIT	147.4	7	3	3	76966
83	O77791|S10AC_RABIT	140.45	71	4	4	10668
84	P16973|LYSC_RABIT	121.98	36	3	3	14722
88	P09809|APOA1_RABIT	124	26	5	5	30591
90	P46409|GSTMU_RABIT	113.73	14	2	2	25417
91	P35543|SAA3_RABIT	153.18	13	2	2	13806
92	P47845|LEG3_RABIT	81.62	10	2	2	25502
95	P00567|KCRB_RABIT	132.67	12	3	3	42663
96	Q8MK67|PEBP1_RABIT	121.78	55	4	4	20994
98	P09212|SODC_RABIT	111.48	37	2	2	15819
99	P15253|CALR_RABIT	125.17	12	3	3	48275
100	P06813|CPNS1_RABIT	124.92	20	3	3	28239
102	P31347|ANGI_RABIT	78.88	25	2	2	14361
106	P02252|H14_RABIT	94.07	12	2	2	21897
107	P01840|KAC4_RABIT	139.37	40	2	2	11043
108	P53789|VTDB_RABIT	89.61	9	2	2	52912
109	P31097|OSTP_RABIT	114.17	15	3	3	35172
110	P62943|FKB1A_RABIT	98.4	25	2	2	11951
111	P11909|GPX1_RABIT	90.28	14	2	2	21883
113	P01696|KV15_RABIT	86.74	19	2	1	11596
114	P34032|TYB4_RABIT	102.41	32	2	2	5037
120	P01697|KV16_RABIT	70.94	18	2	1	12112
121	P29694|EF1G_RABIT	93.83	11	3	3	50049
122	O19049|HNRPK_RABIT	92.66	9	2	2	50960
130	P23612|SYWC_RABIT	73	7	2	2	53799

Table S 25. Identified proteins in postbiotic treated rabbit 5, right eye.

Protein Group	Accession	-10lgP	Coverage (%)	Peptides	Unique	Avg. Mass
1	P01832|PIGR_RABIT	446.27	51	58	58	83887
2	P49065|ALBU_RABIT	413.54	62	56	49	68910
3	P19007|HPT_RABIT	383.4	65	40	28	38869
4	P19134|TRFE_RABIT	402.14	54	44	42	76670
5	P60990|PIP_RABIT	277.91	61	20	20	16871
7	P29751|ACTB_RABIT	322.79	60	22	1	41756
9	Q95218|DMBT1_RABIT	281.75	16	16	16	172763
11	Q8MI17|AL1A1_RABIT	332.48	60	26	26	54341
12	P51662|ANXA1_RABIT	330.17	53	18	18	38735
13	P46406|G3P_RABIT	288.27	50	16	16	35780
14	P01879|IGHA_RABIT	276.72	31	11	11	32256
15	P23108|IGJ_RABIT	220.21	68	12	12	15556
16	P68105|EF1A1_RABIT	287.57	38	13	13	50141
16	Q71V39|EF1A2_RABIT	203.91	16	5	5	50470
17	C0HJA6|OBP2_RABIT	141.33	100	4	4	1831
18	P11974|KPYM_RABIT	283.49	42	14	14	58048
19	Q9TTC6|PPIA_RABIT	253.75	67	12	12	17837
21	Q9XSC5|CLUS_RABIT	261.43	27	13	13	51851
23	P30946|HS90A_RABIT	227.98	24	12	8	79733
25	P68135|ACTS_RABIT	209.24	25	9	1	42051
25	P62740|ACTA_RABIT	203.79	22	8	1	42009
26	P00883|ALDOA_RABIT	250.31	56	12	12	39343
27	P01870|IGHG_RABIT	224.26	33	6	6	35404
28	O77791|S10AC_RABIT	222.32	71	7	7	10668
29	Q29504|UBA1_RABIT	230.89	17	11	11	117688
30	P30947|HS90B_RABIT	184.88	16	9	5	83467
31	Q28640|HRG_RABIT	226.99	19	9	9	58877
32	P21195|PDIA1_RABIT	215.99	30	11	11	56808
33	P62160|CALM_RABIT	187.23	50	6	6	16838
35	P31097|OSTP_RABIT	180.69	47	8	8	35172
37	Q8HZQ5|EZRI_RABIT	156.18	13	7	7	69220
38	P80191|FETUA_RABIT	220.39	26	5	5	38387
39	Q6Q6X0|1433T_RABIT	168.56	34	8	8	27778
40	P15122|ALDR_RABIT	146.94	27	6	6	35763
41	P13491|LDHA_RABIT	142.37	13	4	4	36565
42	O97529|ANXA8_RABIT	175.11	38	8	8	36680
43	Q08863|GSTA1_RABIT	163.53	28	6	6	25691
44	P39056|OSTCN_RABIT	166.92	90	3	3	5431
46	P09809|APOA1_RABIT	195.63	34	7	7	30591
48	P30801|S10A6_RABIT	146.55	74	6	6	10154
49	P13490|LDHB_RABIT	133.69	18	4	4	24134
50	O19048|PCBP1_RABIT	171.53	22	5	5	37498
51	P25704|ENOB_RABIT	188.56	16	4	4	47069
52	P12247|CO3_RABIT	166.55	14	6	4	81844

55	P01840|KAC4_RABIT	192.85	83	4	4	11043
56	P47845|LEG3_RABIT	142.53	21	4	4	25502
57	P29562|IF4A1_RABIT	178.92	18	5	5	45291
59	C0HJA9|OBP3_RABIT	163.92	58	3	3	4721
60	P08855|ICAL_RABIT	194.6	21	8	8	76966
62	P00939|TPIS_RABIT	161.53	39	6	6	26757
65	Q95MF9|CLIC1_RABIT	147.02	32	6	6	26925
67	O97862|CYTC_RABIT	185.43	47	6	6	16346
68	Q28631|WFDC2_RABIT	151.47	52	3	3	12803
69	P80508|PE2R_RABIT	148.12	19	5	5	36670
70	Q29426|K2C3_RABIT	147.41	8	4	2	64341
74	P00567|KCRB_RABIT	165.04	17	4	4	42663
75	P24480|S10AB_RABIT	162.82	58	3	3	11429
76	Q8WN94|ACBP_RABIT	174.7	60	5	5	9915
77	P35543|SAA3_RABIT	175.6	26	3	3	13806
82	P01696|KV15_RABIT	107.94	31	3	1	11596
83	P50117|S10A9_RABIT	107.59	21	2	2	14787
84	Q8MK67|PEBP1_RABIT	160.93	55	4	4	20994
86	P46409|GSTMU_RABIT	130.73	14	2	2	25417
87	P10160|IF5A1_RABIT	150.28	35	3	3	16816
88	P14422|PA2GA_RABIT	138.14	38	3	3	7607
90	P16973|LYSC_RABIT	129.29	36	3	3	14722
91	P11909|GPX1_RABIT	129.62	36	4	4	21883
94	P08628|THIO_RABIT	152.1	37	4	4	11761
95	P01697|KV16_RABIT	103.62	30	3	1	12112
96	P09212|SODC_RABIT	138.76	37	3	3	15819
99	P06813|CPNS1_RABIT	112.12	20	3	3	28239
100	P79226|ALDOB_RABIT	99.64	8	2	2	39605
102	Q9N1E2|G6PI_RABIT	93.41	6	2	2	62747
103	P53789|VTDB_RABIT	108.5	9	2	2	52912
106	Q28680|CD14_RABIT	123.93	13	3	3	39992
107	P26890|IL1RA_RABIT	117.02	16	2	2	20214
108	P01847|LAC_RABIT	97.66	33	2	2	11484
109	P15253|CALR_RABIT	91.31	7	2	2	48275
110	P31347|ANGI_RABIT	89.9	25	2	2	14361
114	O19049|HNRPK_RABIT	102.54	9	2	2	50960
115	P34032|TYB4_RABIT	111.24	32	2	2	5037
118	Q28619|NHRF1_RABIT	95.61	9	2	2	38562
119	Q9XS70|COR1B_RABIT	95.94	9	2	2	53609
121	P01687|KV06_RABIT	86.53	31	2	2	11281
123	P06815|CAN1_RABIT	87.88	7	2	2	35275
125	O77506|LASP1_RABIT	94.56	19	3	3	29935
126	P58776|TPM2_RABIT	71.62	8	2	2	32837
127	Q09YN4|CAZA2_RABIT	77.66	11	2	2	32951
133	P62943|FKB1A_RABIT	86.11	25	2	2	11951
140	P62493|RB11A_RABIT	62.73	11	2	2	24394

Table S 26. Identified proteins in postbiotic treated rabbit 6, right eye.

Protein Group	Accession	-10lgP	Coverage (%)	Peptides	Unique	Avg. Mass
1	P01832|PIGR_RABIT	407.98	51	44	44	83887
2	P19134|TRFE_RABIT	384.55	57	46	46	76670
3	P19007|HPT_RABIT	347.99	61	33	25	38869
4	P49065|ALBU_RABIT	346.57	56	34	34	68910
5	P60990|PIP_RABIT	271.18	61	21	21	16871
9	Q95218|DMBT1_RABIT	265.69	16	15	15	172763
14	P29751|ACTB_RABIT	269.06	48	13	1	41756
16	P51662|ANXA1_RABIT	301.29	53	16	16	38735
17	P01870|IGHG_RABIT	249.22	51	13	13	35404
19	Q8MI17|AL1A1_RABIT	263.56	53	18	18	54341
21	P23108|IGJ_RABIT	218.18	68	10	10	15556
22	P01879|IGHA_RABIT	266.27	39	12	12	32256
23	C0HJA6|OBP2_RABIT	127.07	100	4	4	1831
24	Q9XSC5|CLUS_RABIT	255.15	27	12	12	51851
25	P46406|G3P_RABIT	255.15	46	12	12	35780
28	P68105|EF1A1_RABIT	249.18	35	11	11	50141
28	Q71V39|EF1A2_RABIT	189.22	18	6	6	50470
34	P62740|ACTA_RABIT	184.22	22	7	1	42009
34	P68135|ACTS_RABIT	184.22	22	7	1	42051
35	Q29426|K2C3_RABIT	206.16	18	11	4	64341
37	Q9TTC6|PPIA_RABIT	186.6	63	9	9	17837
38	P13491|LDHA_RABIT	197.65	33	9	8	36565
40	P13490|LDHB_RABIT	203.62	44	11	10	24134
41	P39056|OSTCN_RABIT	190.09	90	4	4	5431
42	P30801|S10A6_RABIT	155.17	74	10	10	10154
43	Q08863|GSTA1_RABIT	201.78	41	8	8	25691
44	C0HJA9|OBP3_RABIT	185.55	58	5	5	4721
54	P62160|CALM_RABIT	146.92	46	5	5	16838
56	P25704|ENOB_RABIT	181.62	16	4	4	47069
59	P31097|OSTP_RABIT	175.31	37	6	6	35172
61	P11974|KPYM_RABIT	145.71	17	6	6	58048
63	Q28706|K1C12_RABIT	140.98	14	6	2	45727
64	O97862|CYTC_RABIT	176.27	37	5	5	16346
65	Q6Q6X0|1433T_RABIT	161.82	27	5	5	27778
68	P01840|KAC4_RABIT	184.77	54	3	3	11043
69	P24480|S10AB_RABIT	149.15	58	4	4	11429
71	P00939|TPIS_RABIT	139.86	33	5	5	26757
72	P47845|LEG3_RABIT	86.09	10	2	2	25502
76	P00883|ALDOA_RABIT	115.69	12	3	3	39343
77	Q29504|UBA1_RABIT	155.35	6	4	4	117688
78	P30946|HS90A_RABIT	148.65	11	5	4	79733
80	Q8WN94|ACBP_RABIT	157.7	60	4	4	9915
81	P46409|GSTMU_RABIT	139.1	27	4	4	25417

82	P16973|LYSC_RABIT	135.28	29	3	3	14722
85	Q95MF9|CLIC1_RABIT	128.98	17	4	4	26925
86	P14422|PA2GA_RABIT	100.49	38	2	2	7607
87	P35543|SAA3_RABIT	152.48	13	2	2	13806
88	P80191|FETUA_RABIT	144.21	15	3	3	38387
89	Q28640|HRG_RABIT	119.65	11	4	4	58877
93	P21195|PDIA1_RABIT	108.09	12	3	3	56808
94	O19048|PCBP1_RABIT	85.44	7	2	2	37498
95	P01847|LAC_RABIT	96.23	33	2	2	11484
96	P01696|KV15_RABIT	97.03	31	3	2	11596
97	Q28631|WFDC2_RABIT	113.28	33	2	2	12803
98	P08628|THIO_RABIT	128.2	37	3	3	11761
99	O77791|S10AC_RABIT	101.6	36	2	2	10668
100	P00567|KCRB_RABIT	117.78	11	3	3	42663
103	P02252|H14_RABIT	89.29	12	2	2	21897
106	P01697|KV16_RABIT	68.25	18	2	1	12112
108	P31347|ANGI_RABIT	65.39	25	2	2	14361

Table S 27. Identified proteins in postbiotic treated rabbit 7, right eye.

Protein Group	Accession	-10lgP	Coverage (%)	Peptides	Unique	Avg. Mass
1	P49065|ALBU_RABIT	442.65	70	99	81	68910
2	P01832|PIGR_RABIT	442.28	54	69	69	83887
3	P19134|TRFE_RABIT	418.68	65	81	77	76670
4	P19007|HPT_RABIT	319.66	61	27	21	38869
5	P51662|ANXA1_RABIT	327.44	58	23	23	38735
7	P29751|ACTB_RABIT	311.12	59	19	1	41756
8	P60990|PIP_RABIT	248.28	54	16	16	16871
9	Q8MI17|AL1A1_RABIT	312.93	55	27	27	54341
13	P68105|EF1A1_RABIT	296.27	51	19	19	50141
13	Q71V39|EF1A2_RABIT	215.83	20	8	8	50470
14	Q95218|DMBT1_RABIT	243.91	10	12	12	172763
15	P46406|G3P_RABIT	271.26	46	14	14	35780
16	P23108|IGJ_RABIT	231.04	82	16	16	15556
19	Q9TTC6|PPIA_RABIT	230.01	75	15	15	17837
20	P11974|KPYM_RABIT	282.91	44	18	18	58048
21	P00883|ALDOA_RABIT	251.16	61	13	13	39343
22	P80191|FETUA_RABIT	262.51	43	9	9	38387
23	Q28640|HRG_RABIT	264.68	24	14	14	58877
24	P01879|IGHA_RABIT	264.32	31	13	13	32256
25	P68135|ACTS_RABIT	207.77	25	8	1	42051
25	P62740|ACTA_RABIT	201.89	22	7	1	42009
26	Q9XSC5|CLUS_RABIT	257.9	31	13	13	51851
27	P30946|HS90A_RABIT	246.92	32	16	9	79733
28	P09809|APOA1_RABIT	232.29	50	13	13	30591
29	P01870|IGHG_RABIT	244.07	47	9	9	35404
31	P30947|HS90B_RABIT	236.69	31	17	10	83467
33	Q29426|K2C3_RABIT	215.36	24	13	8	64341
34	Q29504|UBA1_RABIT	250.27	22	15	15	117688
36	P30801|S10A6_RABIT	160.86	74	8	8	10154
37	P13491|LDHA_RABIT	186.03	40	11	10	36565
41	O97529|ANXA8_RABIT	213.67	36	9	9	36680
44	P21195|PDIA1_RABIT	231.62	36	13	13	56808
45	P53789|VTDB_RABIT	179.94	28	9	9	52912
50	O77791|S10AC_RABIT	184.79	71	6	6	10668
51	P62160|CALM_RABIT	199.49	59	9	9	16838
56	P15122|ALDR_RABIT	154.41	42	9	9	35763
57	Q95MF9|CLIC1_RABIT	185.16	57	9	9	26925
60	Q6Q6X0|1433T_RABIT	195.08	31	8	8	27778
61	O19048|PCBP1_RABIT	176.22	33	8	8	37498
62	Q8HZQ5|EZRI_RABIT	159.79	19	8	8	69220
64	P00567|KCRB_RABIT	225.59	38	9	9	42663
65	P12247|CO3_RABIT	177.68	17	8	5	81844
70	Q28706|K1C12_RABIT	161.73	24	9	3	45727

71	P20058|HEMO_RABIT	168.29	19	7	7	51767
73	O19049|HNRPK_RABIT	168.55	21	6	6	50960
74	P47845|LEG3_RABIT	130.57	27	5	5	25502
75	C0HJA6|OBP2_RABIT	111.77	61	3	3	1831
76	P16973|LYSC_RABIT	180.38	45	7	7	14722
79	P01840|KAC4_RABIT	199.54	71	4	4	11043
80	P13490|LDHB_RABIT	170.57	34	7	6	24134
81	P14422|PA2GA_RABIT	163.57	40	5	5	7607
82	P80508|PE2R_RABIT	161.17	24	7	7	36670
85	P25704|ENOB_RABIT	180.48	16	4	4	47069
86	P29562|IF4A1_RABIT	175.27	22	6	6	45291
87	P10160|IF5A1_RABIT	166.33	43	5	5	16816
89	P08855|ICAL_RABIT	143.45	17	7	7	76966
90	P00939|TPIS_RABIT	148.83	46	7	7	26757
91	P26890|IL1RA_RABIT	151.83	29	4	4	20214
92	P50117|S10A9_RABIT	159.54	33	4	4	14787
93	P31097|OSTP_RABIT	136.38	30	5	5	35172
94	P35543|SAA3_RABIT	183.55	13	3	3	13806
100	Q28658|SPRR3_RABIT	159.4	55	6	6	24139
101	P46409|GSTMU_RABIT	169.45	27	4	4	25417
102	Q08863|GSTA1_RABIT	145.38	20	5	5	25691
103	C0HJA9|OBP3_RABIT	146.05	58	2	2	4721
105	Q8WN94|ACBP_RABIT	186.64	60	4	4	9915
108	O97862|CYTC_RABIT	134.68	31	4	4	16346
111	P08628|THIO_RABIT	149.84	37	4	4	11761
114	P79226|ALDOB_RABIT	124.82	18	5	5	39605
115	P12337|EST1_RABIT	122.85	10	4	4	62292
116	O18998|DNAS1_RABIT	116.54	25	4	4	31346
117	P09212|SODC_RABIT	121.05	44	3	3	15819
118	Q28631|WFDC2_RABIT	144.64	52	3	3	12803
124	P29694|EF1G_RABIT	116.86	11	4	4	50049
125	P24480|S10AB_RABIT	155.48	58	3	3	11429
126	P11909|GPX1_RABIT	122.24	32	4	4	21883
127	P01847|LAC_RABIT	109.71	33	2	2	11484
128	P06815|CAN1_RABIT	101.42	22	3	3	35275
129	P35324|SPRR1_RABIT	71.85	23	2	2	14044
130	Q8MK67|PEBP1_RABIT	131.29	26	2	2	20994
131	P23775|CBG_RABIT	93.13	9	3	3	42326
132	O77622|TCPZ_RABIT	97.32	7	2	2	58024
133	P58776|TPM2_RABIT	93.05	8	3	1	32837
135	P19943|RLA2_RABIT	121.61	80	2	2	4695
137	P41975|SODE_RABIT	89.77	23	4	4	25688
139	P34826|EF1B_RABIT	123.58	12	2	2	24749
140	P39056|OSTCN_RABIT	99.84	51	2	2	5431
142	P58772|TPM1_RABIT	90.99	8	3	1	32681

143	P01684|KV03_RABIT	89.38	21	3	1	11512
144	Q09YN4|CAZA2_RABIT	100.22	17	3	3	32951
146	O19053|ADHX_RABIT	102.01	10	2	2	39596
147	P27170|PON1_RABIT	93.14	9	2	2	40010
148	P15253|CALR_RABIT	82.54	12	3	3	48275
149	P47844|CBR1_RABIT	80.03	10	2	2	30452
150	P01687|KV06_RABIT	68.84	31	2	2	11281
152	Q95212|TPD52_RABIT	86.03	13	2	2	19809
157	Q28619|NHRF1_RABIT	93.72	15	3	3	38562
158	P23612|SYWC_RABIT	81.92	6	2	2	53799
162	P62943|FKB1A_RABIT	73.88	25	2	2	11951
163	P34032|TYB4_RABIT	97.83	32	2	2	5037
166	P53787|EF1D_RABIT	74.65	9	2	2	31075
168	Q9XS70|COR1B_RABIT	103.79	9	2	2	53609
169	O77506|LASP1_RABIT	82.58	10	2	2	29935
170	P62493|RB11A_RABIT	58.22	11	2	2	24394
171	P26203|P15B_RABIT	79.88	18	2	2	15626
171	P26202|P15A_RABIT	79.88	18	2	2	15675
202	P48738|PIPNA_RABIT	88.7	16	2	2	31906

Table S 28. Identified proteins in postbiotic treated rabbit 8, right eye

Protein Group	Accession	-10lgP	Coverage (%)	Peptides	Unique	Avg. Mass
1	P49065|ALBU_RABIT	450.86	70	78	73	68910
2	P01832|PIGR_RABIT	454.68	53	56	56	83887
3	P19134|TRFE_RABIT	410.86	55	54	52	76670
4	P19007|HPT_RABIT	372.25	61	38	27	38869
5	P60990|PIP_RABIT	266.24	58	19	19	16871
6	P51662|ANXA1_RABIT	371.02	57	23	23	38735
9	P29751|ACTB_RABIT	335.96	54	18	1	41756
10	Q8MI17|AL1A1_RABIT	339.99	64	29	29	54341
11	P68105|EF1A1_RABIT	310.27	46	18	18	50141
11	Q71V39|EF1A2_RABIT	220.47	19	7	7	50470
12	P46406|G3P_RABIT	300.23	50	15	15	35780
14	P11974|KPYM_RABIT	308.97	46	20	20	58048
15	P01879|IGHA_RABIT	301.61	39	17	17	32256
17	P00883|ALDOA_RABIT	283.93	64	13	13	39343
18	Q95218|DMBT1_RABIT	225.99	9	9	9	172763
19	P30947|HS90B_RABIT	225.97	26	13	6	83467
21	P23108|IGJ_RABIT	237.27	60	12	12	15556
23	P30946|HS90A_RABIT	255.68	27	13	7	79733
24	P01870|IGHG_RABIT	232.32	47	9	9	35404
25	Q9XSC5|CLUS_RABIT	266.07	31	13	13	51851
26	Q9TTC6|PPIA_RABIT	239.61	67	13	13	17837
28	P68135|ACTS_RABIT	217.22	19	6	1	42051
28	P62740|ACTA_RABIT	213.97	19	6	1	42009
29	P13491|LDHA_RABIT	207.54	34	10	9	36565
30	Q28640|HRG_RABIT	243.09	20	11	11	58877
32	P30801|S10A6_RABIT	150.71	67	9	9	10154
33	Q29504|UBA1_RABIT	247.37	19	13	13	117688
37	O97529|ANXA8_RABIT	224.45	43	11	11	36680
38	P21195|PDIA1_RABIT	235.41	31	11	11	56808
42	P00567|KCRB_RABIT	249.28	38	9	9	42663
43	P62160|CALM_RABIT	207.88	46	5	5	16838
44	P09809|APOA1_RABIT	231.94	47	11	11	30591
45	Q95MF9|CLIC1_RABIT	193.25	62	10	10	26925
46	P16973|LYSC_RABIT	209.1	46	7	7	14722
48	P80191|FETUA_RABIT	227.43	31	6	6	38387
49	Q6Q6X0|1433T_RABIT	185.75	31	7	7	27778
50	Q8HZQ5|EZRI_RABIT	189.27	18	8	8	69220
51	P53789|VTDB_RABIT	170.5	18	5	5	52912
52	P39056|OSTCN_RABIT	195.69	90	4	4	5431
55	O19048|PCBP1_RABIT	187.1	33	8	8	37498
56	Q29426|K2C3_RABIT	177.78	13	7	4	64341
59	O19049|HNRPK_RABIT	194.68	24	7	7	50960
60	C0HJA9|OBP3_RABIT	172.98	58	3	3	4721

62	P13490|LDHB_RABIT	165.83	28	6	5	24134
66	Q08863|GSTA1_RABIT	183.31	25	5	5	25691
67	P08855|ICAL_RABIT	214.9	23	10	10	76966
68	P29562|IF4A1_RABIT	196.24	27	8	8	45291
69	P15122|ALDR_RABIT	132.48	17	4	4	35763
70	O77791|S10AC_RABIT	185.59	71	6	6	10668
71	P25704|ENOB_RABIT	191.27	16	4	4	47069
76	P10160|IF5A1_RABIT	167.74	43	5	5	16816
80	P12247|CO3_RABIT	189.3	17	8	5	81844
85	P31097|OSTP_RABIT	137.32	19	3	3	35172
86	P00939|TPIS_RABIT	162.2	41	6	6	26757
87	P01840|KAC4_RABIT	198.41	71	4	4	11043
88	P20058|HEMO_RABIT	167.73	16	5	5	51767
89	P24480|S10AB_RABIT	179.88	58	4	4	11429
90	P35543|SAA3_RABIT	176.02	13	3	3	13806
92	Q8WN94|ACBP_RABIT	207.54	60	5	5	9915
93	P47845|LEG3_RABIT	135.69	26	5	5	25502
94	P80508|PE2R_RABIT	144.39	14	3	3	36670
96	O97862|CYTC_RABIT	180.14	37	5	5	16346
97	P46409|GSTMU_RABIT	154.4	22	3	3	25417
98	C0HJA6|OBP2_RABIT	120.27	61	3	3	1831
99	Q28631|WFDC2_RABIT	155.09	59	4	4	12803
100	Q9N1E2|G6PI_RABIT	116.06	14	5	3	62747
102	P23612|SYWC_RABIT	174.78	17	5	5	53799
103	Q8MK67|PEBP1_RABIT	167.66	48	4	4	20994
104	P02057|HBB_RABIT	138.05	30	4	4	16133
107	Q9XS70|COR1B_RABIT	139.65	12	3	3	53609
109	P09212|SODC_RABIT	131.8	49	4	4	15819
110	Q28706|K1C12_RABIT	131.93	8	3	1	45727
111	P06815|CAN1_RABIT	105.52	23	5	5	35275
112	P25230|CAP18_RABIT	161.05	23	3	3	19805
114	Q09YN4|CAZA2_RABIT	122.97	17	3	3	32951
115	P62493|RB11A_RABIT	100.35	16	3	3	24394
116	P08628|THIO_RABIT	150.25	37	4	4	11761
117	P11909|GPX1_RABIT	113.46	32	4	4	21883
118	P14422|PA2GA_RABIT	92.57	38	2	2	7607
121	O18750|ENPL_RABIT	132.86	7	4	3	82608
122	P29694|EF1G_RABIT	120.51	9	3	3	50049
124	P12337|EST1_RABIT	117.59	8	3	3	62292
125	P58776|TPM2_RABIT	83.17	7	2	1	32837
126	P50117|S10A9_RABIT	90.76	21	2	2	14787
127	P26203|P15B_RABIT	129.62	27	4	4	15626
127	P26202|P15A_RABIT	129.62	27	4	4	15675
128	P79226|ALDOB_RABIT	146.06	16	4	4	39605
129	P02252|H14_RABIT	98.68	12	2	2	21897

130	P00489|PYGM_RABIT	89.94	6	3	3	97289
131	P15253|CALR_RABIT	87.2	10	3	3	48275
132	P34032|TYB4_RABIT	116.22	32	2	2	5037
137	Q28619|NHRF1_RABIT	100.37	9	2	2	38562
139	P62943|FKB1A_RABIT	88.77	25	2	2	11951
142	O77622|TCPZ_RABIT	87.18	7	2	2	58024
144	P27170|PON1_RABIT	84.15	9	2	2	40010
147	P58772|TPM1_RABIT	76.54	8	2	1	32681
150	P31347|ANGI_RABIT	62.34	25	2	2	14361
151	P01687|KV06_RABIT	84.98	31	2	2	11281
152	P07466|DEF6_RABIT	66.21	21	2	2	10122
154	Q28739|BPI_RABIT	82.78	6	2	2	48837
159	P35324|SPRR1_RABIT	99	23	2	2	14044
162	P34826|EF1B_RABIT	113.65	21	2	2	24749
163	P03988|IGHM_RABIT	68.42	6	2	2	49897
163	P04221|MUCM_RABIT	68.42	6	2	2	52351
167	P62975|UBIQ_RABIT	86.22	33	2	2	8565
171	P19943|RLA2_RABIT	127.56	80	3	3	4695

Table S 29. Identified proteins in postbiotic treated rabbit 9, right eye

Protein Group	Accession	-10lgP	Coverage (%)	Peptides	Unique	Avg. Mass
1	P19134|TRFE_RABIT	441.18	67	73	70	76670
2	P01832|PIGR_RABIT	448.25	51	56	56	83887
3	P49065|ALBU_RABIT	411.59	66	54	48	68910
4	P19007|HPT_RABIT	393.83	67	42	32	38869
5	P60990|PIP_RABIT	280.02	58	23	23	16871
6	Q95218|DMBT1_RABIT	289.4	16	18	18	172763
7	P29751|ACTB_RABIT	318.6	62	17	1	41756
9	P51662|ANXA1_RABIT	329.16	57	20	20	38735
10	Q8MI17|AL1A1_RABIT	304.27	64	24	24	54341
13	P01879|IGHA_RABIT	300.87	39	14	14	32256
15	P46406|G3P_RABIT	282.6	50	14	14	35780
16	P23108|IGJ_RABIT	247.38	60	10	10	15556
17	P68105|EF1A1_RABIT	291.99	46	15	9	50141
18	Q9XSC5|CLUS_RABIT	276.73	32	14	14	51851
21	P01870|IGHG_RABIT	229.21	33	7	7	35404
22	P68135|ACTS_RABIT	218.81	28	9	1	42051
22	P62740|ACTA_RABIT	214.44	25	8	1	42009
23	P13491|LDHA_RABIT	217.93	40	11	10	36565
25	Q29426|K2C3_RABIT	234.41	22	13	8	64341
26	P00883|ALDOA_RABIT	243.39	52	12	12	39343
27	P11974|KPYM_RABIT	240.18	34	12	12	58048
32	Q9TTC6|PPIA_RABIT	197.43	57	8	8	17837
33	P15122|ALDR_RABIT	164.41	43	9	9	35763
34	P39056|OSTCN_RABIT	207.46	90	5	5	5431
40	Q29504|UBA1_RABIT	190.08	13	9	9	117688
41	Q28640|HRG_RABIT	214.61	14	7	7	58877
45	Q6Q6X0|1433T_RABIT	183.61	27	6	6	27778
48	P13490|LDHB_RABIT	185.45	35	8	7	24134
49	O77791|S10AC_RABIT	178.03	71	6	6	10668
50	C0HJA9|OBP3_RABIT	214.67	58	5	5	4721
51	P30946|HS90A_RABIT	198.8	21	10	6	79733
53	P62160|CALM_RABIT	192.44	46	5	5	16838
55	P30801|S10A6_RABIT	114.43	50	4	4	10154
56	Q8HZQ5|EZRI_RABIT	154.15	11	6	6	69220
61	P09809|APOA1_RABIT	188.61	34	8	8	30591
62	Q28706|K1C12_RABIT	149.02	19	8	3	45727
63	P80191|FETUA_RABIT	205.97	26	5	5	38387
64	P00567|KCRB_RABIT	236.14	27	7	7	42663
70	P25704|ENOB_RABIT	193.58	16	4	4	47069
71	Q08863|GSTA1_RABIT	172.82	37	6	6	25691
72	C0HJA6|OBP2_RABIT	109.61	61	2	2	1831
75	Q95MF9|CLIC1_RABIT	159.18	39	7	7	26925
76	P16973|LYSC_RABIT	170.14	45	5	5	14722

78	P30947|HS90B_RABIT	144	12	7	3	83467
79	P21195|PDIA1_RABIT	183.56	20	6	6	56808
80	P35543|SAA3_RABIT	171.06	13	2	2	13806
82	O97862|CYTC_RABIT	172.37	37	5	5	16346
83	P47845|LEG3_RABIT	110.38	16	3	3	25502
86	Q28658|SPRR3_RABIT	170.61	44	5	5	24139
87	P80508|PE2R_RABIT	154.77	24	6	6	36670
90	P01840|KAC4_RABIT	177.34	63	4	4	11043
91	P24480|S10AB_RABIT	167.06	58	3	3	11429
92	Q8WN94|ACBP_RABIT	154.94	60	4	4	9915
94	O19048|PCBP1_RABIT	125.94	16	4	4	37498
96	P10160|IF5A1_RABIT	161.99	35	3	3	16816
98	P50117|S10A9_RABIT	139.67	33	3	3	14787
99	P14422|PA2GA_RABIT	123.74	40	3	3	7607
103	P00939|TPIS_RABIT	138.76	28	4	4	26757
107	P29562|IF4A1_RABIT	130.9	10	3	3	45291
108	P08628|THIO_RABIT	146.73	37	4	4	11761
109	Q28631|WFDC2_RABIT	130.84	40	3	3	12803
110	O19049|HNRPK_RABIT	134.18	15	4	4	50960
111	P46409|GSTMU_RABIT	119.45	14	2	2	25417
118	P09212|SODC_RABIT	97.86	32	2	2	15819
119	P02252|H14_RABIT	83.95	12	2	2	21897
120	P11909|GPX1_RABIT	94.01	14	2	2	21883
121	P31097|OSTP_RABIT	103.68	19	3	3	35172
122	P01684|KV03_RABIT	88.3	11	2	2	11512
122	P01697|KV16_RABIT	78.48	11	2	2	12112
123	P35324|SPRR1_RABIT	72.02	23	2	2	14044
124	P07466|DEF6_RABIT	75.19	21	2	2	10122
125	P12247|CO3_RABIT	106.04	6	3	3	81844
126	P79226|ALDOB_RABIT	92.7	7	2	2	39605
130	P34032|TYB4_RABIT	112.21	32	2	2	5037
132	P01692|KV11_RABIT	103.12	17	2	2	9469
138	Q09YN4|CAZA2_RABIT	82.45	11	2	2	32951
139	P58776|TPM2_RABIT	62.25	8	2	1	32837
140	P26203|P15B_RABIT	94.72	18	2	2	15626
140	P26202|P15A_RABIT	94.72	18	2	2	15675
146	Q8MK67|PEBP1_RABIT	111.51	26	2	2	20994
173	O19053|ADHX_RABIT	78.97	10	2	2	39596

Table S 30. Identified proteins in postbiotic treated rabbit 10, right eye

Protein Group	Accession	-10lgP	Coverage (%)	Peptides	Unique	Avg. Mass
1	P19134|TRFE_RABIT	468.85	69	102	99	76670
2	P01832|PIGR_RABIT	477.03	55	67	67	83887
3	P19007|HPT_RABIT	393.88	63	42	30	38869
4	P60990|PIP_RABIT	303.17	62	26	26	16871
5	P49065|ALBU_RABIT	375.99	64	39	39	68910
6	Q95218|DMBT1_RABIT	315.91	17	19	19	172763
9	P01879|IGHA_RABIT	300.48	35	14	14	32256
10	P23108|IGJ_RABIT	262.75	74	16	16	15556
11	P01870|IGHG_RABIT	284.98	42	12	12	35404
13	Q9XSC5|CLUS_RABIT	284.82	35	15	15	51851
15	P51662|ANXA1_RABIT	330.36	57	18	18	38735
17	P29751|ACTB_RABIT	299.56	67	17	1	41756
18	C0HJA6|OBP2_RABIT	116.23	61	3	3	1831
19	Q8MI17|AL1A1_RABIT	264.6	50	16	16	54341
20	C0HJA9|OBP3_RABIT	253.86	58	9	9	4721
21	P46406|G3P_RABIT	263.46	47	12	12	35780
22	P39056|OSTCN_RABIT	213.33	90	6	6	5431
27	P68105|EF1A1_RABIT	225.72	28	8	8	50141
27	Q71V39|EF1A2_RABIT	156.54	14	4	4	50470
28	P31097|OSTP_RABIT	199.43	44	9	9	35172
30	Q9TTC6|PPIA_RABIT	175.94	60	8	8	17837
31	P68135|ACTS_RABIT	210.38	25	8	1	42051
31	P62740|ACTA_RABIT	202.9	22	7	1	42009
32	P00883|ALDOA_RABIT	179.49	32	7	7	39343
33	P35543|SAA3_RABIT	208.75	32	6	6	13806
36	Q29426|K2C3_RABIT	173.66	11	6	3	64341
38	P11974|KPYM_RABIT	198.51	27	9	9	58048
39	P01840|KAC4_RABIT	205.88	91	5	5	11043
42	P30801|S10A6_RABIT	151.64	67	6	6	10154
43	P14422|PA2GA_RABIT	156.48	40	4	4	7607
45	P25704|ENOB_RABIT	182.41	16	4	4	47069
47	O97862|CYTC_RABIT	180.96	47	6	6	16346
52	P16973|LYSC_RABIT	177.67	52	6	6	14722
53	P62160|CALM_RABIT	150.54	46	4	4	16838
58	Q28706|K1C12_RABIT	132.94	10	4	3	45727
59	P13490|LDHB_RABIT	117.19	12	2	2	24134
60	Q08863|GSTA1_RABIT	141.01	11	2	2	25691
63	Q6Q6X0|1433T_RABIT	140.62	19	4	4	27778
64	P24480|S10AB_RABIT	168.85	58	3	3	11429
65	O77791|S10AC_RABIT	119.22	58	3	3	10668
68	Q28631|WFDC2_RABIT	152.2	40	3	3	12803
71	Q8WN94|ACBP_RABIT	183.47	60	4	4	9915
72	P50117|S10A9_RABIT	113.23	33	3	3	14787

76	P12247|CO3_RABIT	135.82	9	4	2	81844
77	P00567|KCRB_RABIT	149.97	14	3	3	42663
78	P01696|KV15_RABIT	95.16	31	3	1	11596
79	P46409|GSTMU_RABIT	115.33	14	2	2	25417
82	P98065|TSG6_RABIT	125.45	18	4	4	31081
83	P00939|TPIS_RABIT	122.84	16	3	3	26757
84	Q95MF9|CLIC1_RABIT	103.08	14	3	3	26925
85	P01847|LAC_RABIT	111.43	33	2	2	11484
87	P21195|PDIA1_RABIT	113.44	9	2	2	56808
90	P15253|CALR_RABIT	77.75	7	2	2	48275
91	P47845|LEG3_RABIT	75.22	10	2	2	25502
92	P31347|ANGI_RABIT	82.81	25	2	2	14361
94	P80191|FETUA_RABIT	138.86	9	2	2	38387
95	P12337|EST1_RABIT	99.76	7	3	3	62292
96	P13491|LDHA_RABIT	71.58	7	2	2	36565
98	Q28658|SPRR3_RABIT	107.67	16	2	2	24139
100	P10160|IF5A1_RABIT	84.67	23	2	2	16816
104	P02252|H14_RABIT	82.13	12	2	2	21897
105	P09809|APOA1_RABIT	65.98	9	2	2	30591
106	P25230|CAP18_RABIT	132.29	15	2	2	19805
107	P26890|IL1RA_RABIT	99.15	16	2	2	20214
109	P34032|TYB4_RABIT	90.5	32	2	2	5037
119	P09212|SODC_RABIT	112.15	32	2	2	15819

Table S 31. Wilcoxon rank sum test score

Accession	Gene	Score	Accession	Gene	Score
P58776	TPM2	6.5	P80508	AKR1C5	3
P15253	CALR	6	Q95MF9	CLIC1	3
O19049	HNRNPK	5	P01687	IGKV1-5	2.5
P14422	PLA2G2A	5	P01696	IGKV1-27	2.5
Q09YN4	CAPZA2	5	P13491	LDHA	2.5
Q28619	SLC9A3R1	5	P58772	TPM1	2.5
P09809	APOA1	4.5	P62493	RAB11A	2.5
P10160	EIF5A	4.5	Q28680	CD14	2.5
P11909	GPX1	4.5	Q71V39	EEF1A2	2.5
P15122	AKR1B1	4.5	Q9N1E2	GPI	2.5
P31347	ANG	4.5	Q9XS70	CORO1B	2.5
Q29504	UBA1	4.5	P12337	CES1	2
P00567	CKB	4	P16973	LYZ	2
P06815	CAPN1	4	Q8WN94	DBI	2
P09212	SOD1	4	O18998	DNASE1	2
P12247	C3	4	P47844	CBR1	2
P21195	P4HB	4	P48738	PITPNA	2
P30946	HSP90AA1	4	Q08862	GSTA2	2
P30947	HSP90AB1	4	C0HJA9	Mup4	1.5
P47845	LGALS3	4	C0HJA9	Mup 4	1.5
P62943	FKBP1A	4	O77622	CCT6	1.5
Q8MK67	PEBP1	4	P00489	PYGM	1.5
P35324	Sprr1a	4	P02252	H1-4	1.5
O19048	PCBP1	3.5	P03988	N/A	1.5
P00883	ALDOA	3.5	P04221	N/A	1.5
P01697	N/A	3.5	P06813	CAPNS1	1.5
P01697	/	3.5	P07466	N/A	1.5
P01847	IGLC6	3.5	P11974	PKM	1.5
P08628	TXN	3.5	P34826	EEF1B	1.5
P08855	CAST	3.5	P68105	EEF1A1	1.5
P29694	EEF1G	3.5	P80191	AHSG	1.5
P30801	S100A6	3.5	Q08863	GSTA1	1.5
P34032	TMSB4	3.5	Q08863	NA	1.5
P50117	S100A9	3.5	Q28658	SPRR3	1.5
P53789	GC	3.5	O62695	H2AZ2	1.5
P79226	ALDOB	3.5	O97529	ANXA8	1
Q28640	HRG	3.5	P00949	PGM1	1
Q8HZQ5	EZR	3.5	P01684	IGKV1D-12	1
O77506	LASP1	3	P01684	IGKV1-12	1
O77791	S100A12	3	P19943	RPLP2	1
P00939	TPI1	3	P27170	PON1	1
P23612	WARS1	3	P46409	Gstm2	1
P29562	EIF4A1	3	P53787	EEF1D	1
P31097	SPP1	3	Q28706	KRT12	1

P06814	CAPN2	1	P24480	S100A11	0
P13019	BLMH	1	P25704	ENO3	0
P23775	SERPINA6	1	P41316	CRYAB	0
P29678	MAP2K1	1	P46406	GAPDH	0
P43348	TPT1	1	P49065	ALB	0
P63150	PPP2R2A	1	P51662	ANXA1	0
Q00006	PPP2R2B	1	P60990	PIP	0
Q28719	PTGR1	1	P62160	CALM	0
Q29513	GNMT	1	Q28631	WFDC2	0
Q95212	TPD52	1	Q6Q6X0	YWHAQ	0
Q9N0V7	CBS	1	Q8MI17	ALDH1A1	0
C0HJA6	N/A	0.5	Q95218	Dmbt1	0
C0HJA6	/	0.5	Q9TTC6	PPIA	0
O19053	ADH5	0.5	Q9XSC5	CLU	0
P01840	K-BAS	0.5	P01685	IGKV1-27	-0.5
P13490	LDHB	0.5	P01685	GSTA1	-0.5
P29751	ACTB	0.5	P01885	B2M	-0.5
P35543	SAA3	0.5	P01894	HLA-H	-0.5
P39056	BGLAP	0.5	P06140	HLA-H	-0.5
P41975	SOD3	0.5	P25230	CAP18	-0.5
P62139	PPP1CA	0.5	P26202	N/A	-0.5
P62143	PPP1CB	0.5	P26202	/	-0.5
P62740	ACTA2	0.5	P26203	N/A	-0.5
P68135	ACTA1	0.5	P26203	/	-0.5
P98065	TNFAIP6	0.5	Q28685	DAG1	-0.5
Q29426	KRT3	0.5	Q28739	BPI	-0.5
P62975	UBA52	0.5	Q9BGN0	PON3	-0.5
O18750	HSP90B1	0	P25227	ORM1	-0.5
O97862	CST3	0	P00389	POR	-1
P01832	PIGR	0	P01948	HBA	-1
P01870	IGHG1	0	P02057	HBB1	-1
P01879	N/A	0	P15128	CYP4B1	-1
P01879	/	0	Q28618	YBX1	-1
P19007	HP	0	P00169	CYB5A	-1.5
P19134	TF	0	P01692	N/A	-1.5
P20058	HPX	0	P01692	/	-1.5
P23108	JCHAIN	0	P26890	IL1RN	-1.5

5.2. IgG extraction from rabbit serum (2A)

Table S 32. Online nanoLC-ESI-MS^E set-up

Lock Spray Configuration:		Instrument Configuration:	
Reference Scan Frequency(sec)	30	Lteff	1800
Reference Cone Voltage(V)	40	Veff	7176.85
Reference Trap Collision Energy	6	Resolution	18000
Reference DRE Setting	99.9	Min Points in Peak	2
Wave Velocity Look Up Table		Acquisition Device	WatersADC
Backing	2.96E+00	Acquisition Algorithm	ADC Mode
Source	6.09E-03	ADC Trigger Threshold (V)	0.95
Sample Plate	1.00E-06	ADC Input Offset (V)	-1.62
Trap	8.51E-03	Average Single Ion Intensity	23
Helium Cell	1.68E-04	ADC Amplitude Threshold	4
IMS	2.04E-04	ADC Centroid Threshold	-1
Transfer	8.89E-03	ADC Ion Area Threshold	4
TOF	7.27E-07	ADC Ion Area Offset	10
IMSRFOffset	300	ADC Pushes Per IMS Increment	1
IMSMobilityRFOffset	250	EDC Delay Coefficient	1.41
TrapRFOffset	300	EDC Delay Offset	0.4
Use Automatic RF Settings	TRUE	Acquisition mass range	
AutoStepWave1RFOffset	300	Start mass	50
AutoStepWave2RFOffset	350	End mass	2000
TransferRFOffset	350	Calibration mass range	
MS Profile Type	Profile	Start mass	72.074
MSProfileMass1	400	End mass	1285.59
MSProfileDwellTime1	20	Function Parameters	
MSProfileRampTime1	20	Survey Start Time	10
MSProfileMass2	500	Survey End Time	55
MSProfileDwellTime2	20	Survey Ion Mode	ES Mode
MSProfileRampTime2	40	Survey Polarity	Positive
MSProfileMass3	600	Survey Start Mass	50
PusherInterval	69	Survey End Mass	2000
PusherOffset	0.25	Parent Survey Low CE (V)	10
LockMassValidSigma	5	TIC Threshold	5
PRODUCT IONS		Survey Scan Time	0.5
Use High CE Product Ions Mass List File	NO	Survey Interscan Time	0
High CE Product Ions Mass List Filename		Survey Data Format	Continuum Resolution
Product Ions Match Logic	NO	Analyser Mode	
Product Ions Switch Threshold (Intensity/s)	10	ADC Sample Frequency (GHz)	3
Product Ions Switch Detection Window +/- (mDa)	100	TargetEnhancementMass2	69
Product Ions Retention Time Window +/- (sec)	10	TargetEnhancementMass3	1.75
		Survey Use Tune Page CV	YES

Experimental Instrument Parameters			
Polarity	ES+	Pusher	1900
Capillary (kV)	2.1	Pusher Offset	0.12
Source Temperature (°C)	70	Puller	1370
Sampling Cone	30	Pusher Cycle Time (µs)	Automa
Source Offset	40	Pusher Width (µs)	Automa
Source Gas Flow (mL/min)	0	Collector	60
Desolvation Temperature (°C)	150	Collector Pulse	10
Cone Gas Flow (L/Hr)	30	Stopper	10
Nanoflow Gas Pressure (Bar)	0.4	Stopper Pulse	20
Purge Gas Flow (mL/h)	500	Entrance	60
Desolvation Gas Flow (L/Hr)	500	Static Offset	180
Nebuliser Gas Flow (Bar)	6	Puller Offset	0
LM Resolution	4.7	Reflectron Grid (kV)	1.443
HM Resolution	15	Flight Tube (kV)	10
Aperture 1	0	Reflectron (kV)	3.78
Pre-filter	2	Use Manual Trap DC	TRUE
Ion Energy	0.2	Trap DC Entrance	0
Manual Trap Collision Energy	FALSE	Trap DC Bias	2
Trap Collision Energy	4	Trap DC	0
Manual Transfer Collision Energy	FALSE	Trap DC Exit	0
Transfer Collision Energy	2	Use Manual IMS DC	TRUE
Manual Gas Control	FALSE	IMS DC Entrance	-20
Trap Gas Flow (mL/min)	2	Helium Cell DC	1
HeliumCellGasFlow	180	Helium Exit	-20
IMS Gas Flow (mL/min)	90	IMSBias	2
Detector	3375	IMS DC Exit	20
DetectorCache	2300	USe Manual Transfer DC	FALSE
Sample Infusion Flow Rate (µL/min)	2	Transfer DC Entrance	5
Sample Flow State	LC	Transfer DC Exit	15
Sample Fill Volume (µL)	50	Trap Manual Control	OFF
Sample Reservoir	Wash	Trap Wave Velocity (m/s)	300
LockSpray Infusion Flow Rate (µL/min)	1	Trap Wave Height (V)	0.5
LockSpray Flow State	Infusion	IMS Manual Control	OFF
LockSpray Reservoir	A	IMS Wave Velocity (m/s)	850
LockSpray Capillary (kV)	3	IMS Wave Height (V)	0
Use Manual LockSpray Collision Energy	FALSE	Transfer Manual Control	OFF
Collision Energy	4	Transfer Wave Velocity (m/s)	247
Acceleration1	70	Transfer Wave Height (V)	0.2
Acceleration2	200	Step Wave 1 In Manual Control	OFF
Aperture2	70	Enable Reverse Operation	OFF
Transport1	70	Step Wave 1 In Velocity (m/s)	20
Transport2	70	Step Wave 1 In Height	15
Steering	0.44	Step Wave 1 Out Manual Control	ON
Tube Lens	75	Step Wave 1 Out Velocity (m/s)	300
Step Wave 1 Out Height	5	Mobility Extract Height (V)	0
Step Wave 2 Manual Control	ON	Trag Gate LUT table enabled	FALSE

Step Wave 2 Velocity (m/s)	300	Using Drift Time Trimming	TRUE
Step Wave 2 Height	1	Drift Time Bins	3
Use Manual Step Wave DC	ON	Using Mobility Delay after Trap Release	TRUE
Step Wave TransferOffset	18	IMS Wave Delay (µs)	450
Step Wave DiffAperture1	3	Variable Wave Height Enabled	FALSE
Step Wave DiffAperture2	0	Wave Height Ramp Type	Linear
Use Automatic RF Settings	TRUE	Wave Height Start (V)	8
StepWave1RFOffset	100	Wave Height End (V)	20
StepWave2RFOffset	100	Wave Height Using Full IMS	TRUE
Target Enhancement Enabled	FALSE	Wave Height Ramp (%)	100
Target Enhancement Mode	EDC	Variable Wave Velocity Enabled	TRUE
Target Enhancement Mass	556	Wave Velocity Ramp Type	Linear
Target Enhancement Trap Height (V)	4	Wave Velocity Start (m/s)	800
Target Enhancement Extract Height (V)	15	Wave Velocity End (m/s)	450
Mobility Trapping Manual Release Enabled	TRUE	Wave Velocity Using Full IMS	TRUE
Mobility Trapping Release Time (µs)	500	Wave Velocity Ramp (%)	100
Mobility Trap Height (V)	15		

NEUTRAL LOSS	
Use Neutral Loss Mass List File	NO
Neutral Loss Mass List Filename	
Neutral Loss Match Logic	OR
Neutral Loss Switch Threshold (Intensity/s)	10
Neutral Loss Switch Detection Window +/- (mDa)	100
MS/MS	
MSMS Start Mass	50
MSMS End Mass	2000
Number of components	0
Use MSMS to MS Switch After Time	NO
MSMS Switch After Time (sec)	10
Absence of Neutral Loss	NO
Absence of Product Ion	NO
MSMS Scan Time (sec)	1
MSMS Interscan Time (sec)	0
MSMS Data Format	Continuum
Use Tune Page Cone Voltage	YES
Use MS/MS ipr File	NO
Instrument Parameter Filename	
Peak Detection Window	1
Use Intensity based Peak Detection	YES
Charge State Tolerance Window	3
Charge State Extraction Window	4
Deisotope Tolerance Window	3
Deisotope Extraction Window	4
Discard survey data	NO
[COLLISION ENERGY]	
Using Auto Trap MS Collision Energy (eV)	4
Using Auto Transfer MS Collision Energy (eV)	2
Precursor Selection	Everything
Use Exclude Masses List	NO
Exclude Mass Range	
Use Exclude File Masses	NO
Exclude Mass Filename	
Exclude Window +/- (mDa)	100
Exclude Retention Time Window	10
Reference Frequency	0
Reference Cone Voltage	0
Calibration	Dynamic 2

Autosampler	
Run Time	60.00 min
Loop Option	Partial Loop
LoopOffline	Disable
Weak Wash Solvent Name	Water
Weak Wash Volume	800 uL
Strong Wash Solvent Name	Acetonitrile
Strong Wash Volume	300 uL
Target Column Temperature	35.0 C
Column Temperature Alarm Band	Disabled
Target Sample Temperature	6.0 C
Sample Temperature Alarm Band	Disabled
Full Loop Overfill Factor	Automatic
Syringe Draw Rate	Automatic
Needle Placement	0.5
Pre-Aspirate Air Gap	Automatic
Post-Aspirate Air Gap	Automatic
Column Temperature Data Channel	No
Ambient Temperature Data Channel	Yes
Sample Temperature Data Channel	No
Sample Pressure Data Channel	No
Switch 1	No Change
Switch 2	No Change
Switch 3	No Change
Switch 4	No Change
Chart Out	Sample Pressure
Sample Temp Alarm	Disabled
Column Temp Alarm	Disabled
Run Events	Yes
SampleLoop	5
Saved as Trizaic	No
nanoTile Cool Down	2

Pump	
Pump Type	BSM1
Run Time	60.00 min
Solvent Selection A	A1
Solvent Selection B	B1
Seal Wash	15.0 min
Switch 1	No Change
Switch 2	No Change
Switch 3	No Change
Chart Out 1	System Pressure
Chart Out 2	%B
Run Events	Yes
Gradient Table	
Time(min) Flow Rate(uL/min) %A %B Curve	1. Initial 0.300 97.0 3.0 2. 1.00 0.300 97.0 3.0 6 3. 25.00 0.300 60.0 40.0 6 4. 30.00 0.300 15.0 85.0 6 5. 35.00 0.300 10.0 90.0 6 6. 36.00 0.300 97.0 3.0 6 7. 60.00 0.300 97.0 3.0 6 8. 65.00 0.300 97.0 3.0 6 9. 100.00 0.150 50.0 50.0 6
Analytical Low Pressure Limit	0 psi
Analytical High Pressure Limit	10000 psi
Sample Loading Time	4.00 min
Trapping Flow Rate	8.000 uL/min
Trapping %A	99.9
Trapping %B	0.1
Trapping Low Pressure Limit	0 psi
Trapping High Pressure Limit	5000 psi
Flow Rate A Data Channel	No
Flow Rate B Data Channel	No
Solvent Name A	Water
Solvent Name B	Acetonitrile
Pump A	
Aux Pump Role	Auxiliary
Aux Solvent Name	Water
Aux Flow Rate	0.000 uL/min
Aux Solvent Selection	A1
Aux Low Pressure Limit	0 psi
Aux High Pressure Limit	10000 psi

Pump B	
Aux Pump Role	Lock Mass
Aux Solvent Name	Water
Aux Flow Rate	0.500 uL/min
Aux Solvent Selection	B1
Aux Low Pressure Limit	0 psi
Aux High Pressure Limit	10000 psi

Table S 33. PLGS set-up

Processing parameters	
Chromatographic Peak Width	Automatic
MS TOF Resolution	Automatic
Lock Mass for charge 2	785.8426 Da/e
Lock Mass Window	0.25 Da
Low Energi treshold	135.0 counts
Elevated Energy treshold	30.0 counts
Databank Search Query	
Databank	*Oryctolagus Cuniculu*
Peptide tolerance	Automatic
Fragment Tolerance	Automatic
Min Fragmnet ion match	3
Ion match per protein	7
Maximum protein mass	2500000
Digest reagent	Trypsin
Missed Cleavages	2
Fixed modification	Carbamidomethyl C
Variable modification	Oxidation M
FDR	4

Table S 34. IgG recovery of serum extractions

R1 replicate	Volume (µl)	Concentration (µg/µl)	Recovery (%)
1	50	0.349	5.4
2	40	0.456	5.55
3	42	0.340	4.3
4	66	0.146	7.7
Average recovery (%)			5.7
Standard Deviation			1.4

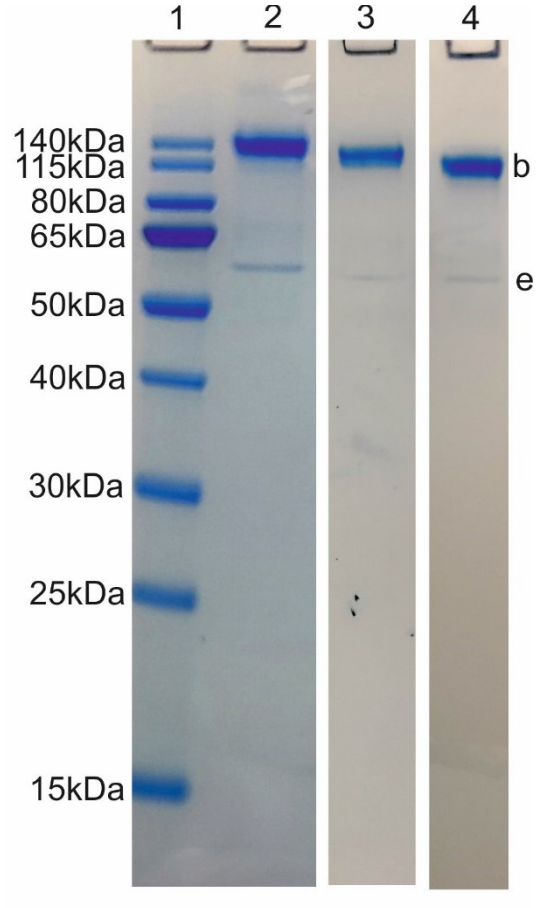

Figure S 1. SDS-PAGE unreduced R1 replicates.

Into pockets 1 were loaded 3 µl of Prestained proteins marker; into pockets 2 was loaded 1.2 µl of R1 replicate2 (0.55 µg of total proteins loaded); into pockets 3 was loaded 1.6 µl of R1 replicate3 (0.54 µg of total proteins loaded); into pockets 4 was loaded 1.6 µl of R1 replicate1 (0.56 µg of total proteins loaded). In all of them is possible to see the fat band b at the apparent mass of ca. 140 kDa, which fit to the average mass of IgG (150 kDa), and the tiny band e between 65 kDa and 50 kDa of apparent mass, this value can be related with Albumin mass.

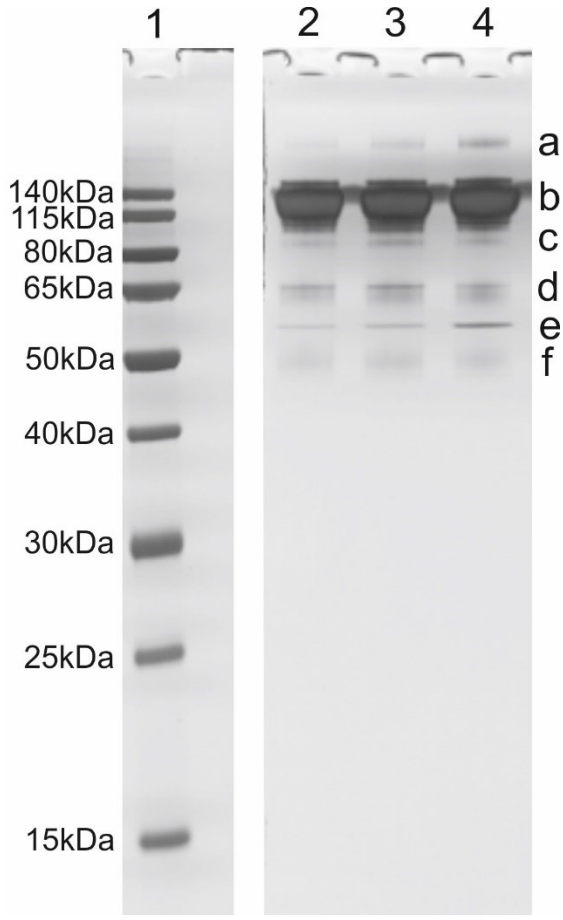

Figure S 2. SDS-PAGE unreduced R1 replicates Silver stained.

Into pockets 1 were loaded 3 µl of Prestained proteins marker; into pockets 2 was loaded 1.2 µl of R1 replicate2 (0.55 µg of total proteins loaded); into pockets 3 was loaded 1.6 µl of R1 replicate3 (0.54 µg of total proteins loaded); into pockets 4 was loaded 1.6 µl of R1 replicate1 (0.56 µg of total proteins loaded). In all of them is possible to see the fat band b at the apparent mass of ca. 140 kDa, which fit to the average mass of IgG (150 kDa), and the tiny band e between 65 kDa and 50 kDa of apparent mass, this value can be related with Albumin mass. In addition, thanks to the major sensitivity of the silver stain method other bands are better visual-

ised. Band a contains traces of unknown protein, band c contains traces of haptoglobin, band d serum transferrin, Ig gamma chain and serum albumin, and the band f was found related to transthyretin. Proteins identification of the reported bands were performed by online nanoLC-ESI-MS^E analysis followed by PLGS raw data analysis (Chapter 3.4) from in-gel digestion Coomassie stained gel of R1 replicate 4 as it was for the before descripted gel (Figure 32, chapter 3.3 and 3.4)

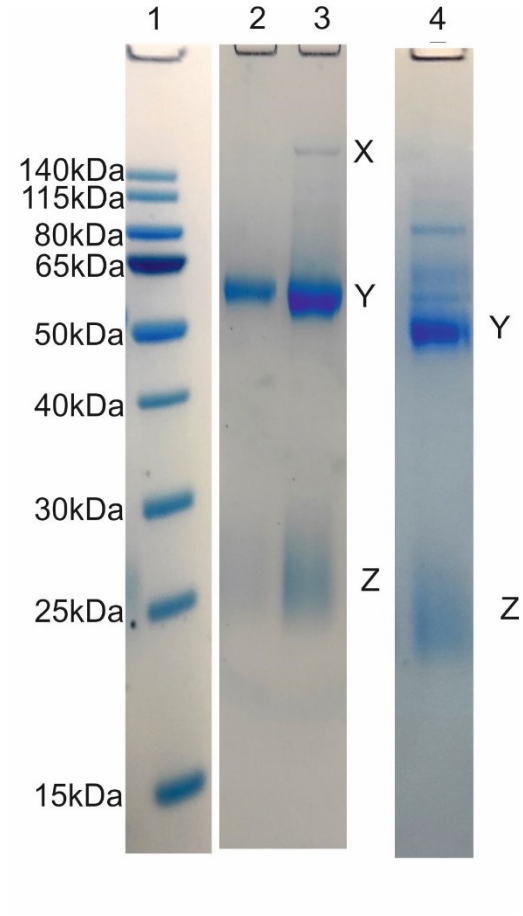

Figure S 3. SDS-PAGE reduced R1 replicates.

To confirm the presence of IgGs was performed another SDS-PAGE, but this time the replicates solutions were treated with the Reducing buffer, in order to disassemble the IgGs and obtain light and heavy chains bends. Into pockets 1 were loaded 3 µl of Prestained proteins marker; into pockets 2 was loaded 1.2 µl of R1 replicate2 (0.55 µg of total proteins loaded); into pockets 3 was loaded 1.6 µl of R1 replicate3 (0.54 µg of total proteins loaded); into pockets 4 was loaded 1.6 µl of R1 replicate1 (0.56 µg of total proteins loaded). In all of them is possible to see the big band Y of the apparent mass of 50 kDa, which fit to the average mass of

IgG heavy chains (50 kDa), the band Z, broad and less coloured, is visible at about 25 kDa, these fit with the average mass of IgG light chains (25 kDa). In addition, in lane 3 is possible to see band X related to unreduced IgG.

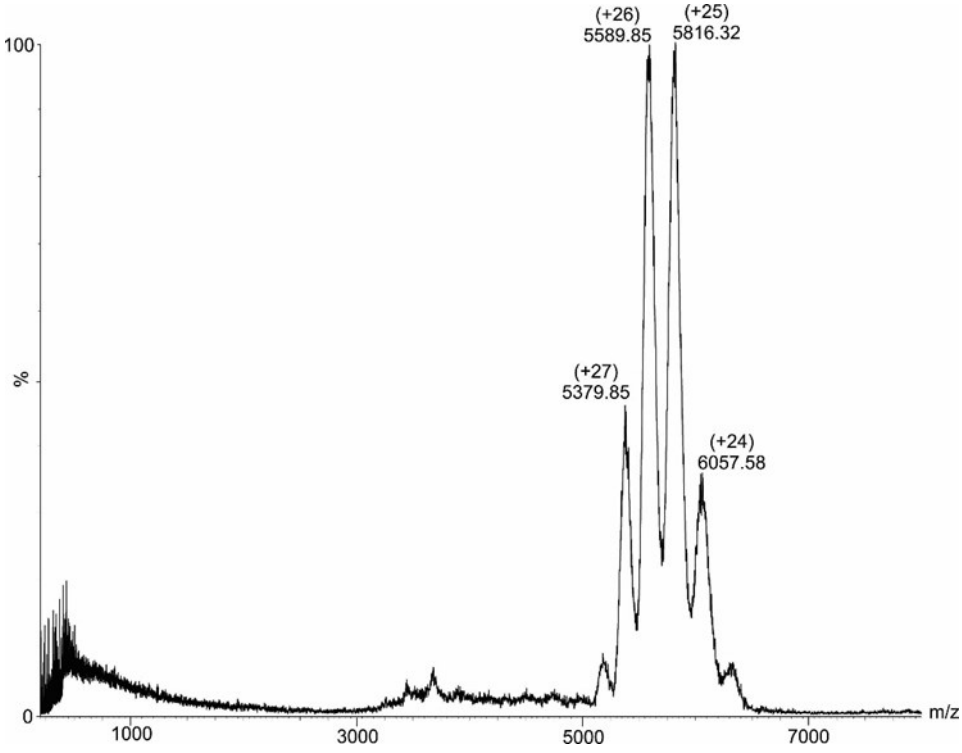

Figure S 4. Offline nanoESI-MS spectra of R1 replicate 1 0.27 µg/µl. Ion signals are labelled with m/z values and charge states are given in parentheses. Solvent: 200 mM ammonium acetate, pH 6.7.
The mass spectrum shows a clean antibody solution obtained after the desalting and buffer exchange process with the typical pattern of multiply charged ion signals between m/z 5000 and m/z 6500. Ion signal intensities follow a Gaussian distribution and the most intense ion signal is recorded for the 25-fold protonated ion. The from the multiply charged ion signals determined molecular mass is 145319.99 ± 67.81 Da. In the m/z range between m/z 3000 and m/z 4000 there are some low intensity ion signals that can be attributed to the presence of albumin and transthyretin (not labelled in Figure S 4). Same result obtained for the spectrum of R1 replicate 4 (Figure 33)

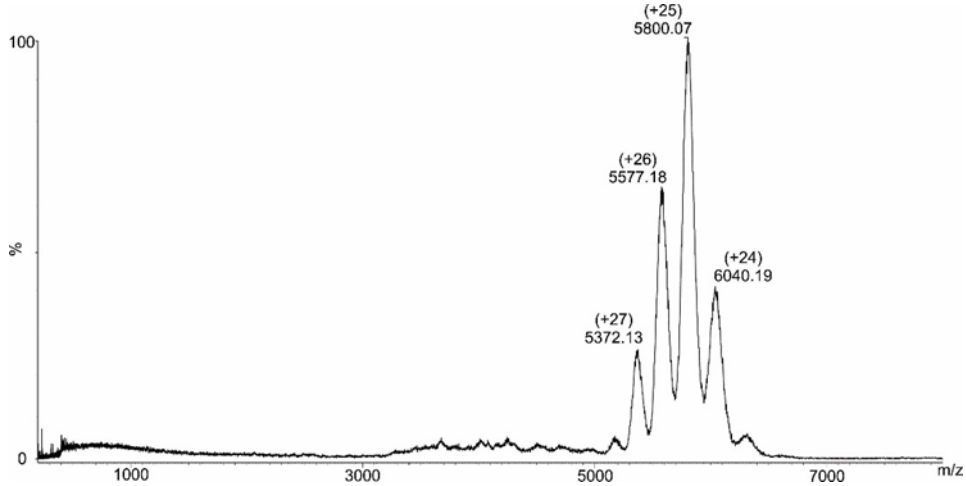

Figure S 5. Offline nanoESI-MS spectra of R1 replicate 2 0.45 µg/µl. Ion signals are labelled with m/z values and charge states are given in parentheses. Solvent: 200 mM ammonium acetate, pH 6.7. The mass spectrum shows a clean antibody solution obtained after the desalting and buffer exchange process with the typical pattern of multiply charged ion signals between m/z 5000 and m/z 6500. Ion signal intensities follow a Gaussian distribution and the most intense ion signal is recorded for the 25-fold protonated ion. The from the multiply charged ion signals determined molecular mass is 144979.63 ± 32.70 Da. In the m/z range between m/z 3000 and m/z 4000 there are some low intensity ion signals that can be attributed to the presence of albumin and transthyretin (not labelled in Figure S 5). Same result obtained for the spectrum of R1 replicate 4 (Figure 33)

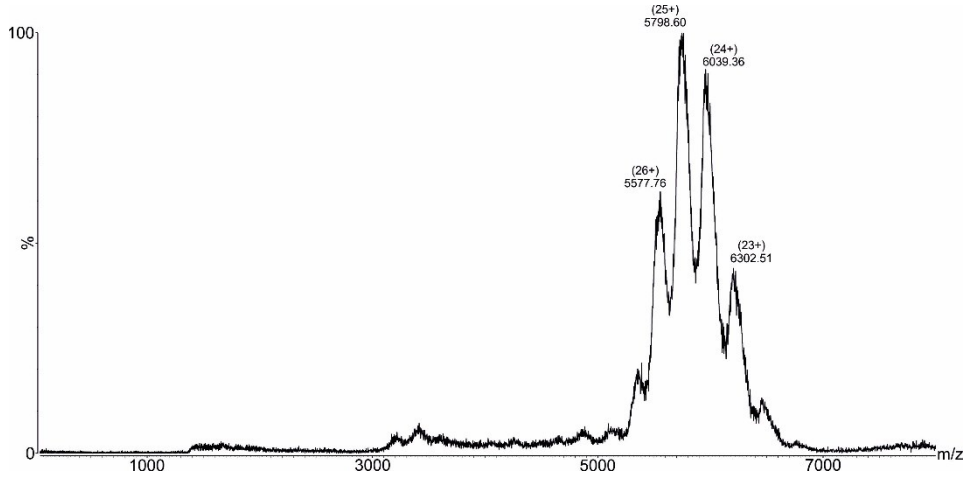

Figure S 6. Offline nanoESI-MS spectra of R1 replicate 3 0.34 µg/µl. Ion signals are labelled with m/z values and charge states are given in parentheses. Solvent: 200 mM ammonium acetate, pH 6.7. The mass spectrum shows a clean antibody solution obtained after the desalting and buffer exchange process with the typical pattern of multiply charged ion signals between m/z 5000 and m/z 6500. Ion signal intensities follow a Gaussian distribution and the most intense ion signal is recorded for the 25-fold protonated ion. The from the multiply charged ion signals determined molecular mass is 144947.73 ± 33.01 Da. In the m/z range between m/z 3000 and m/z 4000 there are some low intensity ion signals that can be attributed to the pres-

ence of albumin and transthyretin (not labelled in Figure S 6). Same result obtained for the spectrum of R1 replicate 4 (Figure 33)

5.3. IgGs extraction from converted serum and characterisation (2B)

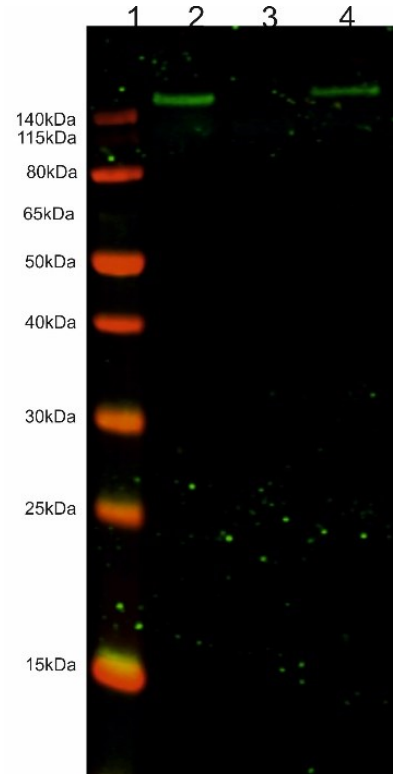

Figure S 7. Western blot of serum mixed with anti-Ovalbumin antibody (Solution 3), IgGs extracted from rabbit serum spiked in with anti-Ovalbumin antibody (Solution 4) and IgGs extracted from rabbit serum (Solution 9).

To assess if the anti-Ovalbumin antibody concentration into IgG extracted from converted serum solution (Solution 4) is enough for Western blot, another electrophoresis was performed (as reported in chapter 3.3.2), on the gel were loaded 3 µl of Prestained proteins marker, 4.5 µl of IgG extracted from converted serum solution (Solution 4, 6.34 µg of total proteins), 14 µl of converted serum solution (Solution 3, 33 µg of total proteins) and 10 µl of IgG extracted from rabbit serum solution (Solution 9, 3.4 µg of IgG). Once the electrophoresis was done, Western blot was performed (as reported in chapter 3.6.4). After blotting, the membrane was blocked putting it into the Blocking solution (ca. 10 ml) shaken for 1 hour at room temperature; then the membrane was immersed in Secondary antibody solution (ca. 3 ml) shaken for 1 hour at

room temperature protected from light. At this point the membrane was washed protected from light 4 times (ca. 10 ml each time), 5 minutes each, and shaken into washing solution at room temperature. The last step consists in putting the membrane into a solution of PBS 1% (ca. 10 ml) and it was scanned at LICOR-System scanner. The green band showed in line 1 demonstrate that the amount of anti-Ovalbumin antibody mixed with the raw rabbit serum, diluted, and loaded on the gel (Solution 3), was enough to be transferred on the membrane and to be linked by antiMouse-IgG antibody from goat labelled with IRDye® 800 CW. The absent green band in line 3, where the IgGs extracted from rabbit serum solution (Solution 9) was loaded suggest that rabbit serum does not contain IgGs available to be bonded by antiMouse-IgG antibody from goat labelled with IRDye® 800 CW. The green band in line 4 suggest that the amount of anti-Ovalbumin antibody, contained into IgG extracted from converted serum solution (Solution 4), that was mixed with the raw rabbit serum and that went through the extraction process still enough to be recognized by antiMouse-IgG antibody from goat labelled with IRDye® 800 CW, and that it still working even if anti-Ovalbumin is among others IgGs.

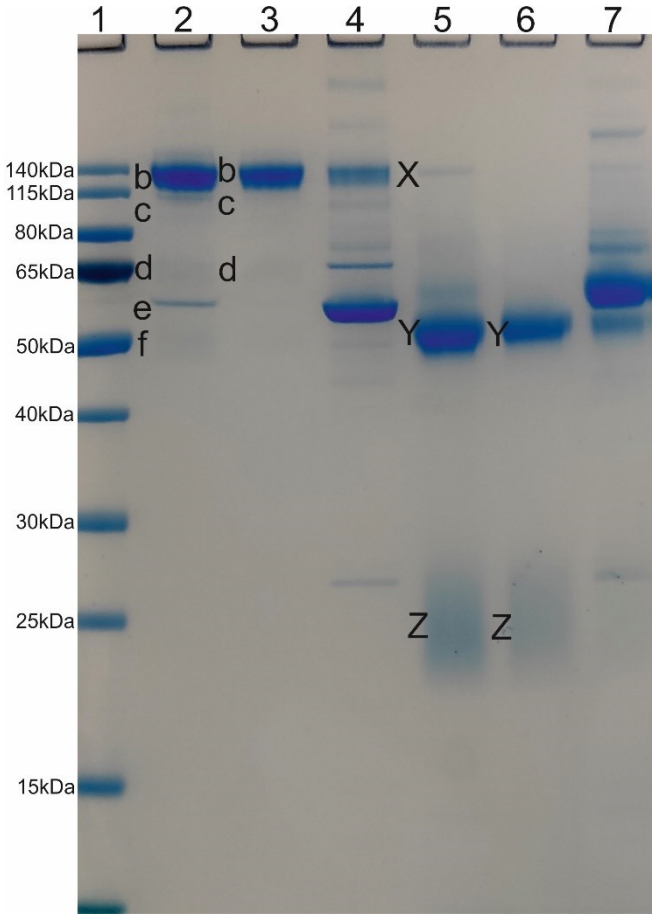

Figure S 8. Comparison between serum mixed with anti-Ovalbumin antibody (Solution 1), IgGs extracted from rabbit serum spiked in with anti-Ovalbumin antibody (Solution 4) and IgGs extracted from rabbit serum (Solution 9).

Gel related to the electrophoresis performed loading on the gel anti-Ovalbumin antibody (Solution 1), IgGs extracted from rabbit serum spiked in with anti-Ovalbumin antibody (Solution 4) and IgGs extracted from rabbit serum (Solution 9), each of them were mixed with both reducing and unreducing buffer. Into pockets 1 were loaded 3 µl of Prestained proteins marker each; into pocket 2 was loaded 0.75 µl of IgG extracted from converted rabbit serum solution (Solution 4), 1.41 µg/µl of protein concentration; into pockets 3 1.6 µl of IgG extracted from rabbit serum solution (Solution 9), 0.34 µg/µl; into pocket 4 0.8 µl of converted serum (Solution 3), 2.38 µg/µl; into pocket 5 was load the same amount of IgG extracted from converted serum (Solution 4) but it was treated with reducing buffer; the same for IgG extracted from rabbit serum solution (Solution 9) in pocket 6 and converted serum solution (Solution 3) in pocket 7. It show the same result obtained in before (Figure 32 and 33)

5.4. Ovalbumin digestion and characterisation (2B)

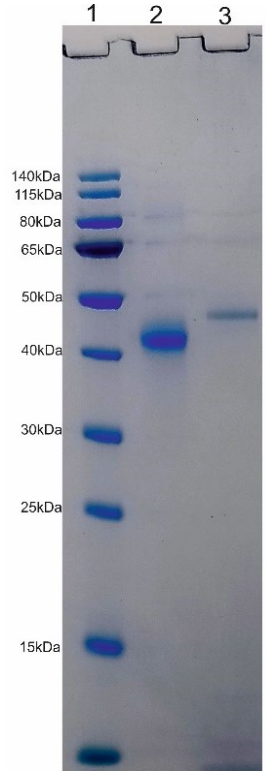

Figure S 9. SDS-PAGE electrophoresis of Ovalbumin tryptic digested solution (Solution 6).

SDS-PAGE electrophoresis was performed loading on the gel 3 µl of Prestained protein marker in pocket 1, Ovalbumin solution (Solution 5) was diluted 1:40 with 50 mM ammonium bicarbonate, pH 8 (0.24 µg/µl) and 3.2 µl of it were mixed with 12.8 µl of deionised water and 4 µl of Non-reducing buffer, then this solution was loaded into pocket 2, 1.2 µl of 0.63 µg/µl of

Ovalbumin tryptic digested solution (Solution 6) were mixed with 14.8 µl of deionised water and 4 µl of Non-reducing buffer, it was loaded into pocket 3. In line 1 we can see the bands related to the Prestained protein marker, in line 2 where just Ovalbumin was loaded is possible to observe one band between 40 and 50 kDa of apparent mass, which fit with the 45 kDa mass of Ovalbumin, in line 3 even if about the same amount of proteins were loaded at ca. 45 kDa of apparent mass is present a smaller band, it suggest that the digestion took place but was not complete.

Table S 35. PLGS set-up

Processing parameters	
Chromatographic Peak Width	Automatic
MS TOF Resolution	Automatic
Lock Mass for charge 2	785.8426 Da/e
Lock Mass Window	0.25 Da
Low Energi treshold	135.0 counts
Elevated Energy treshold	30.0 counts
Databank Search Query	
Databank	Gallus gallus
Peptide tolerance	Automatic
Fragment Tolerance	Automatic
Min Fragmnet ion match	3
Ion match per protein	7
Maximum protein mass	2500000
Digest reagent	Trypsin
Missed Cleavages	3
Fixed modification	Carbamidomethyl C
Variable modification	Oxidation M Glycosylation N Acetylation G Phosphorilation S
FDR	4

Table S 36. BiopharmaLinx set-up

Resolution	
Instrument resolution	Automatic
Lock Mass for charge 2	785.842 Da
Lock Mass tolerance	0.25 Da
Peak Width (Mins)	Automatic
MS ion intensity treshold	250 counts
Process MS^E Data	Yes
MS^E Ion intensity treshold	100 counts
Process HD data	No
Tetention time Range (Mins)	Automatic
Search Parameters	
MS mass tolerance	30 ppm
MS^E Mass tolerance	30 ppm
Missed Cleavages	3
Digest Reagent	Trypsin
Protein	Ovalbumin P01012
Modifications	Acetyl N-Term
	Glycosylation G
	Phosphorylation S
	Carbamidomethil C (fixed)
	Oxidation M
	Deamidation M
	Deamidation Q
	Carbamyl K
	Carbamyl R
	Oxidation 2X M
	Oxidation W
	Na
	K

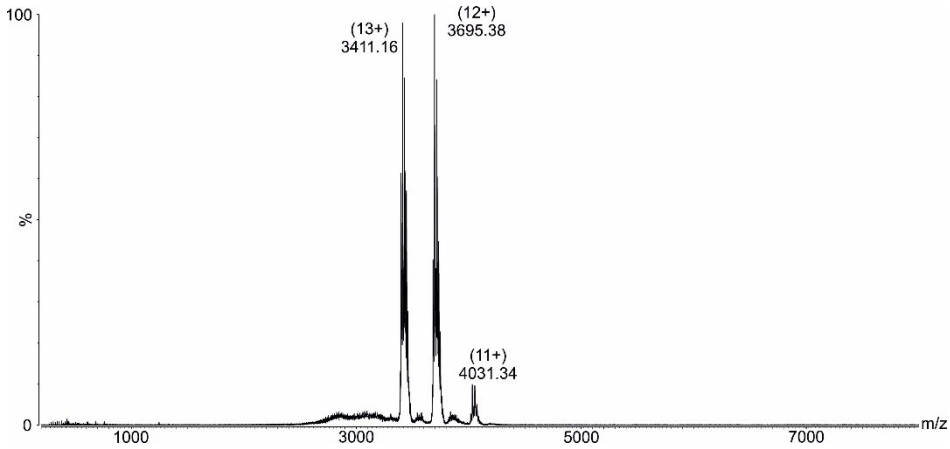

Figure S 10. *Offline nanoESI-MS spectrum of Ovalbumin (Solution 5).*

Native Ovalbumin solution was analysed by offline nanoESI-MS, it was prepared diluting 1:15 the Ovalbumin solution 9.66 µg/µl with ammonium acetate 0.2 M, pH 6.7, (prepared in chapter 3.6.1), to obtain a solution 0.64 µg/µl, on this the exchanging buffer operation was performed using Amicon filter 30 kDa (as reported in chapter 3.3.1. step 3). Concentration measured at Qubit was 0.39 µg/µl. The spectrum of this solution was collected in offline nanoESI-MS filling with 2.5 µl of solution a gold coated needle for nano Spray and the following set-up: capillary voltage was 1.2 KV; Cone voltage 130 V, Extractor voltage 3 V, RF Lens 1.2 V, Source temperature 40 °C, MCP 1950 V, Pusher 124 µs, Inelet Penning vacuum was $1.55 \cdot 10^{-1}$ mbar, Analyser Penning at $3 \cdot 10^{-5}$ mbar, the ToF Penning at $4.5 \cdot 10^{-7}$ mbar and the nitrogen sheath gas flow was at 4 psi. The spectrum was collected from m/z 50 to m/z 8000 and for 9 minutes, it was smoothed 10 times (Window size scans ± 30, used method "mean"). Spectra were recorded using the MassLinx 4.0 data system from Waters (Manchester, UK) and CDR-files were saved on computer drives. The MassLinx software package was used for data analysis and spectral image preparation in conjunction with the CorelDraw 17.0 software package.

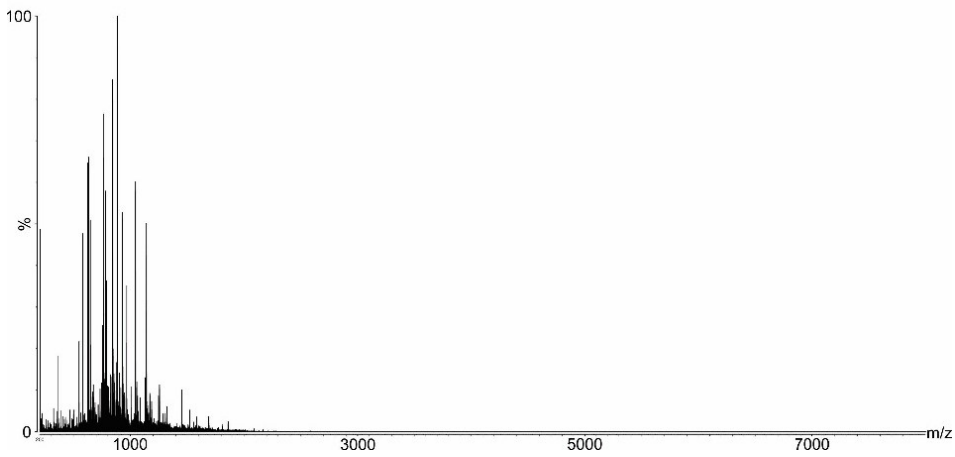

Figure S 11. Offline nanoESI-MS spectrum (set-up chapter 3.6.6) of Ovalbumin digested solution (Solution 6).

Comparing the offline nanoESI-MS spectra of Ovalbumin (Solution 5) and digested Ovalbumin (Solution 6) (Figure S 10 and Figure S 11) is possible to see that after digestion of Ovalbumin, and desalting by OASIS, Ovalbumin signals between m/z 3400 and m/z 4000 are absent in digested Ovalbumin solution (Solution 6) spectrum, therefore undigested Ovalbumin was removed.

Table S 37. Calculated peptides of digested Ovalbumin by GPMAW

From	To	MH+	M2H+	M3H+	Sequence
1	16	1750.99	876	584.33	GSIGAASMEFCFDVFK
1	19	2121.43	1061.22	707.82	GSIGAASMEFCFDVFKELK
1	46	5079.94	2540.47	1693.98	GSIGAASMEFCFDVFKELKVHHANENIFYCPIAIMSALAMVYLGAK
1	50	5539.39	2770.2	1847.14	GSIGAASMEFCFDVFKELKVHHANENIFYCPIAIMSALAMVYLGAKDSTR
17	19	389.47	195.24	130.49	ELK
17	46	3347.97	1674.49	1116.66	ELKVHHANENIFYCPIAIMSALAMVYLGAK
17	50	3807.42	1904.22	1269.81	ELKVHHANENIFYCPIAIMSALAMVYLGAKDSTR
17	55	4392.09	2196.55	1464.7	ELKVHHANENIFYCPIAIMSALAMVYLGAKDSTRTQINK
20	46	2977.53	1489.27	993.18	VHHANENIFYCPIAIMSALAMVYLGAK
20	50	3436.98	1718.99	1146.33	VHHANENIFYCPIAIMSALAMVYLGAKDSTR
20	55	4021.65	2011.33	1341.22	VHHANENIFYCPIAIMSALAMVYLGAKDSTRTQINK
20	58	4376.09	2188.55	1459.37	VHHANENIFYCPIAIMSALAMVYLGAKDSTRTQINKVVR
47	50	478.48	239.74	160.16	DSTR
47	55	1063.14	532.07	355.05	DSTRTQINK
47	58	1417.59	709.3	473.2	DSTRTQINKVVR
47	61	1808.02	904.52	603.35	DSTRTQINKVVRFDK
51	55	603.69	302.35	201.9	TQINK
51	58	958.14	479.57	320.05	TQINKVVR
51	61	1348.57	674.79	450.19	TQINKVVRFDK
51	84	3841.16	1921.09	1281.06	TQINKVVRFDKLPGFGDSIEAQCGTSVNVHSSLR
56	58	373.47	187.24	125.16	VVR
56	61	763.9	382.46	255.31	VVRFDK
56	84	3256.5	1628.75	1086.17	VVRFDKLPGFGDSIEAQCGTSVNVHSSLR
56	104	5520	2760.51	1840.67	VVRFDKLPGFGDSIEAQCGTSVNVHSSLRDILNQITKPNDVYSFSLASR
59	61	409.46	205.23	137.16	FDK
59	84	2902.05	1451.53	968.02	FDKLPGFGDSIEAQCGTSVNVHSSLR
59	104	5165.56	2583.28	1722.52	FDKLPGFGDSIEAQCGTSVNVHSSLRDILNQITKPNDVYSFSLASR
59	110	5927.38	2964.19	1976.46	FDKLPGFGDSIEAQCGTSVNVHSSLRDILNQITKPNDVYSFSLASRLYAEER
62	84	2511.62	1256.31	837.88	LPGFGDSIEAQCGTSVNVHSSLR
62	104	4775.12	2388.06	1592.38	LPGFGDSIEAQCGTSVNVHSSLRDILNQITKPNDVYSFSLASR
62	110	5536.94	2768.98	1846.32	LPGFGDSIEAQCGTSVNVHSSLRDILNQITKPNDVYSFSLASRLYAEER
62	122	7040.73	3520.87	2347.58	LPGFGDSIEAQCGTSVNVHSSLRDILNQITKPNDVYSFSLASRLYAEERYPILPEYLQCVK
85	104	2282.53	1141.77	761.51	DILNQITKPNDVYSFSLASR
85	110	3044.35	1522.68	1015.45	DILNQITKPNDVYSFSLASRLYAEER
85	122	4548.13	2274.57	1516.72	DILNQITKPNDVYSFSLASRLYAEERYPILPEYLQCVK
85	126	5109.76	2555.39	1703.93	DILNQITKPNDVYSFSLASRLYAEERYPILPEYLQCVKELYR
105	110	780.84	390.93	260.95	LYAEER
105	122	2284.63	1142.82	762.21	LYAEERYPILPEYLQCVK
105	126	2846.26	1423.63	949.42	LYAEERYPILPEYLQCVKELYR
105	142	4516.05	2258.53	1506.02	LYAEERYPILPEYLQCVKELYRGGLEPINFQTAADQAR
111	122	1522.81	761.91	508.27	YPILPEYLQCVK
111	126	2084.44	1042.72	695.48	YPILPEYLQCVKELYR
111	142	3754.23	1877.62	1252.08	YPILPEYLQCVKELYRGGLEPINFQTAADQAR
111	158	5595.26	2798.13	1865.76	YPILPEYLQCVKELYRGGLEPINFQTAADQARELINSWVESQTNGIIR
123	126	580.65	290.83	194.22	ELYR
123	142	2250.45	1125.73	750.82	ELYRGGLEPINFQTAADQAR
123	158	4091.48	2046.24	1364.5	ELYRGGLEPINFQTAADQARELINSWVESQTNGIIR
123	181	6534.3	3267.66	2178.77	ELYRGGLEPINFQTAADQARELINSWVESQTNGIIRNVLQPSSVDSQTAMVLVNAIVFK
127	142	1687.84	844.91	563.61	GGLEPINFQTAADQAR
127	158	3529.84	1765.43	1177.29	GGLEPINFQTAADQARELINSWVESQTNGIIR
127	181	5972.67	2986.84	1991.56	GGLEPINFQTAADQARELINSWVESQTNGIIRNVLQPSSVDSQTAMVLVNAIVFK
127	186	6586.38	3293.69	2196.13	GGLEPINFQTAADQARELINSWVESQTNGIIRNVLQPSSVDSQTAMVLVNAIVFKGLWEK
143	158	1860.05	930.53	620.69	ELINSWVESQTNGIIR
143	181	4302.88	2151.94	1434.97	ELINSWVESQTNGIIRNVLQPSSVDSQTAMVLVNAIVFK
143	186	4916.59	2458.8	1639.53	ELINSWVESQTNGIIRNVLQPSSVDSQTAMVLVNAIVFKGLWEK
143	189	5263.01	2632.01	1755.01	ELINSWVESQTNGIIRNVLQPSSVDSQTAMVLVNAIVFKGLWEKAFK
159	181	2461.85	1231.43	821.29	NVLQPSSVDSQTAMVLVNAIVFK
159	186	3075.56	1538.28	1025.86	NVLQPSSVDSQTAMVLVNAIVFKGLWEK
159	189	3421.98	1711.49	1141.33	NVLQPSSVDSQTAMVLVNAIVFKGLWEKAFK
159	199	4613.25	2307.13	1538.42	NVLQPSSVDSQTAMVLVNAIVFKGLWEKAFKDEDTQAMPFR
182	186	632.73	316.87	211.58	GLWEK
182	189	979.15	490.08	327.06	GLWEKAFK
182	199	2170.42	1085.72	724.15	GLWEKAFKDEDTQAMPFR
182	218	4437.06	2219.04	1479.69	GLWEKAFKDEDTQAMPFRVTEQESKPVQMMYQIGLFR

187	189	365.45	183.23	122.49	AFK
187	199	1556.72	778.86	519.58	AFKDEDTQAMPFR
187	218	3823.36	1912.18	1275.12	AFKDEDTQAMPFRVTEQESKPVQMMYQIGLFR
187	226	4627.28	2314.15	1543.1	AFKDEDTQAMPFRVTEQESKPVQMMYQIGLFRVASMASEK
190	199	1210.29	605.65	404.1	DEDTQAMPFR
190	218	3476.93	1738.97	1159.65	DEDTQAMPFRVTEQESKPVQMMYQIGLFR
190	226	4280.86	2140.93	1427.62	DEDTQAMPFRVTEQESKPVQMMYQIGLFRVASMASEK
190	228	4540.23	2270.62	1514.08	DEDTQAMPFRVTEQESKPVQMMYQIGLFRVASMASEKMK
200	218	2285.66	1143.33	762.56	VTEQESKPVQMMYQIGLFR
200	226	3089.59	1545.3	1030.53	VTEQESKPVQMMYQIGLFRVASMASEK
200	228	3348.96	1674.98	1116.99	VTEQESKPVQMMYQIGLFRVASMASEKMK
200	263	7195.42	3598.21	2399.15	VTEQESKPVQMMYQIGLFRVASMASEKMKILELPFASGTMSMLVLLPDEVSGLEQLESIINFEK
219	226	822.95	411.98	274.99	VASMASEK
219	228	1082.32	541.66	361.44	VASMASEKMK
219	263	4928.78	2464.89	1643.6	VASMASEKMKILELPFASGTMSMLVLLPDEVSGLEQLESIINFEK
219	276	6492.47	3246.74	2164.83	VASMASEKMKILELPFASGTMSMLVLLPDEVSGLEQLESIINFEKLTEWTSSNVMEER
227	228	278.39	139.7	93.47	MK
227	263	4124.86	2062.93	1375.62	MKILELPFASGTMSMLVLLPDEVSGLEQLESIINFEK
227	276	5688.55	2844.78	1896.85	MKILELPFASGTMSMLVLLPDEVSGLEQLESIINFEKLTEWTSSNVMEER
227	277	5816.72	2908.86	1939.58	MKILELPFASGTMSMLVLLPDEVSGLEQLESIINFEKLTEWTSSNVMEERK
229	263	3865.49	1933.25	1289.17	ILELPFASGTMSMLVLLPDEVSGLEQLESIINFEK
229	276	5429.18	2715.09	1810.4	ILELPFASGTMSMLVLLPDEVSGLEQLESIINFEKLTEWTSSNVMEER
229	277	5557.35	2779.18	1853.12	ILELPFASGTMSMLVLLPDEVSGLEQLESIINFEKLTEWTSSNVMEERK
229	279	5798.68	2899.84	1933.56	ILELPFASGTMSMLVLLPDEVSGLEQLESIINFEKLTEWTSSNVMEERKIK
264	276	1582.71	791.86	528.24	LTEWTSSNVMEER
264	277	1710.88	855.95	570.97	LTEWTSSNVMEERK
264	279	1952.21	976.61	651.41	LTEWTSSNVMEERKIK
264	284	2580.98	1290.99	861	LTEWTSSNVMEERKIKVYLPR
277	277	147.19	74.1	49.74	K
277	279	388.52	194.77	130.18	KIK
277	284	1017.29	509.15	339.77	KIKVYLPR
277	286	1276.66	638.83	426.22	KIKVYLPRMK
278	279	260.35	130.68	87.46	IK
278	284	889.12	445.06	297.04	IKVYLPR
278	286	1148.48	574.75	383.5	IKVYLPRMK
278	290	1666.08	833.54	556.03	IKVYLPRMKMEEK
280	284	647.79	324.4	216.6	VYLPR
280	286	907.15	454.08	303.06	VYLPRMK
280	290	1424.75	712.88	475.59	VYLPRMKMEEK
280	322	4904.64	2452.82	1635.55	VYLPRMKMEEKYNLTSVLMAMGITDVFSSSANLSGISSAESLK
285	286	278.39	139.7	93.47	MK
285	290	795.99	398.5	266	MKMEEK
285	322	4275.87	2138.44	1425.96	MKMEEKYNLTSVLMAMGITDVFSSSANLSGISSAESLK
285	339	6031.76	3016.38	2011.26	MKMEEKYNLTSVLMAMGITDVFSSSANLSGISSAESLKISQAVHAAHAEINEAGR
287	290	536.62	268.81	179.54	MEEK
287	322	4016.5	2008.76	1339.51	MEEKYNLTSVLMAMGITDVFSSSANLSGISSAESLK
287	339	5772.39	2886.7	1924.8	MEEKYNLTSVLMAMGITDVFSSSANLSGISSAESLKISQAVHAAHAEINEAGR
287	359	7843.44	3922.23	2615.15	MEEKYNLTSVLMAMGITDVFSSSANLSGISSAESLKISQAVHAAHAEINEAGREVVGSAEAGVDAASVSEEFR
291	322	3498.91	1749.96	1166.97	YNLTSVLMAMGITDVFSSSANLSGISSAESLK
291	339	5254.79	2627.9	1752.27	YNLTSVLMAMGITDVFSSSANLSGISSAESLKISQAVHAAHAEINEAGR
291	359	7325.85	3663.43	2442.62	YNLTSVLMAMGITDVFSSSANLSGISSAESLKISQAVHAAHAEINEAGREVVGSAEAGVDAASVSEEFR
291	369	8497.24	4249.12	2833.08	YNLTSVLMAMGITDVFSSSANLSGISSAESLKISQAVHAAHAEINEAGREVVGSAEAGVDAASVSEEFRADHPFLFCIK
323	339	1774.91	887.96	592.31	ISQAVHAAHAEINEAGR
323	359	3845.96	1923.49	1282.66	ISQAVHAAHAEINEAGREVVGSAEAGVDAASVSEEFR
323	369	5017.36	2509.18	1673.12	ISQAVHAAHAEINEAGREVVGSAEAGVDAASVSEEFRADHPFLFCIK
323	381	6344.89	3172.95	2115.63	ISQAVHAAHAEINEAGREVVGSAEAGVDAASVSEEFRADHPFLFCIKHIATNAVLFFGR
340	359	2090.08	1045.54	697.36	EVVGSAEAGVDAASVSEEFR
340	369	3261.47	1631.24	1087.83	EVVGSAEAGVDAASVSEEFRADHPFLFCIK
340	381	4589	2295	1530.34	EVVGSAEAGVDAASVSEEFRADHPFLFCIKHIATNAVLFFGR
340	385	4974.46	2487.73	1658.82	EVVGSAEAGVDAASVSEEFRADHPFLFCIKHIATNAVLFFGRCVSP
360	369	1190.41	595.71	397.48	ADHPFLFCIK
360	381	2517.95	1259.48	839.99	ADHPFLFCIKHIATNAVLFFGR
360	385	2903.41	1452.21	968.47	ADHPFLFCIKHIATNAVLFFGRCVSP
370	381	1346.56	673.78	449.52	HIATNAVLFFGR
370	385	1732.01	866.51	578.01	HIATNAVLFFGRCVSP
382	385	404.48	202.74	135.5	CVSP

Table S 38. Raw protein list obtained from PLGS analysis of Ovalbumin digested solution (Solution 6) Online nanoLC-ESI-MS^E measurement without redundancy

Accession number	Description	Avg. Mass	Matched Products	Matched Peptides	Seq. Cover(%)
A0A411G5W6	Ovalbumin OS=Gallus gallus	43253.5441	225	16	38.08
P01005	Ovomucoid OS=Gallus gallus	23674.9774	112	7	33.81
Q8JIG5	Alpha-1-acid glycoprotein OS=Gallus gallus	22549.5592	46	3	15.76
E1BTF4	SERPIN domain-containing protein OS=Gallus gallus	44098.5052	67	10	22.16
P00761	Trypsin OS=Sus scrofa	25093.8291	18	3	16.45
A0A1Y4NLR6	Uncharacterized protein OS=Lachnoclostridium sp.	96744.451	22	5	1.96
F1N9L7	Uncharacterized protein OS=Gallus gallus	76862.2827	8	3	3.74
A0A1Y4K0L4	Lon protease OS=Bacteroides clarus	92923.1429	11	3	3.52
A0A1Y4HSI8	BppU_N domain-containing protein OS=Collinsella sp.	68082.6952	11	5	1.11
F1NH25	Uncharacterized protein OS=Gallus gallus	93592.0707	13	5	4.86

Table S 39. Final protein list from *Gallus gallus* obtained from PLGS analysis of Ovalbumin digested solution (Solution 6) Online nanoLC-ESI-MS^E measurement

Accession number	Description	Avg. Mass	Matched Products	Matched Peptides	Seq. Cover(%)
A0A411G5W6	Ovalbumin OS=Gallus gallus	43253.5441	225	16	38.08
P01005	Ovomucoid OS=Gallus gallus	23674.9774	112	7	33.81
Q8JIG5	Alpha-1-acid glycoprotein OS=Gallus gallus	22549.5592	46	3	15.76
E1BTF4	SERPIN domain-containing protein OS=Gallus gallus	44098.5052	67	10	22.16

Figure S 12. Ovalbumin sequence coverage from online nanoLC-ESI-MS^E spectrometry of digested Ovalbumin peptides (Solution 6) by BiopharmaLinx.

5.5. Egg white digestion and characterisation (2B)

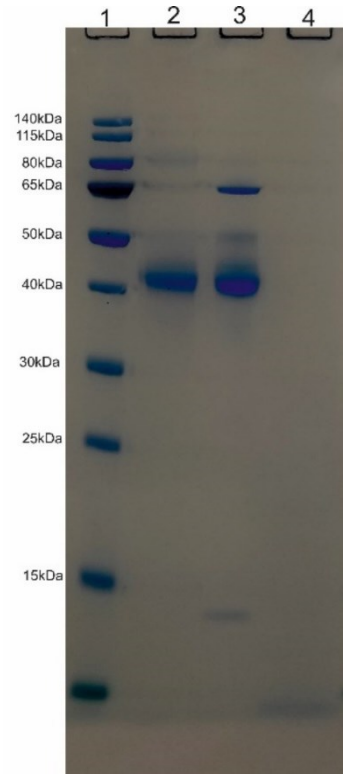

Figure S 13. SDS-PAGE electrophoresis of egg white digested solution (Solution 8)

On the gel were loaded 3 µl of Prestained protein marker in pocket 1, Ovalbumin 9.66 µg/µl (Solution 5) was diluted 1:40 with 50 mM ammonium bicarbonate, pH 8, (0.24 µg/µl) and 3.2 µl of it were mixed with 12.8 µl of deionised water and 4 µl of Non-reducing buffer, than the solution was mixed at vortex and centrifugated for 2 minutes at room temperature 6000 rpm, eventually it was loaded into pocket 2, 1.5 µl of 0.75 µg/µl of egg white solution (Solution 7) was mixed with 14.5 µl of deionised water and 4 µl of Non-reducing buffer, than the sample was mixed at vortex and centrifugated for 2 minutes at room temperature 6000 rpm, eventually it was loaded into pocket 3, 3 µl of egg white digested solution (Solution 8) were mixed with 13 µl of deionised water and 4 µl of Non-reducing buffer, than the sample was mixed at vortex and centrifugated for 2 minutes at room temperature 6000 rpm, eventually it was loaded into pocket 4. In line 1 we can see the bands related to the Prestained protein marker, in line 2 where just Ovalbumin was loaded is possible to observe one band between 40 and 50 kDa of apparent mass, which fit with the 45 kDa mass of Ovalbumin, in line 3 a diluted egg white solution (0.75 µg/µl) was loaded, in line 4 digested egg white solution (So-

lution 8) was loaded, and no bands appear on the gel after electrophoresis, therefore after digestion and OASIS cartridge treatment no proteins still into the solution.

Table S 40. Raw protein list obtained from PLGS analysis of egg white digested solution (Solution 8) Online nanoLC-ESI-MS^E measure without redundancy

Accession number	Description	Avg. Mass	Matched Products	Matched Peptides	Seq. Cover(%)
A0A1Y3VY82	AAA family ATPase OS=Butyricimonas sp. An62	48604.1139	12	4	5.59
A7UEB0	Alpha-1-acid glycoprotein OS=Gallus gallus	22549.5592	47	4	18.23
A0A140T8H8	Folate_rec domain-containing protein OS=Gallus gallus	28309.1312	19	5	15.13
D5GR60	Gallin protein OS=Gallus gallus	7496.852	10	2	33.33
B8YK69	Lysozyme C OS=Bambusicola thoracicus	16802.1128	43	4	21.09
G3XDT7	Lysozyme C OS=Dromaius novaehollandiae	16956.2412	21	2	10.2
B8YK71	Lysozyme C OS=Francolinus pondicerianus interpositus	16756.0003	50	5	25.85
P00698	Lysozyme C OS=Gallus gallus	16751.9202	114	7	44.9
B8YK77	Lysozyme C OS=Gallus lafayettii	16751.9202	93	7	44.9
B8YK75	Lysozyme C OS=Gallus sonneratii	16751.9202	93	7	44.9
B8YK73	Lysozyme C OS=Gallus varius	16765.0614	43	4	21.09
G3XGC2	Lysozyme OS=Struthio camelus	16994.3316	21	2	10.2
P01012	Ovalbumin OS=Gallus gallus	43223.5178	327	21	49.48
R9TNA6	Ovalbumin-related protein X OS=Gallus gallus gallus	45658.723	131	14	34.08
P01014	Ovalbumin-related protein Y OS=Gallus gallus	44057.4526	128	13	29.64
I0J178	Ovalbumin-related Y OS=Gallus gallus	44057.4526	121	13	29.64
P10184	Ovoinhibitor OS=Gallus gallus	59627.9789	79	11	19.34
P01005	Ovomucoid OS=Gallus gallus	23674.9774	88	7	36.67
P02789	Ovotransferrin OS=Gallus gallus	79601.5131	608	41	50.92
P02752	Riboflavin-binding protein OS=Gallus gallus	28295.0609	21	5	15.13
A0A1D5PI58	SERPIN domain-containing protein OS=Gallus gallus	43855.6049	116	13	32.99
P00761	Trypsin OS=Sus scrofa	25093.8291	42	4	29.44
A0A1Y4DPF5	Uncharacterized protein OS=Elusimicrobium sp. An273	18916.4107	6	3	23.95
A0A1Y4WAQ3	Uncharacterized protein OS=Flavonifractor sp. An100	31846.4095	10	3	8.48
R4GI90	Uncharacterized protein OS=Gallus gallus	7563.9051	10	2	33.33
R4GFM6	Uncharacterized protein OS=Gallus gallus	7493.8514	10	2	33.33
A0A1D5P3C4	Uncharacterized protein OS=Gallus gallus	224069.2941	40	19	6.05
A0A486WY81	Uncharacterized protein OS=Salmonella enterica subsp. enterica serovar Stanley	38224.0112	11	5	6.78
A0A1Y4EXL6	V-type ATP synthase subunit I OS=Anaeromassilibacillus sp. An250	75123.4524	12	3	8.51
A0A1Y3TFF0	Zinc ribbon domain-containing protein OS=Lachnoclostridium sp. An76	18223.8816	10	3	5.56

Table S 41. Final protein list of *Gallus gallus* obtained from PLGS analysis of egg white digested solution (Solution 8) Online nanoLC-ESI-MS^E measure

Accession number	Description	Avg. Mass	Matched Products	Matched Peptides	Seq. Cover(%)
A7UEB0	Alpha-1-acid glycoprotein OS=Gallus gallus	22549.5592	47	4	18.23
A0A140T8H8	Folate_rec domain-containing protein OS=Gallus gallus	28309.1312	19	5	15.13
D5GR60	Gallin protein OS=Gallus gallus	7496.852	10	2	33.33
P00698	Lysozyme C OS=Gallus gallus	16751.9202	114	7	44.9
P01012	Ovalbumin OS=Gallus gallus	43223.5178	327	21	49.48
P10184	Ovoinhibitor OS=Gallus gallus	59627.9789	79	11	19.34
P01005	Ovomucoid OS=Gallus gallus	23674.9774	88	7	36.67
P02789	Ovotransferrin OS=Gallus gallus	79601.5131	608	41	50.92
P02752	Riboflavin-binding protein OS=Gallus gallus	28295.0609	21	5	15.13
A0A1D5PI58	SERPIN domain-containing protein OS=Gallus gallus	43855.6049	116	13	32.99

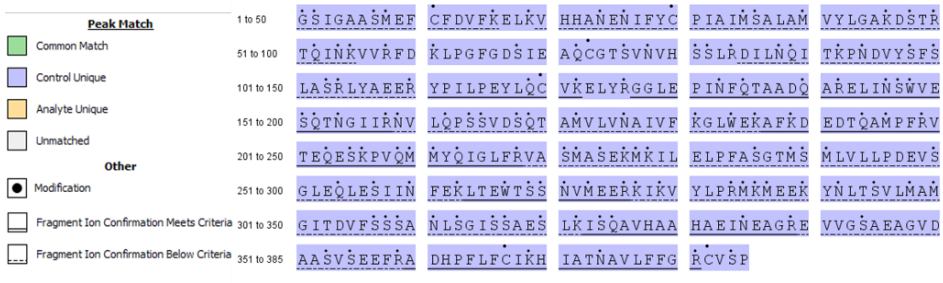

Figure S 14. Ovalbumin sequence coverage from online nanoLC-ESI-MS^E spectrometry of digested egg white peptides (Solution 8) by BiopharmaLinx.

5.6. ITEM Analysis (2B)

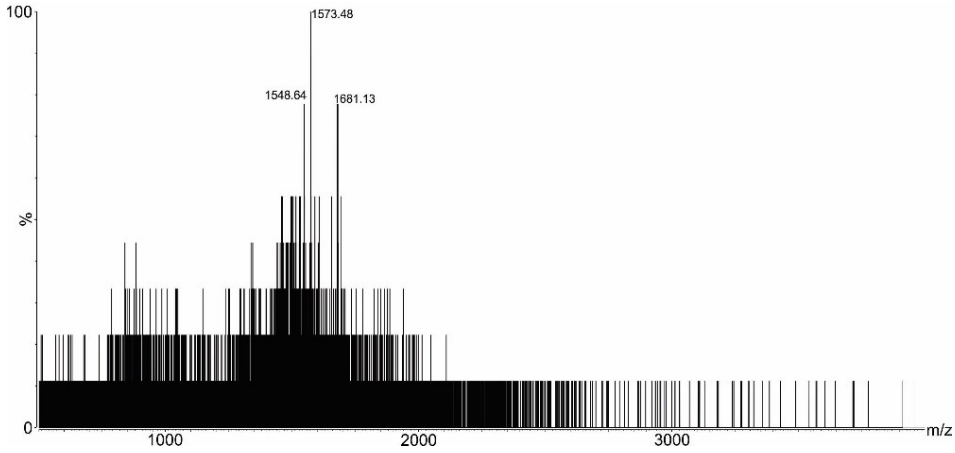

Figure S 15. Offline nanoESI-MS spectrum of Ovalbumin digested solution (Solution 6) in ITEM condition.

Capillary voltage was 1.6 KV; Cone voltage 130 V, Extractor voltage 3 V, RF Lens 1.2 V, Source temperature 80 °C, MCP 1950 V, Pusher 124 µs, Inelet Penning vacuum was 1.55• 10^{-1} mbar, Analyser Penning at 4.5• 10^{-5} mbar, the ToF Penning at 4.5• 10^{-7} mbar, the nitrogen sheath gas flow was at 4 psi, Quadrupole transmission blocked at m/z 2000, collecting from m/z 50 to m/z 8000, for 5.5 minutes, collision gas pressure 4 psi and collision cell voltage difference 3 V. Spectrum unsmoothed. The spectrum was recorded using the MassLinx 4.0 data system from Waters (Manchester, UK) and CDR-files were saved on computer drives. The MassLinx software package was used for data analysis and spectral image preparation in conjunction with the CorelDraw 17.0 software package.

The more intense signal related to peptides that can "survive" the blocked transmission of the quadrupole are at m/z 1548.64, 1573.48 and 1681.13, (Table 11) they can be related to the signal 1555.97, 1582.02 and 1687.12 (Figure 40).

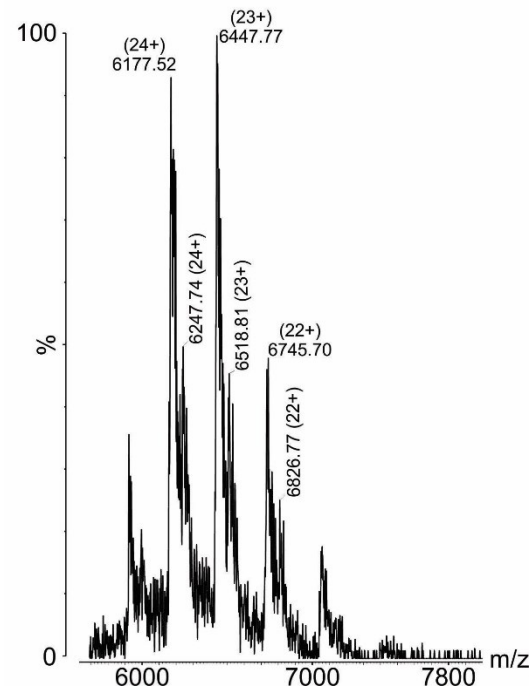

Figure S 16. Satellite signals of antibody in Positive Control 1 ITEM experiment of anti-Ovalbumin antibody + Ovalbumin digested solution (Solution 1 and 6)

To calculate the average mass added to the antibody the average difference between each pair of peaks multiplicated by the charge and subtracted by the proton number was done (Table S 42). The estimation of additional mass in the immune complex is 1677.91, close to the value of released peptide 1688.04

Table S 42. Epitope mass estimation from satellite signals in Positive Control 1 ITEM experiment

m	m'	Charge	((m-m')*Charge)-Charge
6247.74	6177.52	24	1661.28
6518.81	6447.77	23	1610.92
6826.77	6745.7	22	1761.54
Average			1677.91

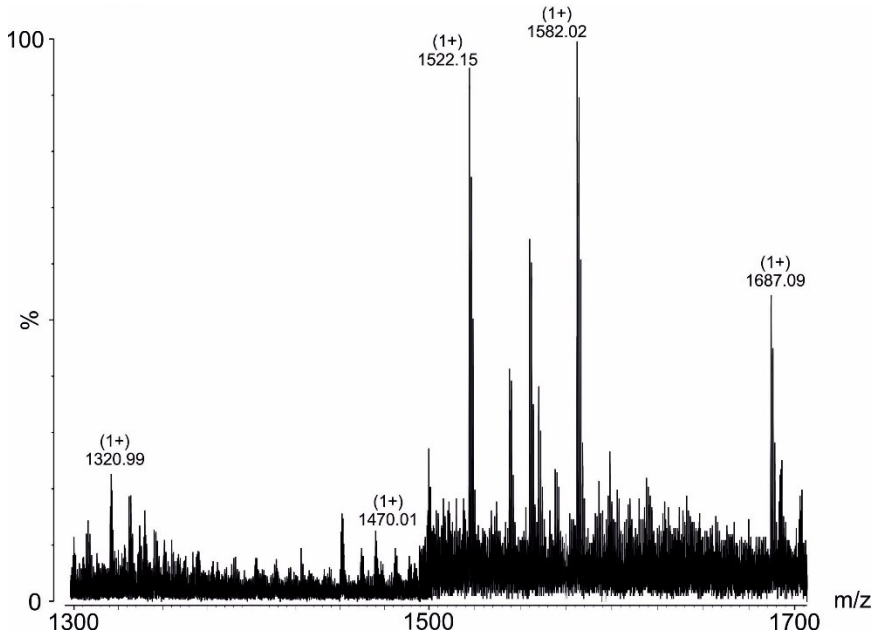

Figure S 17. Zoomed offline nanoESI-MS spectrum (set-up chapter 3.6.6) of Egg White digested solution (Solution 6). Ion signals are labelled with m/z values and charge states are given in parentheses. Protein concentration is 0.28 µg/µl. Solvent: 200 mM ammonium acetate, pH 6.7.

6. List of Figures

7. List of Tables

8. Bibliography

1. Tiffany, J. The normal tear film. *Dev. Ophthalmol.* (2008) doi:10.1159/000131066.

2. D. W. Lamberts. Punctal occlusion. *Int Ophthalmol Clin* **34**, 145–150 (1994).

3. Coffey, M. J., Decory, H. H. & Lane, S. S. Development of a non-settling gel formulation of 0.5% loteprednol etabonate for anti-inflammatory use as an ophthalmic drop. *Clinical Ophthalmology* (2013) doi:10.2147/OPTH.S40588.

4. Mishima, S., Gasset, A., Klyce, S. D. & Baum, J. L. Determination of tear volume and tear flow. *Invest. Ophthalmol.* (1966).

5. Sack, R. A., Kah Ooi Tan & Tan, A. Diurnal tear cycle: Evidence for a nocturnal inflammatory constitutive tear fluid. in *Investigative Ophthalmology and Visual Science* (1992).

6. de Souza, G. A., Godoy, L. M. F. & Mann, M. Identification of 491 proteins in the tear fluid proteome reveals a large number of proteases and protease inhibitors. *Genome Biol.* (2006) doi:10.1186/gb-2006-7-8-r72.

7. Rantamäki, A. H., Seppänen-Laakso, T., Oresic, M., Jauhiainen, M. & Holopainen, J. M. Human tear fluid lipidome: From composition to function. *PLoS One* (2011) doi:10.1371/journal.pone.0019553.

8. Li, K., Chen, Z., Duan, F., Liang, J. & Wu, K. Quantification of tear proteins by SDS-PAGE with an internal standard protein: A new method with special reference to small volume tears. *Graefe's Arch. Clin. Exp. Ophthalmol.* (2010) doi:10.1007/s00417-009-1275-3.

9. Small, D., Hevy, J. & Tang-Liu, D. Comparison of tear sampling techniques for pharmacokinetic analysis: Ofloxacin concentrations in rabbit tears after sampling with schirmer tear strips, capillary tubes, or surgical sponges. *J. Ocul. Pharmacol. Ther.* (2000) doi:10.1089/jop.2000.16.439.

10. Kalsow, C. M., Reindel, W. T., Merchea, M. M., Bateman, K. M. & Barr, J. T. Tear cytokine response to multipurpose solutions for contact lenses. *Clin. Ophthalmol.* (2013) doi:10.2147/OPTH.S44642.

11. Fullard, R. J. & Snyder, C. Protein levels in nonstimulated and stimulated tears of normal human subjects. *Investig. Ophthalmol. Vis. Sci.* (1990).

12. Markoulli, M., Papas, E., Petznick, A. & Holden, B. Validation of the flush method as an alternative to basal or reflex tear collection. *Curr. Eye Res.* (2011) doi:10.3109/02713683.2010.542867.

13. Balafas, E. *et al.* A noninvasive ocular (Tear) sampling method for genetic

ascertainment of transgenic mice and research ethics innovation. *Omi. A J. Integr. Biol.* (2019) doi:10.1089/omi.2019.0057.

14. van Der Meid, K. R., Su, S. P., Krenzer, K. L., Ward, K. W. & Zhang, J. Z. A method to extract cytokines and matrix metalloproteinases from Schirmer strips and analyze using Luminex. *Mol. Vis.* (2011).

15. Green-Church, K. B., Nichols, K. K., Kleinholz, N. M., Zhang, L. & Nichols, J. J. Investigation of the human tear film proteome using multiple proteomic approaches. *Mol. Vis.* (2008).

16. M.A., L. *et al.* The definition and classification of dry eye disease: Report of the definition and classification subcommittee of the international Dry Eye WorkShop (2007). *Ocul. Surf.* (2007).

17. Stern, M. E., Schaumburg, C. S. & Pflugfelder, S. C. Dry eye as a mucosal autoimmune disease. *International Reviews of Immunology* (2013) doi:10.3109/08830185.2012.748052.

18. Stevenson, W., Chauhan, S. K. & Dana, R. Dry eye disease: An immune-mediated ocular surface disorder. *Archives of Ophthalmology* (2012) doi:10.1001/archophthalmol.2011.364.

19. Lemp, M. A., Crews, L. A., Bron, A. J., Foulks, G. N. & Sullivan, B. D. Distribution of aqueous-deficient and evaporative dry eye in a clinic-based patient cohort: A retrospective study. *Cornea* (2012) doi:10.1097/ICO.0b013e318225415a.

20. Chia, E. M. *et al.* Prevalence and associations of dry eye syndrome in an older population: The Blue Mountains Eye Study. *Clin. Exp. Ophthalmol.* (2003) doi:10.1046/j.1442-9071.2003.00634.x.

21. Ridder, W. H., Zhang, Y. & Huang, J. F. Evaluation of reading speed and contrast sensitivity in dry eye disease. *Optom. Vis. Sci.* (2013) doi:10.1097/OPX.0b013e3182780dbb.

22. Deschamps, N. *et al.* The impact of dry eye disease on visual performance while driving. *Am. J. Ophthalmol.* (2013) doi:10.1016/j.ajo.2013.02.019.

23. Labbé, A. *et al.* Dry eye disease, dry eye symptoms and depression: The Beijing eye study. *Br. J. Ophthalmol.* (2013) doi:10.1136/bjophthalmol-2013-303838.

24. Yu, J., Asche, C. V. & Fairchild, C. J. The economic burden of dry eye disease in the United States: A decision tree analysis. *Cornea* (2011) doi:10.1097/ICO.0b013e3181f7f363.

25. Messmer, E. M. Pathophysiology, diagnosis and treatment of dry eye. *Dtsch. Arztebl. Int.* **112**, 71–82 (2015).

26. Foulks, G. N. & Bron, A. J. Meibomian gland dysfunction: A clinical scheme for description, diagnosis, classification, and grading. *Ocul. Surf.* (2003) doi:10.1016/S1542-0124(12)70139-8.

27. Turgut, B. *et al.* Spontaneous corneal perforation in a patient with lamellar ichthyosis and dry eye. *Clin. Ophthalmol.* (2009) doi:10.2147/opth.s8407.

28. Pflugfelder, S. C. *et al.* Management and therapy of dry eye disease: Report of the management and therapy subcommittee of the international Dry Eye WorkShop (2007). in *Ocular Surface* (2007). doi:10.1016/s1542-0124(12)70085-x.

29. S., B. *et al.* The effect of an artificial tear combining hyaluronic acid and tamarind seeds polysaccharide in patients with moderate dry eye syndrome: A new treatment for dry eye. *Eur. J. Ophthalmol.* (2014).

30. Lee, S. Y. & Tong, L. Lipid-containing lubricants for dry eye: A systematic review. *Optometry and Vision Science* (2012) doi:10.1097/OPX.0b013e31826f32e0.

31. Geerling, G. *et al.* Autologous serum and alternative blood products for the treatment of ocular surface disorders. *Ophthalmologe* (2008) doi:10.1007/s00347-008-1750-y.

32. Pflugfelder, S. C. *et al.* A randomized, double-masked, placebo-controlled, multicenter comparison of loteprednol etabonate ophthalmic suspension, 0.5%, and placebo for treatment of keratoconjunctivitis sicca in patients with delayed tear clearance. *Am. J. Ophthalmol.* (2004) doi:10.1016/j.ajo.2004.04.052.

33. Sall, K., Stevenson, O. D., Mundorf, T. K. & Reis, B. L. Two multicenter randomized studies of the efficacy and safety of cyclosporine ophthalmic emulsion in moderate to severe dry eye disease. *Ophthalmology* (2000) doi:10.1016/S0161-6420(99)00176-1.

34. Moscovici, B. K. *et al.* Clinical treatment of dry eye using 0.03% tacrolimus eye drops. *Cornea* (2012) doi:10.1097/ICO.0b013e31823f8c9b.

35. Yoo, S. E., Lee, D. C. & Chang, M. H. The effect of low-dose doxycycline therapy in chronic meibomian gland dysfunction. *Korean J. Ophthalmol.* (2005) doi:10.3341/kjo.2005.19.4.258.

36. Foulks, G. N., Borchman, D., Yappert, M., Kim, S. H. & McKay, J. W. Topical azithromycin therapy for meibomian gland dysfunction: Clinical response and lipid alterations. *Cornea* (2010) doi:10.1097/ICO.0b013e3181cda38f.

37. Barabino, S. *et al.* Systemic linoleic and γ-linolenic acid therapy in dry eye syndrome with an inflammatory component. *Cornea* (2003) doi:10.1097/00003226-200303000-00002.

38. Bielory, L. & Schoenberg, D. Ocular allergy. *Curr. Opin. Allergy Clin. Immunol.* **19**, 495–502 (2019).

39. Nye, M., Rudner, S. & Bielory, L. Emerging therapies in allergic conjunctivitis and dry eye syndrome. *Expert Opinion on Pharmacotherapy* (2013) doi:10.1517/14656566.2013.802773.

40. Bilkhu, P. S., Wolffsohn, J. S., Naroo, S. A., Robertson, L. & Kennedy, R. Effectiveness of nonpharmacologic treatments for acute seasonal allergic conjunctivitis. *Ophthalmology* (2014) doi:10.1016/j.ophtha.2013.08.007.

41. Meier, E. J., Torkildsen, G. L., Gomes, P. J. & Jasek, M. C. Phase iii trials examining the efficacy of cetirizine ophthalmic solution 0.24% compared to vehicle for the treatment of allergic conjunctivitis in the conjunctival allergen challenge model. *Clin. Ophthalmol.* (2018) doi:10.2147/OPTH.S185835.

42. Bakrania, A. K. & Patel, S. S. Combination treatment for allergic conjunctivitis - Plant derived histidine decarboxylase inhibitor and H1 antihistaminic drug. *Exp. Eye Res.* (2015) doi:10.1016/j.exer.2015.05.020.

43. Carr, W., Schaeffer, J. & Donnenfeld, E. Treating allergic conjunctivitis: A once-daily medication that provides 24-hour symptom relief. *Allergy Rhinol.* (2016) doi:10.2500/ar.2016.7.0158.

44. Minami, T. *et al.* In vitro and in vivo performance of epinastine hydrochloride-releasing contact lenses. *PLoS One* (2019) doi:10.1371/journal.pone.0210362.

45. Nolte, H. & Maloney, J. The global development and clinical efficacy of sublingual tablet immunotherapy for allergic diseases. *Allergology International* (2018) doi:10.1016/j.alit.2018.03.008.

46. Blin, P. *et al.* An observational cohort study of the use of five-grass-pollen extract sublingual immunotherapy during the 2015 pollen season in France. *Allergy, Asthma and Clinical Immunology* (2018) doi:10.1186/s13223-018-0262-9.

47. Mösges, R. *et al.* A randomized, double-blind, placebo-controlled, dose-finding trial with Lolium perenne peptide immunotherapy. *Allergy Eur. J. Allergy Clin. Immunol.* (2018) doi:10.1111/all.13358.

48. Senti, G. *et al.* Determinants of efficacy and safety in epicutaneous allergen immunotherapy: Summary of three clinical trials. *Allergy Eur. J. Allergy Clin. Immunol.* (2015) doi:10.1111/all.12600.

49. Dennis-Wall, J. C. *et al.* Probiotics (Lactobacillus gasseri KS-13, Bifidobacterium bifidum G9-1, and Bifidobacterium longum MM-2) improve rhinoconjunctivitis-specific quality of life in individuals with seasonal allergies: A double-blind, placebo-controlled, randomized trial. *Am. J. Clin. Nutr.* (2017) doi:10.3945/ajcn.116.140012.

50. Hirakata, T. *et al.* Dietary ω-3 fatty acids alter the lipid mediator profile and alleviate allergic conjunctivitis without modulating Th2 immune responses. *FASEB J.* (2019) doi:10.1096/fj.201801805R.

51. Horak, F. *et al.* The CRTH2 antagonist OC000459 reduces nasal and ocular symptoms in allergic subjects exposed to grass pollen, a randomised, placebo-controlled, double-blind trial. *Allergy Eur. J. Allergy Clin. Immunol.* (2012) doi:10.1111/all.12042.

52. Wegh, C. A. M., Geerlings, S. Y., Knol, J., Roeselers, G. & Belzer, C. Postbiotics and Their Potential Applications in Early Life Nutrition and Beyond. *Int. J. Mol. Sci. 2019, Vol. 20, Page 4673* **20**, 4673 (2019).

53. Oak, S. J. & Jha, R. The effects of probiotics in lactose intolerance: A systematic review. *https://doi.org/10.1080/10408398.2018.1425977* **59**, 1675–1683 (2018).

54. Kijmanawat, A., Panburana, P., Reutrakul, S. & Tangshewinsirikul, C. Effects of probiotic supplements on insulin resistance in gestational diabetes mellitus: A double-blind randomized controlled trial. *J. Diabetes Investig.* **10**, 163–170 (2019).

55. Ratna, A. U. & Madempudi, S. Probiotics and blood pressure: current insights. (2016) doi:10.2147/IBPC.S73246.

56. Sivamaruthi, B. S., Kesika, P. & Chaiyasut, C. A Mini-Review of Human Studies on Cholesterol-Lowering Properties of Probiotics. *Sci. Pharm. 2019, Vol. 87, Page 26* **87**, 26 (2019).

57. Martín, R. & Langella, P. Emerging health concepts in the probiotics field: Streamlining the definitions. *Front. Microbiol.* **10**, 1047 (2019).

58. O'Toole, P. W., Marchesi, J. R. & Hill, C. Next-generation probiotics: The spectrum from probiotics to live biotherapeutics. *Nat. Microbiol.* **2**, (2017).

59. Collado, M., Isolauri, E., Salminen, S. & Sanz, Y. The Impact of Probiotic on Gut Health. *Curr. Drug Metab.* **10**, 68–78 (2009).

60. Hemarajata, P. & Versalovic, J. Effects of probiotics on gut microbiota: mechanisms of intestinal immunomodulation and neuromodulation. *Therap. Adv. Gastroenterol.* **6**, 39–51 (2013).

61. Bermudez-Brito, M., Plaza-Díaz, J., Muñoz-Quezada, S., Gómez-Llorente, C. & Gil, A. Probiotic Mechanisms of Action. *Ann. Nutr. Metab.* **61**, 160–174 (2012).

62. Sanders, M. E., Merenstein, D. J., Reid, G., Gibson, G. R. & Rastall, R. A. Probiotics and prebiotics in intestinal health and disease: from biology to the clinic. *Nat. Rev. Gastroenterol. Hepatol.* **16**, 605–616 (2019).

63. Gibson, G. R. *et al.* Expert consensus document: The International Scientific

Association for Probiotics and Prebiotics (ISAPP) consensus statement on the definition and scope of prebiotics. *Nat. Rev. Gastroenterol. Hepatol. 2017 148* **14**, 491–502 (2017).

64. Vyas, U. & Ranganathan, N. Probiotics, prebiotics, and synbiotics: Gut and beyond. *Gastroenterol. Res. Pract.* (2012) doi:10.1155/2012/872716.

65. Bertelsen, R. J., Jensen, E. T. & Ringel-Kulka, T. Use of probiotics and prebiotics in infant feeding. *Best Pract. Res. Clin. Gastroenterol.* **30**, 39–48 (2016).

66. Aguilar-Toalá, J. E. *et al.* Postbiotics: An evolving term within the functional foods field. *Trends Food Sci. Technol.* **75**, 105–114 (2018).

67. Vallejo-Cordoba, B., Castro-López, C., García, H. S., González-Córdova, A. F. & Hernández-Mendoza, A. Postbiotics and paraprobiotics: A review of current evidence and emerging trends. *Adv. Food Nutr. Res.* **94**, 1–34 (2020).

68. de Almada, C. N., Almada, C. N., Martinez, R. C. R. & Sant'Ana, A. S. Paraprobiotics: Evidences on their ability to modify biological responses, inactivation methods and perspectives on their application in foods. *Trends Food Sci. Technol.* **58**, 96–114 (2016).

69. Taverniti, V. & Guglielmetti, S. The immunomodulatory properties of probiotic microorganisms beyond their viability (ghost probiotics: proposal of paraprobiotic concept). *Genes Nutr.* **6**, 261–274 (2011).

70. Konstantinov, S. R., Kuipers, E. J. & Peppelenbosch, M. P. Functional genomic analyses of the gut microbiota for CRC screening. *Nat. Rev. Gastroenterol. Hepatol. 2013 1012* **10**, 741–745 (2013).

71. Tsilingiri, K. *et al.* Probiotic and postbiotic activity in health and disease: comparison on a novel polarised ex-vivo organ culture model. doi:10.1136/gutjnl-2011-300971.

72. Adams, C. A. The probiotic paradox: live and dead cells are biological response modifiers. *Nutr. Res. Rev.* **23**, 37–46 (2010).

73. Cuevas-González, P. F., Liceaga, A. M. & Aguilar-Toalá, J. E. Postbiotics and paraprobiotics: From concepts to applications. *Food Res. Int.* **136**, 109502 (2020).

74. De Oliveira Coelho, B. *et al.* In Vitro Probiotic Properties and DNA Protection Activity of Yeast and Lactic Acid Bacteria Isolated from A Honey-Based Kefir Beverage. doi:10.3390/foods8100485.

75. Amaretti, A. *et al.* Antioxidant properties of potentially probiotic bacteria: In vitro and in vivo activities. *Appl. Microbiol. Biotechnol.* **97**, 809–817 (2013).

76. Aguilar-Toalá, J. E. *et al.* Modulatory Effect of the Intracellular Content of Lactobacillus casei CRL 431 Against the Aflatoxin B1-Induced Oxidative Stress in Rats. *Probiotics Antimicrob. Proteins* **11**, 470–477 (2019).

77. Maghsood, F. *et al.* Anti-proliferative and Anti-metastatic Potential of High Molecular Weight Secretory Molecules from Probiotic Lactobacillus Reuteri Cell-Free Supernatant Against Human Colon Cancer Stem-Like Cells (HT29-ShE). *Int. J. Pept. Res. Ther.* **26**, 2619–2631 (2020).

78. Nozari, S. *et al.* Potential anticancer effects of cell wall protein fractions from Lactobacillus paracasei on human intestinal Caco-2 cell line. (2019) doi:10.1111/lam.13198.

79. Chuah, L.-O. *et al.* Postbiotic metabolites produced by Lactobacillus plantarum strains exert selective cytotoxicity effects on cancer cells. doi:10.1186/s12906-019-2528-2.

80. Ardestani, S. K., Tafvizi, F. & Ebrahimi, M. T. Heat-killed probiotic bacteria induce apoptosis of HT-29 human colon adenocarcinoma cell line via the regulation of Bax/Bcl2 and caspases pathway. doi:10.1177/0960327119851255.

81. Kareem, K. Y., Ling, F. H., Chwen, L. T., Foong, O. M. & Anjas Asmara, S. Inhibitory activity of postbiotic produced by strains of Lactobacillus plantarum using reconstituted media supplemented with inulin. *Gut Pathog.* **6**, 1–7 (2014).

82. Moradi, M., Mardani, K. & Tajik, H. Characterization and application of postbiotics of Lactobacillus spp. on Listeria monocytogenes in vitro and in food models. *LWT* **111**, 457–464 (2019).

83. Posadas, G. A. *et al.* Yeast Pro- and Paraprobiotics Have the Capability to Bind Pathogenic Bacteria Associated with Animal Disease. *Transl. Anim. Sci.* **1**, 60–68 (2017).

84. Balzaretti, S. *et al.* A novel rhamnose-rich hetero-exopolysaccharide isolated from Lactobacillus paracasei DG activates THP-1 human monocytic cells. *Appl. Environ. Microbiol.* **83**, (2017).

85. Qi, S. R., Cui, Y. J., Liu, J. X., Luo, X. & Wang, H. F. Lactobacillus rhamnosus GG components, SLP, gDNA and CpG, exert protective effects on mouse macrophages upon lipopolysaccharide challenge. *Lett. Appl. Microbiol.* **70**, 118–127 (2020).

86. Jensen, G. S., Benson, K. F., Carter, S. G. & Endres, J. R. *GanedenBC 30™ cell wall and metabolites: anti-inflammatory and immune modulating effects in vitro*. http://www.biomedcentral.com/1471-2172/11/15 (2010).

87. Rufino, R. D., de Luna, J. M., de Campos Takaki, G. M. & Sarubbo, L. A. Characterization and properties of the biosurfactant produced by Candida lipolytica UCP 0988. *Electron. J. Biotechnol.* **17**, 34–38 (2014).

88. Rodrigues, L. R., Teixeira, J. A., van der Mei, H. C. & Oliveira, R. Isolation and partial characterization of a biosurfactant produced by Streptococcus thermophilus A. *Colloids Surfaces B Biointerfaces* **53**, 105–112 (2006).

89. Varjani, S. J. & Upasani, V. N. Critical review on biosurfactant analysis, purification and characterization using rhamnolipid as a model biosurfactant. *Bioresource Technology* vol. 232 389–397 (2017).

90. Ghasemi, A., Moosavi-Nasab, M., Setoodeh, P., Mesbahi, G. & Yousefi, G. Biosurfactant Production by Lactic Acid Bacterium Pediococcus dextrinicus SHU1593 Grown on Different Carbon Sources: Strain Screening Followed by Product Characterization. *Sci. Rep.* **9**, 1–12 (2019).

91. Patil, S., Sawant, S., Hauff, K. & Hampp, G. Validated Postbiotic Screening Confirms Presence of Physiologically-Active Metabolites, Such as Short-Chain Fatty Acids, Amino Acids and Vitamins in Hylak® Forte. *Probiotics Antimicrob. Proteins* **11**, 1124–1131 (2019).

92. Morelli, L. *et al.* A Novel Postbiotic From Lactobacillus rhamnosus GG With a Beneficial Effect on Intestinal Barrier Function. (2019) doi:10.3389/fmicb.2019.00477.

93. Kim, H. G. *et al.* Lactobacillus plantarum lipoteichoic acid down-regulated Shigella flexneri peptidoglycan-induced inflammation. *Mol. Immunol.* **48**, 382–391 (2011).

94. Timmer, M. S. M. *et al.* Discovery of lipids from B. longum subsp. infantis using whole cell MALDI analysis. *J. Org. Chem.* **79**, 7332–7341 (2014).

95. Bonaventura, G. Di *et al.* Metabolic Characterization of Supernatants Produced by Lactobacillus spp. With in vitro Anti-Legionella Activity. (2019) doi:10.3389/fmicb.2019.01403.

96. Arasu, M. V. *et al.* Identification and Characterization of Lactobacillus brevis P68 with Antifungal, Antioxidant and Probiotic Functional Properties. *Indian J. Microbiol.* **55**, 19–28 (2015).

97. Liu, Z. *et al.* Characterization and bioactivities of the exopolysaccharide from a probiotic strain of Lactobacillus plantarum WLPL04. (2017) doi:10.3168/jds.2016-11944.

98. Aguilar-Toalá, J. E. *et al.* In Silico Prediction and In Vitro Assessment of Multifunctional Properties of Postbiotics Obtained From Two Probiotic Bacteria. doi:10.1007/s12602-019-09568-z.

99. Dean, S. N., Leary, D. H., Sullivan, C. J., Oh, E. & Walper, S. A. Isolation and characterization of Lactobacillus-derived membrane vesicles OPEN. doi:10.1038/s41598-018-37120-6.

100. McLafferty, F. W. *et al.* Top-down MS, a powerful complement to the high capabilities of proteolysis proteomics. *FEBS Journal* vol. 274 6256–6268 (2007).

101. Fournier, M. L., Gilmore, J. M., Martin-Brown, S. A. & Washburn, M. P. Multidimensional separations-based shotgun proteomics. *Chemical Reviews* vol. 107 3654–3686 (2007).

102. Smith, R. D. & Light-Wahl, K. J. The observation of non-covalent interactions in solution by electrospray ionization mass spectrometry: Promise, pitfalls and prognosis. *Biol. Mass Spectrom.* **22**, 493–501 (1993).

103. Rollgen, F. W., Luttgens, U., Dulcks, T. & U, G. Electrospray mass spectrometry of biomacromolecular complexes with non covalent interactions: new analytical perspectives for supramolecular chemistry and molecular recognition processes. *Conf. Am. Soc. Mass Spectrom* **35**, 806–826 (1993).

104. Fenn, J. B. Ion formation from charged droplets: Roles of geometry, energy, and time. *J. Am. Soc. Mass Spectrom.* **4**, 524–535 (1993).

105. Dongré, A. R., Eng, J. K. & Yates, J. R. Emerging tandem-mass-spectrometry techniques for the rapid identification of proteins. *Trends in Biotechnology* vol. 15 418–425 (1997).

106. Sleno, L. & Volmer, D. A. Ion activation methods for tandem mass spectrometry. *J. Mass Spectrom.* **39**, 1091–1112 (2004).

107. Sundqvist, B. *et al.* Californium-252 plasma desorption time of flight mass spectroscopy of proteins. *Biol. Mass Spectrom.* **11**, 242–257 (1984).

108. Zhang, J. *et al.* PEAKS DB: De novo sequencing assisted database search for sensitive and accurate peptide identification. *Mol. Cell. Proteomics* **11**, (2012).

109. Lin, H., He, L., Ma, B. & Cheriton, D. R. Systems biology A combinatorial approach to the peptide feature matching problem for label-free quantification. **29**, 1768–1775 (2013).

110. Motoyama, A. & Yates, J. R. Multidimensional LC separations in shotgun proteomics. *Analytical Chemistry* vol. 80 7187–7193 (2008).

111. Cunsolo, V., Muccilli, V., Saletti, R. & Foti, S. Mass spectrometry in food proteomics: a tutorial. *J. Mass Spectrom.* **49**, 768–784 (2014).

112. Neilson, K. A. *et al.* Less label, more free: Approaches in label-free quantitative mass spectrometry. *Proteomics* **11**, 535–553 (2011).

113. Cox, J. *et al.* Accurate proteome-wide label-free quantification by delayed normalization and maximal peptide ratio extraction, termed MaxLFQ. *Mol. Cell. Proteomics* **13**, 2513–2526 (2014).

114. Domon, B. & Aebersold, R. Options and considerations when selecting a quantitative proteomics strategy. *Nature Biotechnology* vol. 28 710–721 (2010).

115. Chelius, D. & Bondarenko, P. V. Quantitative profiling of proteins in complex mixtures using liquid chromatography and mass spectrometry. *J. Proteome Res.* **1**, 317–323 (2002).

116. H, L. No Title. *Anal. Chem.* **76**, 4193–4201 (2004).

117. T, V. No Title. *Brief. Bioinform.* 1–12 (2017).

118. Liu, Y., Yu, H., Deaton, S. K. & Szaro, B. G. Cellular/Molecular Heterogeneous Nuclear Ribonucleoprotein K, an RNA-Binding Protein, Is Required for Optic Axon Regeneration in Xenopus laevis. (2012) doi:10.1523/JNEUROSCI.5197-11.2012.

119. Moumen, A., Masterson, P., O'Connor, M. J. & Jackson, S. P. hnRNP K: An HDM2 Target and Transcriptional Coactivator of p53 in Response to DNA Damage. *Cell* **123**, 1065–1078 (2005).

120. Eder, S., Lamkowski, A., Priller, M., Port, M. & Steinestel, K. *Radiosensitization and downregulation of heterogeneous nuclear ribonucleoprotein K (hnRNP K) upon inhibition of mitogen/extracellular signal-regulated kinase (MEK) in malignant melanoma cells*. www.impactjournals.com/oncotarget/.

121. Gao, R. *et al.* Heterogeneous Nuclear Ribonucleoprotein K (hnRNP-K) Promotes Tumor Metastasis by Induction of Genes Involved in Extracellular Matrix, Cell Movement, and Angiogenesis. *J. Biol. Chem.* **288**, 15046–15056 (2013).

122. Lynch, M. *et al.* hnRNP K Binds a Core Polypyrimidine Element in the Eukaryotic Translation Initiation Factor 4E (eIF4E) Promoter, and Its Regulation of eIF4E Contributes to Neoplastic Transformation. *Mol. Cell. Biol.* **25**, 6436–6453 (2005).

123. Tharin, S., Dziak, E., Michalak, M. & Opas, M. Widespread tissue distribution of rabbit calreticulin, a non-muscle functional analogue of calsequestrin. *Cell Tissue Res. 1992 2691* **269**, 29–37 (1992).

124. Calreticulin signaling in health and disease | Elsevier Enhanced Reader. https://reader.elsevier.com/reader/sd/pii/S1357272512000659?token=93117463D58166DB18E8785F188222FE5AFB97706219E2D104DB0CED6EFB6ECBD450A5C9AE3290F2F2CB86EA606BCDE7&originRegion=eu-west-1&originCreation=20220604161813.

125. Nanney, L. B. *et al.* Calreticulin Enhances Porcine Wound Repair by Diverse Biological Effects. *Am. J. Pathol.* **173**, 610–630 (2008).

126. Gold, L. I. *et al.* Calreticulin: non-endoplasmic reticulum functions in physiology and disease. *FASEB J.* **24**, 665–683 (2010).

127. Gunning, P., O'Neill, G. & Hardeman, E. Tropomyosin-based regulation of the actin cytoskeleton in time and space. *Physiol. Rev.* **88**, 1–35 (2008).

128. Schevzov, G., Whittaker, S. P., Fath, T., Lin, J. J. C. & Gunning, P. W. Tropomyosin isoforms and reagents. *Ceased* **1**, 135–164 (2011).

129. Shibata, T. *et al.* Tropomyosin 2 heterozygous knockout in mice using CRISPR-Cas9 system displays the inhibition of injury-induced epithelial-mesenchymal transition, and lens opacity. (2018) doi:10.1016/j.mad.2018.03.001.

130. Kubo, E., Hasanova, N., Fatma, N., Sasaki, H. & Singh, D. P. Elevated tropomyosin expression is associated with epithelial–mesenchymal transition of lens epithelial cells. *J. Cell. Mol. Med.* **17**, 212–221 (2013).

131. Kubo, E., Shibata, T., Singh, D. P. & Sasaki, H. Molecular Sciences Roles of TGF β and FGF Signals in the Lens: Tropomyosin Regulation for Posterior Capsule Opacity. doi:10.3390/ijms19103093.

132. Kubo, E. *et al.* FGF2 antagonizes aberrant TGFβ regulation of tropomyosin: role for posterior capsule opacity. *J. Cell. Mol. Med.* **21**, 916–928 (2017).

133. Phospholipase A2 in Rabbit Tears: A Host Defense against Staphylococcus aureus | IOVS | ARVO Journals. https://iovs.arvojournals.org/article.aspx?articleid=2200058.

134. Delalle, I., Pfleger, C. M., Buff, E., Lueras, P. & Hariharan, I. K. Mutations in the Drosophila Orthologs of the F-Actin Capping Protein a-and b-Subunits Cause Actin Accumulation and Subsequent Retinal Degeneration. doi:10.1534/genetics.105.049213.

135. Hopmann, R., Cooper, J. A. & Miller, K. G. Actin Organization, Bristle Morphology, and Viability Are Affected by Actin Capping Protein Mutations in Drosophila.

136. Georgescu, M.-M., Morales, F. C., Molina, J. R. & Hayashi, Y. Roles of NHERF1/EBP50 in Cancer.

137. Vaquero, J., Nguyen Ho-Bouldoires, T. H., Clapéron, A. & Fouassier, L. Role of the PDZ-scaffold protein NHERF1/EBP50 in cancer biology: from signaling regulation to clinical relevance. *Oncogene 2017 3622* **36**, 3067–3079 (2017).

138. Wang, Q. *et al.* NHERF1 inhibits beta-catenin-mediated proliferation of cervical cancer cells through suppression of alpha-actinin-4 expression. doi:10.1038/s41419-018-0711-x.

139. Nielsen, S. S. Phenol-Sulfuric Acid Method for Total Carbohydrates. in 47–53

(Springer, Boston, MA, 2010). doi:10.1007/978-1-4419-1463-7_6.

140. Mishra, S. K. *et al.* Rapid quantification of microalgal lipids in aqueous medium by a simple colorimetric method. *Bioresour. Technol.* **155**, 330–333 (2014).

141. Matyash, V., Liebisch, G., Kurzchalia, T. V., Shevchenko, A. & Schwudke, D. Lipid extraction by methyl-terf-butyl ether for high-throughput lipidomics. in *Journal of Lipid Research* vol. 49 1137–1146 (American Society for Biochemistry and Molecular Biology, 2008).

142. Brekke, O. New technologies in therapeutic antibody development. *Curr. Opin. Pharmacol.* **3**, 544–550 (2003).

143. Gerba, C. P. *Indicator Microorganisms*. *Environmental Microbiology: Third Edition* (Elsevier Inc., 2015). doi:10.1016/B978-0-12-394626-3.00023-5.

144. Townsend, C. L. *et al.* Significant differences in physicochemical properties of human immunoglobulin kappa and lambda CDR3 regions. *Front. Immunol.* **7**, (2016).

145. Kapingidza, A. B., Kowal, K. & Chruszcz, M. Antigen–Antibody Complexes. *Subcell. Biochem.* **94**, 465–497 (2020).

146. Tian, X. *et al.* In-depth analysis of subclass-specific conformational preferences of IgG antibodies. *IUCrJ* **2**, 9–18 (2015).

147. immunology, M. B.-M. & 2000, undefined. Role of natural and immune IgM antibodies in immune responses. *Elsevier*.

148. Grönwall, C., Vas, J. & Silverman, G. J. Protective roles of natural IgM antibodies. *Front. Immunol.* **3**, (2012).

149. Immunology, C. K.-J. of A. and C. & 2010, undefined. Guilt by intimate association: what makes an allergen an allergen? *Elsevier*.

150. Schroeder, H. W. & Cavacini, L. Structure and function of immunoglobulins. *J. Allergy Clin. Immunol.* **125**, (2010).

151. Keskin, O. Binding induced conformational changes of proteins correlate with their intrinsic fluctuations: A case study of antibodies. *BMC Struct. Biol.* **7**, (2007).

152. Khan, T., Immunology, D. S.-T. J. of & 2014, undefined. Adjustable locks and flexible keys: plasticity of epitope–paratope interactions in germline antibodies. *Am Assoc Immnol* (2014) doi:10.4049/jimmunol.1302143.

153. Björling, E. & Uhlén, M. Antibodypedia, a Portal for Sharing Antibody and Antigen Validation Data. *Mol. Cell. Proteomics* **7**, 2028–2037 (2008).

154. Dübel, S., Stoevesandt, O., Taussig, M. J. & Hust, M. Generating recombinant antibodies to the complete human proteome. *Trends Biotechnol.* **28**, 333–339 (2010).

155. Uhlen, M. & Ponten, F. Antibody-based Proteomics for Human Tissue Profiling. *Mol. Cell. Proteomics* **4**, 384–393 (2005).

156. El-Kased, R. F. *et al.* Mass Spectrometric and Peptide Chip Epitope Analysis on the RA33 Autoantigen with Sera from Rheumatoid Arthritis Patients. *https://doi.org/10.1255/ejms.1046* **16**, 443–451 (2010).

157. Stafylis, C. & Klausner, J. D. Evaluation of two 4th generation point-of-care assays for the detection of Human Immunodeficiency Virus infection. *PLoS One* **12**, e0183944 (2017).

158. Chames, P., Van Regenmortel, M., Weiss, E. & Baty, D. Therapeutic antibodies: successes, limitations and hopes for the future. *Br. J. Pharmacol.* **157**, 220–233 (2009).

159. Inman, K. S., Francis, A. A. & Murray, N. R. Complex role for the immune system in initiation and progression of pancreatic cancer. *World J. Gastroenterol.* **20**, 11160 (2014).

160. Kapingidza, A. B., Kowal, K. & Chruszcz, M. Antigen–Antibody Complexes. *Subcell. Biochem.* **94**, 465–497 (2020).

161. Borghesi, L. & Milcarek, C. From B cell to plasma cell: regulation of V(D)J recombination and antibody secretion. *Immunol. Res.* **36**, 27–32 (2006).

162. Wang, X. Y., Wang, B. & Wen, Y. M. From therapeutic antibodies to immune complex vaccines. *NPJ vaccines* **4**, (2019).

163. Wen, Y. mei & Shi, Y. Immune Complex Vaccination. *Curr. Top. Microbiol. Immunol.* **423**, 95–118 (2019).

164. Lehmann, W. D. *Massenspektrometrie in der Biochemie*. vol. ISBN: 3-86025-094-9. (Spektrum Akademischer Verlag, Heidelberg, 1996).

165. Hernández, H. & Robinson, C. V. Determining the stoichiometry and interactions of macromolecular assemblies from mass spectrometry. (2007) doi:10.1038/nprot.2007.73.

166. Al-Majdoub, M. *et al.* A novel strategy for the rapid preparation and isolation of intact immune complexes from peptide mixtures †. (2014) doi:10.1002/jmr.2375.

167. Hoaglund, C. S., Valentine, S. J., Sporleder, C. R., Reilly, J. P. & Clemmer, D. E. Three-Dimensional Ion Mobility/TOFMS Analysis of Electrosprayed Biomolecules. *Anal. Chem.* **70**, 2236–2242 (1998).

168. Wyttenbach, T., Pierson, N. A., Clemmer, D. E. & Bowers, M. T. Ion Mobility Analysis of Molecular Dynamics. *Annu. Rev. Phys. Chem* **65**, 175–196 (2014).

169. Yefremova, Y., Opuni, K. F. M., Danquah, B. D., Thiesen, H. J. & Glocker, M. O. Intact Transition Epitope Mapping (ITEM). *J. Am. Soc. Mass Spectrom.* **28**, 1612–1622 (2017).

170. Hager-Braun, C. & Tomer, K. B. Determination of protein-derived epitopes by mass spectrometry. *http://dx.doi.org/10.1586/14789450.2.5.745* **2**, 745–756 (2014).

171. Opuni, K. F. M. *et al.* ITEM-THREE analysis of a monoclonal anti-malaria antibody reveals its assembled epitope on the pfMSP119 antigen. *J. Biol. Chem.* **295**, 14987–14997 (2020).

172. Danquah, B. D. *et al.* Intact Transition Epitope Mapping - Thermodynamic Weak-force Order (ITEM - TWO). *J. Proteomics* **212**, 103572 (2020).

173. Danquah, B. D. *et al.* Intact transition epitope mapping – Targeted high-energy rupture of extracted epitopes (ITEM-THREE). *Mol. Cell. Proteomics* **18**, 1543–1555 (2019).

174. Ko, K. Y. & Ahn, D. U. Preparation of Immunoglobulin Y from Egg Yolk Using Ammonium Sulfate Precipitation and Ion Exchange Chromatography. *Poult. Sci.* **86**, 400–407 (2007).

175. Hernández-Campos, F. J., Brito-De La Fuente, E. & Torrestiana-SÁNCHEZ, B. Purification of egg yolk Immunoglobulin (IgY) by ultrafiltration: Effect of pH, Ionic strength, and membrane properties. *J. Agric. Food Chem.* **58**, 187–193 (2010).

176. McKinney, M. M. & Parkinson, A. A simple, non-chromatographic procedure to purify immunoglobulins from serum and ascites fluid. *J. Immunol. Methods* **96**, 271–278 (1987).

177. Simpson, D. M. & Beynon, R. J. Acetone precipitation of proteins and the modification of peptides. *J. Proteome Res.* **9**, 444–450 (2010).

178. Crowell, A. M. J., Wall, M. J. & Doucette, A. A. Maximizing recovery of water-soluble proteins through acetone precipitation. *Anal. Chim. Acta* **796**, 48–54 (2013).

179. Yefremova, Y. *et al.* Apparent activation energies of protein–protein complex dissociation in the gas–phase determined by electrospray mass spectrometry. *Anal. Bioanal. Chem.* **409**, 6549–6558 (2017).

180. Röwer, C. *et al.* Mass spectrometric characterization of protein structure details refines the proteome signature for invasive ductal breast carcinoma. *J. Am. Soc. Mass Spectrom.* **22**, 440–456 (2011).

181. Postu, P. A., Ion, L., Drochioiu, G., Petre, B. A. & Glocker, M. O. Mass spectrometric characterization of the zein protein composition in maize flour extracts upon protein separation by SDS-PAGE and 2D gel electrophoresis. *Electrophoresis* **40**, 2747–2758 (2019).

182. Pecks, U. *et al.* Multifactorial analysis of affinity-mass spectrometry data from serum protein samples: A strategy to distinguish patients with preeclampsia from matching control individuals. *J. Am. Soc. Mass Spectrom. 2010 2110* **21**, 1699–1711 (2010).

183. Röwer, C. *et al.* Distinct Ezrin Truncations Differentiate Metastases in Sentinel Lymph Nodes from Unaffected Lymph Node Tissues, from Primary Breast Tumors, and from Healthy Glandular Breast Tissues. *Transl. Oncol.* **11**, 1–10 (2018).

184. Opuni, K. F. M. *et al.* Mass spectrometric epitope mapping. *Mass Spectrom. Rev.* **37**, 229–241 (2018).

185. Kilshaw, P. J., McEwan, F. J., Baker, K. C. & Cant, A. J. Studies on the specificity of antibodies to ovalbumin in normal human serum: technical considerations in the use of ELISA methods. *Clin. Exp. Immunol.* **66**, 481 (1986).

186. Holm, B. E. *et al.* Antibodies with specificity for native and denatured forms of ovalbumin differ in reactivity between enzyme-linked immunosorbent assays. *APMIS* **123**, 136–145 (2015).

187. Betancourt, L. H. *et al.* Quantitative Assessment of Urea In-Solution Lys-C/Trypsin Digestions Reveals Superior Performance at Room Temperature over Traditional Proteolysis at 37 °c. *J. Proteome Res.* **17**, 2556–2561 (2018).

188. Yang, Y., Barendregt, A., Kamerling, J. P. & Heck, A. J. R. Analyzing protein micro-heterogeneity in chicken ovalbumin by high-resolution native mass spectrometry exposes qualitatively and semi-quantitatively 59 proteoforms. *Anal. Chem.* **85**, 12037–12045 (2013).

189. Wang, H. *et al.* Comparison of glycation in conventionally and microwave-heated ovalbumin by high resolution mass spectrometry. *Food Chem.* **141**, 985–991 (2013).

190. Tsai, H. *et al.* Detection of rabbit IgG by using functional magnetic particles and an enzyme-conjugated antibody with a homemade magnetic microplate. *Chem. Cent. J.* **9**, 1–7 (2015).